THESIS FOR THE DEGREE OF DOCTOR OF PHILOSOPHY

# Lithium-ion Battery Safety

# -

# Assessment by Abuse Testing, Fluoride Gas Emissions and Fire Propagation

FREDRIK LARSSON

CHALMERS

Department of Physics

Chalmers University of Technology

Göteborg, Sweden 2017

Lithium-ion Battery Safety - Assessment by Abuse Testing, Fluoride Gas Emissions and Fire Propagation
ISBN: 978-91-7597-612-9

FREDRIK LARSSON
Göteborg, Sweden 2017



Doktorsavhandlingar vid Chalmers tekniska högskola
Ny serie nr 4293
ISSN 0346-718X

Revised version: October 2017

Front cover:
Photo of a commercial 18650 Li-ion cell in external heating abuse test (oven) just at the beginning of the thermal runaway, showing ignited cell material squirting out of the cell.

Department of Physics
Division of Subatomic and Plasma Physics
CHALMERS UNIVERSITY OF TECHNOLOGY
SE-412 96 Göteborg
Sweden

www.chalmers.se

Telephone: +46 (0)31-772 10 00

Author’s e-mail: vegan@chalmers.se

Printed by Chalmers Reproservice

Göteborg, Sweden 2017

# Lithium-ion Battery Safety - Assessment by Abuse Testing, Fluoride Gas Emissions and Fire Propagation

FREDRIK LARSSON

*Department of Physics, Chalmers University of Technology*

## ABSTRACT

Lithium-ion batteries offer high energy and power densities as well as long life time but have a more narrow stability window compared to other battery types and contain reactive and flammable materials. In case of overheating the battery cell can release gas (vent) and, at temperatures of about 150-200 °C, a so called thermal runaway can occur, that is a rapid self-heated temperature increase which is typically accompanied with a large release of smoke and gas, fire and a potential cell case explosion or gas explosion. In this work Li-ion battery safety has been studied by abuse tests; external fire, external heating (oven), external short circuit and overcharge. In total fifteen types of commercial Li-ion battery cells with various chemistries and cell capacity sizes ranging from 1.4 Ah to 45 Ah were studied.

Cell abuse may have a number of consequences. Emissions of toxic and flammable gases have been studied under external heating and fire tests. During such tests cells can vent long time before/without thermal runaway. In external heating abuse tests, three different vents were identified, two of them occurred before the thermal runaway. In case of a delayed ignition of the vented gases mixed with air in a confined/semiconfined space, a gas explosion can occur. The consequences of a gas explosion might be significantly more severe than those of a cell case explosion (explosion due to extreme cell pressure). In external heating tests, 5 of 11 cells underwent a gas explosion, for all levels of cycle ageing studied (0-300 deep C/2 cycles). Released fluoride gas emissions have been studied by FTIR spectroscopy and gas-washing bottles, a parallel independent method, that verified the total emission amounts. In fire tests, toxic hydrogen fluoride (HF) gas was released with 20-200 mg/Wh of nominal electrical energy capacity, according to data from seven types of commercial Li-ion cells at a state of charge (SOC) in the range of 0-100 %. The HF production rate in limited fire tests was temporarily increased when water mist was applied as a fire fighting medium, however, the total HF emission values were similar with or without water mist. Emission of $POF_3$ was also detected in the fire test, but only for one cell type at 0 % SOC. In external heating tests on the same cell type at 100 % SOC, emissions of HF and $POF_3$ were also detected. The measured amounts indicate that HF might pose a severe and acute toxic threat.

Heat spreading from a single Li-ion cell failure to adjacent cells, the cell-to-cell propagation, has been studied both experimentally and by numerical simulations. The use of fire walls between modules can significantly influence the propagation. A general risk assessment for Li-ion is presented and it is concluded that there is a lack of data on failure mechanisms, probability and consequences today.

The shut-down principle for future metal-air batteries, has also been studied as an additional safety aspect, utilizing primary (non-rechargeable) commercial Zn-Air cells. Besides offering an additional shut-down technique, it also offers possibilities to reduce electrical hazard voltages, by temporarily bringing the voltage down to zero volt.

**Keywords:** Lithium-ion, safety, abuse testing, thermal runaway, fire, cell case explosion, gas explosion, propagation, gas emission, hydrogen fluoride

# LIST OF PUBLICATIONS

**I.** Fredrik Larsson, Bengt-Erik Mellander, "Abuse by external heating, overcharge and short circuiting of commercial lithium-ion battery cells", *Journal of The Electrochemical Society*, 161 (10), A1611-A1617 (2014).

**II.** Fredrik Larsson, Petra Andersson, Bengt-Erik Mellander, "Lithium-ion battery aspects on fires in electrified vehicles on the basis of experimental abuse tests", *Batteries*, 2, 9 (2016).

**III.** Fredrik Larsson, Simon Bertilsson, Maurizio Furlani, Ingvar Albinsson, Bengt-Erik Mellander, "Gas explosions and thermal runaways during external heating abuse of commercial lithium-ion graphite-$LiCoO_2$ cells with different levels of ageing", *manuscript submitted to Journal of Power Sources.*

**IV.** Fredrik Larsson, Petra Andersson, Per Blomqvist, Anders Lorén, Bengt-Erik Mellander, "Characteristics of lithium-ion batteries during fire tests", *Journal of Power Sources*, 271, 414-420 (2014).

**V.** Fredrik Larsson, Petra Andersson, Per Blomqvist, Bengt-Erik Mellander, "Toxic fluoride gas emissions from lithium-ion battery fires", S*cientific Reports*, 7, article number 10018 (2017).

**VI.** Fredrik Larsson, Petra Andersson, Per Blomqvist, Bengt-Erik Mellander, "Gas emissions from lithium-ion battery cells undergoing abuse from external fire", Conference proceedings of Fires in vehicles (FIVE) 2016, Baltimore, USA, 5-6 October 2016, edited by Petra Andersson, Björn Sundström, *SP Technical Research Institute of Sweden*, Borås, Sweden, p. 253-256 (2016).

**VII.** Fredrik Larsson, Johan Andersson, Petra Andersson, Bengt-Erik Mellander, "Thermal modelling of cell-to-cell fire propagation and cascading thermal runaway failure effects for lithium-ion battery cells and modules using fire walls", *Journal of The Electrochemical Society*, 163 (14), A2854-2865 (2016).

**VIII.** Fredrik Larsson, Antti Rytinki, Istaq Ahmed, Ingvar Albinsson, Bengt-Erik Mellander, "Overcurrent abuse of primary prismatic zinc-air battery cells studying air supply effects on performance and safety shut-down", *Batteries*, 3, 1 (2017).

# CONTRIBUTION REPORT

**Paper I**
FL conceived the idea, planned and performed the experiments and made the data process. FL and BEM analysed the results and wrote the paper.

**Paper II**
FL planned the experiments, the SBI fire tests were planned together with PA and BEM. All authors were involved in the analyses of the data and wrote the paper.

**Paper III**
FL conceived the idea and planned the experiments. Analysis of cell separator and cell electrolyte as well as FTIR gas measurements during abuse tests were conducted by SB and MF. FL made the data process. All authors analysed the results and wrote the paper.

**Paper IV**
FL and PA planned the experiments. PB and AL developed the FTIR measuring method used. PA made the initial data process of the SBI data. PB planned and performed the FTIR measurements and made the data processing. FL prepared the batteries and performed the measurement of temperature and cell voltage. FL performed the overall data collection. All authors were involved in the analyses of the data and wrote the paper.

**Paper V**
FL planned the experiments, partially together with PA and BEM. PA made the initial data process of the SBI data. PB planned and performed the FTIR and gas-washing bottles measurements and made the initial data processing. FL prepared the batteries and performed the measurement and data analyses of temperature, cell voltage and water mist, and did the post-measurements and final data processing. Water mist setup was planned and constructed by BEM and FL. All authors were involved in the analyses of the data and wrote the paper.

**Paper VI**
FL planned the experiments, partially together with PA and BEM. PA made the initial data process of the SBI data. PB planned and performed the FTIR and gas-washing bottles measurements and made the initial data processing. FL prepared the batteries and performed the measurement and data analyses of temperature and cell voltage, and did the post-measurements and final data processing. All authors were involved in the analyses of the data and wrote the paper.

**Paper VII**
FL conceived the idea. JA, FL and PA planned the numerical simulations which were implemented and performed by JA. FL made the battery module design and material specification. FL, PA and JA planned the experimental tests. All authors were involved in the analyses of the data and wrote the paper.

**Paper VIII**
FL and IAh conceived the experiments. FL designed and planned the experiments and AR performed the experiments. All authors were involved in the analyses of the data and wrote the paper.

# OTHER RELATED PUBLICATIONS, NOT INCLUDED IN THE THESIS

**1.** Simon Bertilsson, Fredrik Larsson, Maurizio Furlani, Ingvar Albinsson, Bengt-Erik Mellander, "Lithium-ion battery electrolyte emissions analyzed by coupled thermogravimetric/Fourier-transform infrared spectroscopy", *Journal of Power Sources*, 365, 446-455 (2017).

**2.** Petra Andersson, Johan Wikman, Magnus Arvidson, Fredrik Larsson, Ola Willstrand, "Safe introduction of battery propulsion at Sea", *Research Institutes of Sweden*, Göteborg, Sweden, SP Rapport 2017:34, ISSN 0284-5172 (2017).

**3.** Petra Andersson, Per Blomqvist, Anders Lorén, Fredrik Larsson, "Using Fourier transform infrared spectroscopy to determine toxic gases in fires with lithium-ion batteries", *Fire and Materials*, 40 (8), 999-1015 (2016).

**4.** Fredrik Larsson, Johan Anderson, Petra Andersson, Bengt-Erik Mellander, "Safer battery systems in electrified vehicles – an electrified bus perspective", *Eurotransport*, June edition 2016, Russell Publishing Ltd, Kent, United Kingdom, 3, 50-53 (2016).

**5.** Petra Andersson, Per Blomqvist, Fredrik Larsson, Anders Lorén, "Fire risks with lithium-ion batteries - measurements of gas emissions", *2nd IAFSS European Symposium of Fire Safety Science (ESFSS)*, Nicosia, Cyprus (2015).

**6.** Petra Andersson, Johan Anderson, Fredrik Larsson, Bengt-Erik Mellander, Modelling of thermal events in lithium-ion batteries, *2nd IAFSS European Symposium of Fire Safety Science (ESFSS)*, Nicosia, Cyprus (2015).

**7.** Johan Anderson, Fredrik Larsson, Petra Andersson, Bengt-Erik Mellander, "Thermal modeling of fire propagation in lithium-ion batteries", *24th International Technical Conference on the Enhanced Safety of Vehicles (ESV) 2015*, Paper Number 15-0073, Gothenburg, Sweden (2015).

**8.** Fredrik Larsson, Petra Andersson, Bengt-Erik Mellander, "Battery aspects on fires in electrified vehicles", Conference proceedings of Fires in vehicles (FIVE) 2014, Berlin, Germany, 1–2 October 2014, edited by Petra Andersson, Björn Sundström, *SP Technical Research Institute of Sweden*, Borås, Sweden, p. 209–220 (2014).

**9.** Johan Anderson, Fredrik Larsson, Petra Andersson and Bengt-Erik Mellander, "Fire spread due to thermal runaway in a lithium-ion battery cell", Conference proceedings of Fires in vehicles (FIVE) 2014, Berlin, Germany, 1–2 October 2014, edited by Petra Andersson, Björn Sundström, *SP Technical Research Institute of Sweden*, Borås, Sweden, p. 268-271 (2014).

**10.** Fredrik Larsson, Petra Andersson, Bengt-Erik Mellander, "Are electric vehicles safer than combustion engine vehicles?", in: Systems perspectives on Electromobility, edited by Björn Sandén, Pontus Wallgren, *Chalmers University of Technology*, Göteborg, Sweden, ISBN 978-91-980973-9-9, p. 33-44 (2014).

**11.** Petra Andersson, Per Blomqvist, Anders Lorén, Fredrik Larsson, "Investigation of fire emissions from Li-ion batteries", *SP Technical Research Institute of Sweden*, Borås, Sweden, SP Report 2013:15, ISBN 978-91-87461-00-2 (2013).

**12.** Fredrik Larsson, Bengt-Erik Mellander, "Energy storage system safety in electrified vehicles", Conference proceedings of Fires in vehicles (FIVE) 2012, Chicago, USA,

27-28 September 2012, edited by Petra Andersson, Björn Sundström, *SP Technical Research Institute of Sweden*, Borås, Sweden, p. 303-306 (2012).

**13.** Fredrik Larsson, Jesper Martaeng, Bengt-Erik Mellander, "Design for safety", *Proceedings of Advanced Automotive Battery Conference (AABC) 2012*, Orlando, USA (2012).

# ACKNOWLEDGEMENTS

My warmest appreciation and gratitude to my main supervisor Professor Bengt-Erik Mellander, you are great. I am also grateful to my assistant supervisors Dr. Petra Andersson and Associate Professor Ingvar Albinsson, for all your helpful support.

Many thanks to colleagues in the Electrophysics group at Chalmers University of Technology; especially to Dr. Maurizio Furlani, Mr. Simon Bertilsson and Mr. Antti Rytinki. Many thanks to colleagues at RISE Research Institutes of Sweden (former SP); especially to Associate Professor Johan Anderson, Dr. Per Blomqvist and Mr. Ingvar Karlson.

A special thank you to my former employer and the former battery development company Effpower and CEO Per Svantesson for the solid support in the initiation of my PhD-project and the strong trust in my capabilities. A special thanks also to Professor Peter Leisner, head of Electronics department at RISE, for arranging the continuation of the project from Effpower. The project partners of the FFI-project "*Safer battery systems in electrified vehicles – develop knowledge, design and requirements to secure a broad introduction of electrified vehicles*" are also gratefully acknowledged, special thanks to Mr. Patrik Roth.

The Swedish Energy Agency, The Swedish Fire Research Board (Brandforsk), Swedish Fire Protection Association (free translation of Brandskyddsföreningen) and Carl Tryggers Stiftelse för vetenskaplig forskning are gratefully acknowledged for their financial support. Special thanks to the Scandinavian Automotive Supplier Association (FKG) and Stephen Wallman for their support. A special thanks also to Dr. Istaq Ahmed for collaboration in the Zn-Air study.

To my family, Malin and Holger ❤️

Fredrik Larsson

Göteborg, August 2017

# NOMENCLATURE

| | |
|---|---|
| AEGL | Acute exposure guideline level |
| BMS | Battery management system |
| CFD | Computational fluid dynamics |
| CID | Current interrupt device |
| CV | Cell voltage |
| DEC | Diethyl carbonate |
| DMC | Dimethyl carbonate |
| EA | Ethyl acetate |
| EC | Ethylene carbonate |
| EIS | Electrochemical impedance spectroscopy |
| EMC | Ethyl methyl carbonate |
| EV | Electric vehicle |
| FDS | Fire dynamics simulator |
| FEC | Fractional effective dose |
| FED | Fractional effective concentration |
| FEM | Finite-element method |
| FTIR | Fourier transform infrared spectroscopy |
| HDPE | High-density polyethylene |
| HEV | Hybrid electric vehicle |
| HF | Hydrogen fluoride |
| HRR | Heat release rate |
| IDLH | Immediate dangerous to life or health |
| LATP | Lithium aluminium titanium phosphate |
| LCO | Lithium cobalt oxide |
| LFL | Lower flammability limit |
| LFMP | Lithium iron manganese-phosphate |
| LFP | Lithium iron-phosphate |
| LMO | Lithium manganese oxide |
| LTO | Lithium titanium oxide |
| NCA | Lithium nickel cobalt aluminum oxide |
| NHTSA | National Highway Traffic Safety Administration |
| NiMH | Nickel-metal hydride |
| NIOSH | National Institute of Occupational Safety and Health |
| NMC | Lithium nickel manganese cobalt oxide |
| PC | Propylene carbonate |
| PCM | Protection circuit module |
| PE | Polyethylene |
| PHEV | Plug-in hybrid electric vehicle |
| $POF_3$ | Phosphoryl fluoride |
| PP | Polypropylene |
| PTC | Positive temperature coefficient |
| PTFE | Polytetrafluoroethylene |
| PUR | Polyurethane |
| PVC | Polyvinyl chloride |
| PVdF | Polyvinylidene fluoride |
| SBI | Single burning item |
| SEI | Solid electrolyte interface |

| | |
|---|---|
| SOC | State of charge |
| SOH | State of health |
| SOS | State of safety |
| TGA | Thermogravimetric analysis |
| THR | Total heat release |
| TR | Thermal runaway |
| UFL | Upper flammability limit |
| UN | United Nations |

# CONTENTS

# INTRODUCTION

Batteries of different types, sizes and applications are widely used today. There are many requirements on the battery depending on the use such as low weight, small volume, low cost, long life time as well as being safe. Batteries can be divided into two main categories, primary batteries, i.e. non-rechargeable and secondary batteries that are rechargeable and can be used multiple times. There are different battery technologies for each main category. A battery can consist of one or several cells. Common primary batteries are small consumer batteries type AA or AAA consisting of one cell of e.g. alkaline type. Type AA and AAA cells are also available as secondary rechargeable batteries.

The lead-acid battery is a rechargeable battery widely used as vehicle start battery and backup-battery. The lead-acid battery technology is mature, it has been used for more than 150 years, it provides however relatively low energy density, low cycle life time and long charging time. The nickel-metal hydride (NiMH) technology is another type of secondary battery that offers a higher energy density and a longer cycle life time. NiMH has been widely used, however its market has decreased in favor of the lithium-ion (Li-ion) batteries. The Li-ion batteries are rechargeable and offer a long life time combined with high energy and power densities, resulting in compact and low weight high-performance batteries, but have drawbacks in terms of safety. The first commercial Li-ion battery was introduced by Sony in 1991, for a review of the development of lithium-ion batteries see Blomgren [1].

Lithium is a very light element and offers a high cell voltage when used in batteries. The term lithium battery is sometimes used for both rechargeable Li-ion and non-rechargeable Li-metal batteries, which have very different properties. Today's primary lithium batteries, named lithium-metal (Li-metal), are typically found in coin cells (e.g. CR2026 type). Even though secondary Li-ion batteries do not use lithium in metallic form today, it might be used in the future also for rechargeable batteries, increasing the confusion even more regarding the vocabulary. In some situations, e.g. in case of fire-fighting with water, it is essential not to mix up Li-ion and Li-metal battery types as water and lithium-metal produces hydrogen.

## INCIDENTS AND FIELD FAILURES

There are billions of Li-ion battery cells in use world-wide and every year a number of incidents happen. Relatively few incidents are widely reported by media, some are only

locally reported, while some are not reported at all. There are thus limited statistics about Li-ion battery incidents and there is no organization that specifically handles battery accidents. For consumer Li-ion cells, a cell failure rate of less than 1 ppm (<1 cell failure in 1 million cells) are reported in a few scientific papers [2,3,4] however just as a number without further information, discussion or references how they were obtained. Thus, the knowledge of cell failure rates is limited or not publicly available. The known incidents are typically referred to as field failures, that is, failures in the field. There are a number of possible causes for battery failures and at least a part of the field failures are often considered as spontaneous internal cell short circuits. They start at a micrometer scale inside a cell with a short circuit rapidly increasing the local temperature. It is extremely difficult, if not impossible, to detect these types of failures before they happen. Internal cell short circuits are just one of possible causes for fires or explosions, external factors are also very important.

Nowadays Li-ion batteries are used in different environmental conditions, with a more complex ageing profile and power usage, e.g. with large current (high C-rate[*] values), in larger packs, with larger cell sizes, with newly developed electrode materials, electrolyte mixtures, etc. For example, "automotive cells", i.e. cells with high quality manufacturing (e.g. more pure raw materials) and larger size than that of typical consumer products, are exposed to road vibrations, humidity and temperature variations, high charge and discharge pulses, thus the environmental conditions are quite different compared to those for small consumer cells of e.g. the 18650 type. However, 18650 cells are sometimes used also in larger battery systems e.g. the electric car manufacturer Tesla Motors have used 18650 cells but have now announced a change to a somewhat larger cylindrical cell of type 2170, i.e. 21 mm in diameter and 70 mm long [5].

When a new technology is introduced the knowledge on associated risks is often limited. When risks become better known steps are taken (counter actions) to handle these risks. For example, the use of gasoline is a natural part of the handling of vehicles today, however gasoline is a rather extreme, dangerous substance in terms of risks for fire and explosions. Anyhow, today the society has learnt how to handle gasoline so that the safety level is relatively high. For electric vehicles as well as for other applications using Li-ion batteries the learning curve is still on the rise.

[*] The C-rate relates the size of the current to the capacity size of the cell, where 1 C means a current equal to 1 hour discharge of the battery cell. For example a 10 Ah cell have a 1 C-rate of 10 A, while the 10 C-rate is 100 A and C/10 is 1 A.

Over the years there have been repeated incidents involving Li-ion batteries in cell phones, laptops and other portable electronic devices but with the growing use of larger battery systems incidents can have more serious consequences, for example in case of a fire in a grid power storage plant using Li-ion batteries. Laptop computer batteries have been, and still are, involved in battery incidents, due to e.g. cell manufacturing problems, that have led to major recalls, costly for the manufacturer, e.g. Sony [6]. As another example, many cell phones of type Samsung Galaxy Note 7 did catch fire in 2016. That lead to a massive recall by Samsung [7]. Fire incidents with smaller-sized consumer products, including e.g. batteries for electric bicycles and hover boards, having a Li-ion battery are reported relatively often, however taking into account the billions of battery cells used, the failure rate is low. Additionally, the consequences from a single cell or small Li-ion battery failure are typically not so severe. There are however examples of fatal consequences from small Li-ion battery failures. In 2009 in Staffanstorp, Sweden, a family of five people were killed in their sleep during a house fire, and the fire investigation identified an overheated laptop computer as the probable origin of the fire [8,9].

Some incidents involving electrified vehicles have attracted considerable media attention. In 2011 there was an incident involving the electrified vehicle Chevrolet Volt [10]. The vehicle had been crash tested according to common test procedures without problems. However, three weeks later a battery fire accompanied with an explosion occurred as reported in the investigation of the event by the National Highway Traffic Safety Administration (NHTSA). The cause was found to be short circuit by leaking coolant from the mechanical crash damage. After the incident the failure modes were repeated and the delayed fire could also be reproduced. Another incident reported by media occurred in 2012 when hurricane Sandy flooded the harbor in Newark, New Jersey, USA. Thousands of vehicles parked in the harbor were immersed in about 1.5-2.5 meters of sea (salt) water and there were reports of burned HEVs and PHEVs, from Toyota Prius and Fisker Karma. Sea water is a good electrical conductor that can cause an electrical short circuit, e.g. in the Li-ion battery but also in the vehicle´s 12 V lead-acid battery and system. This was an extreme situation, cars are not designed to be submerged in sea water. In order to avoid consequences of such an incident, cars need to be designed with a tightness level of IP68 or equal, something that is not easily accomplished in a Li-ion battery and particularly not for the 12 V system.

At the end of 2013 the media attention was high since three electric vehicles, Tesla Model S, went into fire within a time period of six weeks. The first incident was caused by the driver

hitting road debris at highway speed which mechanically abused the battery pack from underneath by penetration. The second incident involved severe mechanical deformation when the driver hit a concrete wall and thereafter a tree. The third incident was also caused by mechanical abuse when the car was hit by road debris. Thus, the three electric vehicles were exposed to large mechanical forces and one could argue what level of damage a vehicle should be designed to handle. NHTSA conducted an investigation but did not find any defect trends [11]. After these incidents Tesla Motors reinforced the construction to better protect the battery from mechanical abuse [12]. There have been a few more fires in the same type of vehicle, e.g. one in Norway and another in Sweden [13], both when the vehicle was being charged. Vehicle fires in the USA comprise about 1 fire in 1400 vehicles [14]. The statistics for electric vehicles is still very limited, but this far the EVs are significantly less prone to fire as discussed in Paper II. EVs offer in principle several safety advantages [15], anyhow real-world potential safety disadvantages are yet not known to the full extent, for example, the EVs on the streets today are still relatively new thus potential ageing effects on safety are not yet accounted for.

The risks for fire and explosion are of special concern in cases where there are limited possibilities to escape the consequences of a battery incident. In 2013-2014 there were a series of fire incidents involving the then new airplane Boeing 787 Dreamliner [16,17]. Given the occurrence of fires and the number of installed batteries, the cell failure probability rate in 2014 was extremely high, magnitudes above the typical failure rate values found of about 1 ppm. The Dreamliner was the first commercial airliner to use Li-ion batteries but after a reconstruction of the battery system no further incidents have been reported. Battery fires have occurred in airplanes earlier but then involving Li-ion batteries in the cargo hold of the airplane. In 2010 and 2011 two fires occurred in Boeing 747 cargo planes resulting in airplane crashes where the crew was killed. The fires were blamed on the transported Li-ion batteries [18]. The airline industry has since then imposed strict regulations for transporting Li-ion batteries as cargo, but restrictions have also been imposed for batteries transported as hand luggage on airplanes [19]. Another example of a battery fire that may have consequences for the application is the RoboSimian fire in 2016, where the Li-ion batteries of the robot did undergo thermal runaway and a subsequent fire in Nasa's Jet Propulsion Laboratory [20].

All this incidents and accidents show the importance of safety of batteries. The increased use of Li-ion batteries emphasizes the need even more.

# LITHIUM-ION BATTERIES

## THE LITHIUM-ION BATTERY CELL

The term Li-ion battery is used as a family name of a type of batteries using intercalation electrodes and lithium ion conducting electrolytes of different chemical compositions. The batteries are typically characterized by a high cell voltage of about 4 V, high energy and power densities, short charging times, low self-discharge, high efficiency and long life time [21]. Compared to many other battery technologies Li-ion batteries have some drawbacks in terms of safety, e.g. the electrolyte is flammable, and the cell has a limited stable operational window in terms of voltage and temperature ranges. In case of overheating, the cell in itself internally provides all three elements (in the fire triangle) necessary for fire; heat/igniter, combustible material and oxygen.

Li-ion battery cells are sealed during normal use and can be found in different shapes, the most common are cylindrical, hard prismatic and pouch prismatic, see examples in Figure 1. A common cylindrical size is the so called 18650, which is 18 mm in diameter and 65 mm long. It was originally used in battery packs for laptop computers. Li-ion cells are today commercially available in a large range of different capacities, the most common ones are in the range of about 2-20 Ah per cell.

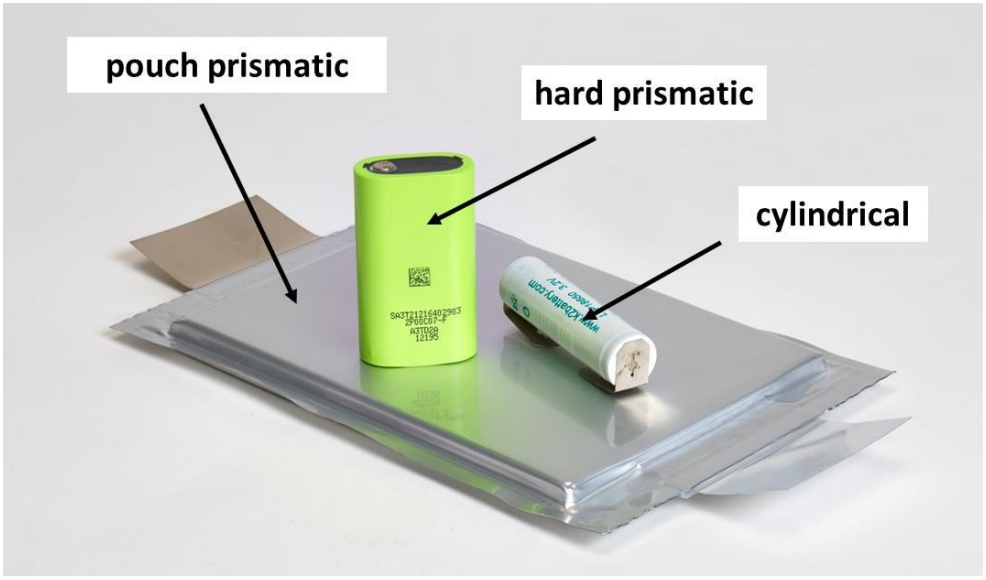


Figure 1. Photo showing commercial Li-ion cells of three types; cylindrical, hard prismatic and pouch prismatic.

Li-ion batteries are produced in very large numbers and are used in many different applications; e.g. in consumer products such as cell phones, laptop computers, digital cameras, handheld power tools, electrified vehicles, ships and for stationary energy storage used in the electrical grid. The small powerful Li-ion batteries have revolutionized the consumer market enabling for example the smart phones. The attractive properties of the Li-ion technology, especially the energy and power densities (corresponding to low weight and volume) and long life time, have resulted in an increasing use of Li-ion batteries for electrified vehicles, i.e. hybrid electric vehicles (HEV), plug-in HEV (PHEV) and electric vehicles (EV), all with different degree of electrification and battery sizes. The diverse applications meet different demands and environmental conditions. For example, in vehicles there are road vibrations, potential crash forces/deformation and vast temperature and humidity variations, while desired battery properties are low cost, long electrical driving range (high energy density), high acceleration and top speed (high power density), fast charging (high charge power density) and long life time. From a physical science perspective, there is always a trade-off between the desired properties, e.g. it is simply not possible to have the highest energy density at the same time as having the highest power density. The battery optimization is, within reasonable ranges, a matter of constructional design. For vehicle applications this means for example, that having a fast charging capability limits the driving range but also lowers the battery life time, since high currents (both charge and discharge) typically wear out the battery faster.

In Li-ion battery cells, the lithium ion, $Li^+$, is transferred between the cathode (positive electrode) and the anode (negative electrode), during charging and discharging, this is sometimes referred to as a “rocking chair”. Figure 2 shows a schematic illustration of the Li-ion cell. During electrical discharge the current goes through the electrical load from plus pole to minus pole and the circuit is closed by the lithium ion transport in the electrolyte. The porous separator is soaked with electrolyte and prevents cathode-anode contact while the holes in the separator allow electrolyte penetration, thus can $Li^+$ pass through. The electrical current is conducted via current collectors, using thin metal foils of aluminum at the cathode and copper at the anode.

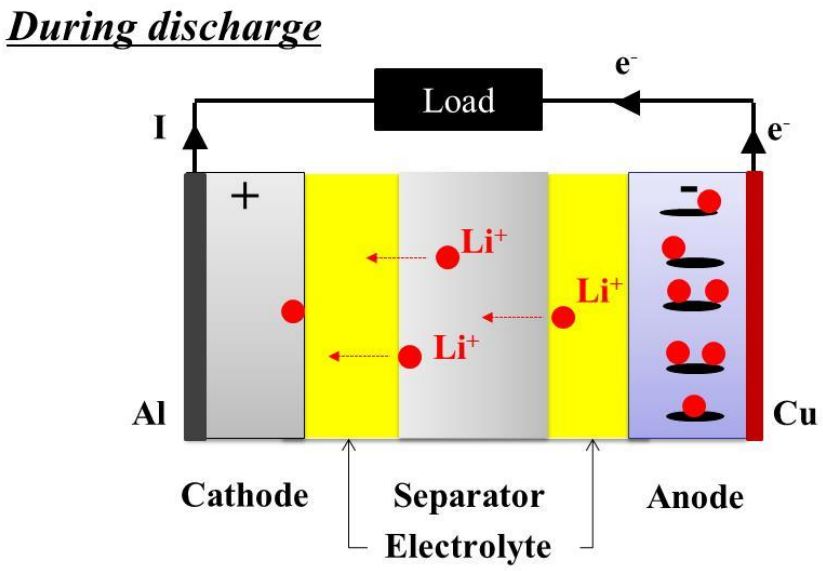


Figure 2. Schematic illustration over the Li-ion battery cell, the directions of the arrows are valid during discharging (opposite direction during charging).

There are a large number of possible electrode materials and many of them have been studied in research laboratories, while just a few have been commercialized. For the anode, different types of carbon/graphite are the most used commercially. Another commercial anode material is lithium titanium oxide (LTO), $Li_4Ti_5O_{12}$ or other titanium compounds, e.g. LATP, $LiAlTiPO_4$. For the cathode a wider range of materials are commercially available. The first cathode material used by Sony was lithium cobalt oxide (LCO), $LiCoO_2$ and it is still in use. Other metal oxides are also used e.g. based on nickel, manganese and aluminum in various combinations. Lithium nickel manganese cobalt oxide (NMC), $LiNi_xMn_yCo_zO_2$ is a common cathode materials in different combinations where x+y+z=1. (NMC is sometimes also referred to as NCM.) Lithium nickel cobalt aluminum oxide (NCA), $LiNi_xCo_yAl_zO_2$, and lithium manganese oxide (LMO), $LiMn_2O_4$, with manganese spinel are other common cathode materials. Another group of cathode materials are based on phosphates, and a few of them are commercialized, the most common one is lithium iron-phosphate (LFP), $LiFePO_4$. The different electrode materials offer various pros and cons.

There are also different types of commercial separators. The most common separator material is a polymer made from e.g. polyethylene (PE) or polypropylene (PP). The melting temperature of PE is about 130 °C while PP melts at about 160 °C. Sometimes a combination of PE and PP is used as a two layer PE-PP or a trilayer PP-PE-PP separators. These are called

shutdown separators and offer some safety advantages. The polymer separator can also be reinforced by ceramics to allow physical rigidity at higher temperatures, usually 200 °C or somewhat higher.

The electrolyte is typically a mixture of a Li-salt, organic solvents and a number of additives. The exact electrolyte composition used in commercial Li-ion batteries is seldom or never revealed and considered key knowhow and treated with large secrecy. Water based electrolytes have an electrochemical stability window of about 1.2 V and cannot be used in Li-ion due to the higher cell voltage [22]. The Li-salt is needed to enable the $Li^+$ conductivity and the currently outmost used commercial Li-salt is lithium hexafluorophosphate, $LiPF_6$. The fluorine in the $LiPF_6$ may give rise to toxic gas emissions but it has so far been a difficult and complex task to replace the $LiPF_6$ in the electrolyte. The organic solvents are typically a mixture of linear and cyclic carbonates in order to achieve optimal properties in terms of e.g. viscosity, dielectric constant, melting and boiling temperature. Common linear carbonates include dimethyl carbonate (DMC), diethyl carbonate (DEC) and ethyl methyl carbonate (EMC) while common cyclic carbonates are ethylene carbonate (EC) and propylene carbonate (PC). Other common solvents are, e.g. ethyl acetate (EA). A number of additives, typically in small concentrations, are often used since they are important for various purposes, e.g. performance, life time and safety.

The cell layers of cathode, separator and anode are soaked with electrolyte and then the layers are either rolled forming a so called jelly-roll or cut in rectangular shapes and stacked on top of each other with electrical parallel connectors between each layer. The jelly-roll is typically used in cylindrical or hard prismatic cans, while the stacked layers are more common in prismatic pouch cells. Figure 3 shows X-ray photos of an 18650 cell where the layers in the jelly-roll are clearly seen.

Several safety mechanisms can be integrated into the Li-ion cell. All Li-ion cells today need to be fully sealed since the electrolyte would otherwise evaporate and react with humid air. In a situation when the battery cell undergoes excessive temperatures, the cell pressure will increase and in order to prevent build-up of extreme cell pressure and the consequence of a cell case explosion, a safety vent is integrated into cylindrical and hard prismatic cells, while a pouch cell typically has no safety vent since it cannot build similar high pressures before naturally bursting. A pouch cell can still have a predesigned spot or spots with less strength in order to predetermine the location of the pouch cell opening. The interior of the cell can also

have a (partly) reversible integrated current limiter such as a positive temperature coefficient (PTC) or a non-reversible current breaker such as a current interrupt device (CID).

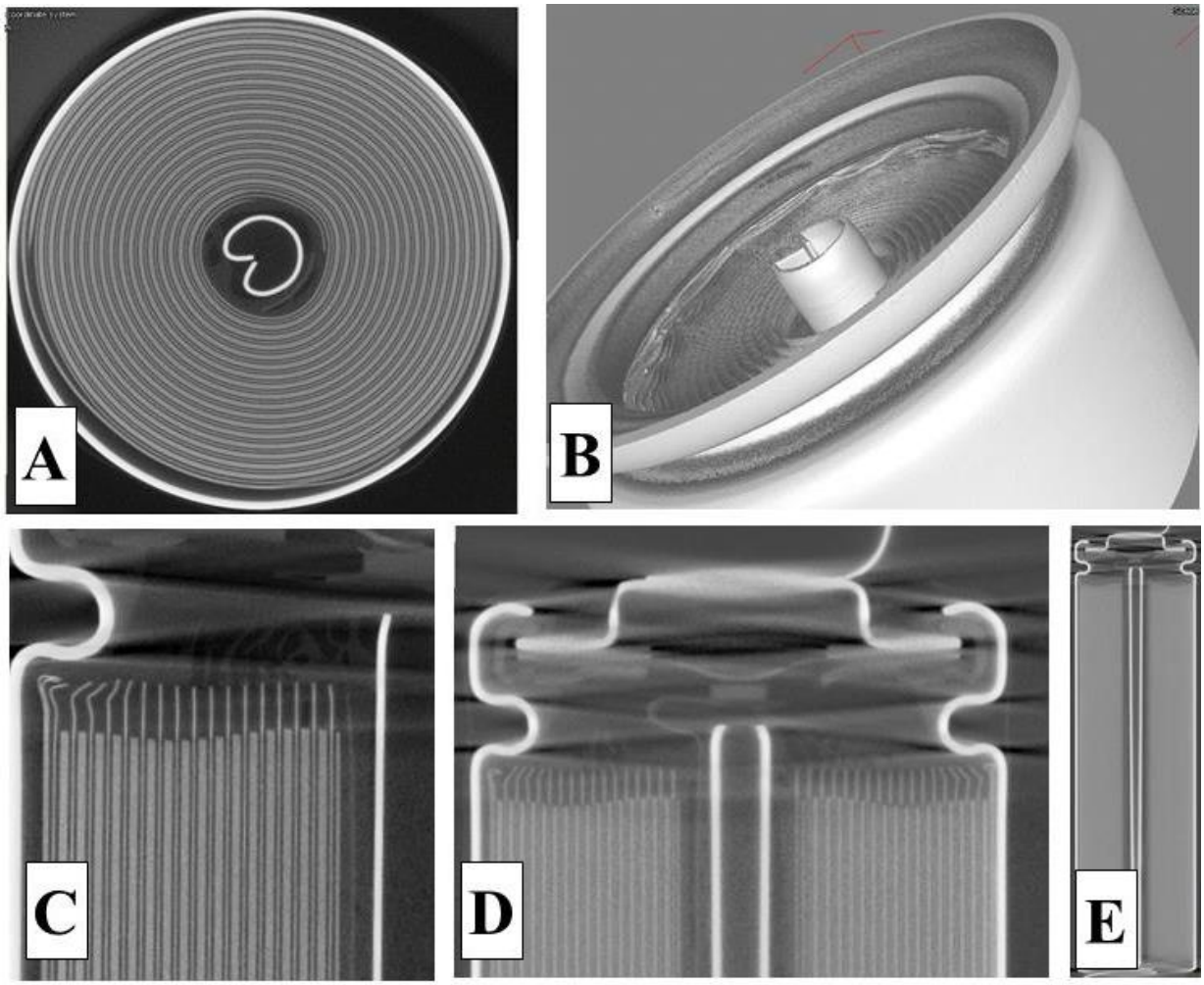


Figure 3. X-ray photos of a 18650 cylindrical cell of type Sanyo UR18650F where A-E is not of the same scale, (**A**) showing a cross-section of the jelly-roll, (**B**) showing a 3D of the top of the jelly-roll, (**C**) showing the jelly-roll from the side, (**D**) showing a cross-section of the top of the cell and (**E**) showing a cross-section of the full cell-length.

Thus the Li-ion battery cannot be described as one single type, but rather as a wide range of different types of batteries. New materials in terms of cathode, anode, separator and electrolyte for Li-ion batteries are constantly developed. Li-ion batteries are often considered positive for the environment and climate change, however the full picture is complex. There are environmental challenges for Li-ion batteries during e.g. material processing and battery manufacturing. The amount of easily accessible lithium sources in the world are concentrated to a few sources and countries [23], even more than for oil, causing potential future political

and market problems. There are huge amounts of highly diluted lithium in sea water, but it is technically and commercially challenging to extract it. Material recycling of Li-ion batteries today focuses on the expensive metals in the battery but might need to focus also on recycling lithium in the future in order obtain enough lithium for the wide use of Li-ion batteries. Development of future sodium-ion batteries [24] may decrease the need for lithium, but lithium ion batteries are and will still be dominant for an extended period of time.

## THE LITHIUM-ION BATTERY SYSTEM

A commercial Li-ion battery today consists of one or multiple cells but also includes electronics for monitoring and control of the cell/cells, cables/connector, all placed inside a battery box (e.g. plastic/metal). Li-ion batteries for cell phones typically consist of just one battery cell, while a Li-ion battery for a power tool can consist of e.g. 6 cells. Larger batteries for electrified vehicles and stationary grid applications can consist of hundreds or thousands of cells or even higher numbers of cells. The application determines the need for power and energy capacity of the battery and thereby the requirements on the cell. By electrically connecting battery cells in series the total voltage is increased, and by parallel electrical connection the capacity is increased. For large batteries cells can be connected both in series and parallel, and they can be arranged in different ways, forming one or several so called cell strings.

Today typically about 10-20 cells are placed together into a battery module with a voltage of about 50 V, and then a number of modules are connected together to form the battery pack with a voltage of about 300-1000 V. For very large systems, a multiple of battery subpacks/packs are connected together to form a battery system. If just one battery pack is used that will be the battery system.

The outer battery case or box is needed to protect the battery from the environmental conditions which vary for different applications. Is should protect from; dust, moisture from rain or air humidity, low and high temperatures, mechanical abuse e.g. drop or deformation by crash, vibrations from e.g. road applications, as well as from accidental short-circuits.

A thermal management system that controls the heating and/or cooling of the battery system, is needed for larger batteries, and can be passive or active using air or a liquid as cooling

agent. It is important to keep the battery within a certain temperature range for reasons of safety, life time and performance.

The battery management system (BMS) is the brain of the battery system and has a number of sensors to monitor and control the battery. The BMS is needed for Li-ion batteries in order to maintain a safe operation. For small batteries only one BMS is used, such a BMS is sometimes called protection circuit module (PCM). Larger battery system can have a master BMS and a multiple of slave BMS, typically one slave BMS per battery module.

The BMS must measure the voltage of each battery cell in order to prohibit overvoltage and undervoltage. Cells connected in parallel can be treated as one cell in terms of cell potential, however in case of separated battery strings, the cells are not connected in parallel and in such a case all the battery cells need to be monitored. In addition to the individual cell voltage sensors, the battery module and pack voltages are typically also measured, and are important in order to validate potential errors in the voltage sensors. The current in the battery system is also measured at one or several locations.

The temperature is typically measured at a numbers of places in the battery system. In large systems, it was earlier relatively common to have one temperature sensor per cell or per two cells. Nowadays it is more common to have fewer temperature sensors, e.g. 1-2 sensors per battery module (e.g. 10-20 cells) in the automotive industry, in order to lower the cost of the battery. The temperature sensors are important in order to establish the overall battery temperature for operational purposes, e.g. power output and for control of the thermal management system.

The battery system also consists of electrical components such as current cables, connectors and circuit breakers. Typically one or several fuses are used for short circuit protection of the battery pack, and there are usually electrical circuit breakers in form of contactors at each battery pole, a negative contactor and a positive contactor. Figure 4 shows a simplified schematic illustration of a battery system focusing on the current path and battery voltage connections. When powering up the battery system the voltage goes from 0 to the system voltage of typically hundreds of volt, and in order to lower the transient current peaks, a pre-charge circuit is often used, typically consisting of a contactor and a resistance (not shown in Figure 4).

The battery voltage has so called floating ground, meaning that there is no electrical connection between either of the battery poles and the outer reference ground potential (e.g. chassis ground in vehicles). The floating ground increases the general electrical hazard safety since two isolation faults are needed in order to create a circuit. The isolation between the battery poles and the ground is typically monitored by an isolation monitor circuit in the BMS.

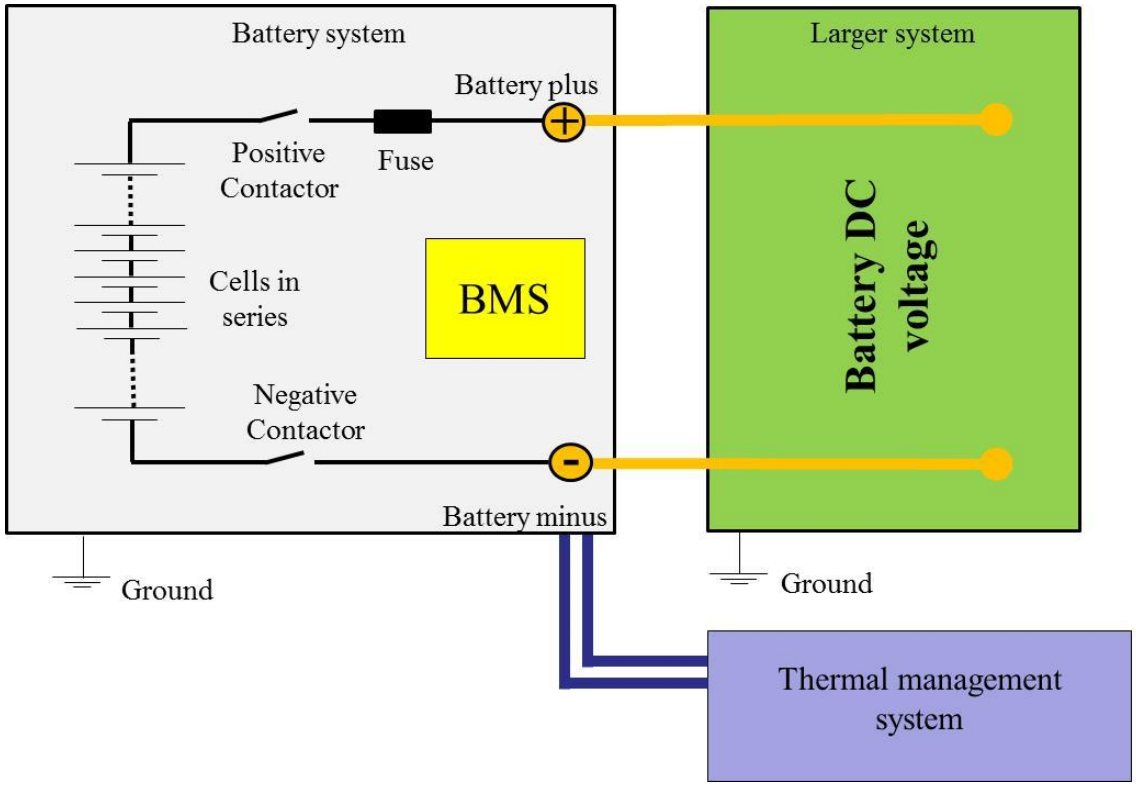


Figure 4. Simplified schematic illustration of a battery system.

During usage the cells will show somewhat different behavior due to small variations in the cell from the manufacturing, from temperature variations within the battery pack and from various electrical connections (resistances) of the cells. Therefore the cells need to be balanced, in order to achieve similar conditions for the cells by adjusting their cell potential. The BMS controls the cell balancing which can be achieved with different passive (resistive burning of the cell(s) with the highest voltage) or active (shifting energy from high to low voltage cells) techniques.

The BMS typically also determines the state of charge (SOC), i.e. the remaining capacity, of the battery pack and also the state of health (SOH), i.e. the ageing (wear) of the battery. The BMS or the battery application establishes the maximum discharge and charge currents (power) given the status of the system, e.g. cell temperature, SOC and SOH. The BMS, especially in larger battery systems, communicates with the application, via e.g. CAN communication protocol. State of safety (SOS) is a novel term which yet not has an established definition and seldom reported [25].

In a situation where the battery cells can be damaged, the BMS can shut down the battery pack via request to the application or simply via opening of the contactors. This can occur in case of isolation faults, overcurrent, overvoltage or undervoltage (for a single cell), too low or too high cell temperatures.

## SAFETY OF LITHIUM-ION BATTERIES

Lithium-ion batteries contain a flammable and volatile electrolyte [26]. The Li-ion cell, even without contact with the outside environment, in itself contains all three parts of the fire triangle in case of overheating; heat, combustible material and released oxygen. In case the temperature of a Li-ion battery cell increases the electrolyte starts to evaporate increasing the internal cell pressure, which can lead to a swollen cell, see an example in Figure 5. If the temperature continues to increase the cell pressure will increase further and to avoid extreme internal cell pressure, cells are designed to vent and thereby release the gases. If the internal cell temperatures increase too much exothermic reactions will increase the temperature even further which can lead to a so called thermal runaway (TR), that is a rapid self-heated cell temperature increase typically accompanied by one or several of the following events; strong venting (smoke and gas release), cell case rupture/explosion, gas explosion and fire. Figure 6 shows a photo of a Li-ion cell at the moment the thermal runaway start, showing the cell squirting out ignited material, less than a second later the cell is engulfed in fire. The released gases can be ignited at once but in case of a delayed ignition there may be a risk of a gas explosion, with more severe consequences, particularly in confined or semi-confined environments. Different Li-ion electrode materials have different thermal runaway characteristics [Paper I-III,27,28,29,30]. The emitted gases consist of the organic electrolyte solvents, such as DMC, DEC, EC, or decomposition products such as CO, $H_2$ and $CH_4$. Besides being flammable the vented gases are also toxic and corrosive. Toxic gases include

various fluoride gases, e.g. hydrogen fluoride (HF) and phosphoryl fluoride ($POF_3$). The released gases consist also of CO (an asphyxiant gas) and $CO_2$ (induces anoxia).

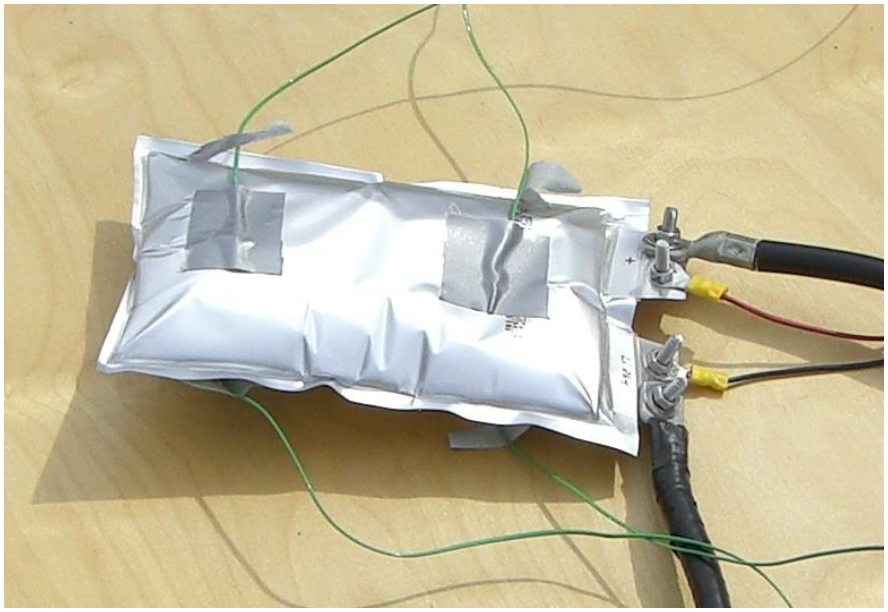

Figure 5. A commercial Li-ion pouch cell which is swollen due to overcharge abuse.

Figure 6. A commercial Li-ion cell of type 18650 undergoing thermal runaway in external heating abuse test.

The cell temperature increase can originate from many sources, Figure 7 shows different types of abuse, potentially leading to TR in a single cell which could propagate to adjacent cells and eventually to the complete battery system. The critical temperature depends on cell

type and ambient conditions, and it is a matter of heat generation vs cooling. The exothermic reactions can start already at about 30 °C [31], but typically higher temperatures are required, starting from about 120 °C with the breakdown of the solid electrolyte interface (SEI) layer [30]. After the SEI breakdown and if the temperature increases further, the next step is exothermic reactions between the electrodes and the electrolyte, typically the anode-electrolyte reaction starts first followed by a larger exothermic cathode-electrolyte reaction. The point of no return for the thermal runaway is typically about 150-200 °C [Paper I-III,27,28,29,30], different for different time scales, cells, battery pack layouts, abuse type and method.

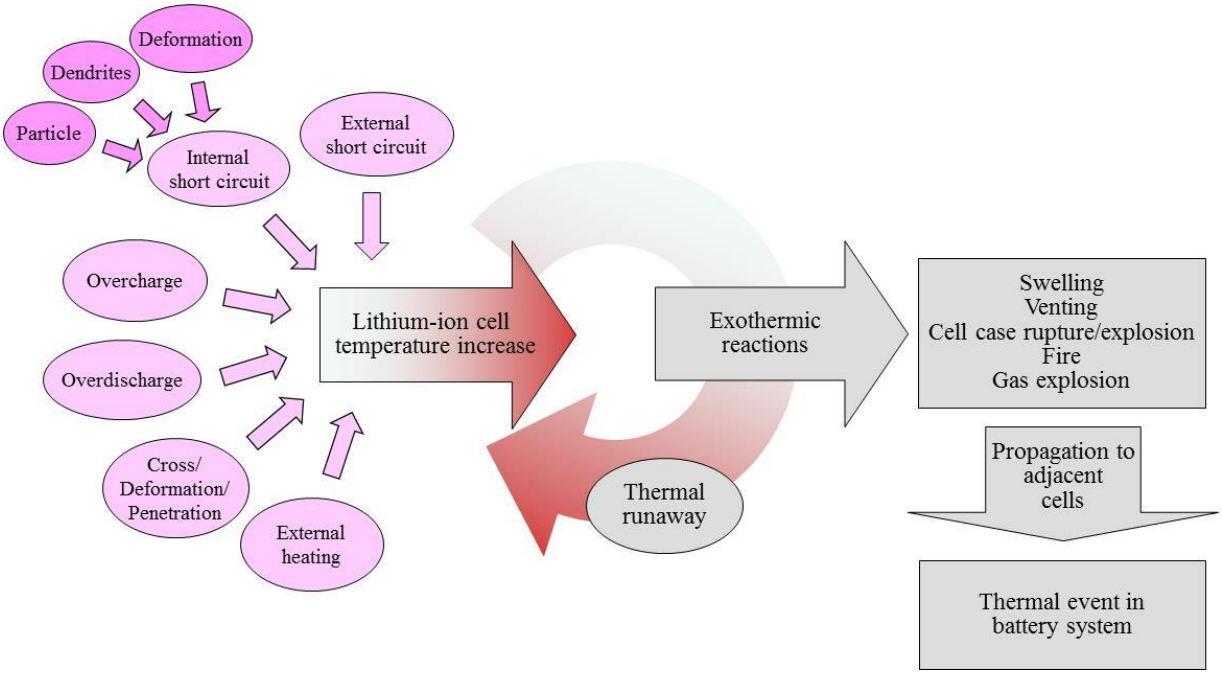


Figure 7. Thermal runaway in a single cell and its potential propagation to complete battery system level.

In abuse testing the battery is exposed to different types of violence in order to study the battery response to the abuse. The level of violence ranges from mild to severe, in different abuse test types and within the same abuse test type. Some of the abuse tests are close to possible events in real-world situations, e.g. external fire, while other failure types that may happen are difficult or impossible to mimic in an abuse test in a controlled laboratory, e.g. spontaneous internal cell short circuits. Batteries are often designed to be safe in some abuse situations, for example having a fuse to offer protection for external short circuit, however,

protection from all types of abuse is impossible. There are several international abuse test standards, such as the commonly referred to FreedomCAR [32], the SAE J2464 [33] and UL1642 [34]. For transportation requirements of batteries, United Nations (UN) have a test standard, UN 38.3 [35] assessing the batteries when they are not in use, i.e. during transportation. Cells/batteries that are to be transported needs to pass this standard otherwise they may not be transported and thus are very difficult to sell and distribute.

Abuse testing is a valuable tool to assess safety, however passing an abuse test does not necessarily mean that the battery is safe. The nail penetration abuse test is a relatively common test, where a metallic nail is forced through a Li-ion cell. Those tests are unfortunately not well understood and typically considered having poor reproducibility [36] and being non-reliable by Li-ion battery safety experts. By varying e.g. the size and shape of the nail and its speed and impact angle, the cell response can vary greatly [37].

There are no intrinsically safe Li-ion cells, which mean that fires and other thermal incidents will occur. The consequences of a single cell failure may be insignificant while the same failure affecting all the cells in a battery pack may be serious. For high safety in battery systems it is therefore essential to handle the consequences from cell failure and minimize cell-to-cell, module-to-module and pack-to-pack propagation. It is a complex task and it can be difficult to completely stop the propagation, however, to delay it might be important as well, achieving valuable time for warning/detection, evacuation of personal, fire fighters to arrive, etc.

From a general physical principle perspective: the higher amount of energy per unit, the higher potential for safety risks, i.e. an increased energy density results in an increased safety challenge. Additionally, the higher the cell voltage the higher the safety challenge, since the voltage stress on the electrolyte increases and there is an increased pressure on undesired side-reactions. The development towards higher cell voltage in Li-ion batteries is therefore challenging.

# EXPERIMENTAL WORK

Experimental work has been carried out in paper I-VIII in order to evaluate the safety of Li-ion and zinc-air batteries. An overview and summary of the experimental methods is presented here. More detailed experimental descriptions can be found in the respective papers.

## TESTED BATTERY CELLS

Fifteen commercial Li-ion battery cells types and two commercial primary Zn-air cell types were tested, see Table 1. The most common battery chemistries for Li-ion batteries were thus investigated as well as different size and packaging of the cells. Li-ion cells for consumer products as well as "automotive" cells were included. Automotive classed cells are typically characterized as high quality cells made from more pure raw materials and with high quality manufacturing process and having long life, capable of higher currents, robustness for e.g. vibrations, humidity and temperature variations occurring on road conditions.

Table 1. List of tested commercial battery cells, sorted by nominal capacity size.

| Commercial battery cells | Nominal capacity (Ah) | Nominal voltage (V) | Anode/cathode material | Cell packaging |
|---|---|---|---|---|
| Secondary cells (rechargeable): Lithium-ion | | | | |
| K2 Energy LFP18650E | 1.4 | 3.2 | carbon/LFP | cylindrical |
| Sanyo UR18650F | 2.2 | 3.7 | carbon/cobalt based | cylindrical |
| Samsung ICR18650–24F | 2.4 | 3.6 | carbon/cobalt based | cylindrical |
| Lenovo laptop battery pack (Sanyo cells) | 2.8 | 3.7 | unknown | cylindrical* |
| K2 Energy LFP26650EV | 3.2 | 3.2 | carbon/LFP | cylindrical |
| Saft MP176065 | 6.8 | 3.75 | graphite/LCO | hard prismatic |
| EiG ePLB-F007A | 7 | 3.2 | carbon/LFP | pouch |
| EiG ePLB-F007H, "older design" | 7 | 3.2 | carbon/LFP | pouch |
| Lifetech X-1P 8Ah 38123 | 8 | 3.3 | carbon/LFP | cylindrical |
| EVE F7568270 | 10 | 3.2 | carbon/LFP | pouch |
| Altairnano LTO | 13 | 2.26 | LTO/NMC | pouch |
| Ener1 SPB150140260 | 20 | 3.2 | graphite/LFP | pouch |
| Leclanche LecCell 30Ah High Energy | 30 | 2.3 | LATP/NCO | pouch |
| Zhejiang GBS Energy GBS-LFMP40Ah | 40 | 3.2 | carbon/LFMP** | soft prismatic |
| European Batteries EBattery 45 Ah v1.4 | 45 | 3.2 | graphite/LFP | pouch |
| Primary cells (non-rechargeable): Zinc-Air | | | | |
| QuantumSphere MetAir® SC Series 4.8, "new design" | 48 | 1.1 | Zn/Air with Mn-C | prismatic |
| QuantumSphere MetAir® SC Series 4.8, "old design" | 48 | 1.1 | Zn/Air with Mn-C | prismatic |

** A complete battery pack included six of the 18650 Sanyo cells, with connectors and electronics as well as outer battery plastic box.*
*** LFMP is lithium iron manganese-phosphate.*

## ABUSE TEST TYPES

Five different abuse test types have been used in the evaluation.

## EXTERNAL HEATING

External heating was used in Papers I, II and III to evaluate the thermal response, in paper III gas emissions were also evaluated. The tests were performed on one cell at a time. The battery cell was heated up in an oven. The cell was placed on one or two bricks in the center of the oven. The oven was of type Binder FED 115, it had 115 liter inner volume and was thermostatically controlled and equipped with a fan for circulation of air in order to have a uniform temperature inside the oven. Two different heating procedures were used, continuous heating or temperature ramping. In the continuous heating procedure, the oven was heated with maximum power, reaching about 200 °C after 1 hour. In the ramping procedure, the oven was first set to 80 °C and thereafter the temperature was increased in steps of 10 °C every 15 minutes. The maximum temperature of the oven was about 300 °C and in some tests the cell was heated to that temperature, however for the majority of the tests the heating was manually stopped after the thermal runaway/exothermic response, which occurred at temperatures below 300 °C.

## EXTERNAL FIRE

External fire was used in papers II, IV, V, VI and VII in order to evaluate the energy release, fire characteristics and gas emissions upon fire. The battery cells were exposed to external fire by a propane burner of about 16 kW, placed beneath the cells. Several cells were put together and burnt in the same test and the numbers of cells put together varied with cell type, in order to achieve similar battery capacity. The tests used the Single Burning Item (SBI) method, EN 13823 [38], which is normally used for fire tests of building materials according to EN 13501 [39]. Fire characteristics were measured, e.g. heat release rate, total heat release, gas emissions, battery temperature and voltage. In the fire calorimetry calculations the oxygen consumption method was used and corrected for $CO_2$ [38]. In the tests a ventilation flow of 400-600 liter/s were used and the fire was considered as well ventilated (oxygen rich).

## EXTERNAL SHORT CIRCUIT

External short circuit tests were performed in papers I and II. A fully charged battery cell was tested, one at the time, via a low-ohmic short circuit. The cell was short circuited via cable shoes with 50 $mm^2$ cables connected to a high-current rated contactor. The current was measured via a current core capable of measuring up to 6000 A.

### OVERCHARGE

Overcharge tests were conducted in papers I and II. A fully charged cell was charged above its limit with different C-rate values of currents and up to a maximum voltage of 15.3 V. The current was measured via a current shunt, different types of shunts were used depending on the charge current.

### OVERCURRENT

Overcurrent tests were conducted in paper VIII for primary Zn-Air battery cells. In the overcurrent test one cell at the time was exposed to a current greater than the maximum allowed current. The maximum allowed current is specified by the cell manufacturer. The overcurrent used was less than the short circuit current.

### DATA LOGGING

Data logging of battery temperature, voltage and current (when applicable) was performed every second (1 Hz measurements) using high-resolution data loggers. During this work the loggers, Pico Technology ADC-24 and Agilent 34972A using an Agilent 34902A reed multiplexer module were utilized in different tests and sometimes combined. In the fire tests, the SBI equipment had its own logging system and the gas measurement also had its own logging computer and specific program.

### CAPACITY, ELECTROCHEMICAL IMPEDANCE SPECTROSCOPY AND AGEING

Cell capacities were measured using a Digatron battery tester or a Metrohm Autolab PGSTAT302N with 20 A booster module. Electrochemical Impedance Spectroscopy (EIS) was performed as a four wire measurement in a Faraday box using the Metrohm Autolab.

Cycle ageing of battery cells was conducted using the Digatron battery tester with a current rate of C/2 and utilizing the full SOC-window. Ageing was also performed by storing fully charged cells for 10 months in a 60 °C oven.

### GAS MEASUREMENT SETUPS

Gas measurements were performed in external fire tests and in some of the external heating tests. The gas emission measurements were focused on detecting fluoride gas emissions, HF, $POF_3$ and $PF_5$. Two different Fourier transform infrared spectroscopy (FTIR) instruments were used, in some experiments gas-washing bottles were also used. Gas-washing bottles continuously collect gas samples which chemically react with a reagent. The contents of the bottles are later analysed to obtain total amounts of fluorine.

In the fire tests quantitative gas measurements were performed using a Thermo Scientific Antaris IGS analyzer (Nicolet) with a gas cell. The spectral resolution was 0.5 $cm^{-1}$ and the gas cell had an optical path length of 2.0 m and an inner volume of 0.2 L. The gas cell and the PTFE hose were both heated to 180 °C to avoid condensation. The FTIR gave a new spectrum about every 12 seconds consisting of 10 scans, enabling relatively fast real-time measurements. The FTIR had been calibrated, the detection limit was 2 ppm for HF and 6 ppm for $POF_3$ but $PF_5$ could be qualitatively detected [40]. Figure 8 shows a schematic illustration of the measurement setup used in the fire tests. The fire tests were performed in three test periods. In the first and second test period the FTIR measurements used both primary and secondary filters. In the third test period the FTIR was used without secondary filter and an additional independent parallel measurement technique was used utilizing gas-washing bottles.

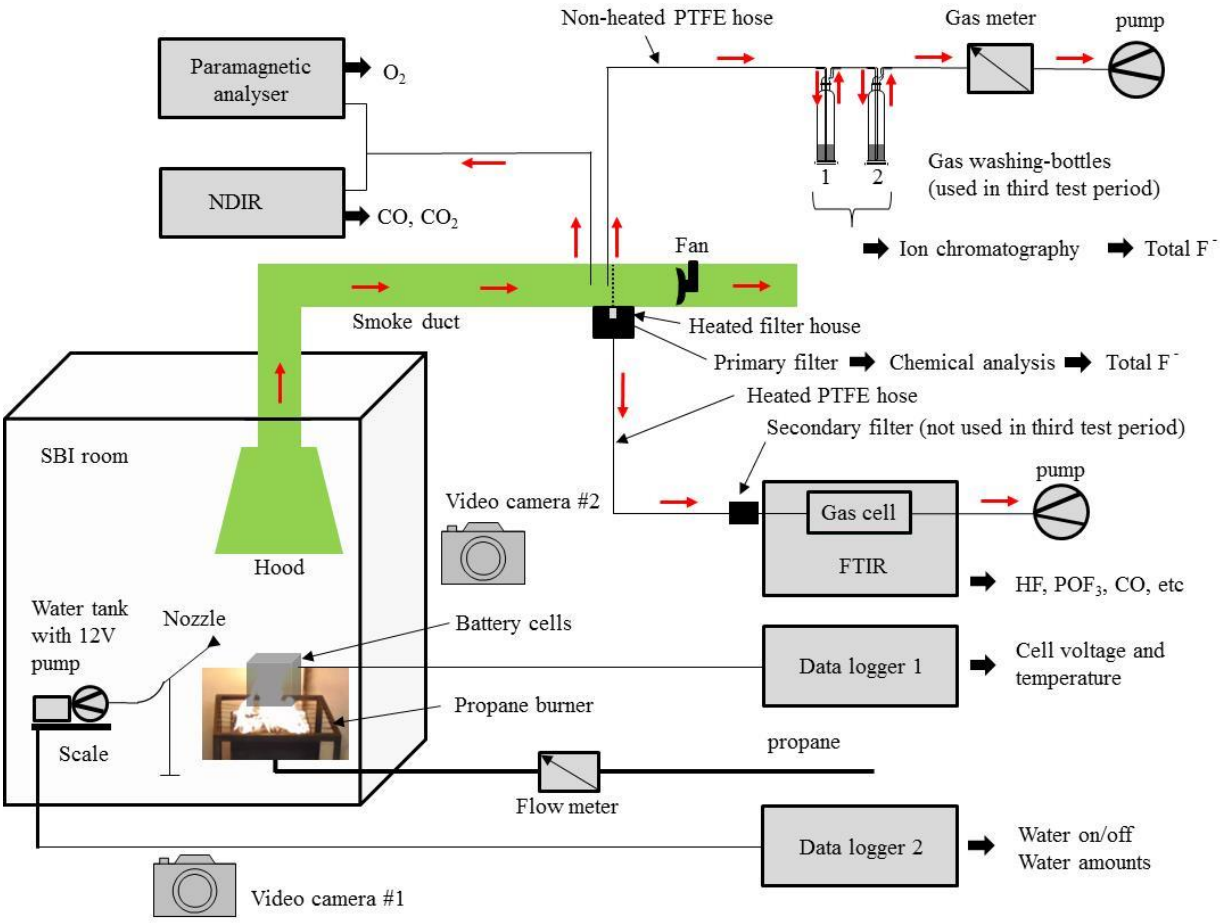


Figure 8. Experimental setup using gas measurements during external fire tests performed during three test periods.

The primary filter for each test was analyzed for fluorine content since it is known that HF may be partly adsorbed by this type of filter [41]. The FTIR setup gave time-resolved quantitative measurements as well as total emissions by integration of the time-resolved measurements. The gas-washing bottles gave only a total value of the emissions.

Gas emission measurements were performed in some of the external heating (oven) tests in paper III. The setup is schematically shown in Figure 9, it used a Bruker Alpha FTIR spectrophotometer with a DTGS detector equipped with a gas cell. The gas cell had an optical path length of 7 cm and an inner volume of 12.4 mL. In order to have rapid measurements, a resolution of 4 $cm^{-1}$ was used with an accuracy of 0.19 $cm^{-1}$, and an average of 8 scans was used which gave a new spectrum about every 12 seconds, offering a reasonable signal to noise ratio. In this setup the gas cell and the hose were not heated, thus condensation could happen in the sampling system.

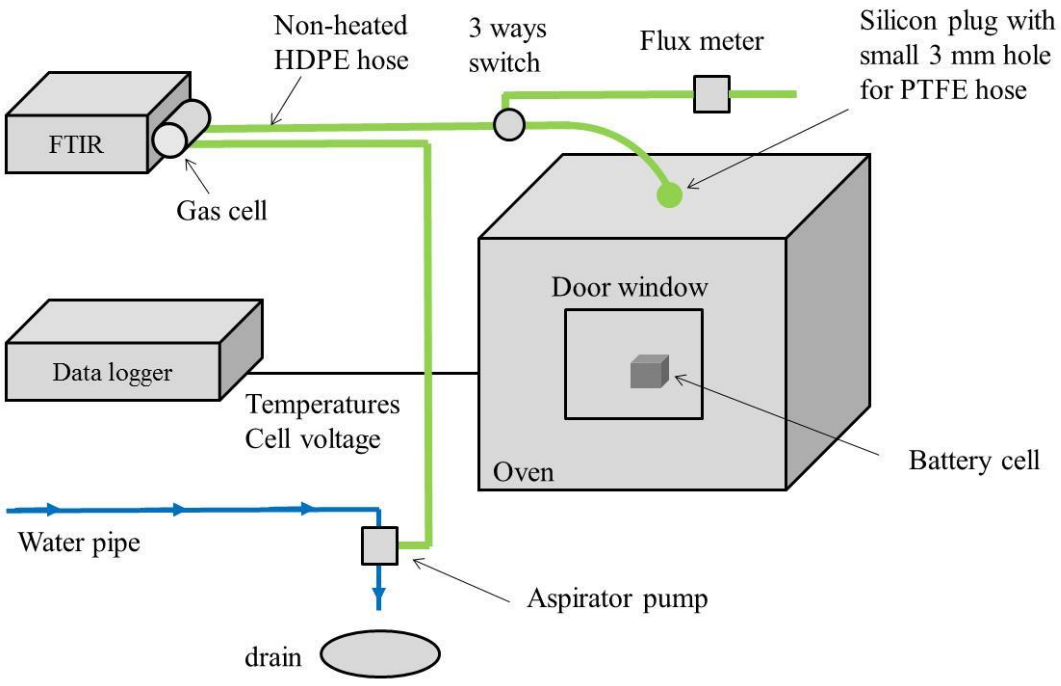


Figure 9. Experimental setup using FTIR gas measurements during external heating tests in oven.

# NUMERICAL SIMULATIONS

Propagation of fire/thermal runaway between Li-ion cells was studied both experimentally and by numerical simulation in paper VII. Experimental fire tests were used as an input to the model and for validation of the model. The main aim of the numerical model was to study cell-to-cell propagation in different scenarios.

The Li-ion battery pouch cell was modelled as a prismatic 3D shape with homogenous but anisotropic material properties, with the Finite-element method (FEM) utilizing the heat transfer module in COMSOL Multiphysics program version 5.1. Total heat generation and time dependent heat release from one cell was calculated based on experimental fire tests using a propane burner. The thermal data of the cell was taken from literature values. In order to validate the model, the propane burner was modelled with the Fire dynamics simulator (FDS) program version 6.1.1. FDS use a Computational fluid dynamics (CFD) model.

The numerical simulation work were implemented and performed by Johan Anderson (RISE Research Institutes of Sweden).

# OVERVIEW OF THE INCLUDED PAPERS

## PAPER I - ABUSE BY EXTERNAL HEATING, OVERCHARGE AND SHORT CIRCUITING OF COMMERCIAL LITHIUM-ION BATTERY CELLS

### SUMMARY

The aim of Paper I is to study the cell response of commercial cells exposed to three types of abuse tests.

Abuse tests:

- Overcharge
- Short circuit
- External heating by oven

Cells:

- Samsung ICR18650–24F, carbon/cobalt based, 2.4 Ah, cylindrical
- EiG ePLB-F007A, “newer design”, carbon/LFP, 7Ah, pouch
- EiG ePLB-F007H, ”older design”, carbon/LFP, 7Ah, pouch
- European Batteries EBattery 45 Ah v1.4, graphite/LFP, 45 Ah, pouch

### MAIN FINDINGS

- During external heating, the Samsung 18650 cell went into an energetic thermal runaway at a temperature of about 220 °C, squirting out ignited cell materials, generating a pressure wave and immediate fire with a temperature increase rate of about 5000 °C/min, see Figure 10.
- The LFP cells were less energetic during external heating than the Samsung 18650 cells, however the three different LFP cells show relatively large diversity. The newer design of the EiG LFP 7 Ah cell showed a very small temperature increase, close to showing no sign of thermal runaway, in contrast to the older design which showed a clear thermal runaway temperature peak, see Figure 11. These results underline that LFP is just one component of a LFP-cell in terms of safety.
- One LFP cell went into fire during 2C overcharge, while three repeated tests did not result in fire, see Figure 12.
- The short circuit currents were very large for the single cells, about 1000 A, see Figure 13.

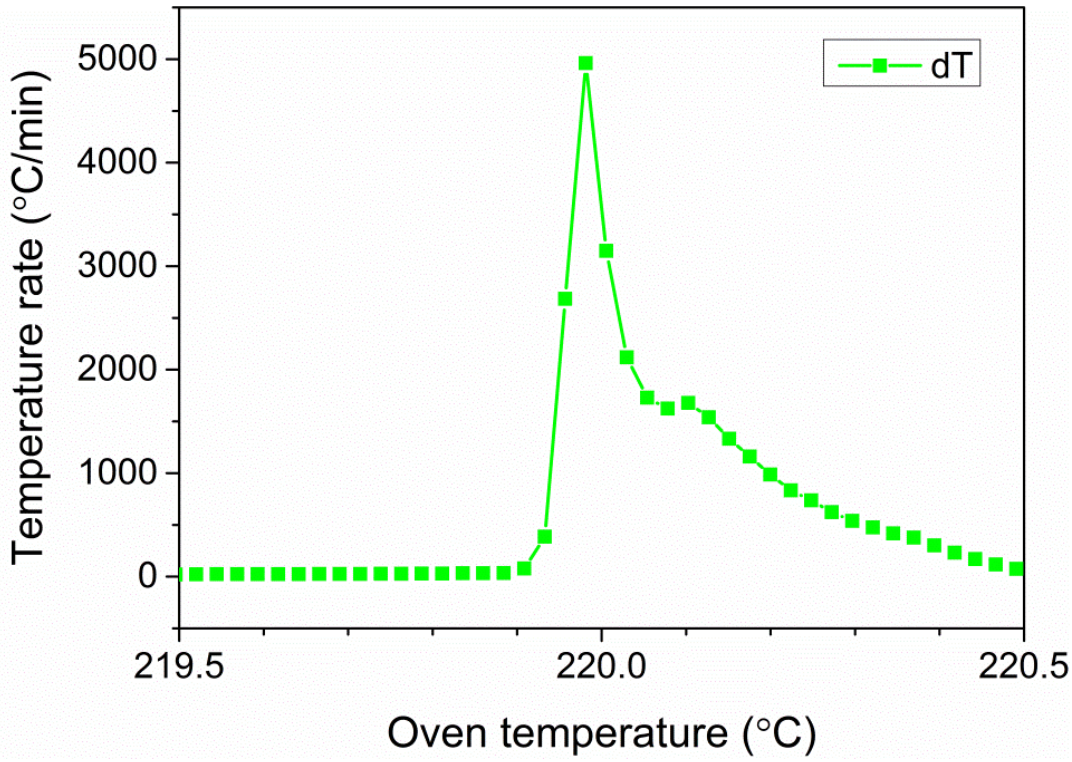


Figure 10. Temperature rate of the average surface temperature of the Samsung 18650 cell, clearly showing the rapid temperature increase at thermal runaway, occurring at an oven temperature of 219.9 °C

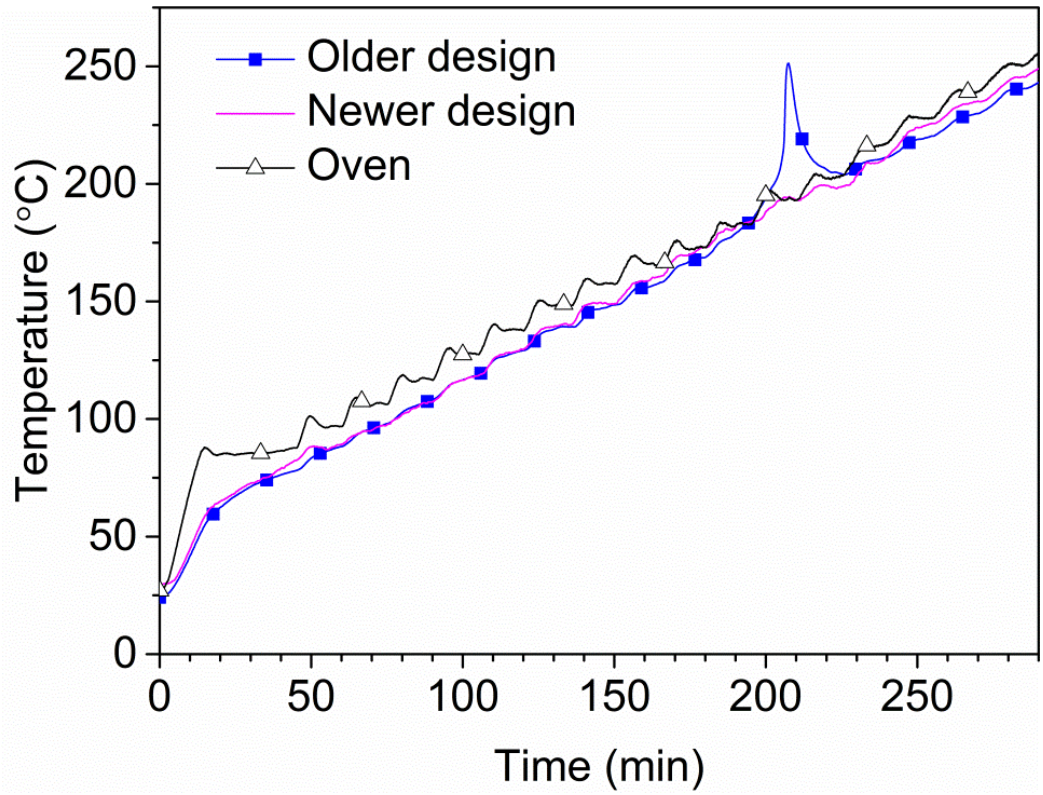


Figure 11. Temperature results from external heating of EiG LFP 7Ah cells with older and newer design.

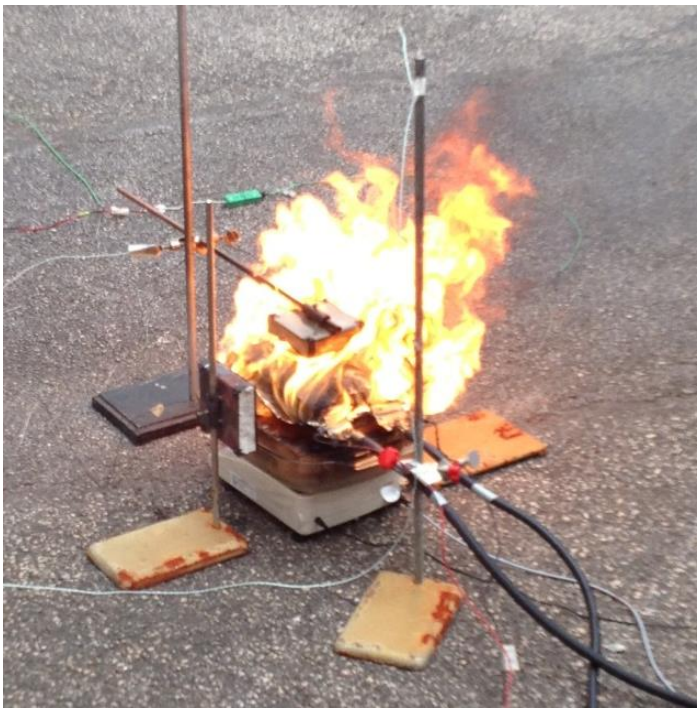

Figure 12. Cell ignited during 2C (90A) overcharge of a 45 Ah LFP pouch cell from European batteries.

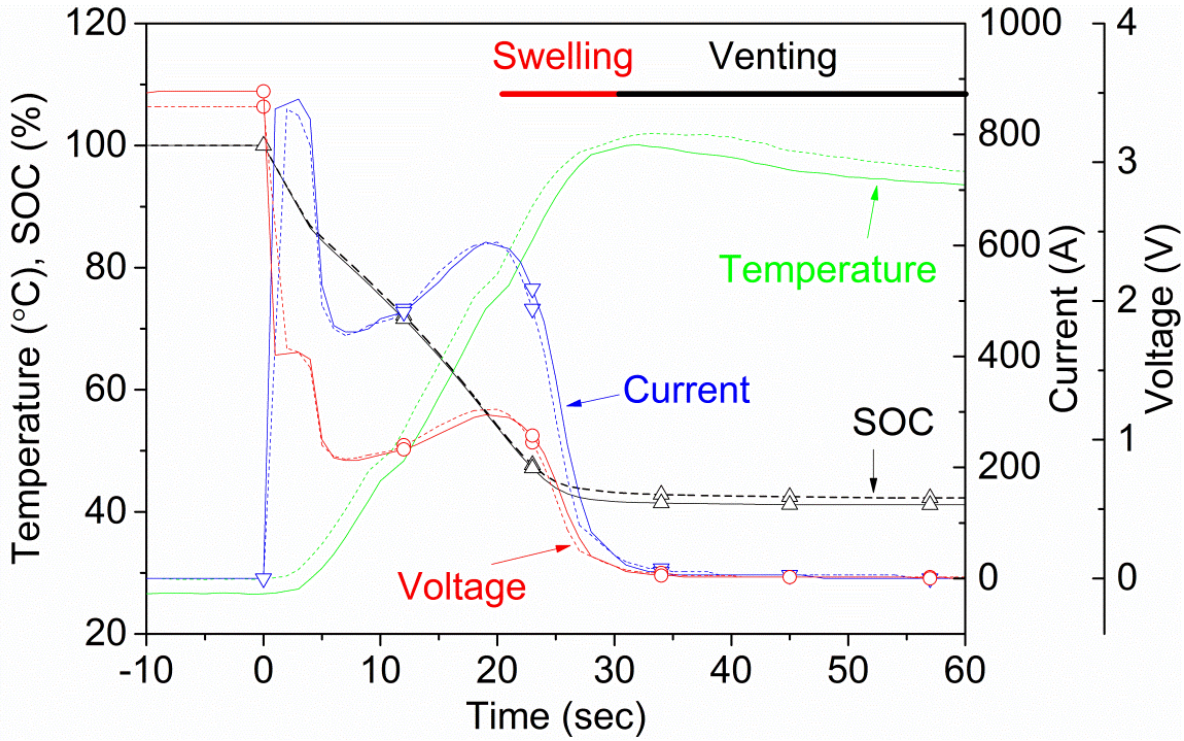


Figure 13. Results from short circuit abuse tests of EiG older design (solid lines) and EiG newer design (dashed lines).

## PAPER II - LITHIUM-ION BATTERY ASPECTS ON FIRES IN ELECTRIFIED VEHICLES ON THE BASIS OF EXPERIMENTAL ABUSE TESTS

### SUMMARY

The aim of Paper II is to discuss and study aspects of Li-ion safety from an electrified vehicle perspective. Some principles on how to make a battery system safe and a review of incidents and statistics of EV fires are discussed. Experimental results from abuse tests of commercial Li-ion cells, part of them automotive-classed Li-ion cells, are presented.

Abuse tests:

- Overcharge
- Short circuit
- External heating by oven
- External fire

Cells:

- Samsung ICR18650–24F, carbon/cobalt based, 2.4 Ah, cylindrical
- EiG ePLB-F007A, carbon/LFP, 7Ah, pouch
- Lifetech X-1P 8Ah 38123, carbon/LFP, 8 Ah, cylindrical
- European Batteries EBattery 45 Ah v1.4, graphite/LFP, 45 Ah, pouch
- EVE F7568270, carbon/LFP, 10 Ah, pouch
- Zhejiang GBS Energy GBS-LFMP40Ah, carbon/LFMP, 40 Ah, soft prismatic

### MAIN FINDINGS

- The fire tests showed that the higher the SOC-value the higher HRR peaks and more rapid heat release, see Figure 14.
- Safety protection can fail, e.g. a cell safety vent malfunction occurred in one of the tested cylindrical cell. There is thus a risk of hazardous projectiles in the event of a cell case explosion, see Figure 15.
- Large short circuit currents, >1000 A, was measured for a single 45 Ah cell as illustrated in Figure 16. As a consequence, the positive terminal tab burnt off with flames.
- High amounts of toxic HF emissions can be released during a battery fire and the toxic gases can pose a severe risk
- High safety is achieved by many safety layer-by-layers, see the "safety onion" in Figure 17.
- Studies of the occurrence of vehicle fires involving electric vehicles compared to non-electric vehicles showed:
    - Very limited statistics available for EVs.
    - Tesla Model S: one vehicle fire in about 20000 vehicles, based on more than 100,000 vehicles manufactured and 6 fires during October 2013 and February 2016 (estimation based on internet search, February 2016). Comparable numbers for vehicle fires in USA is of the order of about 1 fire in 1000 vehicles per year.

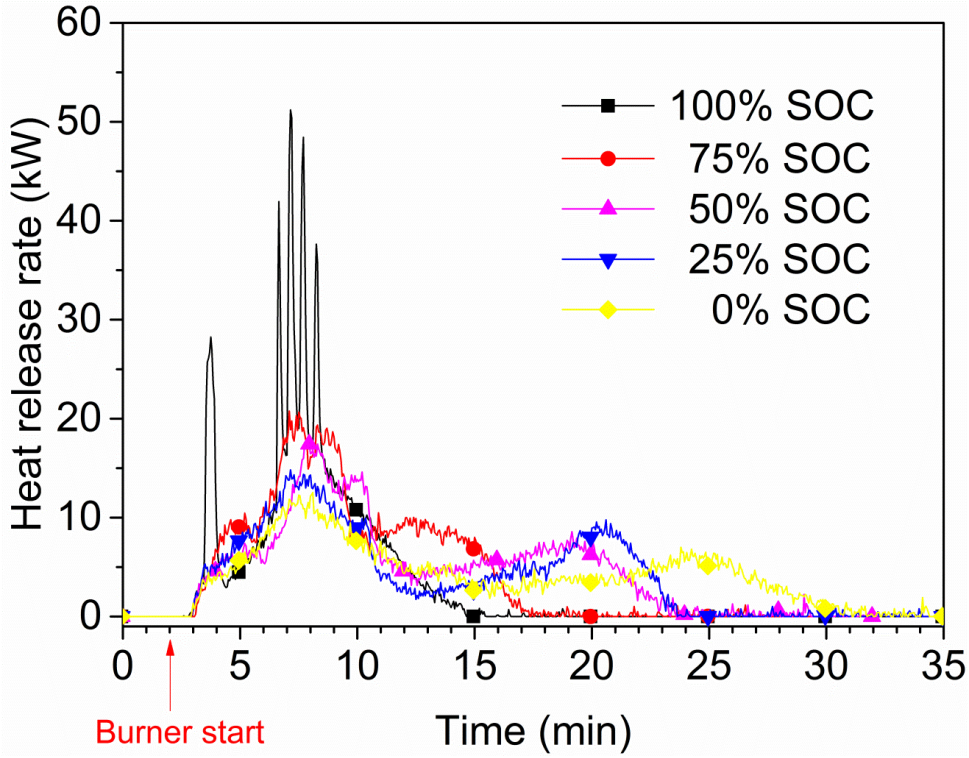


Figure 14. Heat release rate vs time in external fire test, for SOC 0-100% with inter-SOC steps of 25%, for EiG 7 Ah LFP pouch cell, exposed to an external propane burner (burner contribution subtracted).

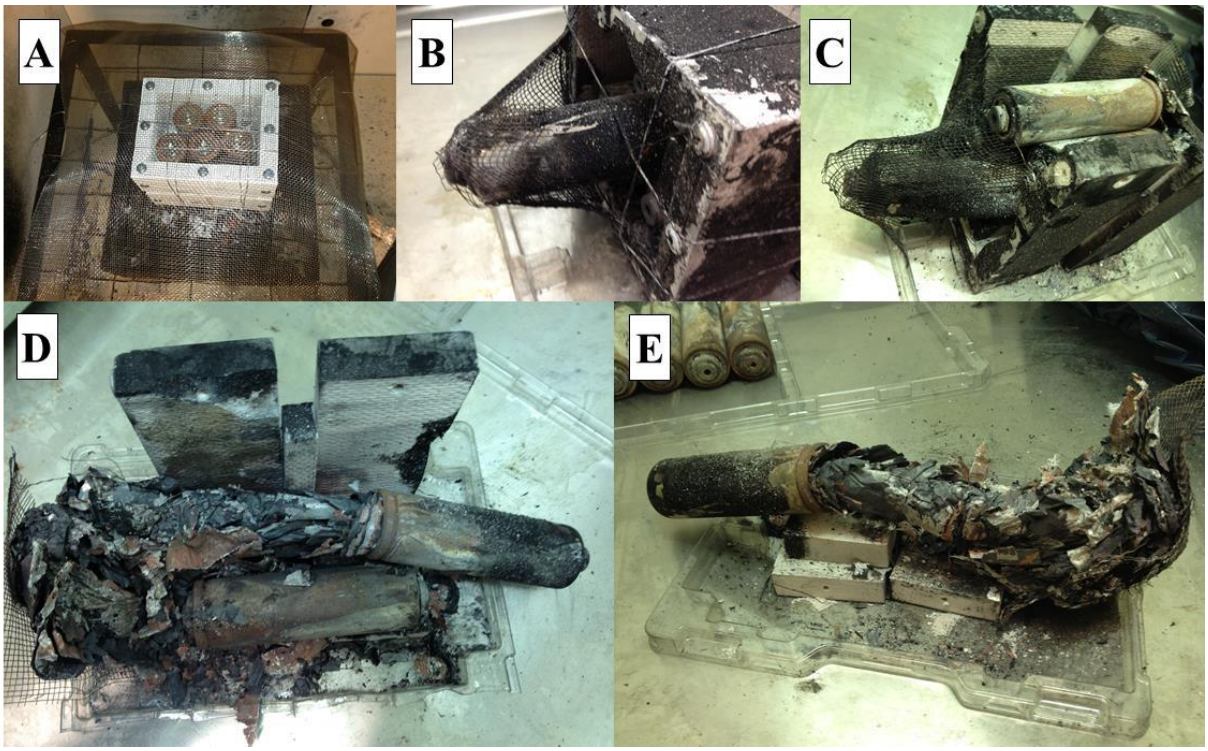


Figure 15. Photos (**A**) before fire test, (**B**) after the fire test showing one cell propelled and was caught in the protected net box. (**C**)-(**E**) show photos during tear down.

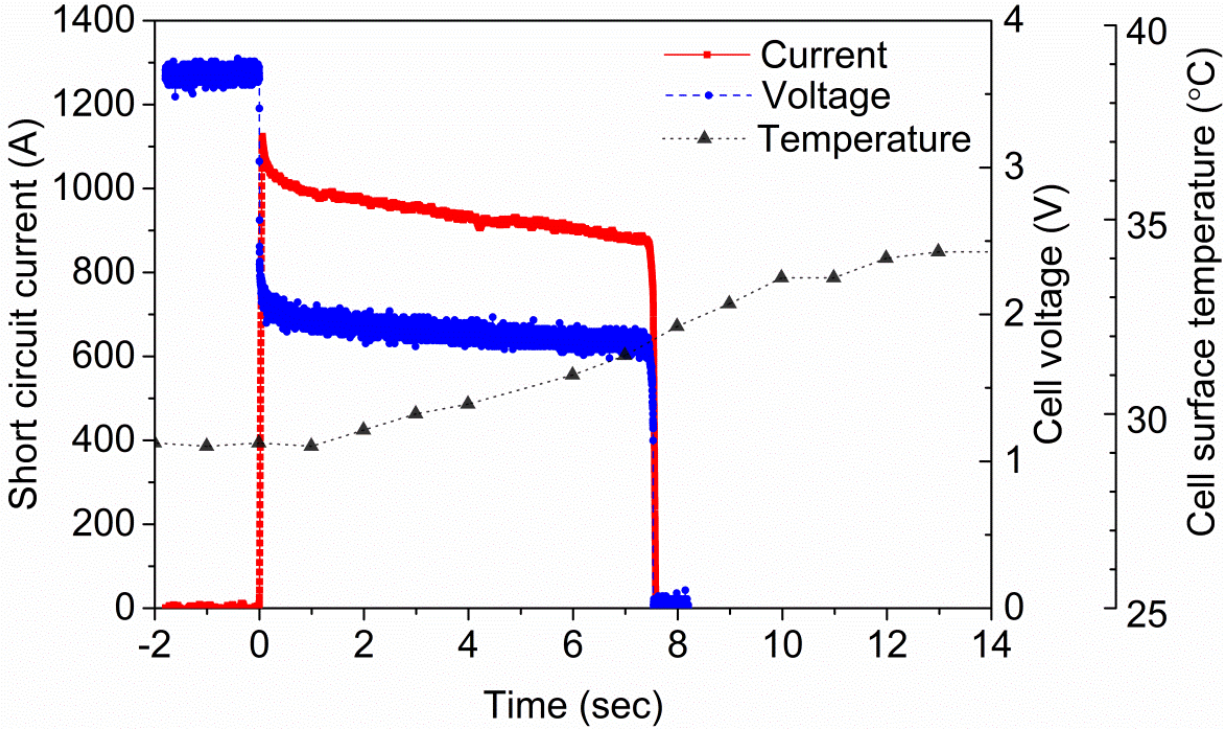


Figure 16. Results from short circuit abuse test of a European battery LFP pouch cell with 45 Ah.

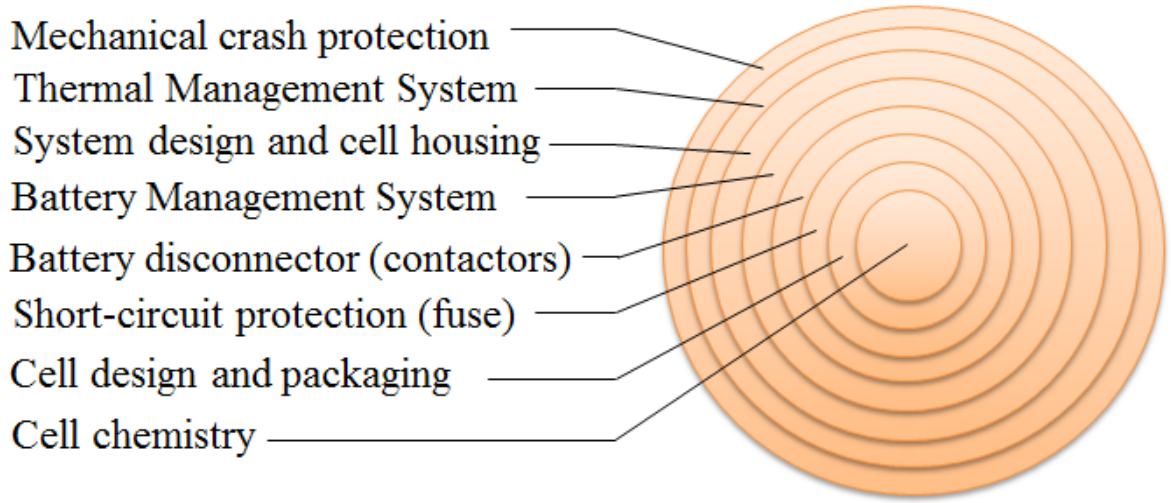


Figure 17. The safety onion, illustration of how to build-up of high safety using layer-by-layer.

## PAPER III - GAS EXPLOSIONS AND THERMAL RUNAWAYS DURING EXTERNAL HEATING ABUSE OF COMMERCIAL LITHIUM-ION GRAPHITE-$LiCoO_2$ CELLS WITH DIFFERENT LEVELS OF AGEING

### SUMMARY

The aim of Paper III is to investigate cell response upon external heating for various ageing/status. Selected cells were cycled aged for 100, 200 and 300 cycles, and some other cells were stored for 10 months at 60 °C. The study included both working cells (functional cells) as well as dead cells. Limited gas measurements by FTIR were conducted in some of the tests to measure HF and $POF_3$ gas emissions as well as emissions from electrolyte solvents.

Abuse tests:

- External heating by oven

Cells:

- Saft MP176065, graphite/LCO, 6.8 Ah, hard prismatic

### MAIN FINDINGS

- Gas explosions occurred in 5 of 11 tests, for cells aged at all cycle ageing levels; 0, 100, 200 and 300 charge/discharge cycles. The gas explosion occurred about 15 seconds after the thermal runaway temperature was reached due to delayed ignition of battery vented gases mixed with the air inside the oven. The oven door was forced open by the explosion and the video camera outside was typically blown away. The oven was not airtight and after first gas explosion actions were taken to protect the oven via pressure release actions (gas explosion mitigations), however still four more gas explosions occurred.
- Thermal runaway occurred in all cells.
- Cycling ageing was found to have an influence on the thermal runaway temperature, see Figure 18, with a weak minimum between 100 and 200 cycles (within the tested range 0-300 cycles), see Figure 19.
- Dead cells were significantly less reactive, however they still went into thermal runaway, releasing heavy smoke and reaching high temperatures.
- Three different vents could be specified, see Figure 20 and Figure 21, the 3$^{rd}$ vent occurred when the thermal runaway was initiated while the 1$^{st}$ and 2$^{nd}$ vents occurred well before thermal runaway.
- HF and $POF_3$ emissions were detected simultaneously and were first observed in the 3$^{rd}$ vent.
- The temperature varied significantly over the cell surface by, about 100 °C, see Figure 22, while in other tests a temperature peak variation of up to 300 °C was found. The 2$^{nd}$ vent is clearly shown in the temperature rate plot, see Figure 22, due to outflowing gases. Neither the 1$^{st}$ nor the 2$^{nd}$ vents are visually seen on the video.

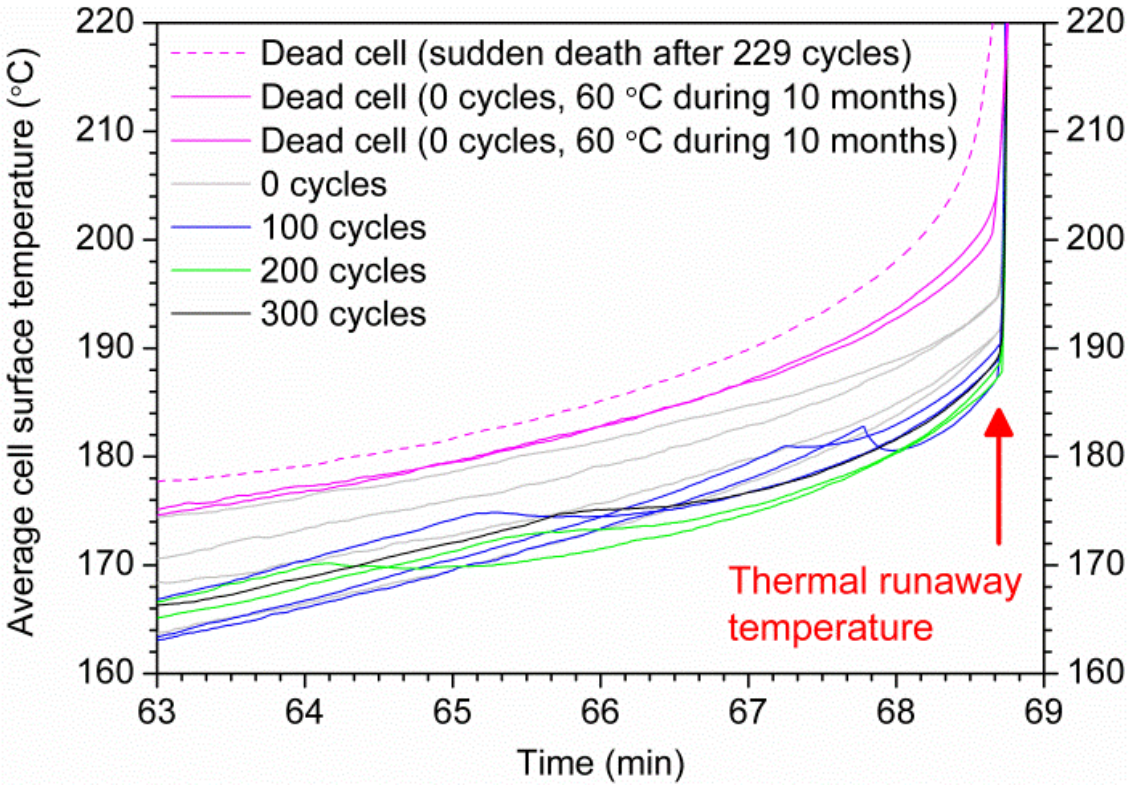


Figure 18. Temperature development before and at thermal runaway for cells with different ageing/status.

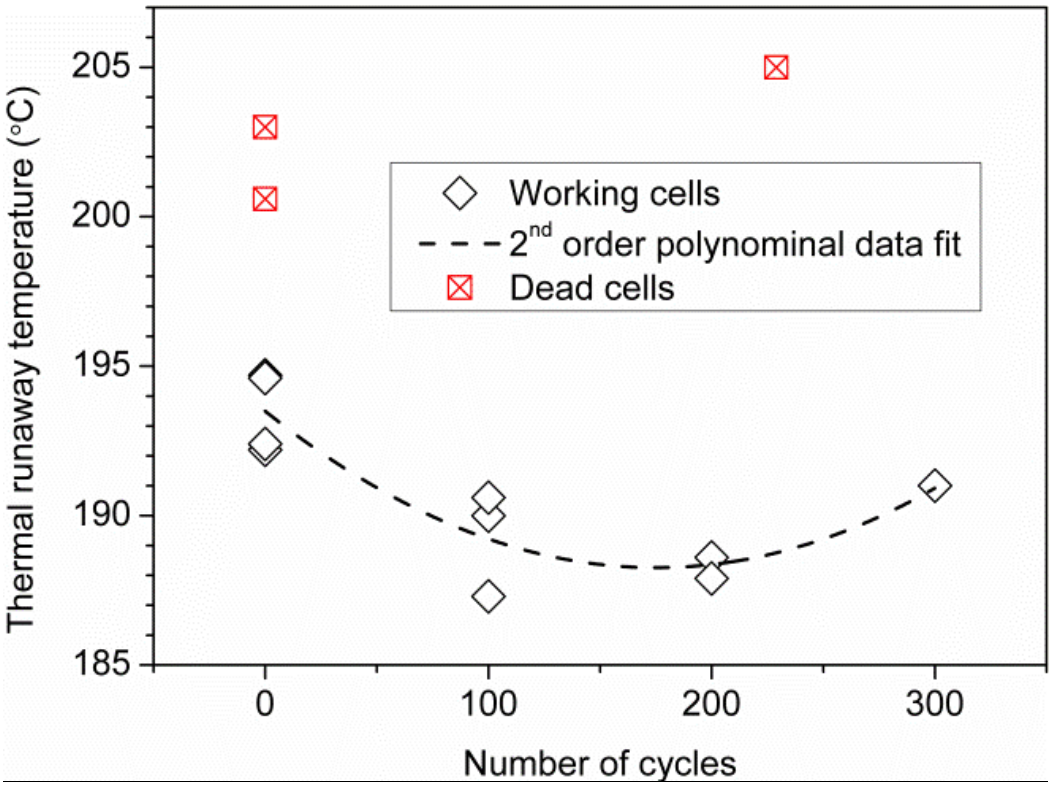


Figure 19. Thermal runaway temperature for cells with different cycle ageing.

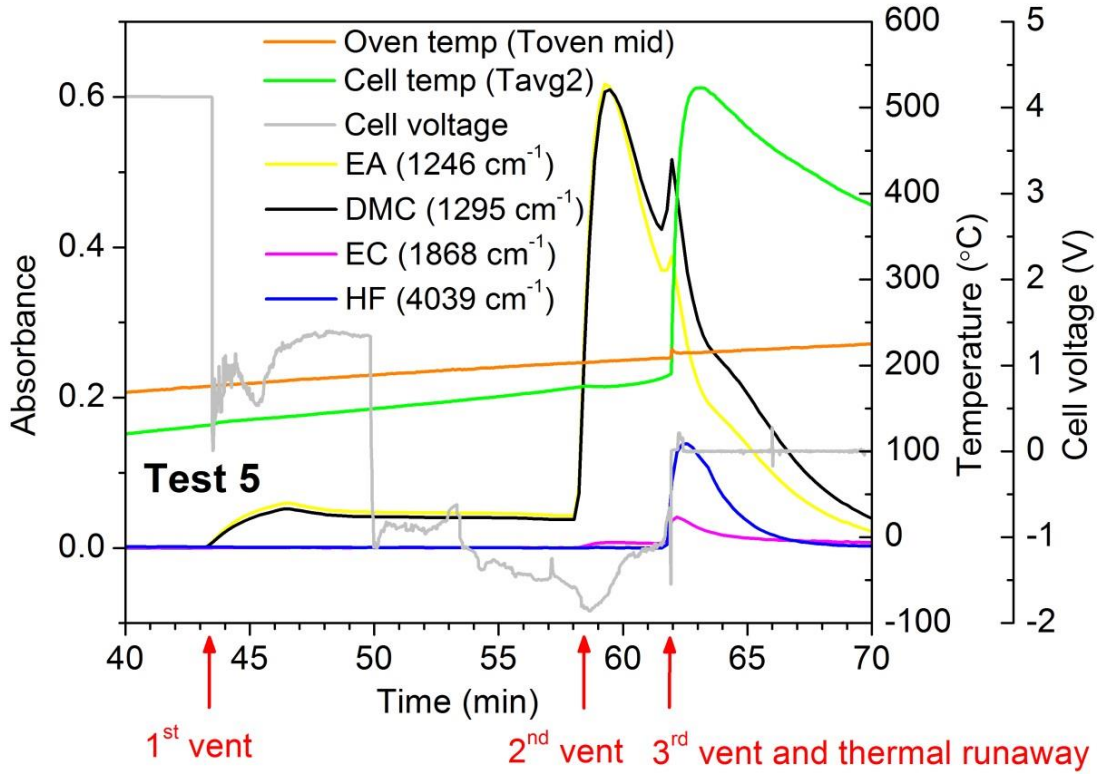


Figure 20. Results from external heating abuse of a cell aged with 100 cycles. The cell ejected small and short jets and fire flames, but neither gas explosion nor major fire occurred.

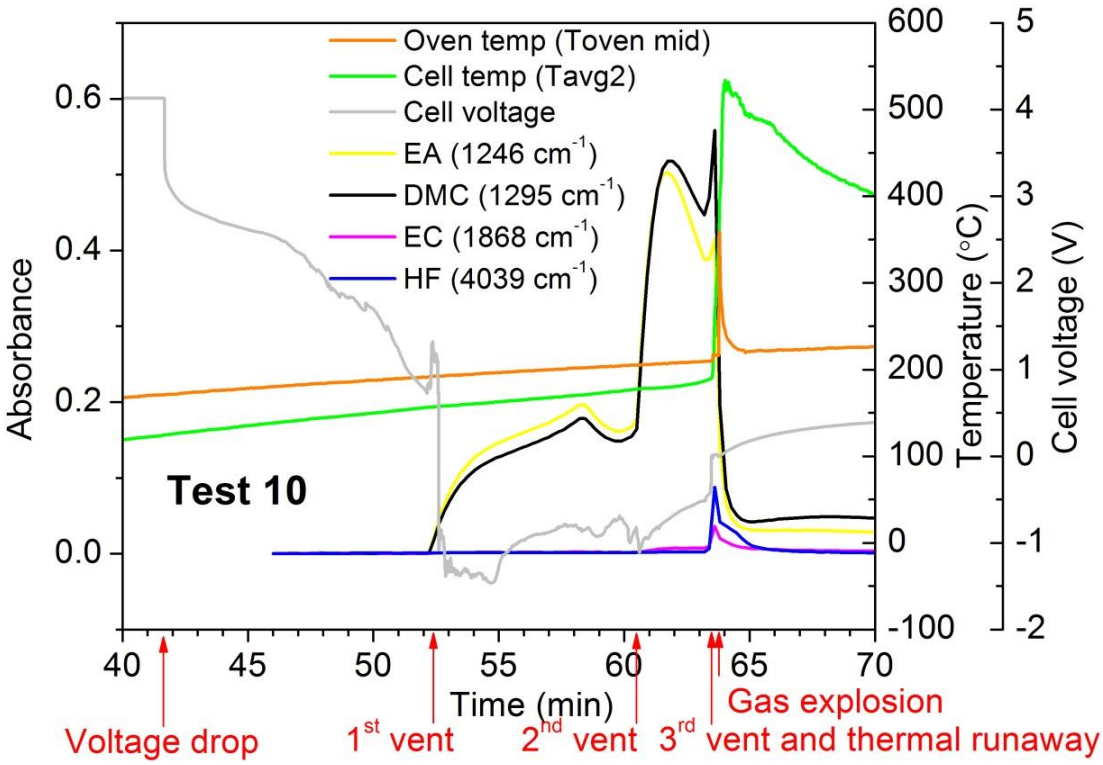


Figure 21. Results from external heating abuse of a cell aged with 300 cycles. A gas explosion occurred shortly after the third vent.

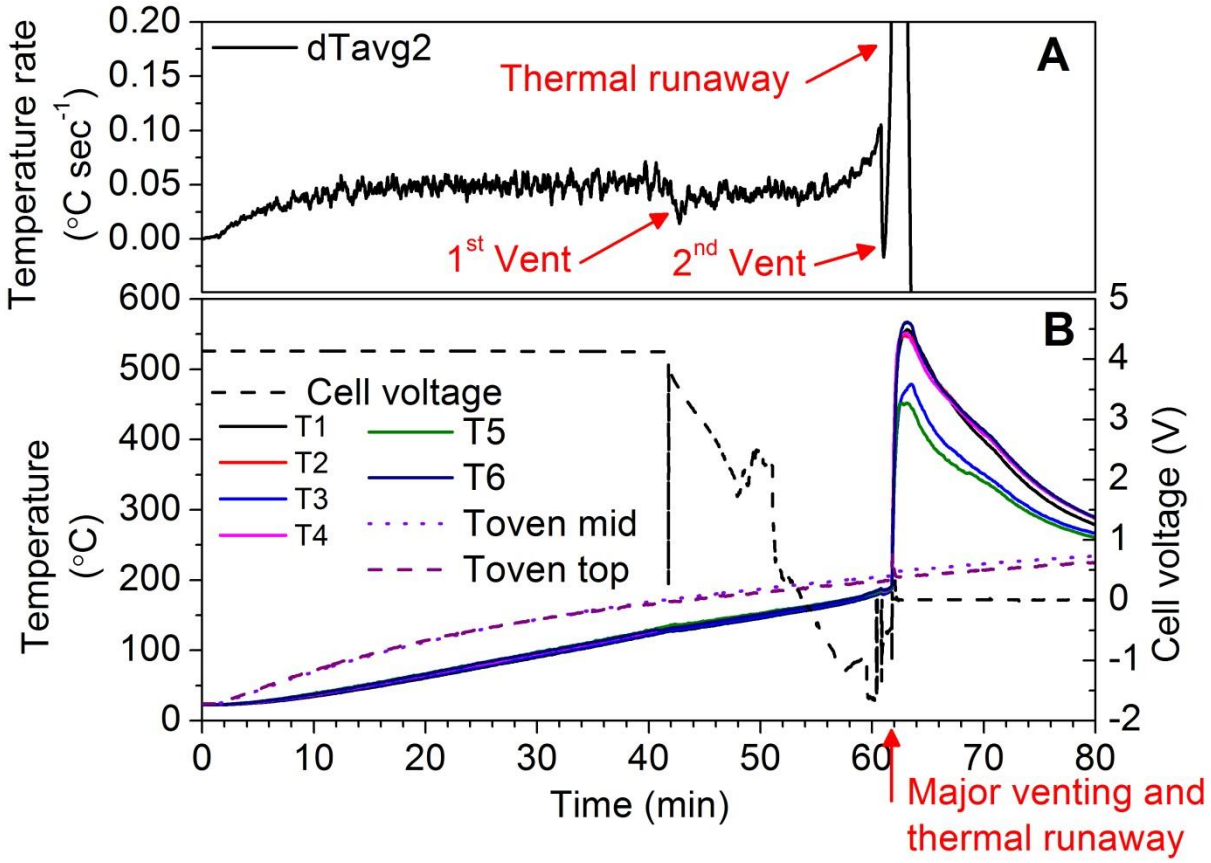


Figure 22. Results from external heating abuse of a cell, (**A**) showing average cell surface temperature rate, and (**B**) cell voltage, six cell surface temperatures (T1-T6) and two oven temperatures.

## PAPER IV - CHARACTERISTICS OF LITHIUM-ION BATTERIES DURING FIRE TESTS

### SUMMARY

The aim of Paper IV is to study the characteristics of commercial Li-ion battery cells exposed to an external fire. Measurements of toxic gas emissions, heat release rate, temperature and cell voltage were performed. The influence of water mist was also studied in one of the fire tests.

Abuse tests:

- External fire

Cells:

- EiG ePLB-F007A, carbon/LFP, 7Ah, pouch
- K2 Energy LFP26650EV, carbon/LFP, 3.2 Ah, cylindrical
- Lenovo laptop battery pack (Sanyo 18650 cells), unknown type, 2.8 Ah, cylindrical

## Main findings

- HRR shows a distinct dependence with SOC.
- The total heat release (THR), i.e. the integrated HRR values, showed low SOC dependence.
- HF emission rates varied with SOC, the highest HF peaks and total values were obtained for 50% SOC, see Figure 23.
- HF emission peak rate was more or less doubled when water mist was applied, see Figure 23 to Figure 26. However, total released HF amounts with and without water mist was similar.
- $POF_3$ was not detected.

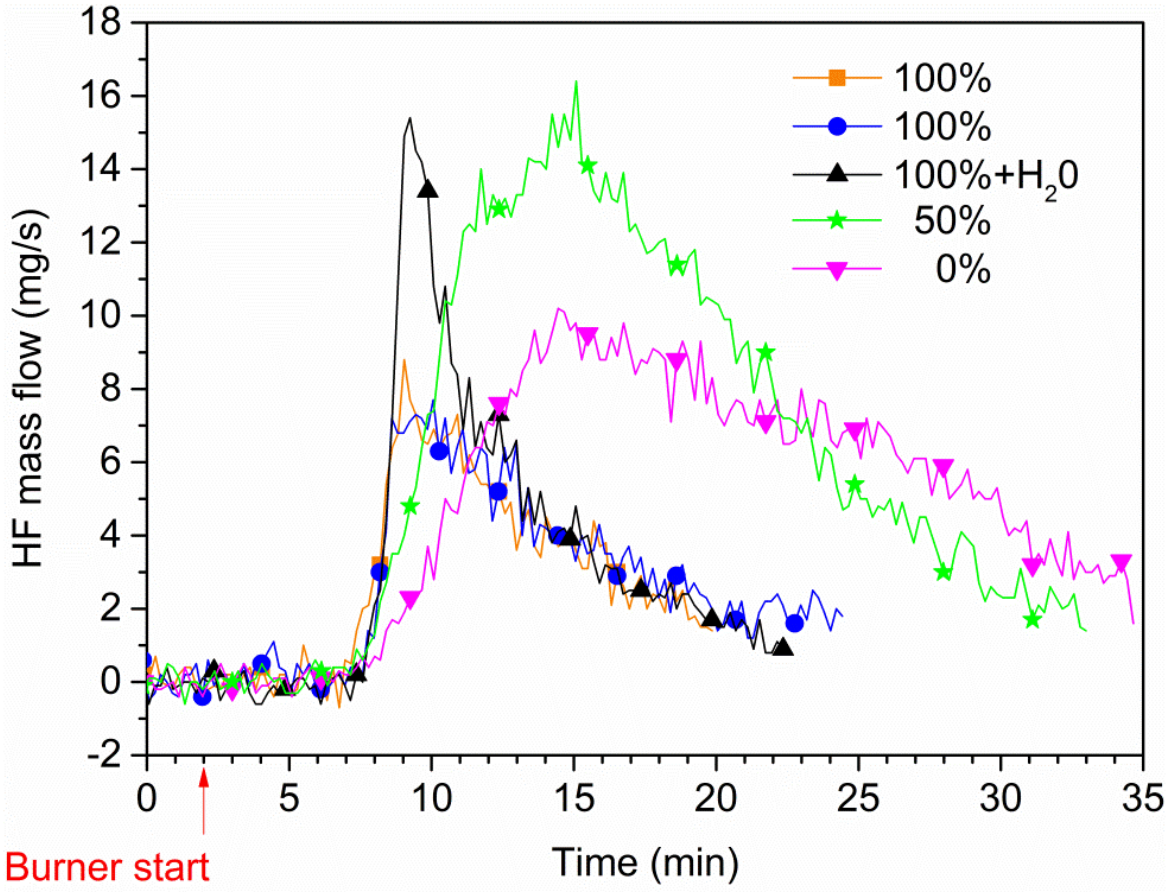


Figure 23. Quantitative time-resolved FTIR measurement of HF mass flow vs time for 0-100% SOC of EiG 7 Ah LFP, exposed to external propane fire.

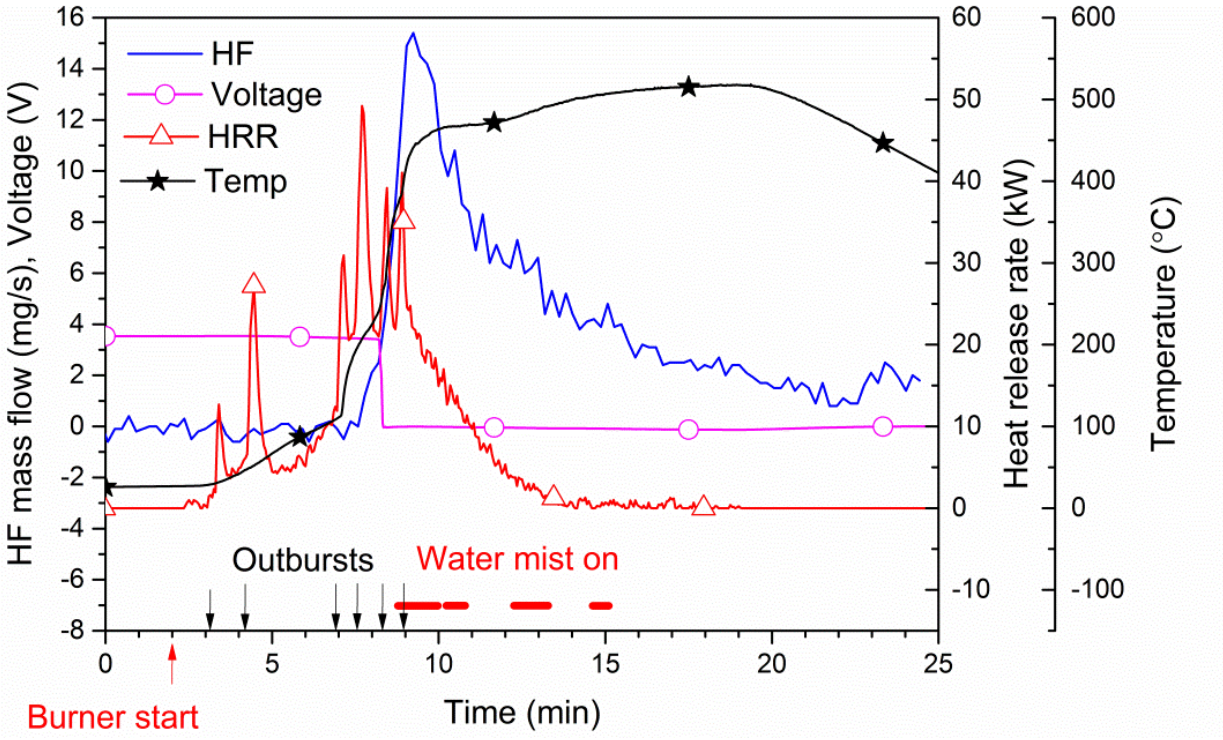


Figure 24. External propane fire test of EiG 100% SOC cells showing the effect of water mist.

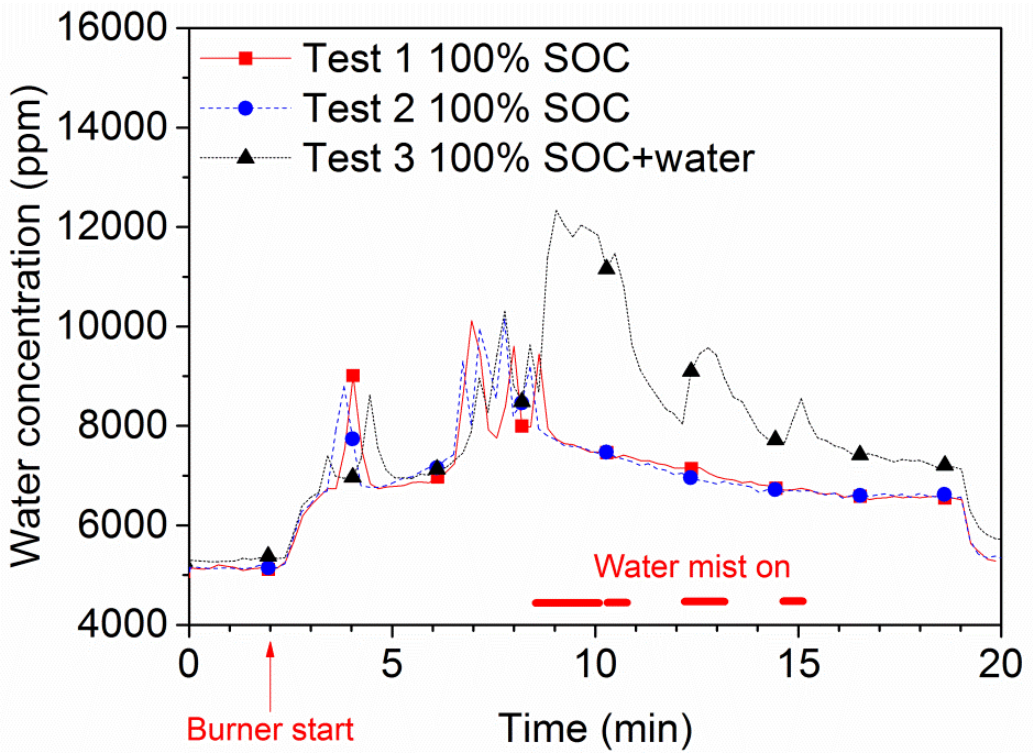


Figure 25. Water concentrations measured for EiG 100% SOC, test 1-3. The increased water level in test 3 due to water mist application is clearly seen.

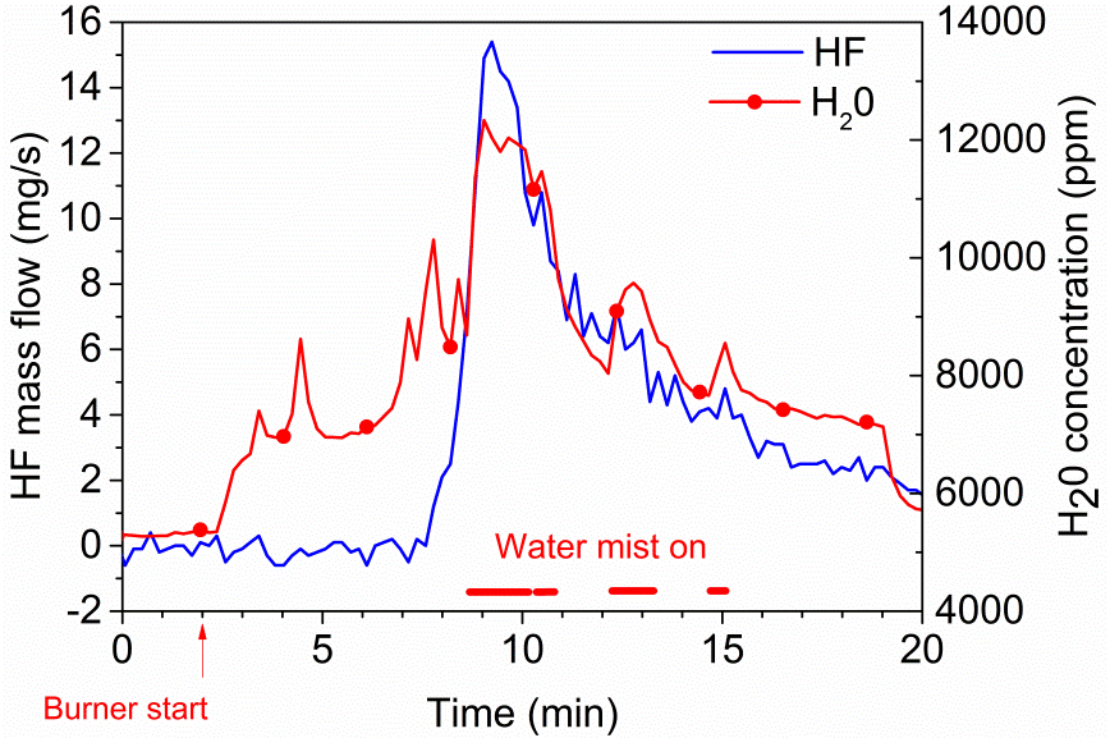


Figure 26. Correlation between water concentration and HF production rate, for water mist test.

## PAPER V - TOXIC FLUORIDE GAS EMISSIONS FROM LITHIUM-ION BATTERY FIRES

### SUMMARY

The aim of Paper V is to study the release of toxic gas emissions, primarily HF and $POF_3$, as well as fire characteristics, e.g. heat release rate and total heat release. Two independent measurement techniques were used to measure gas emissions, FTIR and gas-washing bottles.

Abuse tests:

- External fire

Cells:

- EiG ePLB-F007A, carbon/LFP, 7Ah, pouch
- K2 Energy LFP26650EV, carbon/LFP, 3.2 Ah, cylindrical
- Lenovo laptop battery pack (Sanyo 18650 cells), unknown type, 2.8 Ah, cylindrical
- Saft MP176065, graphite/LCO, 6.8 Ah, hard prismatic
- Lifetech X-1P 8Ah 38123, carbon/LFP, 8 Ah, pouch
- Ener1 SPB150140260, graphite/LFP, 20 Ah, pouch
- Leclanche LecCell 30Ah High Energy, LATP/NCO, 30 Ah, pouch

### MAIN FINDINGS

- HF emission rates varied significantly for the different battery types and with different SOC values, 20-200 mg/Wh, see Figure 27, possibly indications of a general weak local maxima at 50 % SOC.
- The total heat release, the integrated HRR values, showed low dependence with SOC
- HRR showed a high SOC dependence.

- The energy ratio, i.e. the ratio between the energy released from the burning battery (THR) and the nominal electrical energy content varies significantly for the seven Li-ion battery cell types, ranging from 5 to 21, however, with low SOC dependence, see Figure 28.
- $POF_3$ was detected, but only for one of the seven battery types and only for the 0% SOC case, see Figure 29 and Figure 30.
- HF emission rates increased momentary with about 35% when water mist was applied, however, the total values of released HF with and without water mist were about the same. Thus, similar result as in paper IV.

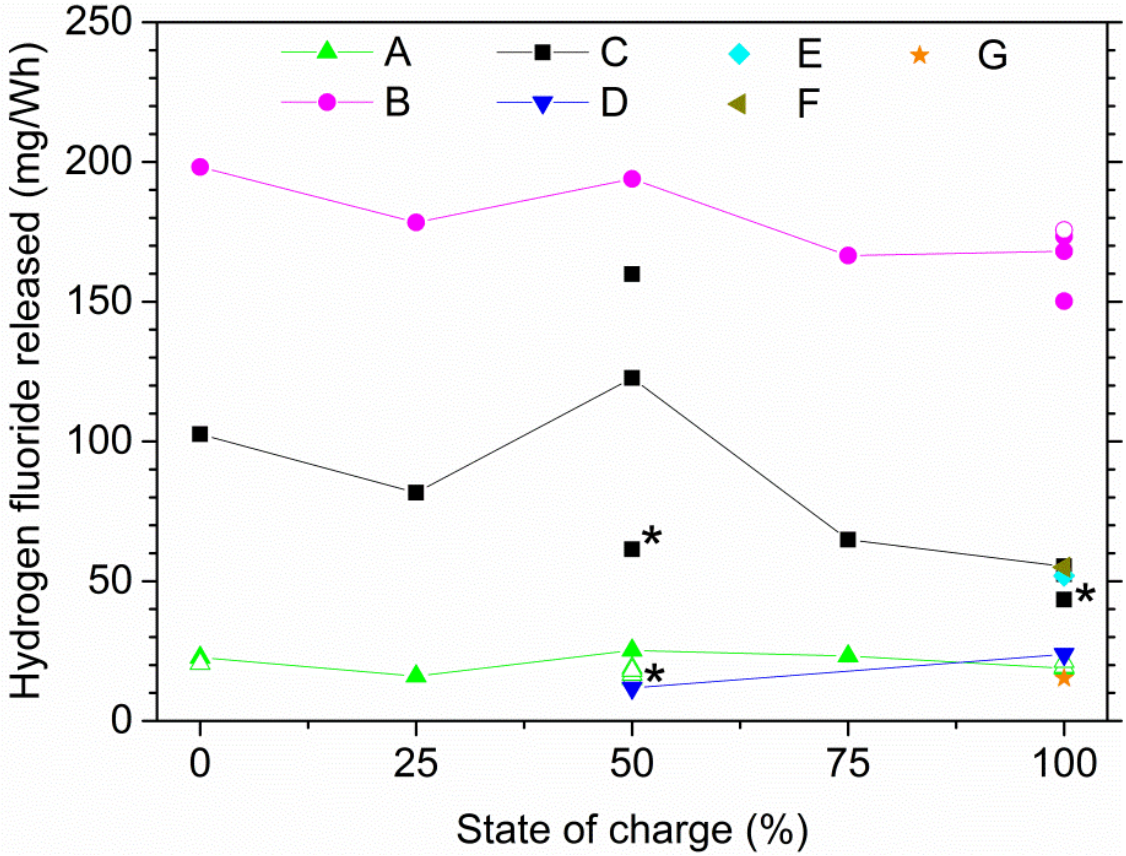


Figure 27. The total amount of HF measured by FTIR for seven types of Li-ion battery cells and for 0-100% SOC. Open symbols indicate that the test included a variant, e.g. water mist. The lines are intended as a guide for the eye.
** Low value due to that a pre HF-saturation was not applied, therefore a part of the HF release was likely to be saturated in the gas sampling system, for type C at 50% and 100% SOC and type D at 50% SOC.*

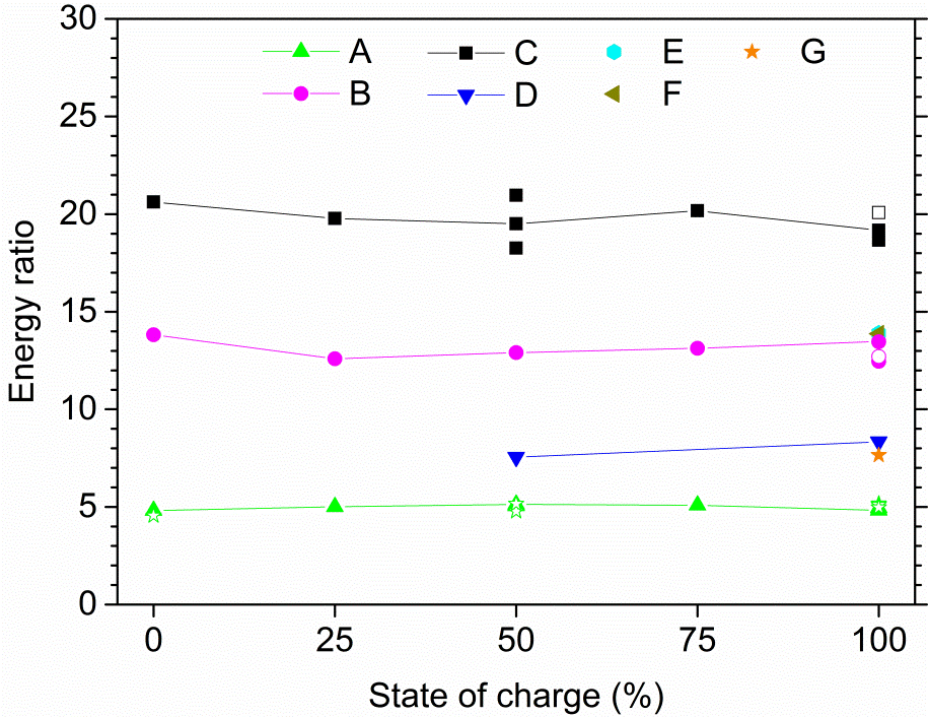


Figure 28. Energy ratio, i.e. the total heat release divided by the nominal electrical energy, and a measure of the chemical energy vs the electrical energy, for seven types of Li-ion battery cells and for 0-100% SOC. Open symbols indicate that the test included a variant, e.g. water mist. The lines are intended as a guide for the eye.

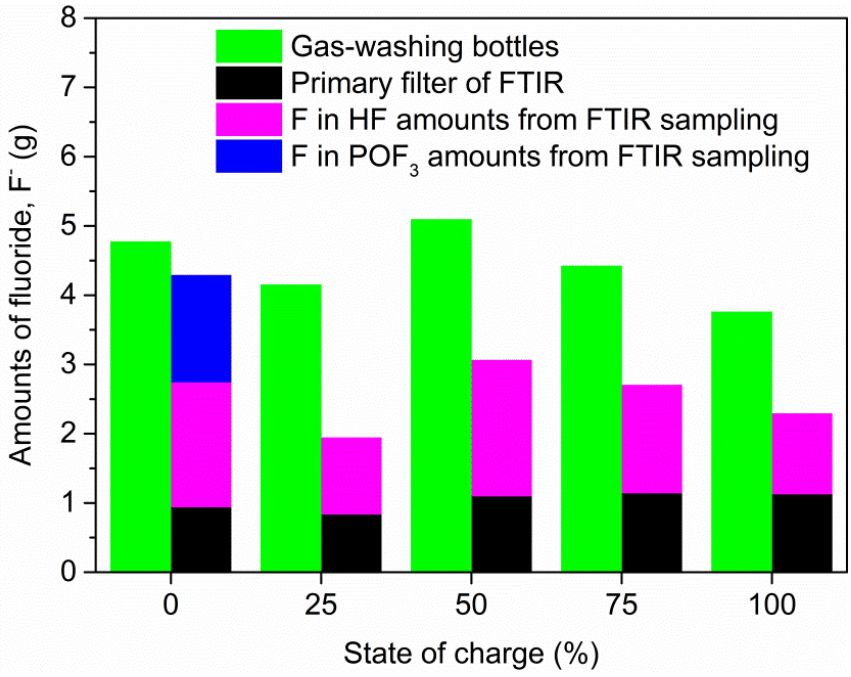


Figure 29. Total amounts of fluoride emitted during external fire tests, $F^-$ vs SOC for 5-cells of Li-ion hard prismatic 6.8 Ah cells with graphite/LCO electrodes. The results from two independent measurement techniques presented. $POF_3$ was only found for the 0% SOC case.

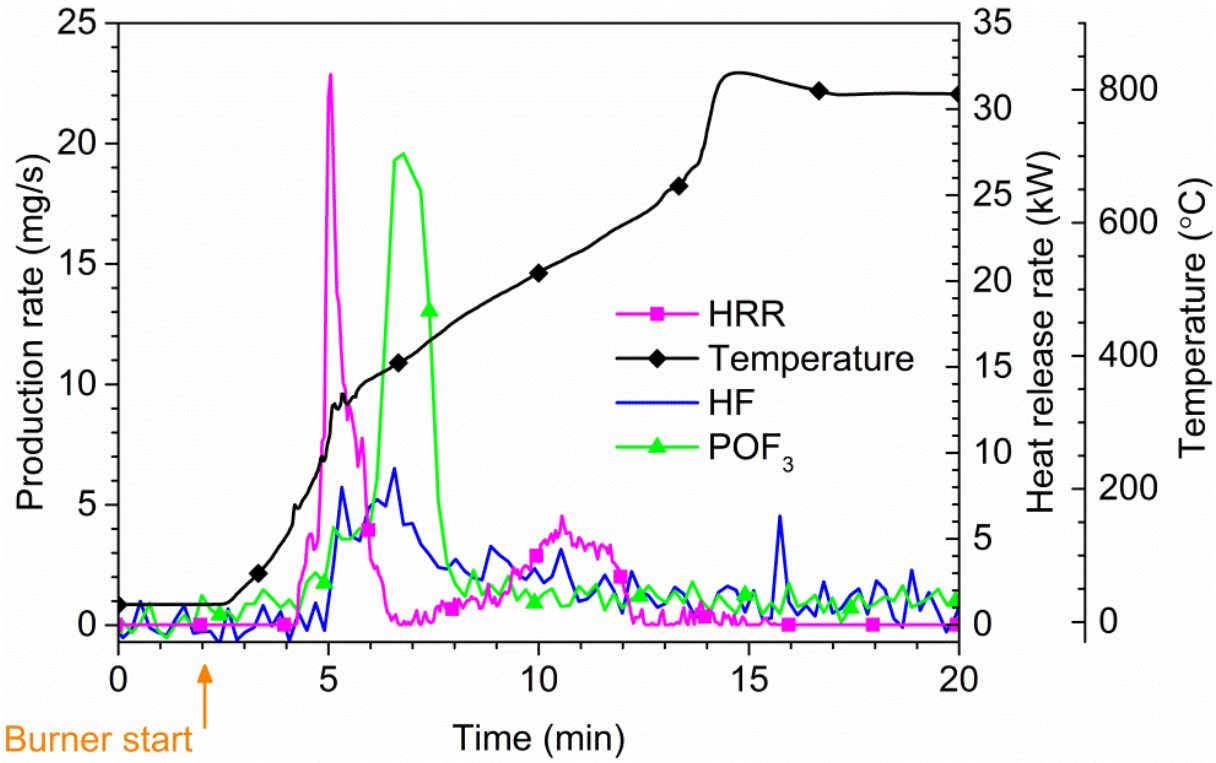


Figure 30. Results for 5-cells of Li-ion hard prismatic cell of 6.8 Ah with graphite/LCO electrodes during external fire test, showing average cell surface temperatures, HRR and production rate of HF and $POF_3$.

## PAPER VI - GAS EMISSIONS FROM LITHIUM-ION BATTERY CELLS UNDERGOING ABUSE FROM EXTERNAL FIRE TESTS

### SUMMARY

The aim of Paper VI is to study the release of toxic gas emissions of HF and $POF_3$ as well as fire characteristics, e.g. heat release rate and total heat release on different cells. Two independent measurement techniques were used to measure gas emissions in one of the tests, FTIR and gas-washing bottles.

Abuse tests:

- External fire

Cells:

- K2 Energy LFP26650EV, carbon/LFP, 3.2 Ah, cylindrical
- Lifetech X-1P 8Ah 38123, carbon/LFP, 8 Ah, pouch
- Leclanche LecCell 30Ah High Energy, LATP/NCO, 30 Ah, pouch

### Main findings

- HF emissions occurred with some delay compared to the peaks in HRR, see Figure 31.
- HF was detected at about the same time as the cell voltage of the bottom cell (in tests with 2 cells) drops to 0 V, see Figure 31.
- The amounts of released HF for FTIR and gas-washing bottles measurements were similar.
- The toxic HF gas released from a large Li-ion battery pack can pose a severe risk, especially in a confined space.

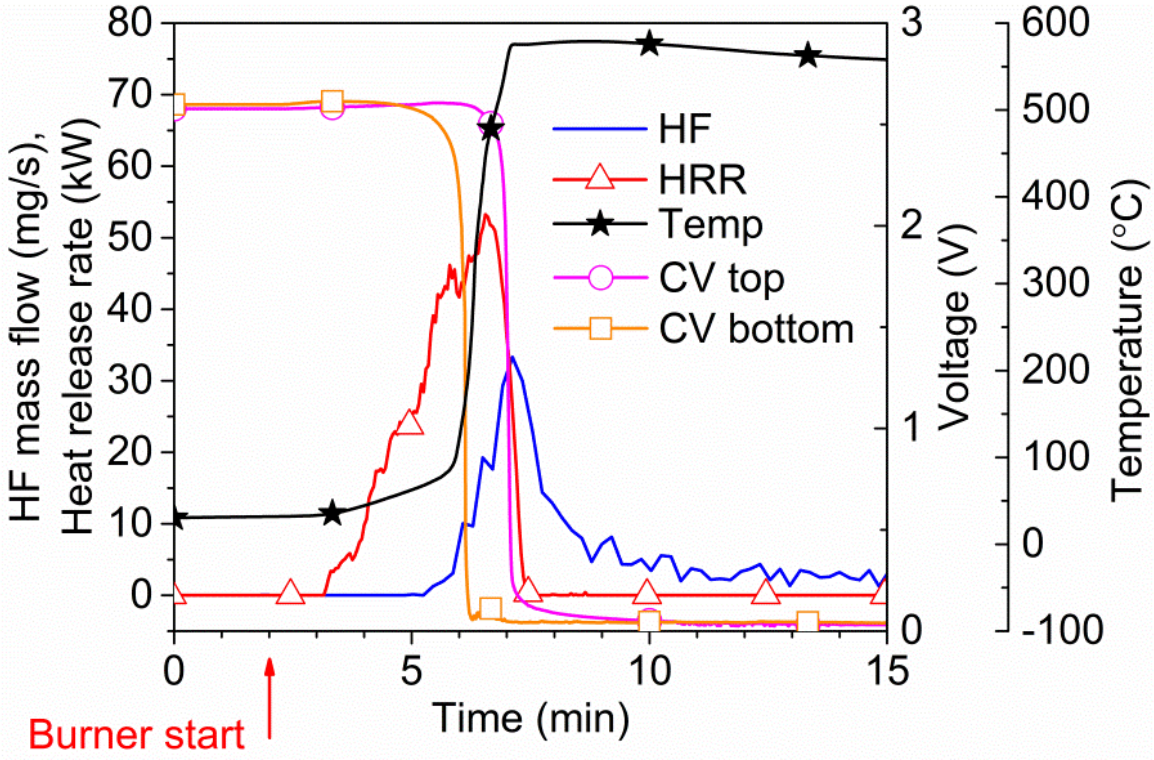


Figure 31. Results from external fire test of two Leclanche LecCell 30Ah high energy cells.

## Paper VII - Thermal modelling of cell-to-cell fire propagation and cascading thermal runaway failure effects for lithium-ion battery cells and modules using fire walls

### Summary

The aim of Paper VII is to study spreading of heat between cells and modules. A numerical model is formulated to predict cell-to-cell propagation. The model is validated by experiments. Heat release from a cell is established by external fire tests. A part of a battery system with one module and two half-modules on each side, with fire walls between the modules are constructed, see Figure 32.

Abuse tests:

- External fire

Numerical tools:

- Comsol Multiphysics, heat transfer module
- Fire dynamics simulator

Cells:

- EiG ePLB-F007A, carbon/LFP, 7Ah, pouch

## MAIN FINDINGS

- A model for evaluating different measures to prevent cascading thermal runaways was developed.
- Substantial risk for cascading effects from the thermal runaway, see Figure 33 to Figure 35.
- Cell-to-cell propagation can be affected by cooling and use of firewalls, see Figure 36.

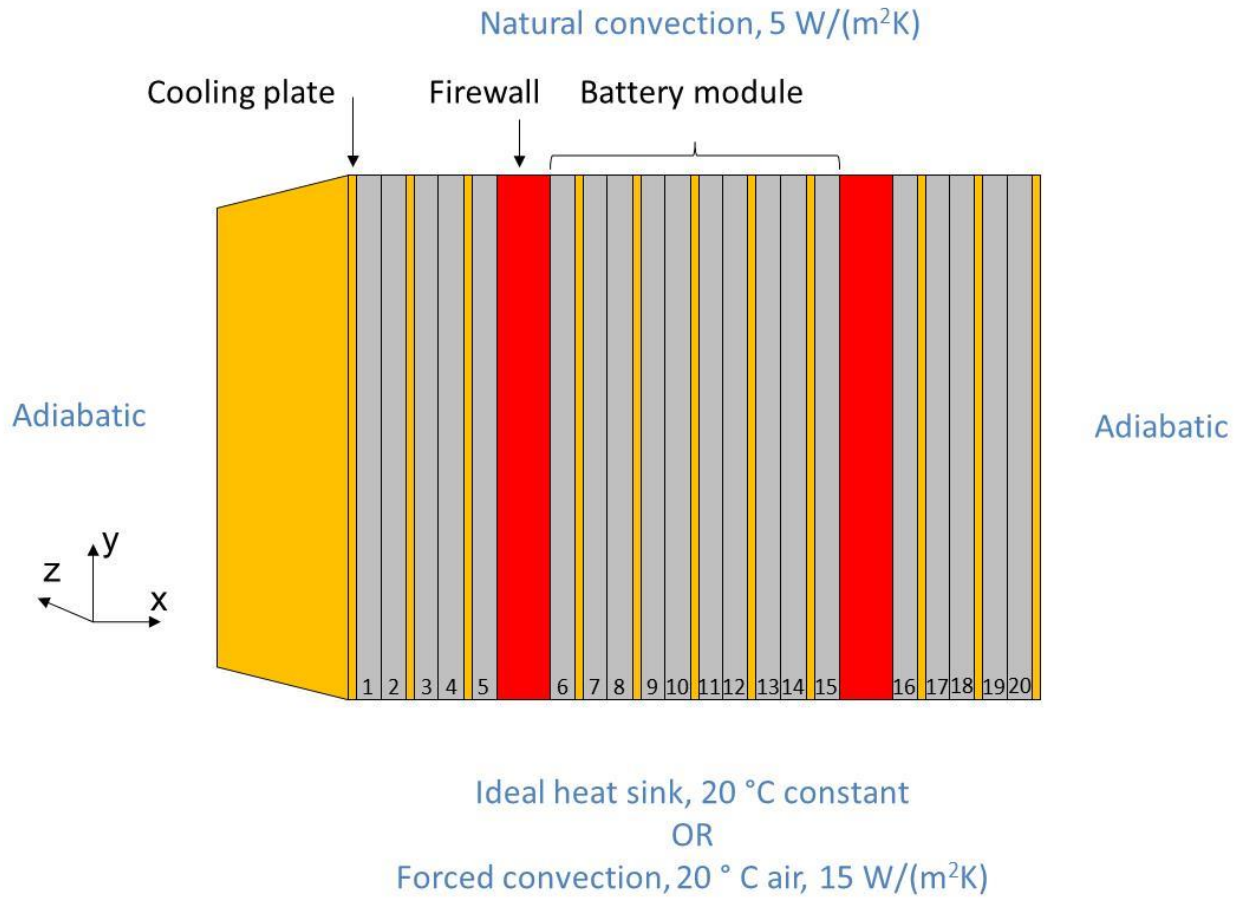


Figure 32. Schematic drawing of part of the battery pack, with one module with 10 cells (cell 6-15) and with a firewall between the modules. The boundary conditions are shown in the figure.

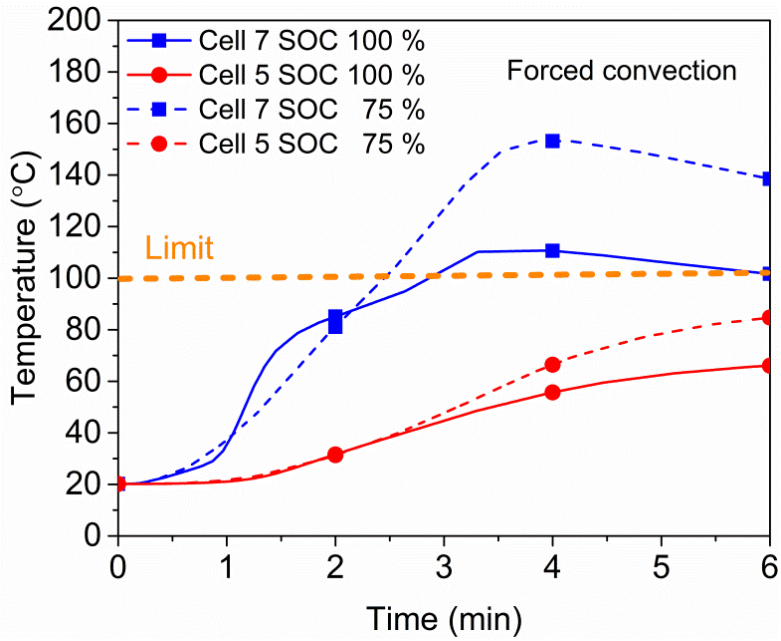


Figure 33. Thermal runaway in cell 6, the first cell in the module closest to the fire wall, and neighbour cell 5 on the other side of the firewall and cell 7 next to cell 6 undergoing thermal runaway.

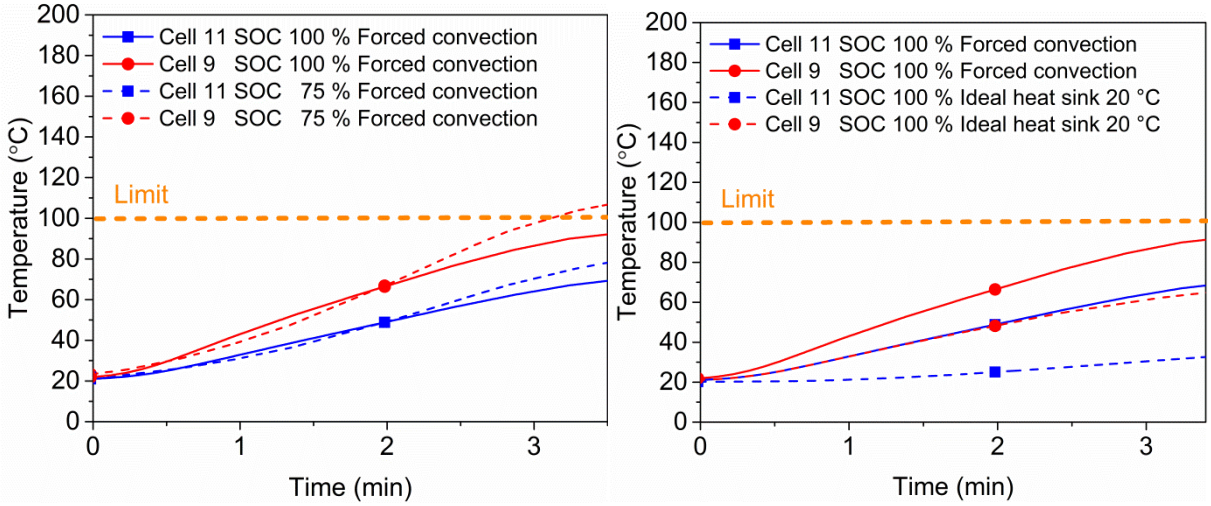


Figure 34. Thermal runaway in cell 10, and temperature development in the neighbouring cell 9 and cell 11, for 100% SOC and 75 % SOC, for forced convection (left) and comparison between forced convention and ideal heat sink 20 °C for 100% SOC (right).

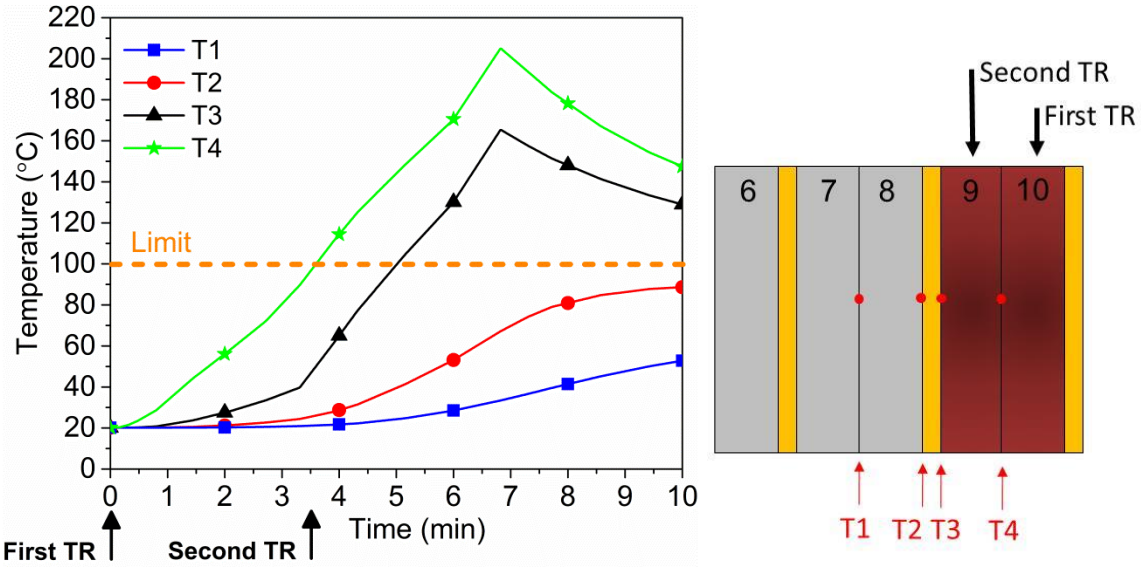


Figure 35. Thermal runaway in cell 10, creating an overtemperature in the neighbour cell 9, going into thermal runaway 3.5 min later and the temperature development (left) for some adjacent cells (right).

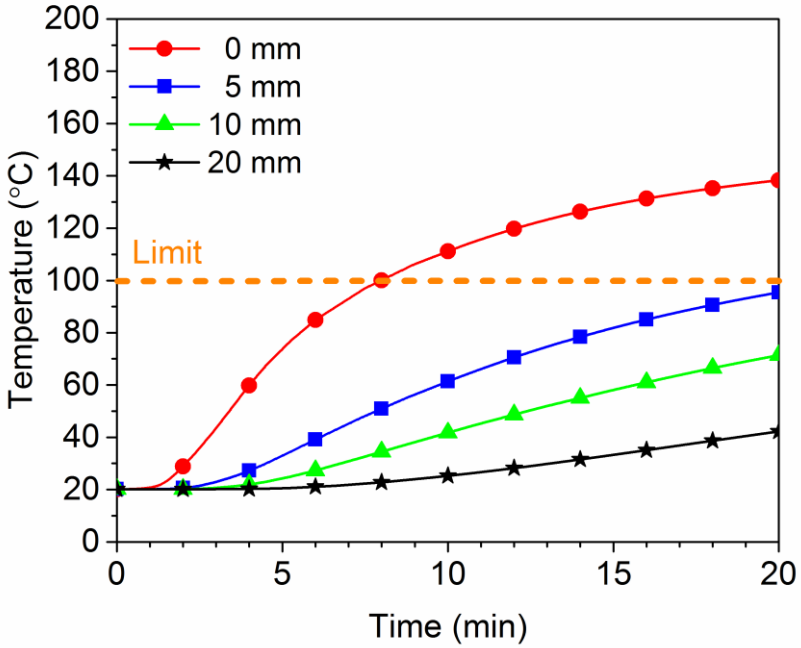


Figure 36. Thermal runaway in the complete module, cell 6-15, all cells initiated at the same time and the cell temperature in the adjacent cell (cell 6 and 16, due to symmetry) located in the adjacent module with different thicknesses, between 0 and 20 mm, of an alumina firewall between the modules.

## PAPER VIII - OVERCURRENT ABUSE OF PRIMARY PRISMATIC ZINC-AIR BATTERY CELLS STUDYING AIR SUPPLY EFFECTS ON PERFORMANCE AND SAFETY SHUT-DOWN

### SUMMARY

The aim of Paper VIII is to study a novel safety enhancement principle for metal-air batteries, for battery shut-down utilizing shut-off of air supply (suffocation).

Abuse tests:

- Overcurrent

Cells:

- New and old design of primary commercial Zn-Air cells, QuantumSphere MetAir® SC Series 4.8, Zn/Air with Mn-C, 48 Ah, prismatic

### MAIN FINDINGS

- The Zn-Air cell was shut-down when its air supply was shut-off, see Figure 37 and Figure 38.
- Demonstrated that shutting-off air supply offers an additional battery shut-down possibility for metal-air batteries.
- Air shut-down also offers possibilities to reduce electrical hazards in large battery systems, bringing the battery voltage towards zero while maintaining its capacity.
- The time to zero Volt was shown to mainly be determined by the trapped air volume.
- The tested primary Zn-Air cell did not show any particular risks when abused by overcurrents.

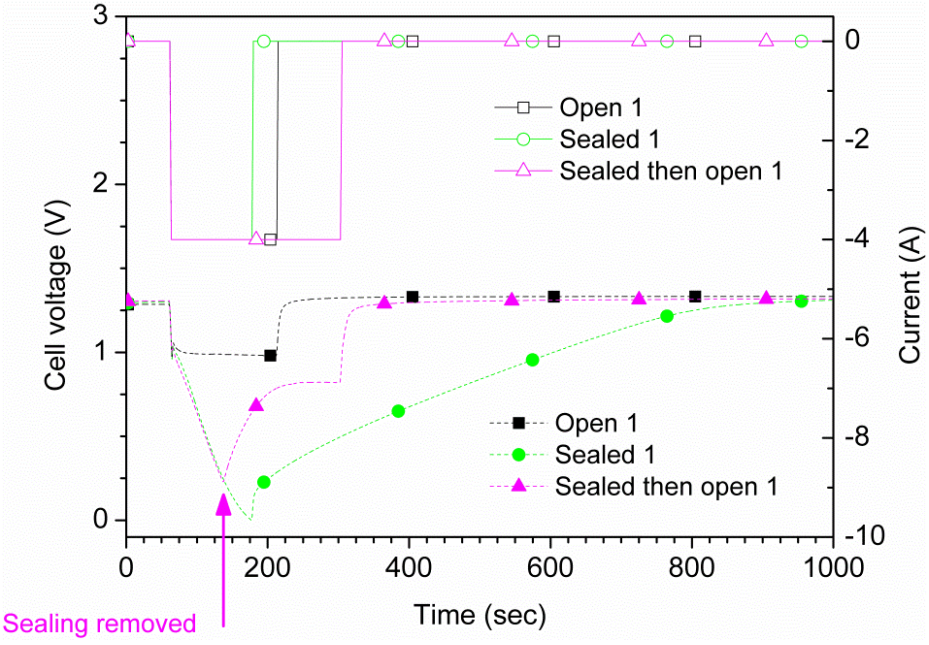


Figure 37. Results from discharge with 4 A (maximum discharge current according to the manufacturer's cell data sheet) with full air supply (Open 1), with sealed air supply from the start of the test (Sealed 1) and with sealed air supply until 135 seconds and then full access to air supply (Sealed then open 1). Voltage as filled symbols and current as open symbols.

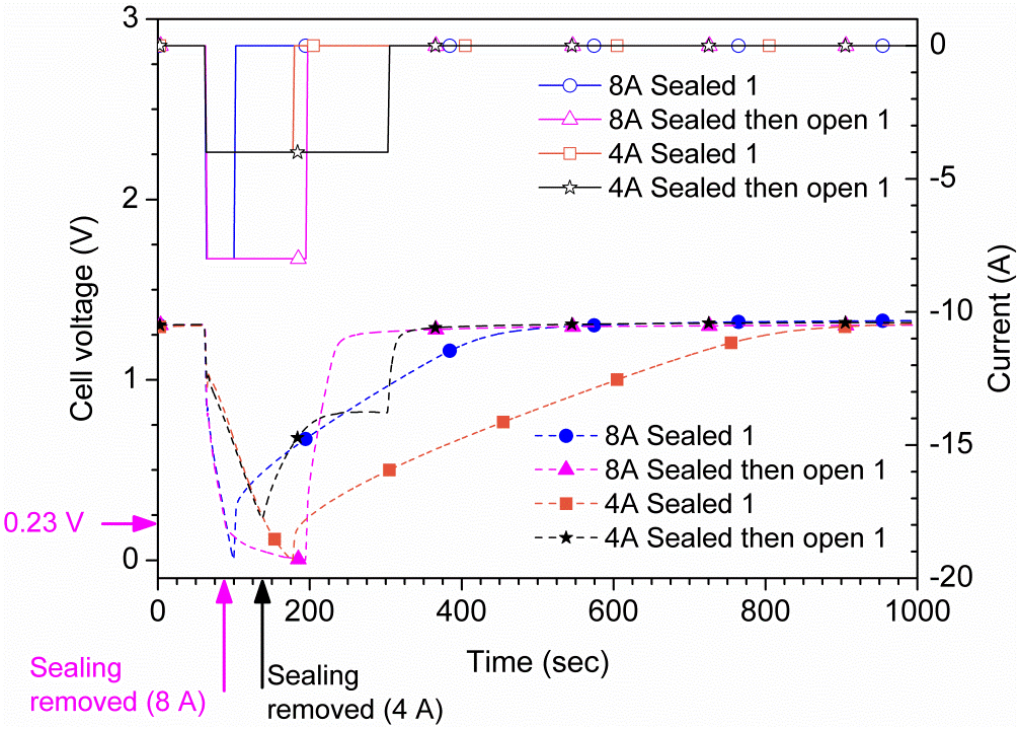


Figure 38. Results from discharge with a current of 4 A and with an overcurrent to 8 A. Voltage is shown as filled symbols and current as open symbols.

# DISCUSSION

## RISKS WITH LI-ION BATTERIES

The risks with lithium-ion batteries are yet not fully studied nor understood. Failure incidents, failure mechanisms and failure states are complex and incidents are often seen as stochastic, perhaps simply due to lack of knowledge. Examples of research areas that have not been studied or have been studied to a very limited extend are; the impact on safety from e.g. battery ageing, toxic gas release, risk for gas explosions, firefighting, failure propagation and size effects when going from small consumer batteries to large battery systems. More studies on these aspects as well as the development of protection strategies (counter actions to mitigate risks) are thus urgently needed.

Today's knowledge is available mainly for small consumer batteries while it is limited for large battery systems, especially regarding how the safety aspects are influenced by the size of the battery system, its environment and possible new failure modes, e.g. failure propagation within the battery system. Safety knowledge and techniques have their origin in the development of safer consumer Li-ion batteries, however, the use in large battery systems can be different and some of the cell safety mechanisms developed for consumer batteries, e.g. CID and PTC, do not work well in a large battery system [42].

For small battery cells and battery packs, e.g. ranging from 10 to 100 Wh, used in consumer products, e.g. cell phones or laptops, significant knowledge has been collected through recent years. Even though batteries sold on the market have passed all required international safety tests incidents do happen. The failure rate per cell is low but the manufacturing numbers are very high and incidents therefore happen. For example, minor incidents occur in airplanes more or less on a weekly basis and restrictions have been implemented limiting the use of Li-ion batteries on-board airplanes [19]. It is important to mention here that a cell can fail without a resulting severe thermal outcome.

One indirect risk from consumer Li-ion battery failures is that it can act as a fire source to start a large fire involving combustible materials in the surrounding. The small sized consumer batteries can also release toxic gases and could thus cause an acute life threating situation in e.g. confined spaces, however, the author of this thesis has not yet found any reports of such events. Anyhow, the amounts of toxic gas that may be released according to

the presented thesis [paper IV-VI] are, at least theoretically, large enough to possibly cause an acute toxic situation.

The safety and incident knowledge is still limited for large battery systems, e.g. ranging from kWh to MWh size today and probably as large as TWh size in a relative near future. One fundamental source of concern is that a large battery system will use a large numbers of cells, which means that the probability for a cell failure within the battery system will increase. For example if the cell failure rate would be 1 ppm, the failure rate in a large battery system with 1000 cells, will be 1 in 1000. Another, perhaps stronger, concern is that the consequences may be much larger for a large battery pack than from a small battery, simply because it consists of many more cells. Therefore it is motivated to mitigate the risks of propagation, for example, a single cell failure should be hindered to propagate to adjacent cells, in other words, to hinder cell-to-cell propagation. However, it can be difficult to achieve and in case more than one cell is undergoing thermal failure, propagation could still occur. Furthermore, even a single cell failure can result in considerable energy release and accompanied events (gas, fire, explosion). For example, if a battery design would hinder a single cell propagation for one type of abuse conditions, propagation can still occur in case of another abuse type or condition, see Figure 7. It can therefore be argued that the propagating strategy should be treated in relation to the battery size, its installation space and location taking into account the local risk assessment. For a large scale application in an area with high population density, hindering/delay of propagation in general should be even more important in order to e.g. lower the amount of toxic gas emissions in a major event.

The energy release from a cell can vary significantly between different cells/battery designs and between different abuse types. Furthermore, the measurement and evaluation techniques typically strongly affect the energy release values. The energy ratios, i.e. energy release compared to energy capacity, are reported between 0.5 (Paper I) and up to 21 (Paper V) in this theses. Studies using other methods and cells often report energy ratios values in the order of about 1 [43,44].

Figure 39 shows examples of thermal response from various abuse tests on some Li-ion cells. Upon overheating, the electrolyte starts to evaporate and the cell will swell, the amount of swelling depends on how much the cell is physically allowed to swell, e.g. is the cell unconstrained in free air or dense packed in cell modules. If the cell is not allowed to swell enough in case of excessive temperatures, the cell will open and release (vent) gases. The opening can either be controlled e.g. via a cell safety vent, or un-controlled as in a cell case

rupture or in a more severe “cell case explosion” or “cell explosion”. The cell rupture is less aggressive and can typically occur for moderate abuse conditions and in case the cell safety vent does not open or releases pressure to slowly. The cell case explosion can often be avoided by having a cell safety vent, releasing overpressure before an extreme cell pressure is reached. However, Figure 39 shows a cylindrical cell that was propelled away and caught by a protection net due to cell case explosion because of cell safety vent failure. It happened for one of five cells simultaneously exposed to external fire demonstrating that also safety devices can fail.

If the vented gases are not immediately ignited and the flammable gases are accumulated in an air/oxygen-mixture in a confined or semi-confined space, there is a potential risk for a gas explosion upon ignition of these gases. The consequences of the gas explosion can be severe, potentially magnitudes larger than the cell case explosion. Compared to the gas explosion an instant fire or delayed fire without gas explosion might be less severe. In fire science gas explosions are a common phenomenon [45] however not often discussed for Li-ion battery safety.

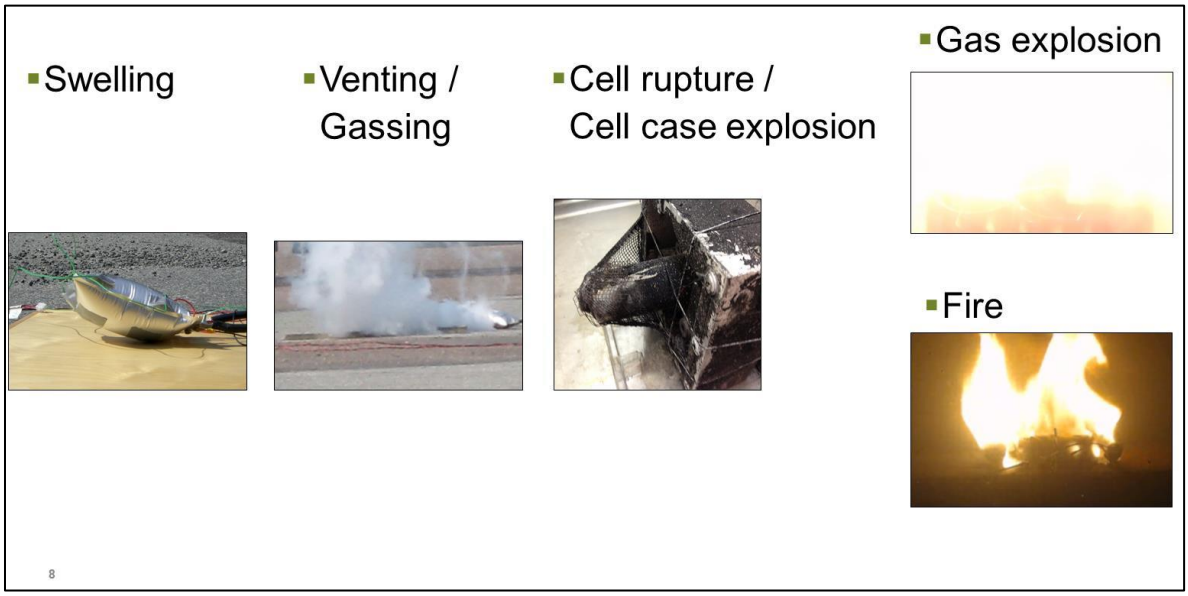


Figure 39. Examples of thermal response upon abuse testing for different Li-ion cells.

The different Li-ion types have different properties in terms of safety. Two important aspects are the heat generation and heat release rate, where LFP is typically considered the safest choice, see for example Figure 40 and Doughty and Roth [30]. Sometimes, rumors say that LFP cells cannot catch fire, but that is not true, LFP cells have a flammable electrolyte and thus it can catch fire. In my abuse testing (fire tests excluded) [Paper I, II, 27], the LFP cells

typically has a lower less frequency of catching fire compared to cells with other cathode materials but some LFP cells still ignited in my abuse tests. LFP cells thus offers an increased safety in terms of heat release, however they might possibly have a safety disadvantage when it comes to emission of gases. There might e.g. be an increased risk for gas explosions, since LFP is more prone to release flammable gases without combustion, and possibly also involving toxic gas emission. This is not yet proven and it is certainly a complex scenario that depends on several parameters, e.g. battery system size and design, environmental conditions, ventilation and possible sources of ignition, but claiming LFP to generally be the safest type of Li-ion battery might not be true. Figure 41 shows examples of burning commercial Li-ion cells with carbon-LFP electrodes. In Figure 41a a European battery graphite/LFP cell catches fire during external heating (oven), in Figure 41b another LFP cell from the same batch catches fire during overcharge. Figure 41c shows five EiG LFP cells, a 5-cell-pack, burning in a fire test using a propane burner. It is important to consider battery fires and thermal response from both internal sources and from external sources, e.g. an external fire adjacent to a Li-ion battery pack. An external fire might actually represent a common failure source.

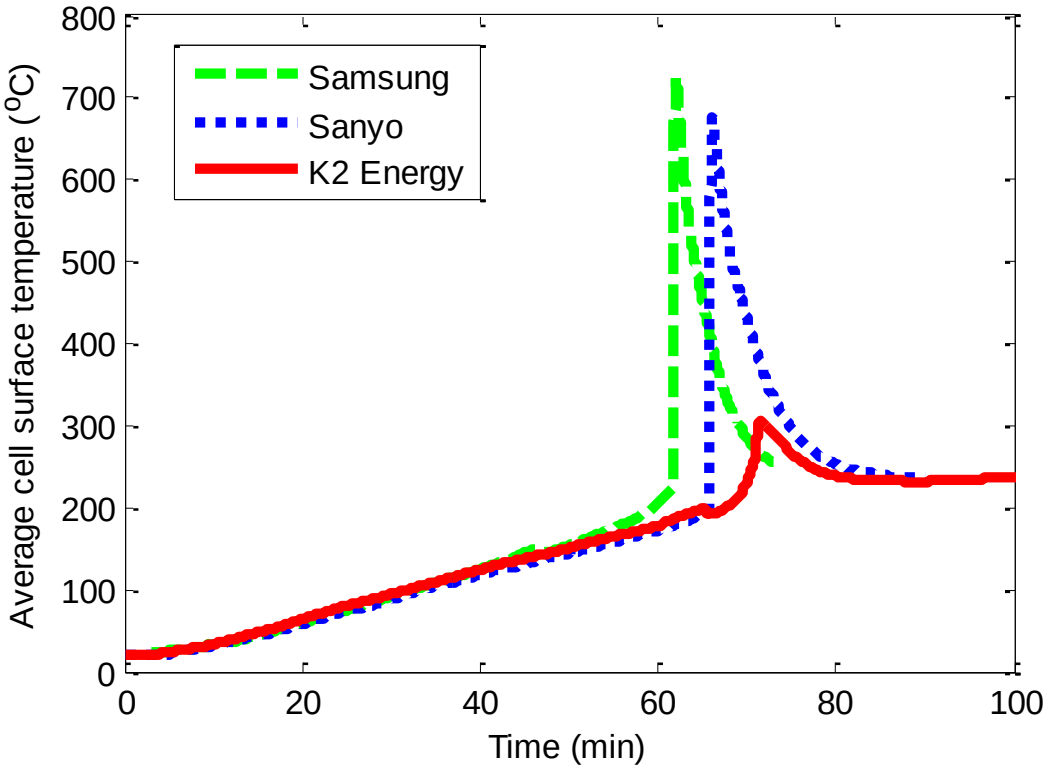


Figure 40. Temperature development for three commercial types of 18650 cells during external heating (oven) abuse tests. The K2 Energy cell has LFP cathode while the cells from Samsung and Sanyo have cobalt-based cathodes.

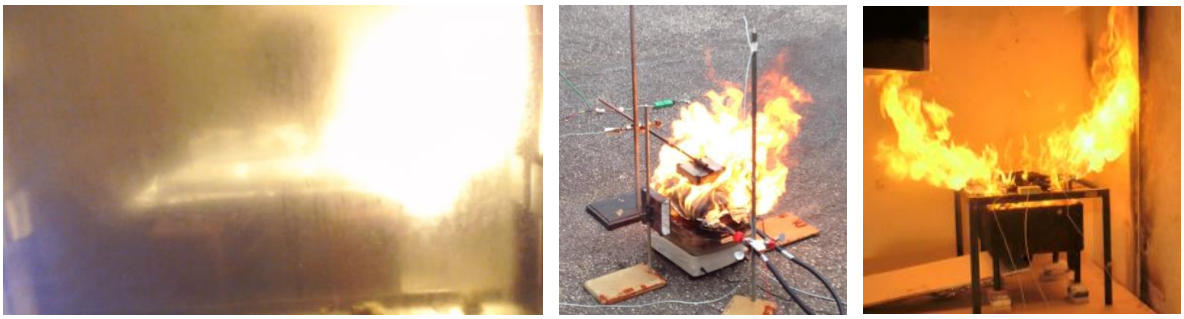

(**A**) (**B**) (**C**)

Figure 41. Fires due to abuse testing in commercial Li-ion cells having carbon-LFP electrodes, showing external heating (**A**), overcharge (**B**) and external fire where the cells are exposure to propane fire (**C**).

Using LTO, $Li_4Ti_5O_{12}$, anodes instead of graphite can improve the safety since LTO shows no Li-plating and less heat generation [30]. It is however essential to consider a holistic perspective as LTO and other variants, e.g. LATP cells, still have a cathode and a flammable electrolyte. In an overcharge abuse test, the LATP cell went into fire as shown in Figure 42. Another titanium based cell having a different cathode (NMC), did not ignite during the 2C overcharge, while it went into fire during a 7C overcharge, see Figure 43. However, ignited cell materials were ejected out of the cell undergoing 2C overcharge, which can be barely seen in Figure 43B to the right in the photo.

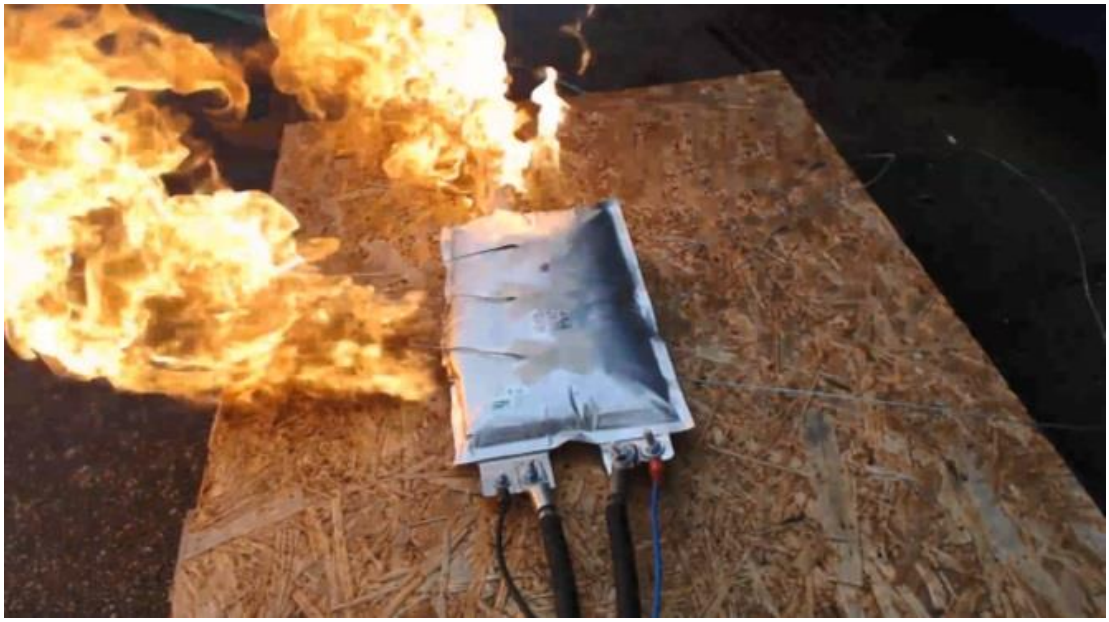

Figure 42. Overcharge abuse with a 2 C-rate current of a 30 Ah cell with LATP/NCA during fire caused by the abuse.

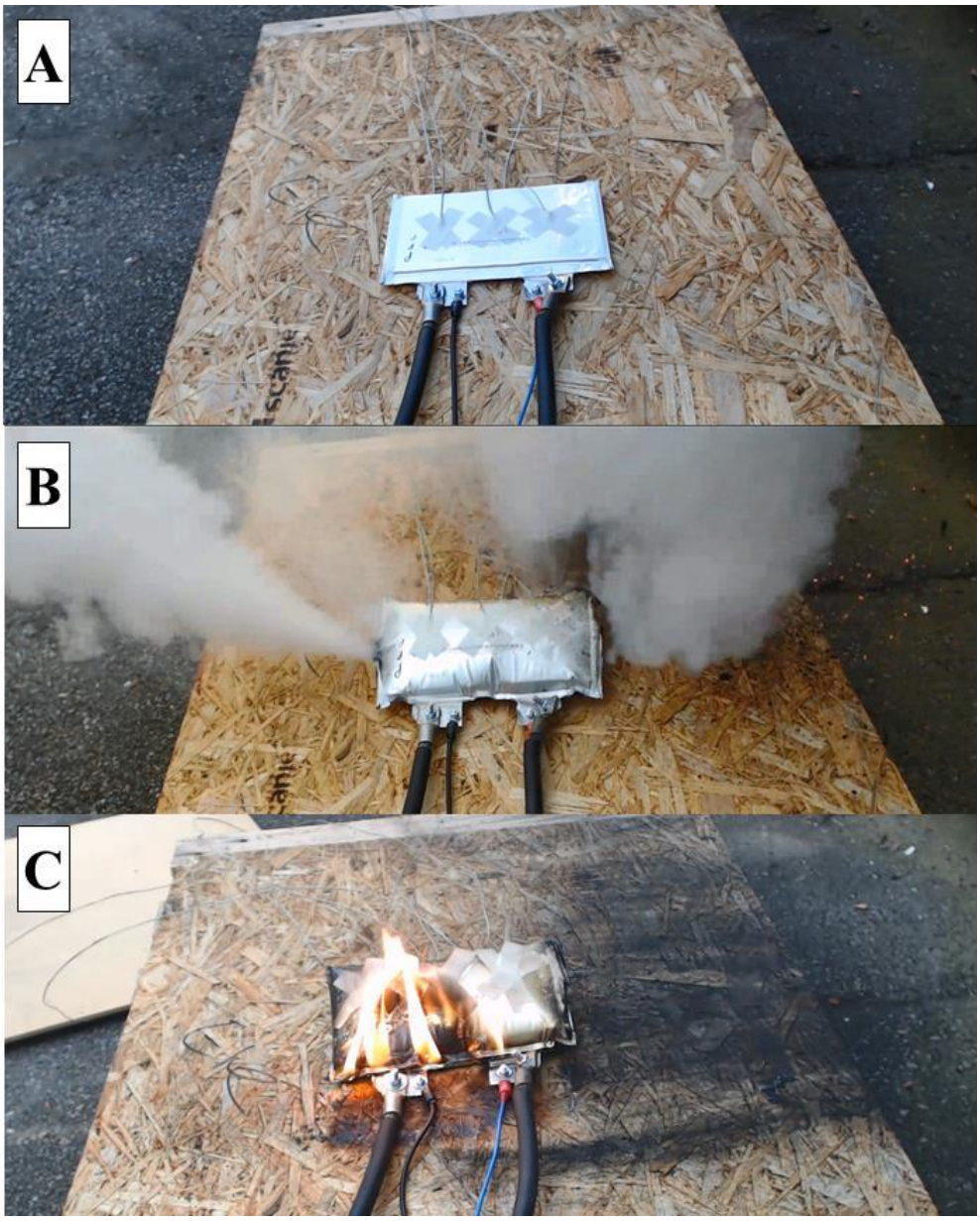


Figure 43. Photos from overcharge abuse tests of Altairnano 13 Ah LTO/NMC pouch cells. (**A**) before overcharge (**B**) shows gas release during overcharge with a current of 2 C-rate (26 A) and (**C**) for another cell during overcharge with a current of 7 C-rate (91 A) that ignited after gas release.

## GAS RELEASE

Upon heating, the Li-ion cell is designed to let the gas out. If the temperature is high enough it will be impossible to contain the internal cell pressure and therefore flammable and toxic gases will be released from the battery cell, either controlled or via a cell rupture or cell case explosion. A safety mechanism for controlled gassing can be implemented in cylindrical and hard prismatic cells by an electrolyte additive with the function of gassing at a predesigned

temperature below critical temperatures, the generated gas pressure can then mechanically activate a CID built-in in consumer cells, thereby electrically disconnect the cell. This safety mechanism can offer protection from e.g. overcharge. This type of mechanism can in general not be used for pouch cells due to the significantly different cell design.

The electrolyte used in Li-ion batteries contains volatile organic solvents which start to evaporate at relatively low temperatures as can be seen in Figure 44 where the results from the Bertilsson study [46] on evaporation (weight loss) is seen by means of presenting the sample weight as function of temperature for some common electrolyte solvents in thermogravimetric analysis (TGA) is shown. The boiling temperature and flammability data for some solvents are presented in Table 2.

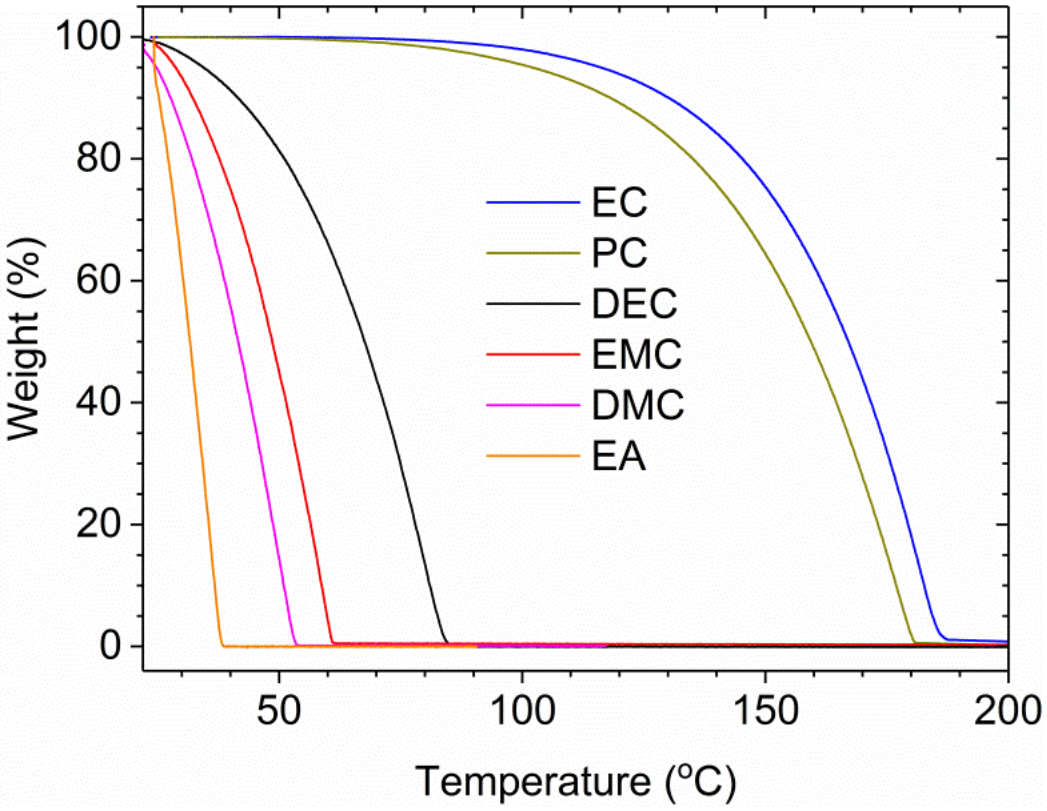


Figure 44. Thermal analysis of some electrolyte solvents commonly used in Li-ion cells, showing the weight loss (evaporation) vs temperature with a constant heating rate of 10 °C/min, using a Perkin-Elmer TGS-2 thermogravimetric analyser. The sample was purged with $N_2$ gas. Reprinted with permission from Bertilsson [46].

Table 2. Flammability data for some common solvents used in Li-ion electrolytes.

| Electrolyte solvent | Molecule weight (g/mol) | Flash point (°C) [47] | Boiling temperature (°C) [47] | Autoignition temperature (°C) [47] | Flammable limits lower / upper (vol %) |
|---|---|---|---|---|---|
| Ethyl acetate (EA) | 88 | -3 | 77 | 427 | 2.2 / 9 [48] |
| Dimethyl carbonate (DMC) | 90 | 16 | 91 | 458 | 4.22 / 12.87 [48] |
| Ethyl methyl carbonate (EMC) | 104 | 24 | 110 | 440 | N/A |
| Diethyl carbonate (DEC) | 118 | 25 | 126 | 445 | 1.4 / 11 [49] |
| Propylene carbonate (PC) | 102 | 132 | 242 | 455 | 1.8 / 14.3 [48] |
| Ethylene carbonate (EC) | 88 | 143 | 248 | 465 | 3.6 / 16.1 [50] |

The cell is typically gassing before thermal runaway and gas will be emitted whether the cell undergoes thermal runaway or not. In Paper III three different vents for hard prismatic cells undergoing external heating are identified. The first vent occurs about 20 minutes before the thermal runaway and the second vent a few minutes before TR and the external heating time from room temperature to reach TR was about 60 minutes. The gas release in the first two vents was not visually observable. Gases are released as single electrolyte components (e.g. DMC, EC) or as decomposed products, e.g. CO, $CO_2$, $CH_2$ and $H_2$. Figure 45 shows an example of gas release with white/grey smoke and gas from overcharge abuse of a Li-ion cell during venting.

Figure 45. Gas release before fire upon overcharge abuse with a 2 C-rate current of a 30 Ah cell with LATP/NCA.

## TOXIC GAS EMISSIONS

Li-ion batteries are totally sealed under normal conditions and do not emit any gases. When a Li-ion battery cell is heated, abused or undergoes failures the cell can emit a large number of different and complex toxic substances [2,51,52,53]. The cell can also release $CO_2$ as in most combustion processes as well as CO. Toxic fluoride gases in form of a large number of other complex fluoride substances may also be emitted from a Li-ion battery cell, yet there are only limited studies on this subject. Emissions of hydrogen fluoride have this far gained the most attention, however there is so far just a few studies available for complete Li-ion cells. Besides emissions from the Li-ion cells, the battery system consists also of other materials, plastics, cables, electronics, coolant media, etc which can emit toxic gases during a fire. For example, combustion of PVC plastic generates hydrogen chloride (HCl) and combustion of polyurethane (PUR) generates hydrogen cyanide (HCN).

Today all commercial Li-ion cells contain at least one of several possible sources of fluorine. The electrolyte contains a Li-salt, mostly, if not always, $LiPF_6$, which has important properties needed for a functional Li-ion cell, e.g. it protecting the aluminum anode from dissolution and it takes part in the SEI layer formation [22]. Fluorine can also be used for binder materials in the electrode, e.g. polyvinylidene fluoride (PVdF). Furthermore, fluorine compounds can be found in the electrode materials, e.g. fluorophosphates [54,55] and $AlF_3$-coating of the cathode [30,56,57] used as a safety enhancement. Additionally, additives in the electrolyte and the separator may contain fluorine, e.g. in flame retardants.

The fire safety may thus be improved by adding flame retardants; however in terms of toxic gas emissions and gas explosion risks such an addition can at the same time result in a decreased safety. The resulting safety is application dependent and not easily determined and has not yet been studied nor evaluated, at least not publicly. Getting a complete picture of the risks is a difficult task and a solution appropriate for one application might not be appropriate for another application, it is important to include all safety measures including e.g. extinguishing systems in any analysis.

The decomposition of $LiPF_6$ occurs according to the following reactions [58,59]:

$$LiPF_6 \rightarrow LiF + PF_5 \quad (1)$$

$$PF_5 + H_2O \rightarrow POF_3 + 2HF \quad (2)$$

$$LiPF_6 + H_2O \rightarrow LiF + POF_3 + 2HF \quad (3)$$

$$POF_3 + H_2O \rightarrow POF_2(OH) + HF \quad (4)$$

In an inert environment, $LiPF_6$ decomposes upon heating to lithium fluoride, LiF, which is a solid compound at temperatures below 845 °C and phosphorus pentafluoride, $PF_5$, which is a very reactive gas and a strong Lewis acid. Hydrogen fluoride, HF, and phosphorous oxyfluoride, $POF_3$, produced when water/moisture reacts with $PF_5$ according to eq. (2) or with $LiPF_6$ directly according to eq. (3). Kawamura et al. [59] suggested that $POF_3$ and water/moisture can react and produce $POF_2(OH)$ and HF according to eq. (4).

The toxicity of HF is well known. The National Institute for Occupational Safety and Health (NOISH) in USA stated the immediate dangerous to life or health (IDLH) value for HF to be 0.025 g/m$^3$ (30 ppm) [60]. The IDLH is typically considered as a 30 minute value before irreversible damage/death. The lethal 10 minutes HF toxicity value (AEGL-3) is 0.139 g/m$^3$ (170 ppm) [61]. The Swedish Work Environment Authority has exposure limits for HF [62] and the maximum allowed concentration of HF in a working environment at any time[†] is 1.7 mg/m$^3$ (2 ppm) and the mean value during a full working day (e.g. 8 hours)[‡] is 1.5 mg/m$^3$ (1.8 ppm).

HF is a light molecule, lighter than air. However, HF can attach via a hydrogen bound to a water molecule thereby resulting in a "gas" heavier than air. HF is also very easily solvable in water and form very toxic and corrosive hydrofluoric acid, other names are fluoric acid or fluorhydric acid. Surrounding surfaces and walls as well as runoff water from e.g. fire fighting may contain high toxic levels and possibly even lethal levels of fluorhydric acid.

There are no toxicity data for $POF_3$. $POF_3$ is a precursor to produce HF [63]. However $POF_3$ might be toxic by itself, and act with other poisoning mechanisms than just by formation of three equivalents of HF. Critical limits of exposure might be lower for $POF_3$ than for HF as in the chlorine analogue $POCl_3$/HCl [62].

There are few studies on HF gas release from commercial Li-ion batteries undergoing abusive conditions. Time-resolved quantitative HF gas emission measurement from commercial Li-ion cells under abuse were studied by Ribière et al. [64] and by Larsson et al. [Paper IV, V, VI] and for non-commercial Li-ion cells by Lecocq et al. [65]. Lecocq et al. also performed time-resolved quantitative HF measurements of gas release from EV and non-EV fire tests [66], and found HF emissions from both types of vehicles. The AC coolant medium was

[†] "Korttidsgränsvärde", KGV value
[‡] "Nivågränsvärde", NGV value

suggested as a possible source for the HF. Other studies have detected HF during abuse on cells [Paper III,51,53,67] and battery packs [68,69], however, they do not report time dependent rates or total amounts of HF and other fluoride gas emissions. There are somewhat larger numbers of studies of other gas emissions released from Li-ion cells [27,29,70,71,72,73,74,75,76] and from electrolytes alone under fire or external heating abuse conditions [77,78,79,80,81], where a few present quantitative measurements of HF and $POF_3$ [80,81]. Electrolytes heated to moderate temperatures, 50-85 °C, were also studied and various fluorine compounds were found [58,59,82,83,84] while some other studies include both electrolyte and electrode material [2,85]. There is a large need of more studies on real conditions having real/complete cells and battery pack.

Blum et. al. [68] abused a 100 kWh stationary battery pack by a 400 kW propane burner and measured HF using a portable HF gas meter, with a simple measurement setup, e.g. without a controlled ventilation flow. However, the maximum detection value of 100 ppm was reached already after 2 minutes, even though no visible smoke could be seen until an additional 33 minutes later. Thus, life threating levels might be present without visual observation of gas release.

The time-resolved quantitative detection of $POF_3$ gas emissions from commercial Li-ion cells under abuse is so far only reported by Larsson et al. [Paper V] as well as time-resolved detection [Paper III]. Andersson et al. [81] studied the production of HF and $POF_3$ from electrolyte burning tests and detected HF and $POF_3$ in all tests with HF:$POF_3$ production ratios varying between 8:1 to 53:1. Figure 46 shows an example where $POF_3$ and HF are produced during a combustion of the $LiPF_6$ salt dissolved in the pure DMC electrolyte [81].

The use of water as firefighting medium for Li-ion battery fires may increase the production of HF gases, according to eqs. (2)-(4). There are, however, few studies about this in the literature [Paper IV, V, 81]. Two fire tests with water mist as firefighting medium are presented in Paper IV and Paper V, in both cases the total HF emission is the same, however the HF production rate increased significantly when applying water mist, yet only two tests were performed. Further studies are thus needed to evaluate the water influence on HF production, as well as the toxicity of the run-off water.

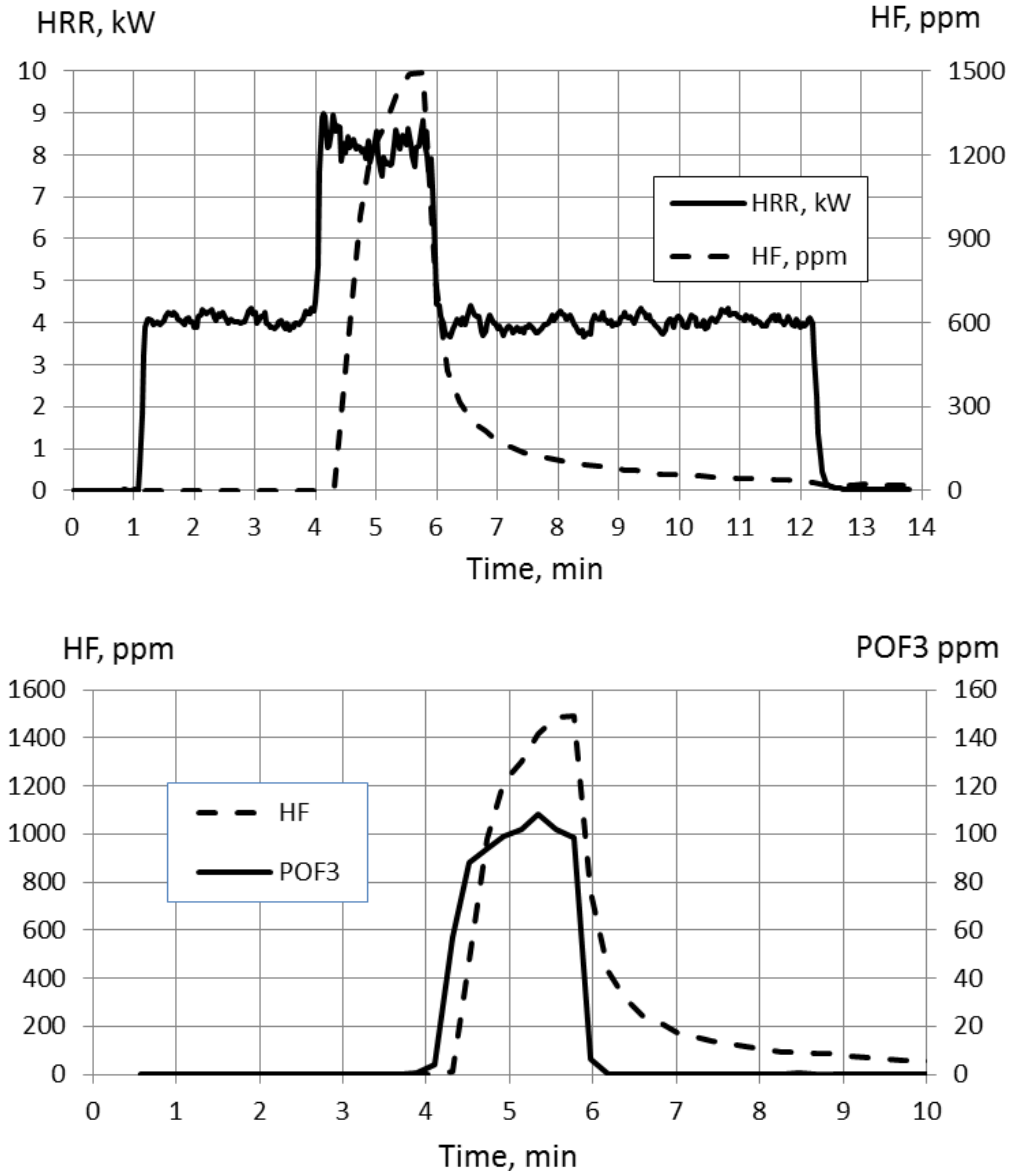


Figure 46. Burning of 1 M $LiPF_6$ in DMC (dimethyl carbonate) with a spray of 18 ml/min during two minutes into a propane burner of 4 kW, showing (**top**) heat release rate and HF concentration and (**bottom**) concentration of HF and $POF_3$. Reprinted from Andersson [81].

## SOME BASIC SCENARIOS REGARDING TOXIC GAS EMISSIONS

When Li-ion batteries are burning, HF is released. Measurements [Paper V] have shown amounts of HF between 20 and 200 mg/Wh of nominal electrical energy capacity. These values were obtained for seven types of commercial cells with SOC ranging from 0% to 100% and a nominal electrical energy capacity ranging from 92 to 138 Wh. These values are state-

of-the-art and valid for external fire. In order to assess the toxic threat due to HF from large Li-ion battery packs undergoing fire, the values can be extrapolated.

Below are some simplified examples presented as theoretical cases, i.e. they will not represent a real case. They are presented only to give the reader a rough indication of the toxicity.

**Scenario 1**

- Fire of a Li-ion battery pack of 100 kWh
- Homogenously distributed HF, no losses
- IDHL value: 0.025 g/$m^3$ [60]
- HF: 20-200 mg/Wh → 100 kWh Li-ion battery pack: 2 - 20 kg HF will be released

In order to reach IDHL the HF amount needs to be diluted in 80 000 – 800 000 $m^3$ of air. This corresponds for example to a fire in one EV with a 100 kWh battery parked in a multi-car park with a volume of one to ten floor levels (each of 3 m height) of 250 x 100 m.

**Scenario 2**

- Fire in one parked EV with a 100 kWh battery
- Underground car park: 50 x 50 m, 3 m height (7500 $m^3$)
- Concentration: 2 – 20 kg HF / 7500 $m^3$ = 0.27 – 2.7 g/$m^3$ = 320 – 3200 ppm
  → Death likely to happen within a time frame of maximum a few minutes.

When comparing toxicity it is essential to compare different materials and scenarios. For example, a non-EV will emit significant amounts of toxic gases during fire, originating from e.g. plastics and rubber in the wheels [86,87,88]. There is a lack of emission studies of burning of new vehicles, which typically have significantly larger amounts of plastics. Also the AC coolant media, R1234yf (2,3,3,3 Tetrafluoropropene, HFO-1234yf), used nowadays for replacing tetrafluoroethane (R134a), produce HF when burning [89], supplying an additional source for HF in vehicle fires, for both EVs and non-EVs. However, comparing a non-fire case is also important, e.g. the Li-ion battery can emit HF and other toxic compounds without fire as shown in Paper III. Comparing toxicity on scenario basis taking into account e.g. production rates, ventilation, different types of toxic substances and combinations of them can be performed via e.g. the ISO 13571 standard [90]. Asphyxiant gases are handled by the fractional effective dose (FED) and irritant-gases are handled by fractional effective concentration (FEC) [90].

## DEGREE OF IGNITION AND CONSEQUENCES OF FIRE, EMISSIONS AND GAS EXPLOSIONS

The gases released from a Li-ion battery are flammable. In principle, after a gas emission there may be either no ignition, an immediate ignition or a delayed ignition. If there is no ignition, there will only be smoke and gas, probably both toxic and flammable gas. Smoke and gas emissions from heated materials are often more toxic if there is no fire or if there is not enough oxygen to have complete combustion (under ventilated fire) than with a fire with complete combustion. The impact of limited oxygen on burning Li-ion batteries has not been studied here, however it is highly probable that limited oxygen will have an adverse impact on the emissions from any part of the battery system. The impact of gas emissions released from a Li-ion cell is thus probably worse in general without ignition or in under ventilated conditions, however no studies are available.

For a battery system, there may be several ignition sources including an external source (outside of the battery system), sparks or hot cable/connection/electronic parts inside the battery system, sparks from electrical arcing at internal cell short circuits undergoing separator melting or thermal runaway, jet flames or small fire flames due to thermal runaway or hot battery surfaces [Paper III]. The autoignition temperature of the electrolyte is about 450 °C, see Table 2, and a Li-ion cell undergoing thermal runaway can reach even higher temperatures [Paper I, II, III, 27].

The gases are often ignited rather instantly, at the same time as the thermal runaway occurs, resulting in a fire. However if ignition takes place later when a flammable mixture has accumulated in a confined or semi-confined environment, the ignition will result in a pressure build-up since the heated gases cannot expand, which can be called a "gas explosion" [45], a "smoke gas explosion" or a "smoke explosion". The study of external heating abuse of 6.8 Ah single Li-ion cells reported in [Paper III] showed the occurrence of repeated gas explosions, also for different cycle ageing level. Although the cells are relatively small the gas explosions were strong enough to open the oven door and to move the video camera, even though the oven was not an airtight confinement and additional pressure releases actions were taken to mitigate gas explosions in the oven, see Paper III.

Note that it is important to distinguish a gas explosion from a cell case explosion. When using the term "battery explosion" it is unclear which of the two types one is referring to.

The gas release due to venting often occurs before thermal runaway and can be difficult to observe visually [Paper III, 68], even though relatively large amounts of gas release can occur

[Paper III]. Thus, without adequate detection equipment/possibilities, situations will occur where flammable as well as toxic gases are released without being detected.

A flammable gas/air mixture can only be ignited if the concentration is within the flammability limits. The lower flammability limit (LFL) and the upper flammability limit (UFL) for some common electrolyte solvents can be seen in Table 2. The LFL is about 3 % for these solvents which means that 30 liters (3 % of 1 $m^3$) of electrolyte in gas phase is needed to create a flammable mixture with 1 $m^3$ of air. This amount corresponds to about 100 g of solvent (calculated from the ideal gas law with a volume of 30 liters and normal temperature and pressure) which in turn corresponds to a cell weight of about 500-1000 g (given that the electrolyte weight is 10-20 % of total cell weight). A room of 10 $m^3$ can easily accommodate a MWh sized Li-ion battery system. With a lower flammability limit of 100 $g/m^3$, only 1 kg of electrolyte, thus just a small fraction of the total amount of electrolyte in the system, is needed to create a flammable mixture with risk of gas explosion.

Upon ignition the gases expand about 5-8 times, causing an overpressure of 5-8 bar if confined. Many building structures can withstand only a very limited pressure increase, e.g. doors and windows typically about 100 mbar.

## BRIEF OVERVIEW ON TODAY'S SAFETY SOLUTIONS

High safety is achieved using many layers of safety, see the safety onion in Figure 17. For high safety, the cell should be made of high quality pure materials using a flawless manufacturing process and selected "safe materials". Since there are no intrinsically safe Li-ion cells, this is not easily done. Various safety mechanisms are often implemented into the battery with the intention to protect the cells from abuse conditions [91]. The BMS is essential, without its protection the battery cells will e.g. easily be over/under-charged. For high safety, the BMS should be of high quality with adequate sensing enabling adequate detection and hinder operation out of battery cell limits. Prudent design also includes keeping the cells within an operating window that minimizes the use of the maximum possible cell limits, in order to create a safe margin, this is typically done by the BMS. The size of the margin will however depend on manufacturer and type of application. The BMS can however unfortunately not protect the battery from all types of abuse situations. Table 3 gives a simplified general overview of abuse situations together with the BMS ability to protect for the situations.

Table 3. A simplified general overview of abuse situations where the BMS can/cannot protect the battery system.

| Abuse type | BMS protection? | Protection strategy |
|---|---|---|
| External battery pack short circuit | YES | Disconnect the battery by using fuse or possibly contactors |
| External cell short circuit | POSSIBLE* | The BMS can protect if the short circuit current is possible to interrupt by a circuit breaker. |
| Internal cell short circuit | NO** | - |
| Overcharge | YES*** | Disconnect the battery by using contactors |
| Overdischarge | YES*** | Disconnect the battery by using contactors |
| Mechanical cross / deformation / penetration | NO | - |
| External heating, mild | YES | Cooling by using Thermal management system |
| External heating, strong | NO | - |

** This case refers to a situation with an external short circuit of one or multiple cells inside the battery pack. Theoretically, many short circuit paths are possible, and if the short circuit happens to be within a current path involving a fuse or possibly contactors then it is possible to stop the short circuit.*
*** Spontaneously starting on micrometer scale inside the cell battery due to e.g. particle contamination or dendrite formation.*
**** The detection and the consequent actions until current shutdown must be rapid enough to ensure that the battery is not exposed to over/under voltages.*

## POTENTIAL FOR IMPROVED FUTURE SAFETY SOLUTIONS

There are complex and sometimes conflicting requirements on the battery. It is desired that the battery has a low cost, long life time, low weight and volume, i.e. high energy and power densities, high safety, high recyclability, low environmental impact, etc. There is always a trade-off between all the requirements. From a pure battery system safety point of view, the safety of the battery system could be improved from a technical and theoretical perspective, but with potential disadvantages regarding other requirements.

The safety level should be adequate, that means it should relate to the risks for the specific situation. There are several factors that determine each situation; the battery size and type, the application that use the battery and what the environment around the battery and the application looks like.

## PROPAGATION PROTECTION/MITIGATION

It is essential to mitigate/hinder failure propagation/spreading. The propagation can occur on several levels. So far cell-to-cell propagation has been briefly studied [Paper VII,92,93], while higher levels of propagation have been the subject of very limited studies [68].

Figure 47 illustrate four different interfaces of levels where the propagation protection can be implemented. The design and installation of the battery system determine to a high degree the propagation protection. Installed firewalls as well as passive and active cooling systems can have a strong impact on propagation [Paper VII]. In case of a single cell failure the propagation should be stopped/delayed at least at the module level. In case of severe damage to multiple cells, e.g. by mechanical forces, multiple modules can be engaged in the fire/thermal event and the event can be handled on the next level; subpack/pack. In very large lithium-ion battery systems separation in different rooms/locations will be an important safety enhancement.

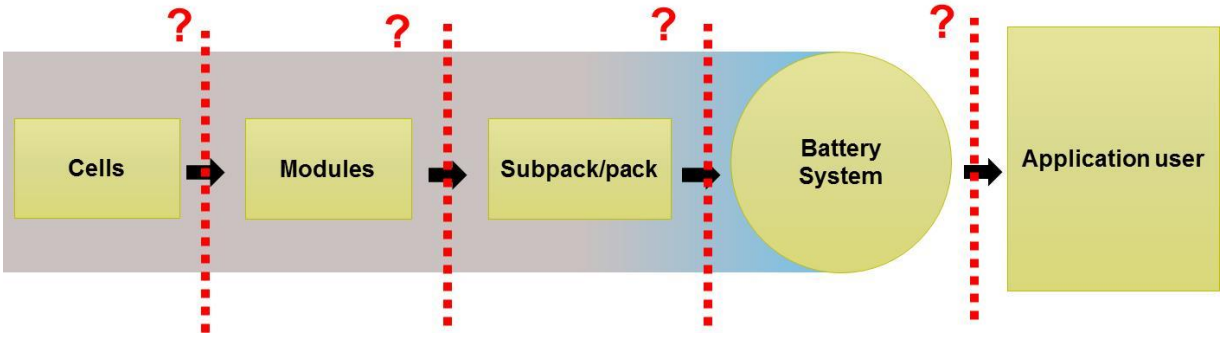


Figure 47. Propagation can occur between many levels within the battery system and the application user (e.g. the electrified vehicle). The thermal event can be initiated at many different levels by different failures/abuse. What will the consequences of various initiation scenarios be? Can they be stopped? At what level can the propagation be stopped?

For cell-to-cell propagation for pouch cells, the cell intercooling plates can play an important role. For example, if a relatively thick inter-cell plate of e.g. 2-5 mm aluminum would be implemented, it would probably significantly decrease the propagation. It might be commercially questionable, especially for automotive applications due to increased weight, volume and cost, while it might be a more viable option for batteries used for grid storage or

for vessels at sea. Separation of the battery system by using distance (free air) could perhaps be part of a low cost solution for applications not limited by volume.

## GAS PROTECTION/MITIGATION

The release of flammable and toxic gas from heated Li-ion battery cells can be handled by different approaches. If the propagation is stopped, the amount of gas release will be limited, which is an important achievement. The released flammable gases should be ventilated out and possibly with a controlled combustion, e.g. a pilot flame. It might be challenging to keep the gas emissions out of the flammability range, but it is important to hinder the occurrence of a gas explosion. The toxic gas emissions can be handled with different solutions, e.g. ventilation to move emissions to other places and by dilution, to lower exposure concentrations. Toxic gas emissions can also be treated by different filters, e.g. $CaCl_2$ for HF. Another possible solution not yet studied is the possibility to wash down the toxic gas emissions by e.g. water mist, however, the run-off water will contain toxic compounds, e.g. hydrofluoric acid, potential lethal concentrations and needs to be handled, yet it might transform the toxicity problem from gas to liquid phase.

For detection of gas release, which can occur before/without thermal runaway, gas sensors can be used inside the battery packs and/or inside battery compartments/rooms. Gas sensors might offer a significant increase in safety since a gas sensor might be the only detecting device of some gas release scenarios [Paper III] as well as offer early detection, which can be very valuable in order to increase the time for evacuation and counter actions to take place. There may be a need for different types of gas sensors, e.g. one for measuring toxic gases such as HF and CO, and one measuring flammable gases, e.g. evaporated solvents, methane and hydrogen gas. In large battery installations, e.g. for electrical grid energy storage, it is probably very relevant to install gas sensors. For example, failure in a large Li-ion battery system having LFP cells, might not induce a cell fire but there is a potential risk that non-combusted released flammable gases may accumulate in the battery compartment/room, posing a risk for a gas explosion. Also, in order to minimize the consequences of a gas explosion in large battery installations, explosion reliefs could be utilized.

## BMS ADDITIONAL IMPROVEMENT

In order to improve detection and detection time, the BMS could have better sensoring and better and faster algorithms. Better sensing can be obtained using more sensors and/or more accurate sensors. For example, having temperature sensor(s) on each cell surface adequately placed for a rapid response of cell temperature increase. More rapid, but still accurate, sensor monitoring, to limit the time from event to detection and protective action is desired, e.g. to hinder over/undervoltage to occur, particularly in the case of high currents. An increased data process capacity and improved algorithms can be the key to finding anomalous cells and detect them before failure, e.g. finding high ohmic internal cell short circuits.

Algorithms and hardware can be used to conduct impedance measurements, in order to e.g. monitor ageing and anomalous cell(s). In case a "bad" cell is identified, it could be bypassed if cells have individual cell circuit breakers. This is, however, probably far from commercially viable at cell level. It can also be important to have capabilities to validate BMS failures as well as sensor failures by having increased redundancy.

## GENERAL AND BROAD RISK ASSESSMENT

A risk assessment is a well-established important method in order to determine risks. There are various types of risk assessment procedures and all of them need adequate reference data (input-data). The input-data, i.e. the existing knowledge, is crucial for the robustness of the assessment. With poor input-data the risk assessment will generate unreliable output-data and not the desired adequate risk determination. At present, major parts of the input-data, particularly for large battery systems, are missing or have too low quality.

Below is a general simplified risk assessment for Li-ion batteries presented. The risk assessment aims to be broad and general, covering Li-ion batteries from small size to large size Li-ion battery systems, for various applications and environments, and the method therefore needs to be simplified. The Li-ion battery hazards are identified and listed and the risk assessment is presented in two tables, Table 4 and Table 5. Table 4 presents the hazards and its sources and how the sources typically can be mitigated or hindered (protection strategy). All hazards in Table 4 can potentially come from any of the sources. In Table 5 the

same hazards are presented together with its consequences as well as possible mitigation strategies.

The probability and the severity of each hazard are not quantified in detail, since there are not enough data available to determine that. Consequently it is not possible to present the rating, i.e. probability multiplied by severity. The ultimate goal of a risk assessment is to present the real-world risks. In order to do that probability, severity and ratings are needed for each hazard and for each battery type/size and application/environment conditions. Today, some values might be estimated for small sized Li-ion batteries in consumer products, e.g. a general cell failure rate of about 1 ppm, as described in the introduction, anyhow it is difficult to apply such data to the detailed hazards in the presented general risk assessment. The data from field failures in large Li-ion battery systems are very limited since there are yet too few systems and incident statistics available. The risks are also depending on the battery use, the environmental conditions and the battery applications. That is, unfortunately not all risk numbers are known. Therefore, it is not possible today to conduct a full covering real-world risk assessment and it is particularly difficult for large Li-ion systems. Anyhow, risk assessments have to be conducted and are important, however, the risk assessment, if done properly, can only be as good as the available reference data. Statistical data from incidents in the field and investigations of such incidents will obviously be important input-data to improve future Li-ion battery risk assessments.

The risks typically have a strong dependence of battery size and application as well as the application environment. The focus has for some time been on reducing the risk of fire for Li-ion cells by several approaches, e.g. by increased onset temperatures, more stable and less reactive cell materials, use of flame retardants etc. For consumer Li-ion batteries a fire is typically a worst case scenario that should be avoided. However, for large Li-ion battery systems, things become much more complex and the risk analysis is significantly more challenging to conduct because it is a new technology and e.g. statistics, failure distribution, consequences and mechanisms of the risks are still not well known. Especially for large battery system, risks associated with flammable and toxic gases can induce dangerous situations in terms of gas explosion and lethal gas concentrations in the battery vicinity. If in the future it is found that fire should by all means be avoided the gas threat must anyhow be removed by changing the cell chemistry or by other means, e.g. ventilation, minimization of the size of the cell(s) involved etc. A fire is a potential source of further fire spreading within buildings/vehicles/vessels and should of course be avoided (or handled, e.g. by fire fighting)

however not to the cost of a much more severe gas explosion or potential toxic gas emission release. However, there are no publicly available studies about these complex aspects and the author is not aware of any studies/reports that even mention/discuss this matter. Consequently, there is a huge need for future studies about this.

Table 4. General simplified risk assessment of Li-ion batteries for all battery sizes/applications; hazard, its sources and mitigation/protection.

<table>
<tr><th>Hazard</th><th>Source</th><th>Mitigation/protection strategy</th><th>Probability</th><th>Severity</th><th>Rating</th></tr>
<tr><td rowspan="10">1. Swelling<br>(but no gas release)<br>2. Gas release / venting:<br>2.1 Toxic gas emissions<br>2.2 Corrosive acid / gas<br>2.3 Gas explosion*<br>3. Electrolyte leakage<br>4 High cell pressure<br>4.1 Cell case rupture<br>4.2 Cell case explosion<br>5. High temperatures<br>6 Gas explosion**<br>7. Fire***<br>7.1 Fire in battery cell<br>7.2 Fire in battery pack material</td><td>External heating</td><td>If minor, BMS by cooling via thermal management system</td><td colspan="3" rowspan="11">Lack of data to conduct</td></tr>
<tr><td>External fire</td><td>Fire barriers, fire fighting</td></tr>
<tr><td>Mechanical cross / deformation / penetration</td><td>Battery protected box, reinforced deformation structure, placing of the battery.</td></tr>
<tr><td>Short circuit, external cell</td><td>Circuit breakers, e.g. fuse</td></tr>
<tr><td>Short circuit, internal cell</td><td>Not possible for cell, propagation protection by system</td></tr>
<tr><td>Overcharge</td><td>BMS, possible cell internal cell safety mechanisms</td></tr>
<tr><td rowspan="4">Overdischarge</td><td rowspan="4">BMS</td></tr>
<tr></tr>
<tr></tr>
<tr></tr>
<tr><td rowspan="2">8. Electrical voltage hazards</td><td>BMS fault</td><td rowspan="2">Electrical insulation, correct personal handling technique and equipment.</td></tr>
<tr><td>Mechanical cross / deformation / penetration</td></tr>
</table>

** Gas explosion of battery vented gases, at relatively low temperature without a thermal runaway, can generate a gas explosion in case of ignition and within the flammability limit.*
*** Gas explosion of battery vented gases, in case of thermal runaway having its own ignition source (e.g. cell temperature higher than autoignition temperature, spark) in case of within the flammability limit.*
**** Fire from the battery cell and/or from fire of non-cell material, e.g. plastics, cables, electronics, within the battery system.*

Table 5. General simplified risk assessment of Li-ion batteries for all battery sizes/applications; hazard, its consequence and mitigation/protection.

| Hazard | Consequence (worst case) | Possible mitigation / protection strategy | Probability | Severity | Rating |
|---|---|---|---|---|---|
| 1. Swelling (but no gas release) | Acute safety typical ok, a balloon of flammable gases have increased fire risks. | • BMS<br>• Detection and remove/replace cell probably important. | Lack of data to conduct | | |
| 2. Gas release / venting:<br>2.1 Toxic gas emissions<br>2.2 Corrosive acid / gas<br><br>2.3 Gas explosion* | Acute toxicity<br><br>*See point 6.* | • Early detection – warning and personal evacuation<br>• Propagation mitigation (limit problem size/severity)<br>• Battery placing<br>• Ventilation<br>• Detox (anti-dote) gas filters<br><br>*See point 6.* | | | |
| 3. Electrolyte leakage | Increased risk of fire (flammable vapours) and toxicity (of decomposition products). | • Ventilation<br>• No heat/ignition sources | | | |
| 4 High cell pressure<br>4.1 Cell case rupture<br><br>4.2 Cell case explosion | Spreading out of combustible material, increased fire risk.<br>Ballistic projectile hazards for persons/vehicles/etc. | • Cell designed to release gas before extreme internal pressure is reached<br><br>• Ballistic projectile protection | | | |
| 5. High temperatures | Burn hazards for persons, ignition source | • Cooling by thermal management system (if still operational) | | | |
| 6 Gas explosion** | Damage to building and persons, potentially severe (life threating). | • Pressure release in battery pack<br>• Propagation mitigation (lower amount of gas)<br>• Ventilation (dilution)<br>• Pilot flame / controlled ignition | | | |
| 7. Fire***<br>7.1 Fire in battery cell<br>7.2 Fire in battery pack material | Heat release<br>Fire source to spread to adjacent structures. | • Propagation mitigation<br>• Fire fighting | | | |
| 8. Electrical voltage hazards | From small burn to potential lethal injury. | • Insulation<br>• Floating ground<br>• BMS<br>• Adequate personnel training on electrical hazards and equipment | | | |

**, **, *** See notes in Table 4.*

# CONCLUSIONS

Lithium-ion battery safety is complex and a holistic perspective is needed. The safety aspects differ significantly between small Li-ion batteries in consumer products and for large sized Li-ion battery systems used in e.g. electrified vehicles, electrical grid and vessels at sea. Risks should not be overestimated and there can sometimes be a tendency in media to report battery fires improperly, since battery fires seem to have a rather large news value. The risks and failure mechanisms for Li-ion batteries are still not well known and some areas have been studied to a very limited extent. Examples of areas that need considerable more studies in the future are size scaling effect for large battery systems of various types and for different environments, propagation protection, ageing effects on safety, fire fighting, toxic gas emissions and gas explosion risks. So far failure statistics are limited, particularly for large Li-ion battery system. Because of the lacking knowledge today, a complete risk assessment can simply not be performed. Furthermore, without that knowledge, counteractions cannot be studied/developed to handle potentially severe but still unknown risks. With further studies in the future, adequate risk assessments can be conducted as well as the very important development of counteractions to mitigate risks.

An external fire that spreads to the battery is a probable event that no built-in battery safety mechanism can protect against. Significant amounts of toxic hydrogen fluoride, 20-200 mg/Wh, can be emitted from Li-ion battery fires. Gases can be released before and without going into thermal runaway. If these gases are not instantly ignited a gas explosion can occur if the gases are mixed with air in a confined space and later ignited, e.g. by spark or autoignition (by contact to a hot surface). LFP cells are considerably less thermally active, and ignite more seldom, however, the gas threat might potentially be more severe in terms of gas explosion and toxic gas emissions although this is not studied in the present work, or elsewhere found, at least not publically.

Examples of methods that can offer increased safety are firewalls between modules and suffocation methods for metal-air battery cells. Firewalls have been shown to give significantly propagation protection according to the simulation studies, hindering a thermal event from propagation is essential for battery pack safety. Suffocation might offer an additional safety protection strategy via air shut-down for metal-air batteries without damaging the battery performance.

# RECOMMENDATIONS FOR FURTHER RESEARCH

A wide perspective is essential, including e.g. failure type, battery size, application and environment. Some battery safety aspects need general extra attention:

- Size scaling effect for large battery systems of various types and environments
- Propagation protection/mitigation
- Toxic gas emissions
- Gas explosion (delayed ignition of vented battery gases)
- Fire fighting
- Ageing effects on safety
- Finding counteractions to mitigate risks, especially from gas threats and for large Li-ion batteries.

It is recommended that the use of fluorine components and additives in Li-ion cells are minimized even if those compounds have positive effects from other points of view. In general, a holistic perspective is needed in terms of safety (e.g. heat, fire, toxicity, gas explosion). It is essential to investigate future incidents and compile better failure statistical data including failure mechanism, probability and severity to use in risk assessments. It is also important to follow the development of high energy density batteries, since these have a general built-in increased safety risk. It is recommended to include safety aspects earlier in the research and development (R&D) processes to have safety built-in, instead of trying to achieve high safety at the end of the R&D process, by adding safety additives or functions.

# REFERENCES


[1] G. E. Blomgren, "The development and future of lithium ion batteries", *Journal of The Electrochemical Society*, 164 (1), A5019-A5025 (2017).

[2] A. Hammami, N. Raymond, M. Armand, "Runaway risk of forming toxic compounds", *Nature*, 424, 635-636 (2003).

[3] Z. Chen, Y. Qin, Y. Ren, W. Lu, C. Orendorff, E. P. Roth, K. Amine, "Multi-scale study of thermal stability of lithiated graphite", *Energy & Environmental Science*, 4, 4023-4030 (2011).

[4] Q. Wang, P. Ping, X. Zhao, G. Chu, J. Sun, C. Chen, "Thermal runaway caused fire and explosion of lithium ion battery", *Journal of Power Sources*, 208, 210-214 (2012).

[5] https://www.tesla.com/blog/battery-cell-production-begins-gigafactory (accessed on 13 June 2017).

[6] http://www.washingtonpost.com/wp-dyn/content/article/2006/10/24/AR2006102400278.html (accessed on 12 August 2017)

[7] Samsung Note 7: Press Conference Details, Samsung US, Our safety promise, http://www.samsung.com/us/explore/committed-to-quality/?CID=van-brd-brd-0119-10000141 (accessed on 13 June 2017).

[8] http://www.expressen.se/kvallsposten/brand-i-dator-dodade-fem-personer/ (accessed on 16 August 2017).

[9] O. Andersson, "Fire hazard in laptop computers", Department of Fire Safety Engineering and Systems Safety, *Lund University*, Report 5364, ISSN: 1402-3504, ISRN: LUTVDG/TVBB--5364--SE, Lund, Sweden (2011).

[10] "Chevrolet Volt battery incident overview report", *National Highway Traffic Safety Administration (NHTSA)*, USA, Washington, DC, DOT HS 811 573, January 2012.

[11] "Investigation PE 13-037*"; National Highway Traffic Safety Administration (NHTSA)*, USA, Washington, DC (2014), available online: http://www-odi.nhtsa.dot.gov/acms/cs/jaxrs/download/doc/UCM452870/ INCLA-PE13037-2071.PDF (accessed on 13 June 2017).

[12] https://www.tesla.com/blog/tesla-adds-titanium-underbody-shield-and-aluminum-deflector-plates-model-s?redirect=no (accessed on 19 August 2017)

[13] http://www.st.nu/medelpad/ange/miljonbilen-gick-upp-i-rok-i-ljungaverk-tesla-skakas-av-ny-brand (accessed on 13 June 2017).

[14] M. Ahrens, "Automobile Fires in the U.S.: 2006–2010 Estimates", Conference proceedings of Fires in vehicles (FIVE) 2012, Chicago, 27-28 September 2012, edited by P. Andersson, B. Sundström, *SP Technical Research Institute of Sweden*, Borås, Sweden, p. 95-104 (2012).

[15] F. Larsson, P. Andersson, B.-E. Mellander, "Are electric vehicles safer than combustion engine vehicles?", in: Systems perspectives on Electromobility, edited by B. Sandén, P. Wallgren, *Chalmers University of Technology*, Göteborg, Sweden, ISBN 978-91-980973-9-9, p. 33-44 (2014).

[16] "Aircraft Serious Incident Investigation Report, JA804A", *Japan Transport Safety Board*, Tokyo, Japan (2014), available online: http://www.mlit.go.jp/jtsb/eng-air_report/JA804A.pdf (accessed on 13 June 2017).

[17] "Auxiliary Power Unit Battery Fire, Japan Airlines Boeing 787-8, JA829J, Boston, Massachusetts; NTSB/AIR-14/01", National Transportation Safety Board, Washington, DC, USA (2014), available online: http://www.ntsb.gov/investigations/AccidentReports/Reports/AIR1401.pdf (accessed on 13 June 2017).

[18] http://abcnews.go.com/US/lithium-batteries-spark-catastrophic-plane-fires-faa-warns/story?id=36816040 (accessed on 13 June 2017).

[19] International Air Transport Association (IATA). Lithium Batteries as Cargo in 2016 Update III, (2016), available online: http://www.iata.org/whatwedo/cargo/dgr/Documents/lithium-battery-update.pdf (accessed on 28 June 2017).

[20] M. Prigg, "Nasa reveals shocking video of secretive military 'RoboSimian' EXPLODING as its batteries catch fire" (2016), http://www.dailymail.co.uk/sciencetech/article-3883158/Nasa-reveals-shocking-video-secretive-military-RoboSimian-EXPLODING-batteries-catch-fire.html (accessed on 13 June 2017).

[21] B. Scrosati, K. M. Abraham, W. van Schalkwijk, J. Hassoun, "Lithium batteries advanced technologies and applications", *Wiley*, The electrochemical society series, USA (2013).

[22] J. Kalhoff, G. G. Eshetu, D. Bresser, S. Passerini, "Safer electrolytes for lithium-ion batteries: state of the art and perspectives", *ChemSusChem*, 8, 2154-2175 (2015).

[23] D. Kushnir, B. A. Sandén, "The time dimension and lithium resource constraints for electric vehicles", *Resources Policy*, 37, 93–103 (2012).

[24] K. Vignarooban, R. Kushagra, A. Elango, P. Badami, B.-E. Mellander, X. Xu, T.G. Tucker, C. Nam, A.M. Kannan, ”Current trends and future challenges of electrolytes for sodium-ion batteries”, *International Journal of Hydrogen Energy*, 41, 2829-2846 (2016).
[25] E. Cabrera-Castillo, F. Niedermeier, A. Jossen, “Calculation of the state of safety (SOS) for lithium ion batteries”, *Journal of Power Sources*, 324, 509-520 (2016).
[26] E. P. Roth, C. J. Orendorff, “How electrolytes influence battery safety”, *The Electrochemical Society Interface*, summer 2012, 45-49 (2012).
[27] F. Larsson, B.-E. Mellander, “Energy storage system safety in electrified vehicles”, Conference proceedings of Fires in vehicles (FIVE) 2012, Chicago, 27-28 September 2012, edited by P. Andersson, B. Sundström, *SP Technical Research Institute of Sweden*, Borås, Sweden, p. 303-306 (2012).
[28] A. W. Golubkov, D. Fuchs, J. Wagner, H. Wiltsche, C. Stangl, G. Fauler, G. Voitic, A. Thaler, V. Hacker, “Thermal-runaway experiments on consumer Li-ion batteries with metal-oxide and olivin-type cathodes”, *RSC Advances*, 4, 3633-3642 (2014).
[29] A. W. Golubkov, S. Scheikl, R. Planteu, G. Voitic, H. Wiltsche, C. Stangl, G. Fauler, A. Thaler, V. Hacker, “Thermal runaway of commercial 18650 Li-ion batteries with LFP and NCA cathodes – impact of state of charge and overcharge”, *RSC Advances*, 5, 57171-57186 (2015).
[30] D. Doughty, E. P. Roth, “A general discussion of Li ion battery safety”, *The Electrochemical Society Interface*, summer 2012, 37-44 (2012).
[31] M. Fleischhammer, T. Waldmann, G. Bisle, B.-I. Hogg, M. Wohlfahrt-Mehrens, “Interaction of cyclic ageing at high-rate and low temperatures and safety in lithium-ion batteries”, *Journal of Power Sources*, 274, 432-439 (2015).
[32] D. H. Doughty and C. C. Crafts, “FreedomCAR electrical energy storage system abuse test manual for electric and hybrid electric vehicle applications”, Sandia report SAND2005-3123, *Sandia National Laboratories*, USA (2006).
[33] D. Doughty, “SAE J2464 Electric and hybrid electric vehicle rechargeable energy storage system (RESS) safety and abuse testing procedure”, *SAE Technical Paper* 2010-01-1077 (2010).
[34] UL 1642, "Standard for Safety Lihtium Batteries", Fifth Edition, *Underwriters Laboratories Inc.*, USA (2012).
[35] “Recommendations on the Transport of dangerous goods, Manual of tests and test criterias”, Fifth edition, Sub-section 38.3, United Nations (2009).
[36] W. Zhao, G. Luo, C.-Y. Wanga, "Modeling Nail Penetration Process in Large-Format Li-Ion Cells", *Journal of The Electrochemical Society*, 162 (1), A207-A217 (2015).
[37] M. Rona, Y. Hyung, B. Barnett, S. Sriramulu, "The relationship of the nail penetration test to safety of Li-ion cells", *2013 DOE annual merit review meeting*, May 13-17 2012, Tiax Llc. (2012), available online: https://energy.gov/sites/prod/files/2014/03/f13/es142_sriramulu_2013_p.pdf (accessed on 19 August 2017).
[38] EN 13823:2010, “Reaction to fire tests for building products – building products excluding floorings exposed to the thermal attack by a single burning item”, *European Committee for Standardization* (2010).
[39] EN 13501-1:2007+A1:2009, “Fire classification of construction products and building elements - part 1: classification using data from reaction to fire tests”, *European Committee for Standardization* (2009).
[40] P. Andersson, P. Blomqvist, A. Lorén, F. Larsson, “Investigation of fire emissions from Li-ion batteries”, *SP Technical Research Institute of Sweden*, Borås, Sweden, SP Report 2013:15, ISBN 978-91-87461-00-2 (2013).
[41] ISO 19702:2006, “Toxicity testing of fire effluents -- guidance for analysis of gases and vapours in fire effluents using FTIR gas analysis”, *International Organization for Standardization* (2006).
[42] J. Jeevarajan, “Safety of commercial lithium-ion cells and batteries”, Chapter 17 in Lithium-Ion Batteries: Advances and Applications, edited by G. Pistoia, *Elsevier*, Amsterdam, The Netherlands, p. 387-407 (2014).
[43] X. Liu, Z. Wu, S. I. Stoliarov, M. Denlinger, A. Masias, K. Snyder, “Heat release during thermally-induced failure of a lithium ion battery: impact of cathode composition”, *Fire Safety Journal*, 85, 10-22 (2016).
[44] R. E. Lyon, R. N. Walters, “Energetics of lithium ion battery failure”. *Journal of Hazardous Materials*, 318, 164-172 (2016).
[45] R. J. Harris, “The investigation and control of gas explosions in buildings and heating plants”, *British gas corporation*, Midlands, England (1983).
[46] S. Bertilsson, “Thermal and infrared analysis of a lithium-ion battery electrolyte and its vapours for safety assessments”, Master thesis, *Chalmers University of Technology* (2017).

[47] G. Eshetu, S. Grugeon, S. Laruelle, S. Boyanov, A. Lecocq, J.-P. Bertrand, G. Marlair, "In-depth safety-focused analysis of solvents used in electrolytes for large scale lithium ion batteries", *Physical Chemistry Chemical Physics*, 15, 9145-9155 (2013).
[48] Safety Data Sheet, http://www.sigmaaldrich.com (accessed 7 August 2017).
[49] Safety Data Sheet, http://www.merckmillipore.com (accessed 7 August 2017).
[50] Material Safety Data Sheet, http://www.sciencelab.com (accessed 7 August 2017).
[51] J. Sun, J. Li, T. Zhou, K. Yang, S. Wei, N. Tang, N. Dang, H. Li, X. Qiu, L. Chen, "Toxicity, a serious concern of thermal runaway from commercial Li-ion battery", *Nano Energy*, 27, 313–319 (2016).
[52] N. P. Lebedeva, L. Boon-Brettz, "Considerations on the Chemical Toxicity of Contemporary Li-Ion Battery Electrolytes and Their Components", *Journal of The Electrochemical Society*, 163 (6), A821-A830 (2016).
[53] A. Nedjalkov, J. Meyer, M. Köhring, A. Doering, M. Angelmahr, S. Dahle, A. Sander, A. Fischer, W. Schade, "Toxic Gas Emissions from Damaged Lithium Ion Batteries—Analysis and Safety Enhancement Solution", *Batteries*, 2, 5 (2016).
[54] Y.-U. Park, D.-H. Seo, B. Kim, K.-P. Hong, H. Kim, S. Lee, R. A. Shakoor, K. Miyasaka, J.-M. Tarascon, K. Kang, "Tailoring a fluorophosphate as a novel 4 V cathode for lithium-ion batteries", *Scientific Reports*, 2, article number 704 (2012).
[55] G. F. Ortiz, M. C. López, Y. Li, M. J. McDonald, M. Cabello, J. L. Tirado, Y. Yang, "Enhancing the energy density of safer Li-ion batteries by combining high-voltage lithium cobalt fluorophosphate cathodes and nanostructured titania anodes", *Scientific Reports*, 6, article number 20656 (2016).
[56] H.-B. Kim, B.-C. Park, S.-T. Myung, K. Amine, Jai Prakash, Y.-K. Sun, "Electrochemical and thermal characterization of $AlF_3$-coated $Li[Ni_{0.8}Co_{0.15}Al_{0.05}]O_2$ cathode in lithium-ion cells", *Journal of Power Sources*, 179, 347–350 (2008).
[57] A. Aboulaich, K. Ouzaouit, H. Faqir, A. Kaddami, I. Benzakour, I. Akalay, "Improving thermal and electrochemical performances of $LiCoO_2$ cathode at high cut-off charge potentials by $MF_3$ (M=Ce, Al) coating", *Materials Research Bulletin*, 73, 362–368 (2016).
[58] H. Yang, G. V. Zhuang, P. N. Ross Jr, "Thermal stability of $LiPF_6$ salt and Li-ion battery electrolytes containing $LiPF_6$", *Journal of Power Sources*, 161, 573-579 (2006).
[59] T. Kawamura, S. Okada, J.-i. Yamaki, "Decomposition reaction of $LiPF_6$-based electrolytes for lithium ion cells", *Journal of Power Sources*, 156, 547-554 (2016).
[60] "Documentation for immediately dangerous to life or health concentrations (IDLHs) for hydrogen fluoride (as F)", *The National Institute for Occupational Safety and Health (NOISH)* (1994).
[61] "Acute exposure guideline levels for selected airborne chemicals: volume 4, subcommittee on acute exposure guideline levels", ISBN: 0-309-53013-X, Committee on Toxicology, *National Research Council* (2004).
[62] A. Middelman, "Hygiensiska gränsvärden AFS 2015:7, Hygieniska gränsvärden". Arbetsmiljöverkets föreskrifter om hygieniska gränsvärden och allmänna råd om tillämpningen av föreskrifterna, ISBN 978-91-7930-628-1, ISSN 1650-3163, *Swedish Work Environment Authority* (2015).
[63] R. Yazami, A. Martinent, "Fluorinated anions and electrode/electrolyte stability in lithium batteries", in: edited by T. Nakajima, H. Groult, *Fluorinated Materials for Energy Conversion*, Elsevier, Paris, pp. 173-194 (2015).
[64] P. Ribière, S. Grugeon, M. Morcrette, S. Boyanov, S. Laruelle, G. Marlair, "Investigation on the fire-induced hazards of Li-ion battery cells by fire calorimetry", *Energy & Environmental Science*, 5, 5271-5280 (2012).
[65] A. Lecocq, G. G. Eshetu, S. Grugeon, N. Martin, S. Laruelle, G. Marlair, "Scenario-based prediction of Li-ion batteries fire-induced toxicity", *Journal of Power Sources*, 316, 197-206 (2016).
[66] A. Lecocq, M. Bertana, B. Truchot, G. Marlair, "Comparison of the fire consequences of an electric vehicle and an internal combustion engine vehicle", ", Conference proceedings of Fires in vehicles (FIVE) 2012, Chicago, 27-28 September 2012, edited by Petra Andersson, Björn Sundström, *SP Technical Research Institute of Sweden*, Borås, Sweden, p. 183-193 (2012).
[67] M. D. Chatelain, T. E. Adams, "Lithium ion gas sampling of vented cells", *Proceedings of the Power Sources Conference*, 42, 87-89 (2006).
[68] A. F. Blum, R. T. Long Jr, "Hazard Assessment of Lithium Ion Battery Energy Storage Systems", *Fire Protection Research Foundation*, USA, MA, Quincy (2016).
[69] D. Hill, "Final Report, Considerations for ESS Fire Safety", Consolidated Edison, New York, NY, Report No.: OAPUS301WIKO(PP151894), *DNV GL*, Rev. 3, January 18 (2017).
[70] T. Ohsaki, T. Kishi, T. Kuboki, N. Takami, N. Shimura, Y. Sato, M. Sekino, A. Satoh, "Overcharge reaction of lithium-ion batteries", *Journal of Power Source*, 146, 97-100 (2005).

[71] D.P. Abraham, E.P. Roth, R. Kostecki, K. McCarthy, S. MacLaren, D.H. Doughty, "Diagnostic examination of thermally abused high-power lithium-ion cells", *Journal of Power Sources*, 161, 648-657 (2006).
[72] E.P. Roth, "Abuse response of 18650 Li-ion cells with different cathodes using EC:EMC/$LiPF_6$ and EC:PC:DMC/$LIPF_6$ electrolytes", *ECS Transactions*, 11 (19), 19-41 (2008).
[73] N. S. Spinner, C. R. Field, M. H. Hammond, B. A. Williams, K. M. Myers, A. L. Lubrano, S. L. Rose-Pehrsson, S. G. Tuttle, "Physical and chemical analysis of lithium-ion battery cell-to-cell failure events inside custom fire chamber", *Journal of Power Sources*, 279, 713-721 (2015).
[74] Y. Fu, S. Lu, K. Li, C. Liu, X. Cheng, H. Zhang, "An experimental study on burning behaviors of 18650 lithium ion batteries using a cone calorimeter", *Journal of Power Sources*, 273, 216-222 (2015).
[75] P. Huang, Q. Wang, K. Li, P. Ping, J. Sun, "The combustion behavior of large scale lithium titanate battery", *Scientific Reports*, 5, article number 7788 (2015).
[76] P. Ping, Q. Wang, P. Huang, K. Li, J. Sun, D. Kong, C. Chen, "Study of the fire behavior of high-energy lithium-ion batteries with full-scale burning test", *Journal of Power Sources*, 285, 80-89 (2015).
[77] E. P. Roth, C. J. Orendorff, "How electrolytes influence battery safety", *The Electrochemical Society Interface*, summer 2012, 45-49 (2012).
[78] G. G. Eshetu, S. Grugeon, S. Laruelle, S. Boyanov, A. Lecocq, J.-P. Bertrand, G. Marlair, "In-depth safety-focused analysis of solvents used in electrolytes for large scale lithium ion batteries", *Physical Chemistry Chemical Physic*, 15, 9145-9155 (2013).
[79] J. Lamb, C. J. Orendorff, E. P. Roth, J. Langendorf, "Studies on the Thermal Breakdown of Common Li-Ion Battery Electrolyte Components", *Journal of The Electrochemical Society*, 162 (10), A2131-A2135 (2015).
[80] G. G. Eshetu, J.-P. Bertrand, A. Lecocq, S. Grugeon, S. Laruelle, M. Armand, G. Marlair, "Fire behavior of carbonates-based electrolytes used in Li-ion rechargeable batteries with a focus on the role of the $LiPF_6$ and LiFSI salts", *Journal of Power Sources*, 269, 804-811 (2014).
[81] P. Andersson, P. Blomqvist, A. Lorén, F. Larsson, "Using Fourier transform infrared spectroscopy to determine toxic gases in fires with lithium-ion batteries", *Fire and Materials*, 40 (8), 999-1015 (2016).
[82] S.F. Lux, I.T. Lucas, E. Pollak, S. Passerini, M. Winter, R. Kostecki, "The mechanism of HF formation in $LiPF_6$ based organic carbonate electrolytes", *Electrochemistry Communications*, 14, 47–50 (2012).
[83] S. F. Lux, J. Chevalier, I. T. Lucas, R. Kostecki, "HF formation in $LiPF_6$-based organic carbonate electrolytes", *ECS Electrochemistry Letters*, 2 (12), A121-A123 (2013).
[84] S. Wilken, M. Treskow, J. Scheers, P. Johansson, P. Jacobsson, "Initial stages of thermal decomposition of $LiPF_6$-based lithium ion battery electrolytes by detailed Raman and NMR spectroscopy*", The Royal Society of Chemistry*, 3, 16359-16364 (2013).
[85] C. L. Campion, W. Li, W. B. Euler, B. L. Lucht, B. Ravdel, J. F. DiCarlo, R. Gitzendanner, K. M. Abraham, "Suppression of toxic compounds produced in the decomposition of lithium-ion battery electrolytes", *Electrochemical and Solid-State Letters*, 7 (7), A194-A197 (2004).
[86] A. Lönnermark, P. Blomqvist, "Emissions from Tyre Fires", *SP Technical Research Institute of Sweden*, Borås, Sweden, SP Report 2005:43, ISBN 91-85303-75-5, ISSN 0284-5172 (2005).
[87] S. Krüger, A. Hofmann, A. Berger, N. Gude, "Investigation of smoke gases and temperatures during car fire – large-scale and small-scale tests and numerical investigations", *Fire and Materials*, 40, 785-799 (2016).
[88] A. Lönnermark, P. Blomqvist, "Emissions from an automobile fire", *Chemosphere*, 62, 1043-1056 (2006).
[89] "Ignition behaviour of HFO1234yf", *Bundesanstalt für Materialforschung und -prüfung (BAM)*, Germany, BAM-ref: II-2318/2009, (2009). Available online: https://www.umweltbundesamt.de/sites/default/files/medien/419/dokumente/test_report_hfo1234yf_2010_06.pdf (accessed on 29 June 2017).
[90] ISO 13571:2012, "Life-threatening components of fire – Guidelines for the estimation of time to compromised tenability in fires", *International Organization for Standardization*, Geneva, Switzerland (2012).
[91] P.G. Balakrishnan, R. Ramesh, T. Prem Kumar, "Safety mechanisms in lithium-ion batteries", *Journal of Power Sources*, 155, 401-414 (2006).
[92] C. F. Lopez, J. A. Jeevarajan, P. P. Mukherjee, "Experimental analysis of thermal runaway and propagation in lithium-ion battery modules", *Journal of The Electrochemical Society*, 162 (9), A1905-A1915 (2015).
[93] J. Lamb, C. J. Orendorff, L. A. M. Steele, S. W. Spangler, "Failure propagation in multi-cell lithium-ion batteries", *Journal of Power Sources*, 283, 517-523 (2015).

# Paper I

*Journal of The Electrochemical Society*, **161** (10) A1611-A1617 (2014)
0013-4651/2014/161(10)/A1611/7/$31.00 © The Electrochemical Society


# Abuse by External Heating, Overcharge and Short Circuiting of Commercial Lithium-Ion Battery Cells

**Fredrik Larsson**[a,b,z] **and Bengt-Erik Mellander**[a]

[a]*Department of Applied Physics, Chalmers University of Technology, Goteborg SE-412 96, Sweden*
[b]*SP Technical Research Institute of Sweden, Boras SE-501 15, Sweden*

Lithium-ion batteries offer great energy and power densities but the thermal stability is an issue of concern compared to other battery technologies. In this study different types of abuse testing have been performed in order to compare the battery safety for different types of commercial lithium-ion battery cells. The results show large differences in abuse response for different cells. Exposed to external heating laptop cells with cobalt based cathode developed a thermal runaway resulting in pressure release, fire and temperatures over 700°C. Lithium iron phosphate (LFP) is known to be a very thermally stable cathode material and LFP-cells showed a significantly lower thermal response, a thermal runaway could, however, be detected for some of the cells in the external heating test. The overcharge tests of LFP-cells were in most cases uneventful but in one case the test resulted in a violent fire. The short circuit tests showed modest temperature increases of the cells in spite of high currents peaking at around 1000 A. Although the development of safer lithium-ion battery cells has been successful thermal runaway events may still occur under extreme conditions.
 [DOI: 10.1149/2.0311410jes] 

Manuscript submitted April 28, 2014; revised manuscript received June 4, 2014. Published July 11, 2014.

The high energy and power density of lithium-ion batteries have made them the preferred type of battery for battery electric vehicles as well as for plug-in hybrid electric vehicles. Lithium-ion batteries have many advantages but the reactive, volatile and flammable materials present in the battery are a concern and may be a threat to safety. Lithium-ion batteries are produced in large quantities, mainly for small consumer products such as cellular telephones and other portable electronic devices. Using them in electric vehicles poses another situation since the large size of the battery as well as the environmental conditions that the battery is exposed to in terms of temperature, vibrations etc have an influence on the safety. In addition, requirements such as long life time and the possibility for a fast recharge of the battery calls for other demands on the cells. All these aspects have an effect on the safety of the vehicle, including the safety for people inside and outside the vehicle, for service personnel involved in maintenance and of rescue personnel in case of an accident.

Lithium-ion batteries have a limited window of stability regarding temperature and voltage. Overheating may start exothermal reactions that release even more heat which in turn can lead to an accelerated process called a thermal runaway. A thermal runaway can be devastating if it spreads to a complete battery system, releasing large amounts of energy. Such a process could start due to overcharge, overdischarge, mechanical deformation, external heating or an external or internal short circuit, see Figure 1. The heat generated by any of these events may start exothermal reactions in the battery that in turn could lead to cell venting, fire or explosion.

These risks are well known[1–8] and are not only associated with the heat and high temperatures that may develop, the emission of harmful or poisonous gases also pose a danger that has been emphasized in literature,[9,10] but also other gases which can be flammable may be emitted.[11–13] The reactions during overheating are typically due to the decomposition of the solid electrolyte interphase (SEI) layer, anode and cathode as well as electrolyte decomposition and combustion.[5,14] These reactions are exothermal. In addition to this separator melting, an endotherm event, may occur. Oxygen may be released at the positive electrode during decomposition; this oxygen can provide the oxidant for the combustion of the electrolyte. Large efforts have been spent on improving the safety of Li-ion cells, e.g. by replacing the cobalt based electrode by lithium iron phosphate[15] which is more thermally stable and has long life time and high power density but lower energy density.[16] Another common practice for commercial cells is to use a number of additives to the electrolytes to improve safety, e.g. including fire retarders.[17–20]

Incidents involving lithium-ion batteries have been reported in small as well as large battery systems, see for example Wang et al.[21] and Mikolajczak et al.[22] Abuse tests of batteries are therefore of prime importance in order to evaluate and improve the level of safety for these types of battery systems. In this article results from abuse tests of commercial Li-ion batteries of different type, chemistry and size are presented to illustrate the problems that may arise under abnormal operating conditions.

## Experimental

Four types of commercial cells were tested; a Samsung 18650-cell, i.e. a cylindrical cell 18 mm in diameter and 65 mm long, typically used in laptops; two EiG cells of pouch-type with lithium iron phosphate ($LiFePO_4$) cathode, and a carbon-based anode (a newer and an older cell design); a European Batteries cell of pouch-type with lithium iron phosphate cathode and graphite anode. A summary of the cell specifications is provided in Table I. The EiG cells were optimized for power application while the European Batteries cell as well as the laptop cell was optimized for energy applications. All cells were fully charged, 100% State of Charge (SOC), according to the manufacturer's instructions.

Three types of abuse tests were performed; external heating, overcharge and short circuit tests. All measurements were performed in a similar but not identical condition as described in international test standards for batteries such as FreedomCAR[23] or SAE J2464.[24] Cells of different sizes, packaging, chemistries and manufacturers were tested. Most tests were repeated in order to account for the variations between individual cells. The tests presented in this paper are a selection of representative examples of these tests. For the Samsung 18650 cell only results from external heating tests are presented since overcharge and short circuit tests would not be of interest due the built-in cell protection mechanisms in the cell.

*External heating test.*— In the external heating test, the cells were heated to excessive temperatures in order to examine their thermal stability. This test is sometimes referred to as thermal ramp test. The tested cell was placed inside a thermostatically controlled oven, Binder FED 115. The oven has a microprocessor control and a PT 100 temperature sensor for internal regulation of oven temperature. The oven's internal fan was set on full speed in order to circulate the oven air to obtain a uniform temperature around the tested lithium-ion cell. The cells were placed on one or two bricks in the center of the oven and tested one at a time, see Figure 2. For the pouch cells the oven temperature was first set to 80°C and thereafter increased in steps of 10°C every 15 min until either any thermal runaway had occurred or to the maximum temperature of the oven (300°C). For the 18650 cell the oven was set to the maximum temperature (300°C) with continuous maximum heating. Both heading procedures were relatively slow.

[z]E-mail: vegan@chalmers.se

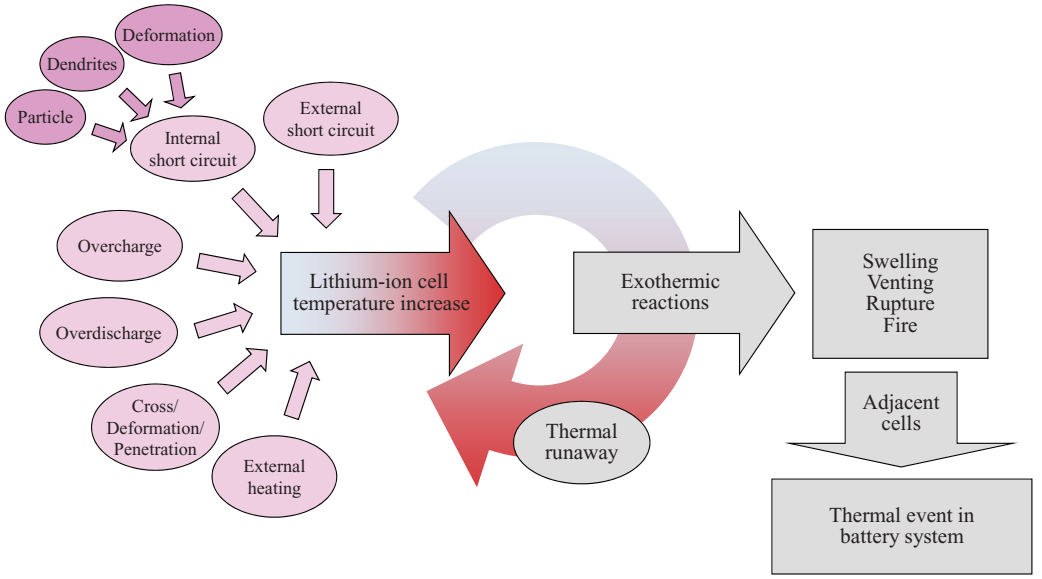


**Figure 1.** Lithium-ion thermal runaway overview from cell event to potential system event.

**Table I. Basic data of tested cells.**

| Cell type | Cell packaging | Nominal voltage (V) | Nominal capacity (Ah) |
|---|---|---|---|
| Samsung ICR18650–24F | Cylindrical | 3.6 | 2.4 |
| EiG ePLB-F007H *In article referred as "older design"* | Pouch | 3.2 | 7 |
| EiG ePLB-F007A *In article referred as "newer design"* | Pouch | 3.2 | 7 |
| European Batteries EBattery 45 Ah v1.4 | Pouch | 3.2 | 45 |

With the continuous heating method it took around 90 min for the oven to reach 200°C.

The cell voltage and the cell surface temperature were measured with a sample rate of 1 Hz with a data logger, Pico Technology ADC-24. There were up to five type K thermocouples evenly distributed on both sides of the cell's surface and one additional thermocouple measuring the oven temperature.

*Overcharge test.*— In the overcharge test, the lithium-ion cells were abused by being charged beyond their limits. The charger was limited to the preset maximum current of each experiment and up to max 15.3 V. The 7 Ah EiG cell was charged with 70 A (corresponding to 10 C-rate) considering that the cell is optimized for power applications while the 45 Ah European Batteries cell was overcharged with 90 A (corresponding to 2 C-rate) due to its optimization for energy applications. The cell surface temperature was measured with five type K thermocouples; one of the sensors was directly attached to the cell surface while four were so called plate-thermometers, that is a thermocouple attached to a 10 × 10 cm metal plate. The plate-thermometers were distributed around the cell, one directly under the cell, the others placed with an air gap from the cell. The current was measured using a current shunt (accuracy 0.5%). Cell voltage, current and temperature were measured with a sample rate of 1 Hz with a data logger, Pico Technology ADC-24.

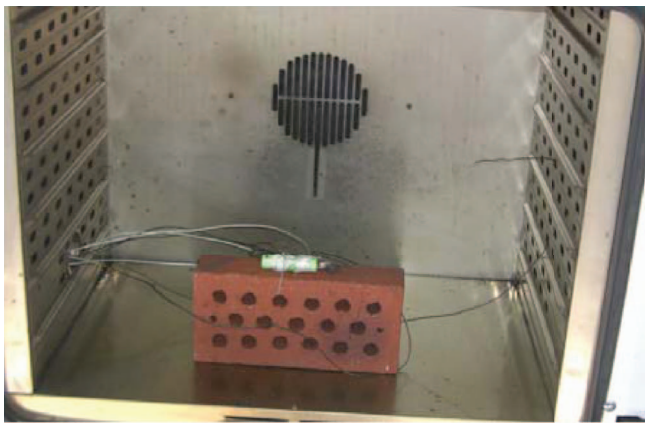

**Figure 2.** Photo of oven set up, showing a cylindrical 18650 cell fastened onto a brick with steel wire.

*Short-circuit test.*— EiG and European Batteries cells were short circuited using 50 $mm^2$ copper cables and a high current contactor, Telemecanique LC1F630, with a low internal resistance of 40 μΩ. The short circuit current was measured by a current core, Hitec 6000E Topacc 1.0, which can measure currents up to 6000 A. The cell surface temperature was measured with eighteen type K thermocouples equally distributed on both sides of the cell surface. The cell voltage, current and temperature were measured at 1 Hz using two data loggers, Pico Technology ADC-24 and Fluke Hydra Series II, as well as by a Tektronix TDS 3034 oscilloscope.

## Results

*External heating test.*— Figure 3 shows the results of an external heating test on the 18650 cell. At 220°C, a very rapid temperature increase occurs when the cell catches fire and a pressure wave is observed. The maximum average temperature at the cell surface reaches 743°C which is higher than the melting temperature of aluminum, 660°C. The maximum cell surface temperature measured by a single sensor was 775°C, the temperature of the cell interior was thus probably even higher. Based on the average surface temperature increase, the corresponding energy released from the thermal runaway

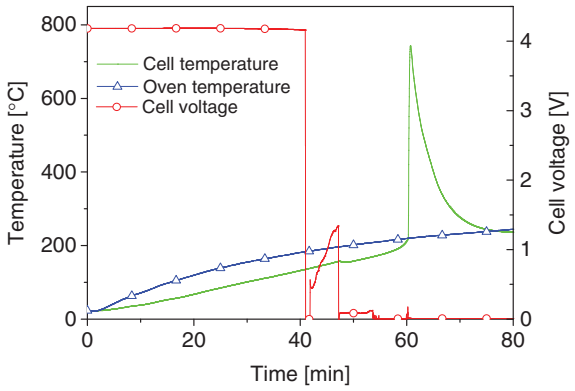


**Figure 3.** Temperature and cell voltage development during external heating of a Samsung 18650 cell.

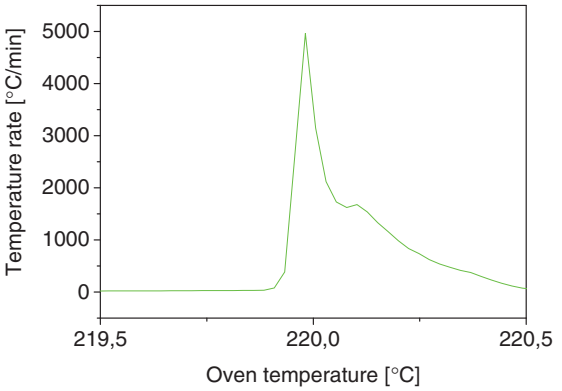


**Figure 5.** The rate of the cell surface temperature for the Samsung 18650 cell in the temperature region of the thermal runaway peak.

can be roughly estimated since the cell is likely to be under adiabatic conditions during the short duration of the thermal runaway, approximately 20 seconds. The specific heat capacity of a complete cell varies between cylindrical and pouch cell packaging and is also dependent on size, energy/power optimization etc. In the estimations we use an approximate value of 700 J/kg°C based on published values for different cell types.[5,25–29] Using the measured temperature increase of 523°C the energy released can be estimated to 15.6 kJ (4.33 Wh). The calculated released energy is thus about half of that of the electrical energy available in the cell, 8.64 Wh. It may also be noted that just prior to the runaway, burning electrolyte is squirting out of the cell seen in Figure 4, which releases energy which is not included in the above value for the energy release calculation. Figure 5 shows the derivative of the average cell surface temperature; the figure shows that the thermal runaway temperature is 220°C and that the rate of temperature increase is very high, initially close to 5000°C/min.

Cells with lithium iron phosphate (LFP) cathode have an enhanced thermal safety compared to cells with cobalt oxide based cathode. Figure 6 shows the results for two LFP-cells during external heating. The old cell design shows a clear but relatively small thermal runaway event while the new cell design shows no obvious signs of thermal runaway. Actually, a minor exothermic event, hardly visible in Figure 6, can be detected in the same temperature region as the thermal runaway in the old cell design also for the new cell design. The chemical and/or physical changes in the cell design are not known or studied in this report. Complementary experiments where the temperature was continuously increased also resulted in a similar behavior as that in Figure 6. The time to reach the thermal runaway temperature was approximately 90 minutes for the test using continuous heating and approximately 200 minutes for the test using temperature-ramping.

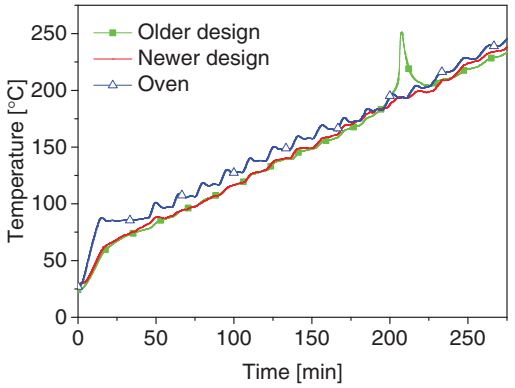


**Figure 6.** Temperature development during external heating of EiG newer and older cell design.

Figure 7 shows the results of the European Batteries cell during external heating. A moderate thermal runaway is detected also for this LFP-cell, with temperatures reaching well above 300°C. The runaway temperature was 183°C within ± 1°C for these cells, this value is close to the value observed for the older design EiG cell, 189°C. The runaway temperature was thus somewhat lower than for the laptop-type cell. The energy released at the detected thermal runaway estimated using the same method and specific heat capacity value as for the Samsung cell above is also much smaller than for the laptop cell. While the ratio of energy released to the electric energy stored in the fully charged battery is of the order of 50% for the laptop battery it is

**Figure 4.** Samsung 18650 cell at the beginning of thermal runaway releasing ignited material.

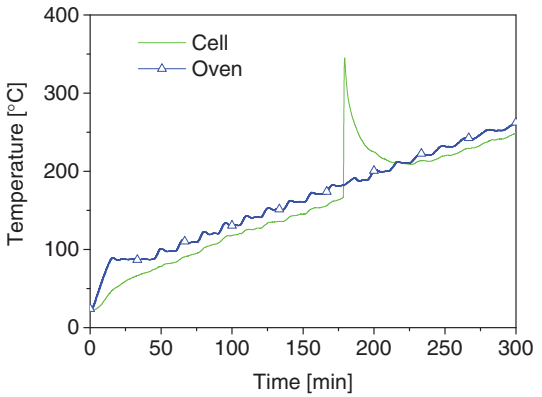


**Figure 7.** Temperature development during external heating of European Batteries cell.

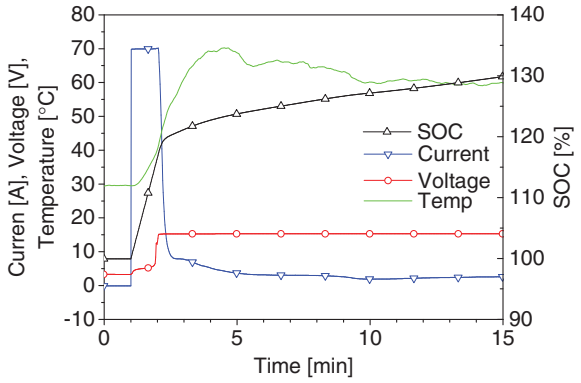


**Figure 8.** Overcharge of EiG cell of newer design.

between 10 and 30% for the LFP-type cells that showed a thermal runaway. The rates of temperature increase at the thermal runaway for the LFP-cells were 500°C/min for European Battery cell and 60°C/min for EiG older design while the rate was not detectable for EiG newer design. The 18650 cell lost 30% of its weight in the external heating tests while the LFP cells lost between 16–26%, the EiG new design had the lowest weight loss of 16%.

*Overcharge test.*— Figure 8 shows the result from an overcharge test of the EiG cell of newer design. The cell surface temperature reached a moderate temperature of 70°C. An almost negligible weight loss was measured, probably due to minor venting of electrolyte. The overcharge test for one of the European Batteries cells is shown in Figure 9. After approximately 5 minutes of charging at a state of charge level of 115%, the cell suddenly caught fire, as seen in Figure 10. The temperature reached 855°C for a sensor placed in the center of the top surface of the cell. During the fire, the top layer of the cell was blown away so the cell temperature presented in Figure 9 may include the temperature of the flames and does not reflect the cell temperature after this event.

The overcharge test on the European Batteries cells was repeated three more times without any occurrence of fire and Figure 11 shows the results of one of the repeated tests. The surface temperature reached a maximum of 79°C, a value comparable to that of the EiG cell. It may be noted that all overcharged cells were swollen with a thickness increase after the test ranging from 350 to 850% of the initial thickness.

*Short-circuit test.*— The results from short circuit tests for EiG cells of both newer and older design are shown in Figure 12. There were no significant differences between the two types of cells. Between 20 and 30 seconds after the start of the short circuit the cell swelled up quickly. The following 2 minutes the cell vented (with no visual smoke) and swelling decreased considerably. The following 5 minutes the cell contracted further to a thickness close to that of the untested cell. The peak current reached almost 900 A which corresponds to a discharge rate of 128C. The maximum cell surface

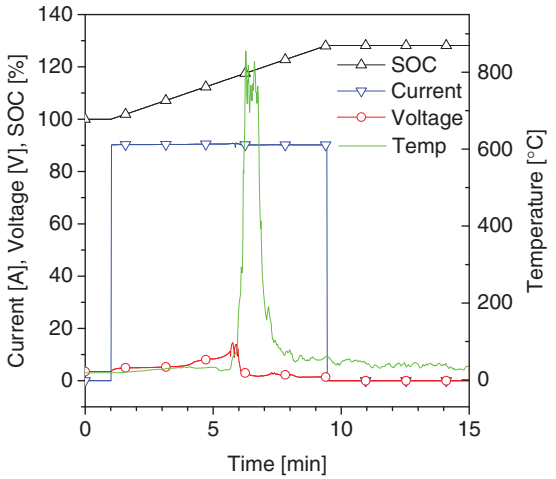


**Figure 9.** Overcharge of a European Batteries cell resulted in fire, in this case the charger was manually stopped at 9.5 min due to the fire.

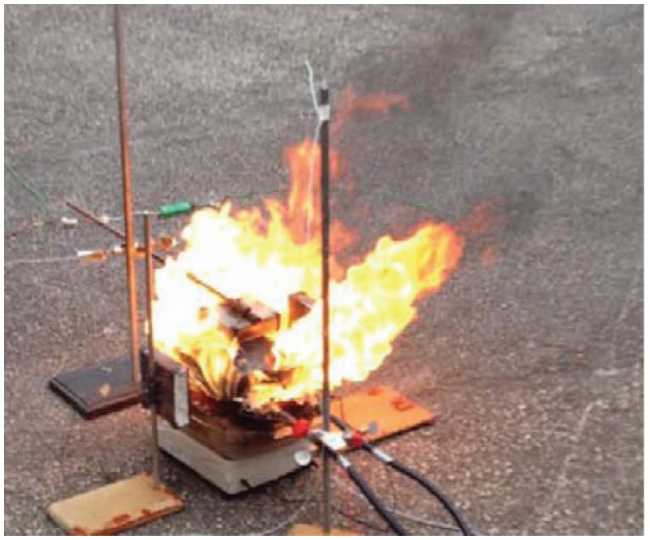

**Figure 10.** Overcharge of a European Batteries cell resulted in fire.

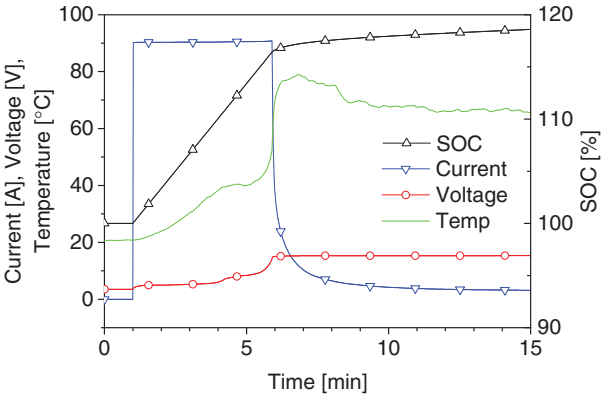


**Figure 11.** Overcharge of a European Batteries cell that did not result in a fire.

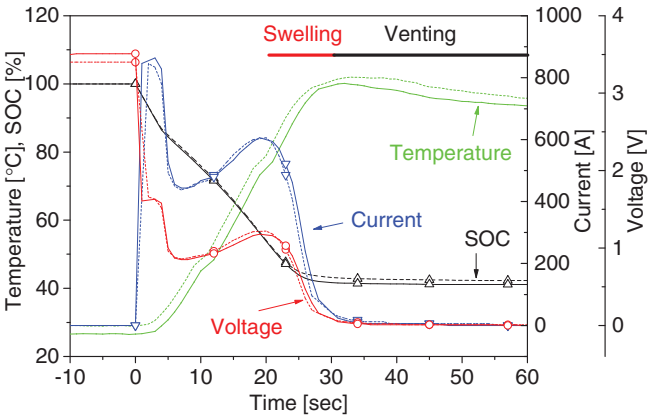


**Figure 12.** Short circuit of EiG cell of newer design (dashed lines) and EiG of older design (solid lines).

**Figure 13.** Short circuit of European Batteries cell, photo (left) showing the flame and smoke from the burnt off positive terminal tab, the photo (right) after the test shows the burnt off tab.

temperature was about 100°C and both types of cells were discharged to about 43% SOC.

In the short circuit test of the European Batteries cell the positive tab of the cell burnt off, which stopped the short circuit current, see Figure 13. The current just before this event was 1084 A and due to the very short time for the short circuit the cell temperature and SOC changed very little, less than 6°C and 4% respectively.

## Discussion

When the Samsung 18650 laptop cell was exposed to external heat, the open circuit voltage remained stable until about 135°C, measured on the cell surface, as seen in Figure 3, then it falls abruptly. The melting points of typical shutdown separator materials, polyethylene and polypropylene, are about 130 and 165°C, the measured values are thus reasonably close to these values, where the final voltage drop occurs at about 158°C. The difference may be due to a delay in the temperature measurement due to the slow heat transfer in the interior of the cell. The runaway temperature, 220°C, and the temperature increase during the thermal runaway, 532°C, is in the same order as reported in our previous study.[30] The rate of temperature increase in the initial phase of the thermal runaway is extremely high, close to 5000°C/min. Jhu et al.[28] found for a similar cell a peak value of about 37000°C/min with a more sensitive technique, and in another study by Jhu et al.[29] temperate rates beyond 70000°C/min were found. The state of charge can have a strong influence on the cell behavior during abuse situations and the influence may vary with different types of abuse. Jhu et al.[28,29] and Doughty et al.[17] showed that lower SOC gives lower energy release during external heating.

A comparison of the results of the external heating tests for the 18650 laptop cell (Figure 3) and the LFP-cells (Figure 6 and Figure 7) shows that the behavior is much less dramatic for the LFP-cells. Two of the three LFP-cells still go into thermal runaway but the energy released is much less than that from a cell with cobalt-based cathode. This is well-known from other studies[2,13,20,31–36] and attributed to the stability of the olivine structure of $LiFePO_4$. The electrode influence on the thermal stability of a LFP-cell is therefore dominated by the anode material. Swelling and venting occurred for all pouch-type cells while the laptop cell vented with a rapid release of gas, accompanied by a pressure wave and immediately followed by fire.

The runaway temperature for the LFP-cells was lower than for the laptop cell, 189°C for the EiG older design and 183°C for the European Batteries cell. The thermal runway in the external heating test for the new design of EiG is significantly reduced compared to that of the older design. It may be noted that the EiG cell is designed to target electrified vehicles in the automotive sector and is currently in use there. The rates of temperate increase at runaway differ considerably for the different cells; 5000°C/min for the Samsung laptop cell, 500°C/min for European Battery cell and 60°C/min for EiG older design. This highlights the large differences for Li-ion cells and particularly underlines the importance of thermal stability.

Cell venting is an important safety factor to protect a Li-ion battery from reaching too high pressure, especially in the case of cylindrical or hard prismatic cell packaging. In fact, cell manufacturers may include so called shutdown additives in the electrolyte in order to activate cell venting at a pre-designed stage by gas generation from polymerizing of the additive molecules, before the cell reaches extreme conditions.[20] Upon heating of a cell, ventilation is also unavoidable since the electrolyte typically consists of a Li-salt dissolved in volatile organic solvents. Even in cases when fire or explosion does not occur, emitted flammable and toxic gas can be a serious problem as mentioned in the introduction.

Abuse by overcharging and external heating adds energy to the system due to the input of electric power or heat, while in a short circuit test no energy is added to the cell. Therefore, the overcharge and external heating test can theoretically be seen as a more severe abuse due to the addition of external energy to the cell. In the overcharge tests presented the additional charged energy is between 20–30% in terms of battery capacity. The energy released in the external heating tests presented in this paper is calculated based on the change of the cell surface temperature and are of the order of 50% or less of the electrical energy within the cell. Those values do not represent the total energy release and neither the possible maximum energy release during the most severe abuse situations when the cell materials are allowed to fully combust. During the external heating, part of the electrolyte, and particularly low boiling components (e.g. dimethyl carbonate), can evaporate due to venting and cell opening. However, some electrolyte is still present since thermal runaway does occur. For example, for the 18650 cell, electrolyte is squirting out of the cell prior to the thermal runaway as seen in Figure 4, releasing energy which is not included in the calculations. Besides, several other parameters also affect the results e.g. abuse test methods, cell chemistry, capacity size, cell design and cell venting characteristics. Values typically found in the literature show a released energy of 2–3 times the electrical energy.[1,38] The results presented in this article are lower presumably due to the reasons discussed above. However, the energy release, 15.6 kJ, of the thermal runaway for the 18650 cell in the external heating test can be compared to 19.2 kJ measured for a similar 18650 cell.[28]

10 C-rate overcharge tests of the EiG newer design did not result in a thermal runaway and the peak surface temperature reached

a moderate 79°C. A similar result was obtained for one of the European Batteries cells, seen in Figure 11. However, one of the European Batteries cells that was overcharged ignited with a resulting fire. This behavior was not reproduced in three other tests. Excluding the ignited cell, no thermal runaway could be detected even though all cells were heavily affected by large swelling and venting. Hund and Ingersoll[38] studied 1 C-rate overcharge of LiFeBatt 10 Ah LFP cells which resulted in a significantly higher temperature of 160°C but no fire or sparks. He et al.[39] used 2 Ah LFP cells and found a temperature peak of 90°C without fire during 1 C-rate overcharging. The incident of the fire in our test is interesting but we can only speculate on the reason. It could be a bad cell due to errors in the manufacturing process or induced by some small variety in the test setup. An event like this in the field could be referred to as a field failure, but field failures rarely happens on cell-level, the probability is typically less than 1 ppm.[21,22] For an overcharge situation to occur in a battery system a failure of the Battery Management System (BMS) is required allowing the cell to be charged above it limits. Secondly, as we have seen above, the cell itself does not necessarily go into thermal runaway because it is overcharged. Studies have, however, shown that LFP-cells have a smaller margin with respect to the amount of overcharged capacity compared to other common Li-chemistries, although the exothermal response for LFP is significantly lower.[2]

The tested large-sized LFP pouch automotive cells have low internal resistance, enabling high short circuit currents known from other studies.[40] The short circuit current of the EiG cells was close to 900 A, corresponding to a 128 C-rate. These cells are power optimized and capable of delivering 20–30 C-rate in normal use. The short circuit current for the six times larger capacity European Batteries cell is close to 1100 A, i.e. a 24 C-rate. The European Batteries cell is energy optimized and made to deliver up to 4 C-rate in normal use. The cell voltage seen in Figure 12 drops quickly due to the short circuit, but does not reach 0 V instantly even if it is a hard short circuit with low connection resistance. The current curve in Figure 12 quickly rises and then falls to about half the value and then increases again. This behavior could be explained by the fact that the extreme current cannot be sustained due to limitations of the transport process of the lithium ion in the cell resulting in a current drop, while the cell is quickly heated due to the ohmic losses. The increased temperature finally enables a higher transportation of lithium ions resulting in an increased current. The time frame for these phases is less than 30 seconds as seen in Figure 12. No thermal runaway is observed, however the cell temperature increases fast during a short period of time.

The short circuit test of the European Batteries cell resulted in that the positive terminal tab burnt off as seen in Figure 13 which stopped the short circuit. In one perspective this can potentially be seen as positive for the safety since the tab functioned as a "fuse" that stopped the short circuit at an early stage. However the flame can be a potential source of ignition of e.g. vented and flammable battery gases or other easily ignitable materials inside a battery system.

Lithium-ion cells can be equipped with a variety of reversible and irreversible safety mechanisms.[41] The 18650 cells typically have protection for short circuit, by the use of for example CID (current interrupture device) and PTC (positive temperature coefficient), the latter causing the cell resistance to increase rapidly at increased temperature reducing the current going through the cell. Many of these safety mechanisms were developed specifically for the Li-ion consumer battery. The use of Li-ion batteries in other applications such as within automotive give rise to more and different demands on the safety as well as other aspects, e.g. cost, life time, energy and power density. The environmental conditions in automotive applications are different to those in consumer products; vibrations, extreme temperatures and varying humidity can be challenging. The risks involved in case of electric vehicle crash deformations must also be taken into consideration. In the automotive industry large capacity cells are required and typically hundreds of these are connected in series. Safety mechanisms within the cell used in commercial Li-ion battery systems do not always give the same protection in e.g. automotive applications. A first example is the shutdown separator which can give an increased safety for some cell abuse situations. However, the use of shutdown separators in a large battery pack with higher voltage due to hundreds of cells connected in series might not give the same safety due to e.g. voltage breakdown of the separator.[42,43] A second example is the PTC which has a relative low voltage tolerance in cell-strings, potentially as low as 30 V, which can result in spontaneous ignition in case of overvoltage.[44] Besides the safety concern the PTC also add parasitic resistance in a large battery pack. A third example is the CID which cannot offer the same safety in case of higher voltage systems.[44]

The battery module design as well as the rate of energy release and the total energy release from a thermal runaway in one cell determines if neighboring cells are effected or not. From a safety perspective it is essential to minimize the probability for a thermal event to occur but also to minimize the consequences of such an event and prevent damage to neighboring cells, avoiding the potential propagation of a thermal runaway from cell to system-level as shown in Figure 1.

## Conclusions

The abuse tests conducted on various types of Li-ion cells give valuable information regarding diverse aspects of the cell safety. Risks associated with thermal runaway situations; fire, smoke and gas emissions are especially important for the use of Li-ion batteries in automotive applications. The external heating test of the 18650 laptop cell resulted in a rapid thermal runaway accompanied with a pressure wave and immediate fire. In large battery packs using multiple cells in series and/or parallel the effect of a propagation scenario in thus a concern. Safer chemistries like the LFP-cells are in general significantly less energetic. Nevertheless our results show that LFP-cells can still go into a thermal runaway event even though the tested LFP cells showed various results. During external heating up to 300°C a LFP-cell with a newer design did not show any substantial thermal runaway while older design LFP cells showed a moderate thermal runaway. Overcharge of the newer designed LFP-cell did not result in thermal runaway either. However, overcharge of another LFP pouch cell did result in a fire, even if that event could not be reproduced in this study.

The energy released during a thermal runaway based on the results reported above for a 18650 cobalt-based cell can be used to estimate how much energy may be released in a thermal runaway of a 300 kg battery system for an electric vehicle. The answer is perhaps somewhat surprising, the calculation shows that the energy released could be in the order of 70 MJ, corresponding to the combustion of about 2 liters of gasoline. However, our estimate is low, as described above, and using the highest value reported earlier one can expect a value up to six times that calculated here. This is still considering the battery type that has the largest energy release while other more safe chemistries, e.g. LFP will have lower values. The presented results thus show that although the safety aspects of Li-ion batteries are still a concern, the safety is improving with safer chemical components and design improvements.

## Acknowledgments

The authors thank the Swedish Energy Agency and the FFI-program for its support.

## References

1. G. G. Eshetu, S. Grugeon, S. Laurelle, S. Boyanov, A. Lecocq, J.-P. Bertrand, and G. Marlair, *Phys. Chem. Chem. Phys.*, **15**, 9145 (2013).
2. D. Doughty and E. P. Roth, *The Electrochem. Soc. Interface: summer* **2012**, 37 (2012).
3. E. P. Roth and C. J. Orendorff, *The Electrochem. Soc. Interface: summer* **2012**, 45 (2012).
4. D. Lisbona and T. Snee, *Process Safety and Environmental Protection*, **89**, 434 (2011).
5. R. Spotnitz and J. Franklin, *J. of Power Sources*, **113**, 81 (2003).
6. P. Biensan, B. Simon, J. P. Pérès, A. de Guibert, M. Broussely, J. M. Bodet, and F. Perton, *J. of Power Sources*, **81–82**, 906 (1999).

7. F. Larsson, P. Andersson and B.-E. Mellander, "Are electric vehicles safer than combustion engine vehicles?", Chapter 4 in Systems perspectives on Electromobility, edited by B. Sandén, *Chalmers University of Technology*, Goteborg, Sweden, ISBN 978-91-980973-1-3, p. 31 (2013).
8. Z. J. Zhang, P. Ramadass, and W. Fang, "Safety of lithium-ion batteries", Chapter 18 in *Lithium-Ion Batteries: Advances and Applications*, edited by G. Pistoia, Elsevier, Amsterdam, The Netherlands, p. 409 (2014).
9. A. Hammami, N. Raymond, and M. Armand, *Nature*, **424**, 635 (2003).
10. H. Yang, G. V. Zhuang, and P. N. Ross Jr, *J. of Power Sources*, **161**, 573 (2006).
11. T. Ohsaki, T. Kishi, T. Kuboki, N. Takami, N. Shimura, Y. Sato, M. Sekino, and A. Satoh, *J. of Power Sources*, **146**, 97 (2005).
12. D. P. Abraham, E. P. Roth, R. Kostecki, K. McCarthy, S. MacLaren, and D. H. Doughty, *J. of Power Sources*, **161**, 648 (2006).
13. E. P. Roth, *ECS Trans.*, **11**(19), 19 (2008).
14. C. Arbizzani, G. Gabrielli, and M. Mastragostino, *J. of Power Sources*, **196**, 4801 (2011).
15. A. K. Padhi, K. S. Nanjundaswarmy, and J. B. Goodenough, *J. Electrochem. Soc.*, **144**, 1188 (1997).
16. K. Zaghib, A. Guerfi, P. Hovington, A. Vijh, M. Trudeau, A. Mauger, J. B. Goodenough, and C. M. Julien, *J. of Power Sources*, **232**, 357 (2013).
17. D. H. Doughty, E. P. Roth, C. C. Craft, G. Nagasubramanian, G. Henriksen, and K. Amine, *J. of Power Sources*, **146**, 116 (2005).
18. S. S. Zhang, *J. of Power Sources*, **162**, 1379 (2006).
19. G. Nagasubramanian and K. Fenton, *Electrochimica Acta*, **101**, 3 (2013).
20. K. Zaghib, J. Dubé, A. Dallaire, K. Galoustov, A. Guerfi, M. Ramanathan, A. Benmayza, J. Prakash, A. Mauger, and C. M Julien, "Lithium-ion cell components and their effect on high-power battery safety", Chapter 19 in *Lithium-Ion Batteries: Advances and Applications*, edited by G. Pistoia, Elsevier, Amsterdam, The Netherlands, p. 437 (2014).
21. Q. Wang, P. Ping, X. Zhao, G. Chu, J. Sun, and C. Chen, *J. of Power Sources*, **208**, 210 (2012).
22. C. Mikolajczak, M. Kahn, K. White, and R. T. Long, "Lithium-ion batteries hazard and use assessment", Fire Protection Research Foundation, Quincy, MA, USA, Doc no 1100034.000 A0F0 0711 CM01 (2011).
23. D. H. Doughty and C. C. Crafts, "FreedomCAR electrical energy storage system abuse test manual for electric and hybrid electric vehicle applications", Sandia report SAND2005-3123, Sandia National Laboratories, USA (2006).
24. D. Doughty, "SAE J2464 Electric and hybrid electric vehicle rechargeable energy storage system (RESS) safety and abuse testing procedure", SAE Technical Paper 2010-01-1077, (2010).
25. L. Fan, J. M. Khodadadi, and A. A. Pesaran, *J. of Power Sources*, **238**, 301 (2013).
26. J. Yi, U. S. Kim, C. B. Shin, T. Han, and S. Park, *J. of the Electrochem. Soc.*, **160**(3), A437 (2013).
27. W. Wu, X. Xiao, and X. Huang, *Electrochimica Acta* **83**, 227 (2012).
28. C.-Y. Jhu, Y.-W. Wang, C.-Y. Wen, C.-C. Chiang, and C.-M. Shu, *J. Therm. Anal. Calorim.*, **106**, 159 (2011).
29. C.-Y. Jhu, Y.-W. Wang, C.-M. Shu, J.-C. Chang, and H.-C. Wu, *J. of Hazardous Materials*, **192**, 99 (2011).
30. F. Larsson and B.-E. Mellander, *Conference proceedings of Fires in vehicles (FIVE) 2012*, edited by P. Andersson and B. Sundstrom, SP Technical Research Institute of Sweden, Sweden, p. 303 (2012).
31. M. Takahaski, S. Tobishima, K. Takei, and Y. Sakurai, *Solid State Ionics*, **148**, 283 (2002).
32. A. Yamada, S. C. Chung, and K. Hinokuma, *J. of the Electrochem. Soc.*, **148**(3), A224 (2001).
33. H. Joachin, T. D. Kaun, K. Zaghib, and J. Prakash, *J. of the Electrochem. Soc.*, **156**(6), A401 (2009).
34. K. Zaghib, J. Dubé, A. Dallaire, K. Galoustov, A. Guerfi, M. Ramanathan, A. Benmayza, J. Prakash, A. Mauger, and C. M. Julien, *J. of Power Sources*, **219**, 36 (2012).
35. G. Chen and T. J. Richardson, *J. of the Electrochem. Soc.*, **156**(9), A756 (2009).
36. G. Chen and T. J. Richardson, *J. of Power Sources*, **195**, 1221 (2010).
37. E. P. Roth, "Lithium ion cell and battery safety", *Tutorials E in Conference proceedings in Advanced Automotive Battery Conference (AABC)*, AABC Europe 2011, Mainz, Germany (2011).
38. T. D. Hund and D. Ingersoll, "Selected test results from the LiFeBatt iron phosphate Li-ion battery", Sandia report SAND2008–5583, Sandia National Laboratories, USA (2008).
39. Y.-B He, G.-W. Ling, Z.-Y. Tang, Q.-S. Song, Q.-H. Yang, W. Chen, W. Lv, Y.-J. Su, and Q. Xu, *J. Solid State Electrochem.*, **14**, 751 (2010).
40. F. V. Conte, P. Gollob, and H. Lacher, *World Electric Vehicle J.*, **3**, 1 (2009).
41. P. G. Balakrishnan, R. Ramesh, and T. P. Kumar, *J. of Power Sources*, **155**, 401 (2006).
42. E. P. Roth, D. H. Doughty, and D. L. Pile, *J. of Power Sources*, **174**, 579 (2007).
43. C. J. Orendorff, *The Electrochem. Soc. Interface: summer* **2012**, 61 (2012).
44. J. Jeevarajan, "Safety of commercial lithium-ion cells and batteries", Chapter 17 in Lithium-Ion Batteries: *Advances and Applications*, edited by G. Pistoia, Elsevier, Amsterdam, The Netherlands, p. 387 (2014).

# Paper II

batteries

MDPI

Article

# Lithium-Ion Battery Aspects on Fires in Electrified Vehicles on the Basis of Experimental Abuse Tests †

**Fredrik Larsson [1,2,*], Petra Andersson [3] and Bengt-Erik Mellander [1]**

1 Department of Physics, Chalmers University of Technology, Kemivagen 9, SE-41296 Goteborg, Sweden; f5xrk@chalmers.se
2 Electronics, SP Technical Research Institute of Sweden, Brinellgatan 4, SE-501 15 Boras, Sweden
3 Fire Research, SP Technical Research Institute of Sweden, Brinellgatan 4, SE-501 15 Boras, Sweden; petra.andersson@sp.se
* Correspondence: vegan@chalmers.se or fredrik.larsson@sp.se; Tel.: +46-010-516-5000
† This paper is based on the one that was originally presented at FIVE 2014. The paper has been modified and is republished with permission from the editors of the FIVE 2014 conference proceedings.

Academic Editor: Andreas Jossen
Received: 25 February 2016; Accepted: 31 March 2016; Published: 11 April 2016

**Abstract:** Safety issues concerning the use of large lithium-ion (Li-ion) batteries in electrified vehicles are discussed based on the abuse test results of Li-ion cells together with safety devices for cells. The presented abuse tests are: overcharge, short circuit, propane fire test and external heating test (oven). It was found that in a fire, cells with higher state of charge (SOC) gave a higher heat release rate (HRR), while the total heat release (THR) had a lower correlation with SOC. One fire test resulted in a hazardous projectile from a cylindrical cell. In the fire tests, toxic gas emissions of hydrogen fluoride (HF) were measured for 100%, 50% and 0% SOC.

**Keywords:** lithium-ion (Li-ion); battery; electrified vehicle; safety; thermal runaway; fire; hydrogen fluoride; toxic gases; abuse test

## 1. Introduction

Lithium-ion (Li-ion) battery technology can enable a broad introduction of electrified vehicles, mainly due to its high energy capacity. Li-ion batteries also have other important properties, e.g., long lifetime and the possibility of fast charging. However, Li-ion batteries have a drawback compared to most other battery technologies in that the electrolyte is flammable and the battery may go into a thermal runaway, that is, the battery may self-heat, resulting in a rapid pressure and temperature increase in the cell; this will release flammable and toxic gases but can also cause projectiles and fire [1–7]. Thermal runaway may happen when the battery moves out of the stable operating window of the Li-ion cell and can be caused by, e.g., short circuiting, overheating, overcharging or mechanical damage.

Li-ion batteries are used in very large numbers for consumer products like cell phones, laptop computers, *etc.* Incidents have occurred with these batteries, but the consequences are in most cases not that serious due to the limited size of the batteries. With the increased number of electric vehicles (EVs) on the roads, the safety issues surrounding Li-ion technology have become more important, taking into consideration the large size of the batteries in automotive applications. Incidents involving EVs have indeed happened, some of them resulting in fires. But these fires have not yet resulted in any more serious consequences.

Notable EV fires include three car fires involving the battery EV (BEV) Tesla Model S that occurred in 2013. In two of them, the driver hit road debris at highway speed, while one was caused by a crash into a concrete barrier and a tree resulting in significant deformations. The first fire was a result of

penetration from beneath of the battery pack. Mass media attention was high regarding these incidents and the fires caused a drop in Tesla Motors stock prices. Up to the present time, the authors are aware of three additional incidents involving the Tesla Model S, however, possibly caused by electrical faults outside of the vehicle. In any case, compared to the annual average number of automobile fires in the USA, of the order of 1/1000 automobiles [8], the number of car fires in the Tesla Model S is significantly lower. Larsson *et al.* [9] estimated in 2014 the number of fires in the Tesla Model S as 1/10,000 cars. With the increased statistics now available, although with still limited amounts of data, and with the sales numbers of more than 100,000 Model S vehicles, the estimate deceases somewhat to about 1/20,000 cars. This comparison does not take into account the age of the cars involved, as older cars may be more prone to fires, but it still shows that the risks involving EVs should not be overstated. In 2014, the National Highway Traffic Safety Administration (NHTSA) investigated the fires and did not find any defect trends [10], but Tesla did voluntarily chose to reinforce the underbody of their cars with arming plates [11] in order to lower the frequency and the effect of hitting road debris.

Other incidents include the Fisker Karma plug-in hybrid EV (PHEV). In October 2012, Hurricane Sandy caused the flooding of a harbor in Newark, New Jersey. The flooding lasted several hours and, thereafter, 16 brand-new Fisker Karma were destroyed by fire. The cars were completely covered with salt water during the flooding, an extreme situation where electrical short circuits are likely to occur. Mass media attention was high on the Fisker Karma fires even though other vehicles including other PHEVs/hybrid EVs (HEVs) also burnt. Prior to Hurricane Sandy, some other fire incidents occurred involving Fisker Karma, one of them outside a supermarket shortly after the driver left the car. These incidents are examples where EV fires have been the focus of the mass media. Other fires have happened, during charging or as spontaneous fires, but have not gained as much media interest.

Besides the few incidents in electrified vehicles, incidents have occurred in other situations. The Boeing 787 Dreamliner Li-ion battery fire incidents in 2013–2014 [12], as well as serious accidents on cargo airplanes involving Li-ion batteries in the cargo hold, have increased the awareness of the safety risks associated with this type of battery [13]. In 2016, the Federal Aviation Administration (FAA) warned that there is a risk of catastrophic aircraft loss if a Li-ion battery fire or explosion occurs in the cargo hold since existing fire suppression systems cannot control such a fire [14]. As a consequence, the ICAO Air Navigation Commission (ANC) has issued strict regulations, effective 1 April 2016, for the transportation of Li-ion batteries as cargo on passenger aircraft [15].

These incidents and their consequences clearly demonstrate the necessity of putting safe vehicles on the market, not only for the safety of humans in or near the vehicles, but also for economic and environmental reasons. The EV has the potential to be safer than conventional combustion engine cars, simply because the main fire source, gasoline/diesel, is removed [16]. In any case, the safety of a battery system depends on several things, e.g., cell chemistry, cell design and system design, including thermal management system and control strategies. Common cathode chemistries contain cobalt, e.g., lithium cobalt oxide (LCO), $LiCoO_2$, lithium nickel manganese cobalt (NMC), $LiNi_xMn_yCo_zO_2$, and lithium nickel cobalt aluminum (NCA), $LiNi_xCo_yAl_zO_2$. Lithium phosphates [17] are also used, e.g., lithium iron phosphate (LFP), $LiFePO_4$. For the anode, various forms of carbon are dominant, while lithium titanate oxide (LTO), $Li_4Ti_5O_{12}$, is used in lower volumes. This paper focuses mainly on carbon-LFP cells, which are currently seen as state of the art on the market when it comes to safety, although many battery systems for automotive applications use less stable chemistries in order to obtain, e.g., higher energy density. Abuse test results from cell level are presented and their impact is discussed on battery system and vehicle level.

## 2. Cells Studied

Cylindrical cells as well as pouch and soft-can prismatic cells have been tested. Cylindrical cells have a spirally wound layers inside an outer metal cylinder. The soft-can prismatic cell has a block shape and an outer cell packaging made of plastic material, in contrast to the hard-can prismatic cell, which has an outer metal packaging. In the pouch cell, the layers are stacked on top of each other and

sealed by an aluminum-polymer bag. The pouch cell is often called a coffee bag cell or a polymer cell. Figure 1 shows an X-ray photo of the EiG pouch cell. The layered structure is clearly visible, where the white-/gray-colored layers are the separator material.

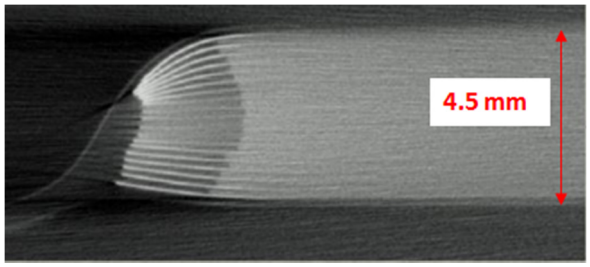


**Figure 1.** X-ray photo of EiG pouch cell seen at one of the edges.

Table 1 shows the cells and their specifications for the abuse tests presented in this paper and Figure 2 shows photos of the cells. Most of the cells have a LFP-cathode and a carbon-based anode as seen from Table 1. The initial state of charge (SOC) level of the cells was achieved by charge/discharge procedures using a Digatron battery test equipment or an ordinary laboratory power aggregate. The cells had not been used prior to the measurements, but had different calendar ageing. The EiG and Lifetech cells had approximately two to three years of calendar aging, while the European Battery cells were less than six months old and the Samsung, EVE and GBS cells were about one year old. Cylindrical cells of type 18650, *i.e.*, 18 mm in diameter and 65 mm long, are produced in very large volumes and are traditionally used in laptops, power tools and electric bikes. Laptop computers are nowadays often too thin to use 18650 cells and use instead pouch cells. Besides the use of 18650 cells in portable devices, Tesla Motors has chosen the 18650 cell format as a basis for its serial-production of EVs, while other vehicle manufacturers have chosen the prismatic or pouch cell type.

**Table 1.** Cell and test specifications. SOC: state of charge; LFP: lithium iron phosphate; and LFMP: LFP with manganese.

| Cell | Nominal Cell Capacity (Ah) | Nominal Cell Voltage (V) | Cathode/Anode | Cell Packaging | Test Type Presented in This Paper | Initial SOC (%) |
|---|---|---|---|---|---|---|
| EiG ePLB-F007A | 7 | 3.2 | LFP/carbon | Pouch | Propane fire, overcharge | 0–100 |
| Lifetech X-1P | 8 | 3.3 | LFP/carbon | Cylindrical | Propane fire | 100 |
| European Battery | 45 | 3.2 | LFP/carbon | Pouch | Short circuit, overcharge | 100 |
| Samsung ICR18650-24F | 2.4 | 3.6 | Cobalt based/carbon | Cylindrical | External heating (oven) | 100 |
| EVE F7568270 | 10 | 3.2 | LFP/carbon | Pouch | Overcharge | 100 |
| GBS LFMP40Ah | 40 | 3.2 | LFMP/carbon | Prismatic | Overcharge | 100 |


**Figure 2.** Photo of tested cells, not at same physical scale.

## 3. Thermal Runaway

Thermal runaway was studied using the external heating abuse test for a commercial 18650 laptop cell that is produced in large quantities by Samsung. The cell was fastened to a brick and placed inside a thermostatically controlled oven, the Binder FED 115, and heated up in about 1 h to the thermal runaway temperature [3]. The cell voltage and the cell surface temperature (measured by four type K thermocouples) as well as the oven air temperature (measured with one type K thermocouple) were measured with 1 Hz. Figure 3 shows the cell voltage and the differential temperature, $\Delta T$, as a function of the oven temperature. The differential temperature is the difference between the average cell surface temperature and the oven temperature. Before the thermal runaway, the cell voltage breakdown occurs due to melting of the separator, an endothermic process which is observable as a small local decrease of $\Delta T$. $\Delta T$ has negative values up to 220 °C due to higher oven temperature than cell temperature, while the thermal runaway occurs at 220 °C. The cell surface temperature increases to close to 800 °C ($\Delta T$ above 500 °C), with a maximum rate of around 5000 °C/min. Observations from the video recording showed that the thermal runaway is accompanied with a pressure wave (*i.e.*, shaking the video camera) and instant ignition. The duration of the fire is approximately 1 min.

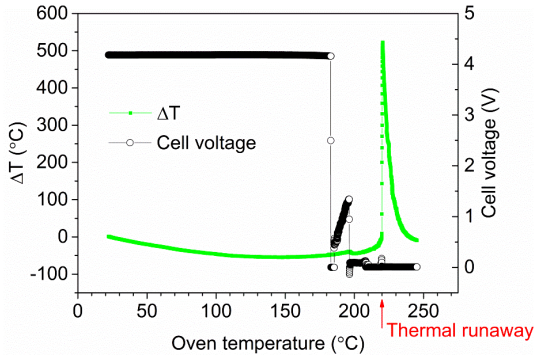


**Figure 3.** External heating test of a Samsung 18650 laptop cell.

## 4. Fire Characteristics on Cell Level

The measurement and gas collection system of the single burning item (SBI) apparatus were used for the fire tests. The SBI apparatus is normally used for the classification of building materials according to the European Classification scheme EN13823 [18]. The experimental setup is shown in Figure 4. The battery cells were placed on a wire grating. A 15 kW propane burner was placed underneath the cells and was ignited 2 min after the start of the test.

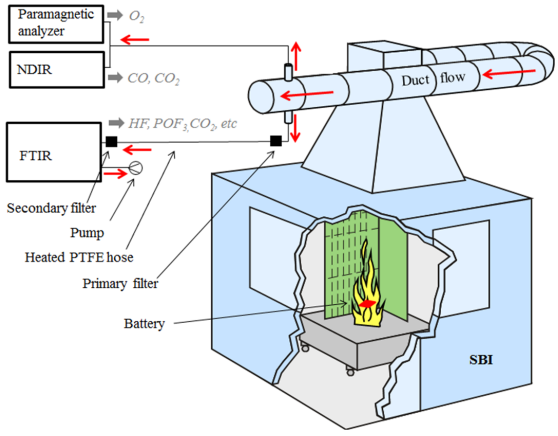


**Figure 4.** Schematic illustration of the experimental setup. NDIR: non-dispersive infrared; FTIR: Fourier transform infrared spectroscopy; and SBI: single burning item.

Tests were performed on EiG and Lifetech cells. Five cells were tested at the same time. The EiG cells were fastened together with steel wire, while the Lifetech cells were placed inside a protection box made of walls of non-combustible silica board and steel net at the bottom and top. Additionally, a secondary layer of steel net was used at the top, nailed to the wire grating to protect from hazardous projectiles (Figure 5). A blank test was conducted at the beginning of each test day in order to make a blank for the gas analysis and to measure the burner influence on the heat release rate (HRR). HRR values were calculated by the oxygen consumption method and corrected for $CO_2$ [18]. The gases from the fire were collected in the duct flow as seen in Figure 4. In the tests of EiG cells with 100% SOC a duct flow of 0.6 $m^3/s$ was used, while for the other tests of EiG cells and for the Lifetech cells, the flow was decreased to 0.4 $m^3/s$ in order to increase emission concentrations. All tests were video recorded. A heated (180 °C) sub-flow was taken out to the Fourier transform infrared spectroscopy (FTIR, Thermo Fisher Scientific, Waltham, MA, USA) with an Antaris IGS analyzer (Nicolet), with a gas cell (heated to 180 °C), that measured gases, e.g., hydrogen fluoride (HF). Each test used a fresh primary filter (heated to 180 °C) which was analyzed for fluoride content after the test. All fluoride found was assumed to be in the form of HF. For the measured HRR the combined expanded uncertainty is +/−5 kW. The detection limit was 2 ppm for HF. For a detailed description of the experiment, see Larsson *et al.* [4] and Andersson *et al.* [19].

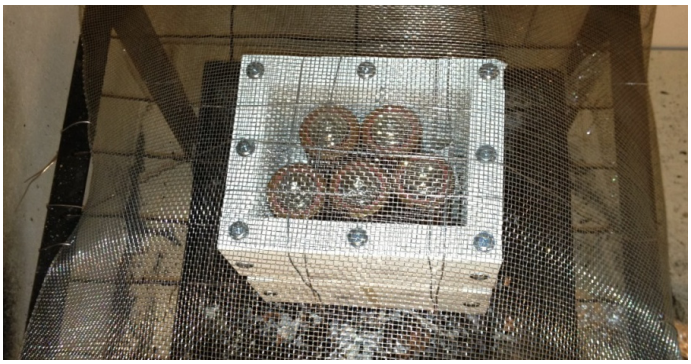

**Figure 5.** Lifetech single cells before the fire test at 100% SOC with external propane burner.

The HRR for various SOC levels for a five-cell-pack of EiG cells is shown in Figure 6. A strong dependence between SOC and HRR can be observed, and lower SOC values result in lower HRR peaks. For a 100% SOC, there are rapid heat releases and outbursts, one per cell, while no outburst or HRR peak can be seen for cells with a lower SOC.

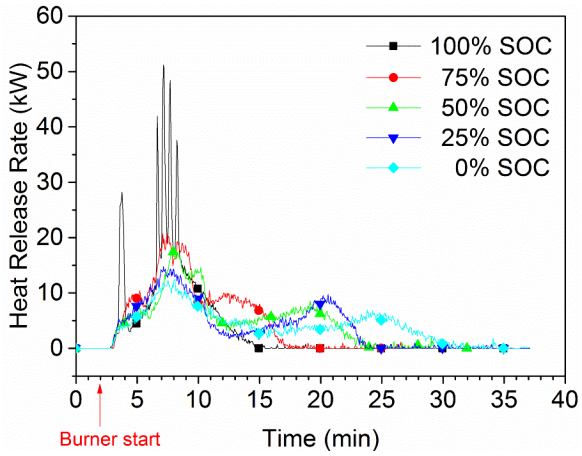


**Figure 6.** Heat release rate (HRR) for the five-cell pack of EiG 7 Ah cell, using an external propane burner (burner HRR has been subtracted from the graph). Cell SOC varied from 0% to 100%.

For an example of an outburst see Figure 7. The total heat release (THR) has a relatively low dependence on SOC and was roughly 8 MJ for the five-cell-pack, corresponding to 6.5 MJ/kg battery cell. Ribière *et al.* [5] found, based on an 11 Wh pouch cell with $LiMn_2O_4$ (LMO) cathode, a heat of combustion of 4 MJ/kg, which is in the same order as that measured in our study.

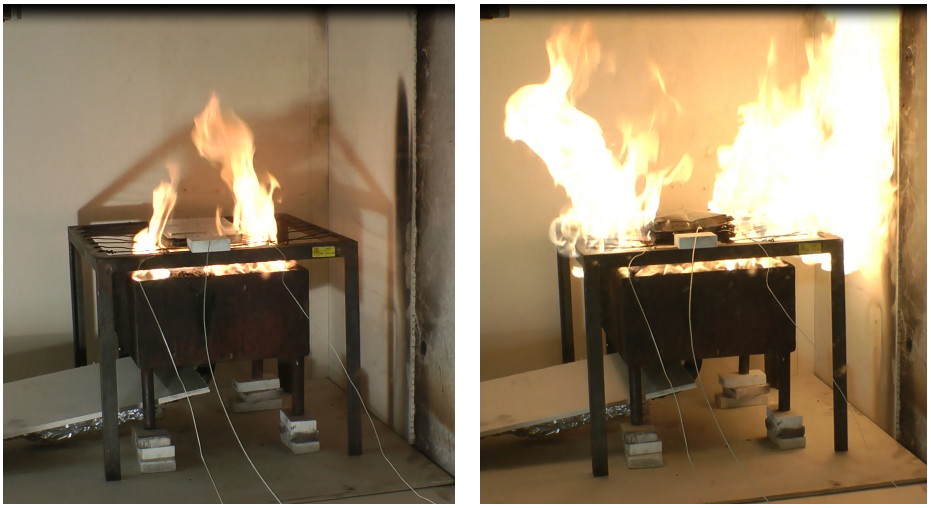

(**a**) (**b**)

**Figure 7.** Photo in the beginning (**a**) of the fire test of a 100% SOC EiG five-cell-pack, and photo of an outburst (**b**) during the fire test.

The nominal energy content of the five-cell-pack is 112 Wh. Electrified vehicles typically have 10–30 kWh of batteries, and an extrapolation of our values to the energy released for this size of battery pack gives a THR of 700–2100 MJ, which corresponds to a fire of about 20–50 L of gasoline.

## 5. Projectile Hazards

Batteries can also cause projectile risks, which was demonstrated in one of the fire tests. Even though the cells were equipped with a safety valve, this did not prevent the explosion of one of the five Lifetech cylindrical cells as shown in Figure 8. Material from the cell interior was expelled while the cell moved backwards with a clear bang and a pressure wave formed a crater in the bed of small stones in the propane burner. No visual flaws of any kind could be observed for any of the five Lifetech cells before the test.

(**a**) (**b**)

**Figure 8.** Photos of the exploded Lifetech cell in the protection box after the fire test at 100% SOC with external propane burner: (**a**) seen from the side of the box; and (**b**) close up of bottom of the box.

A simple teardown was conducted but no indications were found to understand why that cell exploded. Figure 9 shows photos during teardown. No separator could be observed in the cell, which was expected due to the high fire temperatures. The positive current collector of aluminum foil seemed to have melted completely. The copper foil was still present. The weight loss of the cell was 27%.

(**a**) (**b**)

**Figure 9.** Photos of the exploded Lifetech cell during tear-down: (**a**) the exploded cell and part of the protection box and two adjacent cells; and (**b**) exploded cell alone.

## 6. Cell Venting and Toxic Gases

The gases released from a Li-ion battery cell can be toxic, e.g., CO, but the fluoride emissions are of most concern. Hydrogen fluoride (HF) is one of them, but there are also others, e.g., phosphorous oxyfluoride ($POF_3$). They are formed from the fluorine content used in the Li-ion cell; the binder (e.g., PVdF) and the commonly used Li-salt, hexafluorophosphate ($LiPF_6$). The reaction formulas for the salt decomposition can be seen in the following equations [20]:

$$LiPF_6 \rightarrow LiF + PF_5 \quad (1)$$

$$PF_5 + H_2O = POF_3 + 2HF \quad (2)$$

$$LiPF_6 + H_2O \rightarrow LiF + POF_3 + 2HF \quad (3)$$

HF has a relatively well-known toxicity [21], while the toxicity of $POF_3$ is unknown. However, $POF_3$ might be more toxic than HF as in the case of the chlorine analogue $POCl_3$/HCl [22]. $POF_3$ could not be observed in the fire tests on Li-ion cells reported here, but a fire study on electrolytes in a Cone calorimeter by Andersson *et al.* [19] indicated that the $POF_3$ production might be approximately 1:20 of the HF production, which indicates that $POF_3$ may also have been released in the present tests, but that the concentration was below the detection limit (6 ppm). In the previous study [4], the real time HF production rate for EiG cells was determined. Figure 10 shows the HF production rate for EiG cells with different SOC during the fire tests. The highest rate is for 50% SOC, while 100% SOC has the lowest rate. The total amount of HF from both FTIR and the sampling filter is shown in Table 2, and values are between 5.6 g and 14 g HF for a five-cell-pack. Ribière *et al.* [5] measured HF in their studies of another type of pouch cell and, if we normalize their values against the cell electrical energy, a value of 37–69 mg/Wh is obtained, with the higher HF amounts for lower SOC, as seen in Table 2. These amounts are in the same order as our results, 50–120 mg/Wh; however, in contrast to this study, Ribière *et al.* [5] found the highest HF production rate for the fully charged (100% SOC) cells.

The extrapolation of the Larsson *et al.* [4] data to a larger battery pack size typically used in EVs gives an indication of the potential amount of released HF. A battery pack for an EV, based on the tested EiG cell, could, for example, have 432 cells. This corresponds to 108 cells in series and four cells in parallel, which results in a battery pack with 9.7 kWh and a 346 V nominal voltage. The extrapolation factor is then 432/5 = 86.4, resulting in about 400–1200 g HF, depending on the SOC level. These values are in the same order of magnitude as those reported by Lecocq *et al.* [23] for fire tests on a complete EV.

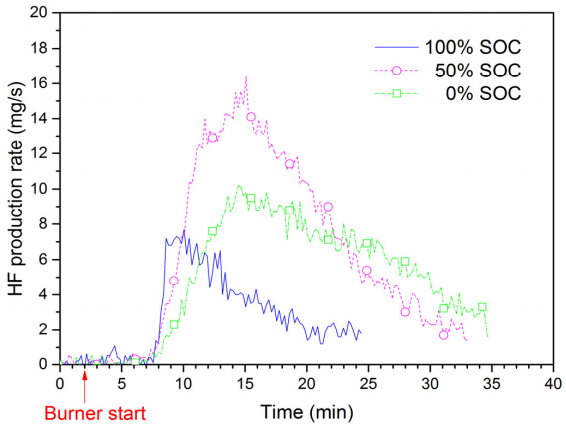


**Figure 10.** The rate of hydrogen fluoride (HF) production for an EiG five-cell pack for 100%, 50% and 0% SOC.

**Table 2.** Emissions of hydrogen fluoride for 100%, 50% and 0% SOC based on results from Larsson *et al.* [4].

| SOC (%) | Max Rate of HF Production (mg/s) | Total Amounts of HF (g) | Total Amount of HF (mg/Wh) | |
|---|---|---|---|---|
| | | | Our Measurements | Calculated from Ribière *et al.* [5] |
| 100 | 8.3 | 5.6 | 50 | 37 |
| 50 | 16 | 14 | 120 | 39 |
| 0 | 10 | 11 | 100 | 69 |

## 7. Cell Safety Mechanisms

Cylindrical 18650 cells for consumer products typically have a cobalt or cobalt mixture-based cathodes (e.g., NMC, NCA), which are not as thermally stable as LFP [24]. A number of safety mechanisms [25] are often included in 18650 cells used in consumer products for low voltage systems. An example of such a safety mechanism is the current interrupter device (CID). The CID is a disc which is part of the current pathway. In case of overpressure in the cell, the CID is mechanically released due to the pressure, letting the cell go into open circuit mode. The CID is typically activated at a predesigned stage, before the cell can go into thermal runaway, by using shutdown additives [26]. Positive temperature coefficient (PTC) is another safety mechanism, which protects the cell by rapidly increasing the resistance in the current pathway when trigged by an overtemperature, significantly lowering the current passing through the cell. In any case, the CID and PTC do not work that well in battery systems with multiple cells that are electrically connected in a series and thereby at a higher voltage [27], e.g., in batteries used in electrified vehicles. Figure 11 shows a cross section X-ray photo of an 18650 cell where PTC and CID are shown.

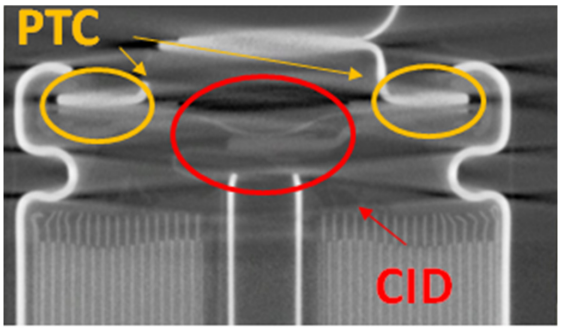


**Figure 11.** X-ray photo of an 18650 cell with the positive temperature coefficient (PTC) and current interrupter device (CID) marked.

Shutdown separators are widely used in commercial Li-ion batteries as a safety protection for some abuse situations, e.g., overcharge and short circuit. The pores in the separator are closed at overtemperatures, which lead to a hindered ion transport between cathode and anode and thus an open circuit. The shutdown separator usually consists of a layered structure where one layer has a lower melting temperature than the other layer. When the first layer melts the pores in the separator are closed, while the second layer sustains the cell integrity, thereby prohibiting internal short circuit. Figure 12 shows differential scanning calorimetry (DSC) measurements of a polypropylene (PP) separator and of a shutdown separator with polyethylene (PE) and PP; the latter exhibits two melting temperatures, corresponding to the two materials. In case of, e.g., an overcharge leading to an increased cell temperature, the PE will melt at around 130 °C, lowering the current and thereby the heating process. It may work less well in some situations, e.g., when the current is interrupted too late or when the cooling is poor due to the battery system design. In those cases, the melting temperature of the second layer of PP, around 160 °C, can be reached, leading to the total disintegration of the separator, followed by an internal cell short circuit. The use of shutdown separators in large battery systems has shown not to have the same safety benefits as in small batteries, since the higher battery voltage in cases where many cells are electrically connected in a series, as with EV batteries, for example, can lead to separator breakdown [28].

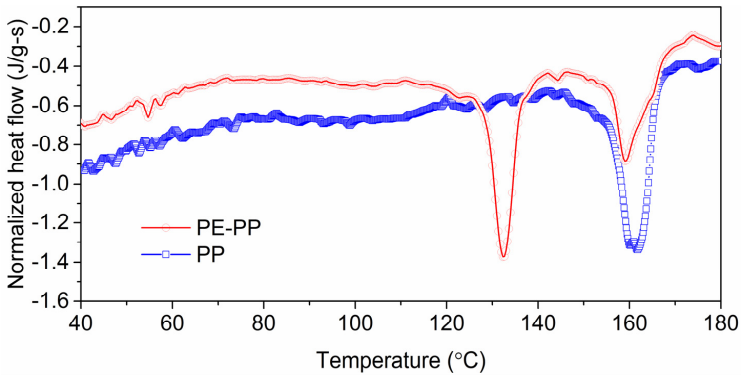


**Figure 12.** Differential scanning calorimetry (DSC) measurements of two different separator materials, one shutdown separator with polyethylene-polypropylene (PE-PP) and one with only PP. The DSC measurements used a liquid $N_2$ cooled Mettler DSC-30 (Greifensee, Switzerland), the samples were purged with $N_2$, and heated between 25 °C and 185 °C with a heating rate of 5 °C/min.

In order to account for the drawback that some of the typical safety devices used in cells for consumer products cannot be used in Li-ion cells for EVs, other safety mechanisms such as special additives in the electrolyte are used. Li-ion cells for EV typically use cells which have higher quality manufacturing, more pure raw materials and safer chemistry such as the LFP, which can withstand abuse better [3]. Figures 13 and 14 show 2C-rate overcharging of four LFP-based cells with a capacity between 7 Ah and 45 Ah. The GBS cell has a cathode of LFMP, *i.e.*, LFP with manganese. The charger voltage was max 15.3 V and the charger was started after 1 min and was active during the complete test; however, for the overcharge of EVE, the charger was switched off at around 17 min, as seen by the voltage drop in Figure 14. The temperatures reached less than 80 °C, well below the onset temperature of the thermal runaway. However, the cells swell and gases are emitted. Four European battery cells were tested and the result from one of them is shown in Figures 13 and 14. In fact, one of the European Battery cell unexpectedly caught fire. A situation of an overcharge abuse in the field might occur in case of a failure in the battery management system (BMS). High charge currents can occur, e.g., during fast charging or during breaking (recuperation) of an EV, which makes those cases especially sensitive to errors in the overcharge protection. In principle, the consequences for overcharging of LFP cells are less dramatic than for other Li-ion chemistries, but the temperature increase starts at a lower state of overcharge [24].

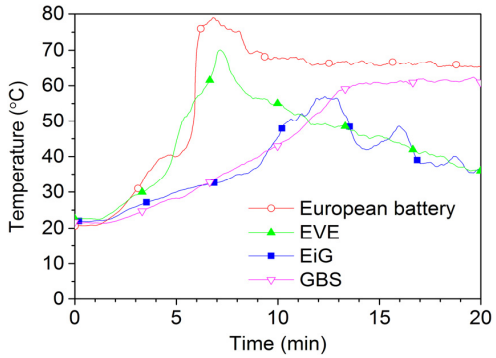


**Figure 13.** Overcharge tests of LFP and LFMP cells, with charge current of 2C-rate, showing average cell surface temperature development.

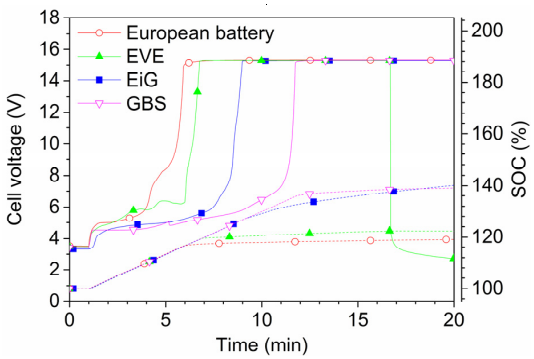


**Figure 14.** Overcharge tests of LFP and LFMP cells, with charge current of 2C-rate, showing cell voltage (solid lines) and SOC development (dashes lines). SOC is calculated by cumulative integration of the measured current and time, divided by the nominal capacity.

In the case of a short circuit of a Li-ion battery, the current can be very high [3]. A measurement of a low-ohmic short circuit on a single pouch cell from European Battery is shown in Figure 15. The voltage and current were measured with 1 kHz by an oscilloscope and cell surface temperatures (by 18 type K thermocouples on both sides of the cell) by a data logger at 1 Hz. The short circuit peak current is close to 1100 A and then lowered to a plateau of about 700 A. High currents generate a lot of heat, but for this cell the average temperature increase is only about 5 °C since the short circuit is stopped when the positive terminal burns off from the cell. In the case of a large battery pack with cell terminals that do not burn off, the current and the generated heat can be substantial, and in the case of burnt off terminal tabs the flames might ignite vented flammable battery gases or plastic parts inside a battery system.

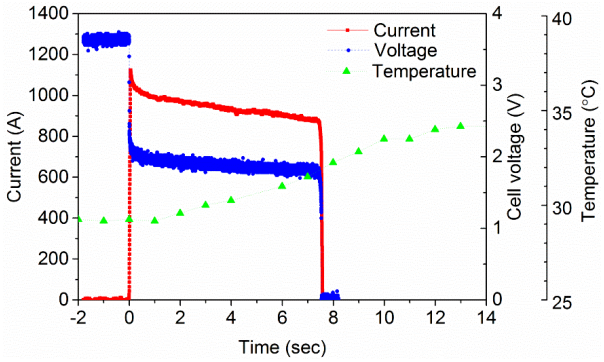


**Figure 15.** Short circuit of a European Battery pouch cell.

## 8. Battery System and Electric Vehicle Level

High battery safety is accomplished by using many layers of actions of various safety techniques. Figure 16 shows the safety onion with examples of diverse safety actions used to ensure a low probability for fault, and to minimize the consequences of a fault. First, the cell chemistry is essential since this is the basis of the thermal stability. Second comes the cell design and packaging. In principle, there are three main levels: cell, battery system and vehicle level.

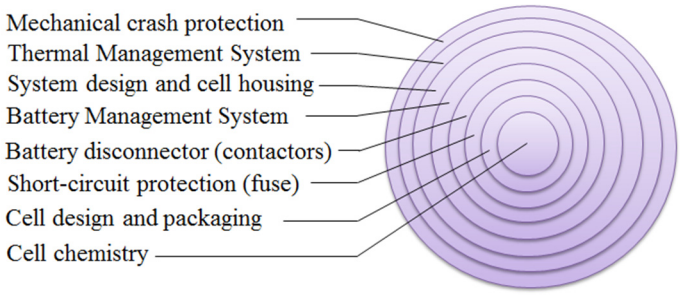


**Figure 16.** The safety onion showing examples, layer by layer, of different safety actions that can be used to establish a safe battery system in electric vehicles (EVs).

## 9. Conclusions

There is relatively good knowledge about the safety risks and safety devices used in consumer cells. Using Li-ion in the automotive sector puts higher demands on the battery since the batteries are significantly larger and have harsher environmental conditions, e.g., vibrations, humidity, larger temperature variations. The different Li-ion chemistries show diverse hazards where the LFP is less reactive but safety measures are still needed for all Li-ion batteries. A high level of safety is achieved by adding several safety layers from the cell to vehicle level; however, the risk for a cascading fire in a complete battery pack starting from a single cell is not yet well studied, and the knowledge about possible counteractions is thus also limited. Sometimes things go wrong even though smart safety strategies are used. The exploded cylindrical cell due to a cell vent malfunction showed this and underlines the importance of using many safety layers.

The toxic gas emissions from Li-ion batteries, e.g., HF and $POF_3$, can pose a serious risk for a person. A replacement of the Li-salt $LiPF_6$ to a non-fluorine salt and change of fluorine binder could resolve this risk. Intense research is ongoing in this field, but the required properties for a Li-ion battery in EVs are complex and demanding.

**Acknowledgments:** The Swedish Energy Agency is gratefully acknowledged for financial support. We are also indebted to several colleagues at SP and Chalmers who have contributed to this work.

**Author Contributions:** Fredrik Larsson conceived, designed and performed the experiments for all abuse types except for the fire tests where Petra Andersson and Fredrik Larsson did it together. All three authors were involved in the analyses of the data and wrote the paper.

**Conflicts of Interest:** The authors declare no conflict of interest.

## References

1. Golubkov, W.; Fuchs, D.; Wagner, J.; Wiltsche, H.E.; Stangl, C.; Fauler, G.; Voitic, G.; Thaler, A.; Hacker, V. Thermal-runaway experiments on consumer Li-ion batteries with metal-oxide and olivin-type cathodes. *RSC Adv.* **2014**, *4*, 3633–3642. [CrossRef]
2. Long, R.T., Jr.; Blum, A.F.; Bress, T.J.; Cotts, B.R.T. *Best Practices for Emergency Response to Incidents Involving Electric Vehicles Battery Hazards: A Report on Full-Scale Testing Results*; Fire Protection Research Foundation: Quincy, MA, USA, 2013.
3. Larsson, F.; Mellander, B.-E. Abuse by external heating, overcharge and short circuiting of commercial lithium-ion battery cells. *J. Electrochem. Soc.* **2014**, *161*, A1611–A1617. [CrossRef]

4. Larsson, F.; Andersson, P.; Blomqvist, P.; Lorén, A.; Mellander, B.-E. Characteristics of lithium-ion batteries during fire tests. *J. Power Sources* **2014**, *271*, 414–420. [CrossRef]
5. Ribière, P.; Grugeon, S.; Morcrette, M.; Boyanov, S.; Laruelle, S.; Marlair, G. Investigation on the fire-induced hazards of Li-ion battery cells by fire calorimetry. *Energy Environ. Sci.* **2012**, *5*, 5271–5280. [CrossRef]
6. Fu, Y.; Lu, S.; Li, K.; Liu, C.; Cheng, X.; Zhang, H. An experimental study on burning behaviors of 18650 lithium ion batteries using a cone calorimeter. *J. Power Sources* **2015**, *273*, 216–222. [CrossRef]
7. Huang, P.; Wang, Q.; Li, K.; Ping, P.; Sun, J. The combustion behavior of large scale lithium titanate battery. *Sci. Rep.* **2015**, *5*. [CrossRef] [PubMed]
8. Ahrens, M. Automobile Fires in the U.S.: 2006–2010 Estimates. In Proceedings of the Fires in Vehicles (FIVE) Conference 2012, Chicago, IL, USA, 27–28 September 2012; Andersson, P., Sundström, B., Eds.; SP Technical Research Institute of Sweden: Borås, Sweden, 2012; pp. 95–104.
9. Larsson, F.; Andersson, P.; Mellander, B.-E. Battery Aspects on Fires in Electrified Vehicles. In Proceedings of the Fires in Vehicles (FIVE) 2014 Conferences, Berlin, Germany, 1–2 October 2014; Andersson, P., Sundström, B., Eds.; SP Technical Research Institute of Sweden: Borås, Sweden, 2014; pp. 209–220.
10. *Investigation PE 13-037*; National Highway Traffic Safety Administration (NHTSA): Washington, DC, USA, 2014. Available online: http://www-odi.nhtsa.dot.gov/acms/cs/jaxrs/download/doc/UCM452870/INCLA-PE13037-2071.PDF (accessed on 7 April 2016).
11. Musk, E. Tesla Adds Titanium Underbody Shield and Aluminum Deflector Plates to Model S, 2014. Available online: http://www.teslamotors.com/blog/tesla-adds-titanium-underbody-shield-and-aluminum-deflector-plates-model-s (accessed on 10 February 2016).
12. *Aircraft Serious Incident Investigation Report*; JA804A; Japan Transport Safety Board: Tokyo, Japan, 2014; Available online: http://www.mlit.go.jp/jtsb/eng-air_report/JA804A.pdf (accessed on 7 April 2016).
13. *Auxiliary Power Unit Battery Fire, Japan Airlines Boeing 787-8, JA829J, Boston, Massachusetts*; NTSB/AIR-14/01. National Transportation Safety Board: Washington, DC, USA, 2014. Available online: http://www.ntsb.gov/investigations/AccidentReports/Reports/AIR1401.pdf (accessed on 7 April 2016).
14. U.S. Department of Transportation, Federal Aviation Administration. Safety Alert for Operators, SAFO 16001, 1/19/2016. Available online: http://www.faa.gov/other_visit/aviation_industry/airline_operators/airline_safety/safo/all_safos/media/2016/SAFO16001.pdf (accessed on 7 April 2016).
15. International Air Transport Association (IATA). Lithium Batteries as Cargo in 2016 Update III, 2016. Available online: http://www.iata.org/whatwedo/cargo/dgr/Documents/lithium-battery-update.pdf (accessed on 25 February 2016).
16. Larsson, F.; Andersson, P.; Mellander, B.-E. Are electric Vehicles Safer than Combustion Engine Vehicles? In *Systems Perspectives on Electromobility*; Sandén, B., Wallgren, P., Eds.; Chalmers University of Technology: Göteborg, Sweden, 2014; pp. 33–44.
17. Padhi, A.K.; Nanjundaswarmy, K.S.; Goodenough, J.B. Phospho-olivines as positive-electrode materials for rechargeable lithium batteries. *J. Electrochem. Soc.* **1997**, *144*, 1188–1194. [CrossRef]
18. *Reaction to Fire Tests for Building Products—Building Products Excluding Floorings Exposed to the Thermal Attack by a Single Burning Item*; EN 13823:2010; European Committee for Standardization: Brussels, Belgium, 2010.
19. Andersson, P.; Blomqvist, P.; Lorén, A.; Larsson, F. *Investigation of Fire Emissions from Li-ion Batteries*; SP Report 2013:5; SP Technical Research Institute of Sweden: Borås, Sweden, 2013.
20. Yang, H.; Zhuang, G.V.; Ross, P.N., Jr. Thermal stability of $LiPF_6$ salt and Li-ion battery electrolytes containing $LiPF_6$. *J. Power Sources* **2006**, *161*, 573–579. [CrossRef]
21. *Documentation for Immediately Dangerous to Life or Health Concentrations (IDLHs) for Hydrogen Fluoride (As F)*; The National Institute for Occupational Safety and Health (NOISH): Washington, DC, USA, 1994.
22. Middelman, A. *Hygiensiska Gränsvärden AFS 2011:18, Hygieniska Gränsvärden Arbetsmiljöverkets Föreskrifter och Allmänna råd om Hygieniska Gränsvärden*; Swedish Work Environment Authority: Stockholm, Sweden, 2011. (In Swedish)
23. Lecocq, A.; Bertana, M.; Truchot, B.; Marlair, G. Comparison of the Fire Consequences of an Electric Vehicle and an Internal Combustion Engine Vehicle. In Proceedings of the International Conference on Fires in Vehicles (FIVE) 2012, Chicago, IL, USA, 27–28 September 2012; Andersson, P., Sundström, B., Eds.; SP Technical Research Institute of Sweden: Borås, Sweden, 2012; pp. 183–194.
24. Doughty, D.; Roth, E.P. A general discussion of Li ion battery safety. *Electrochem. Soc. Interface* **2012**, *2012*, 37–44.

25. Balakrishnan, P.G.; Ramesh, R.; Kumar, T.P. Safety mechanisms in lithium-ion batteries. *J. Power Sources* **2006**, *155*, 401–414. [CrossRef]
26. Zaghib, K.; Dubé, J.; Dallaire, A.; Galoustov, K.; Guerfi, A.; Ramanathan, M.; Benmayza, A.; Prakash, J.; Mauger, A.; Julien, C.M. Lithium-Ion Cell Components and Their Effect on High-Power Battery Safety. In *Lithium-Ion Batteries: Advances and Applications*; Pistoia, G., Ed.; Elsevier: Amsterdam, The Netherlands, 2014; Chapter 19; pp. 437–460.
27. Jeevarajan, J. Safety of Commercial Lithium-Ion Cells and Batteries. In *Lithium-Ion Batteries: Advances and Applications*; Pistoia, G., Ed.; Elsevier: Amsterdam, The Netherlands, 2014; Chapter 17; pp. 387–407.
28. Orendorff, C.J. The role of separators in lithium-ion cell safety. *Electrochem. Soc. Interface* **2012**, *2012*, 61–65.

# Paper III

# Gas explosions and thermal runaways during external heating abuse of commercial lithium-ion graphite-$LiCoO_2$ cells at different levels of ageing

**Fredrik Larsson[1,2,*], Simon Bertilsson[1], Maurizio Furlani[3], Ingvar Albinsson[3], Bengt-Erik Mellander[1]**

[1] Department of Physics, Chalmers University of Technology, Kemivägen 9, SE-41296 Göteborg, Sweden
[2] Division of Safety and Transport, RISE Research Institutes of Sweden, Brinellgatan 4, SE-50115 Borås, Sweden
[3] Department of Physics, University of Gothenburg, Fysikgården 1, SE-41296 Göteborg, Sweden

***** Corresponding author. Department of Physics, Chalmers University of Technology, SE-412 96 Göteborg, Sweden. Tel.: +46 10 5165928; fax: +46 33 125038. E-mail addresses: vegan@chalmers.se, fredrik.larsson@ri.se (F. Larsson)

## Abstract

Commercial 6.8 Ah lithium-ion cells with different ageing/status have been abused by external heating in an oven. Prior to the abuse test, selected cells were aged either by C/2 cycling up to 300 cycles or stored at 60 °C. Gas emissions were measured by FTIR and three separate vents were identified, two well before the thermal runaway while the third occurred simultaneously with the thermal runaway releasing heavy smoke and gas. Emissions of toxic hydrogen fluoride (HF) and phosphorous oxyfluoride ($POF_3$) were detected in the third vent, regardless if there was a fire or not. All abused cells went into thermal runaway and emitted smoke and gas, the working cells also released flames as well as sparks. The dead cells were however less reactive but still underwent thermal runaway. For about half of the working cells, for all levels of cycle ageing, ignition of the accumulated battery released gases occurred about 15 s after the thermal runaway resulting in a gas explosion. The thermal runaway temperature, about 190 °C, varied somewhat for the different cell ageing/status where a weak local minimum was found for cells cycled between 100 and 200 times.

Keywords: gas explosion, lithium-ion, safety, gas emission, ageing, thermal runaway

Highlights:

- Gas explosions due to delayed ignition of battery emitted gases in air mixture
- Three separate vents were detected, two vents before thermal runaway
- Gas emissions of HF and $POF_3$ detected in 3$^{rd}$ vent with and without fire
- Dead cells significantly less thermally reactive than working cells
- Dead cells still undergo thermal runaway

# 1. Introduction

Lithium-ion batteries have revolutionized many products since they have a high energy density combined with several other attractive properties. Li-ion cells are used in very high numbers in e.g. cell phones, laptop computers and power tools. Besides, they are being rapidly introduced in large systems and are found in kWh to MWh energy capacity applications used in e.g. electrified vehicles, ships and stationary grid storage plants.

The use of Li-ion batteries is, however, associated with more pronounced/different risks of developed heat, gas emissions, explosions and fire respect to other battery types. These risks are yet far from being fully understood and there is a potential for increased safety through research studies as well as from the analysis of incidents. The type and the severity of the risks depend on different applications and battery system sizes. Failure consequences can be significantly increased with increasing battery system size due to cell and module failure propagation [1,2,3].

The Li-ion cell contains all three parts of the fire triangle that are necessary to have a fire; heat/igniter, combustible material and oxygen. Furthermore, upon overtemperatures, starting from typically 70-120 °C, the Li-ion battery starts to swell and can release gases (venting). The vented gases are flammable and toxic [4]. If the temperature is high enough, of the order of 150-200 °C, an accelerated self-supporting rapid temperature increase, thermal runaway (TR), can also occur [5,6].The term onset temperature of thermal runaway is referring to the temperature where the exothermic reactions starts that eventually leads to thermal runaway, while the term thermal runaway temperature refers to when the thermal runaway occurs with very rapid temperature increase. The thermal runaway is typically associated by a release of large quantities of smoke and gas, a possible cell case rupture/explosion, fire or a gas explosion. There are thus two main types of explosions, an internal cell case explosion or a gas explosion of the flammable vented gases mixed with air. Cylindrical and hard prismatic cells can build high pressures and are therefore designed to release the gases via a built-in cell safety vent, however in case of e.g. malfunction, extreme pressures can built up inside the battery cell, resulting in the cell case explosion. A gas explosion occurs by a delayed ignition of vented combustible battery gases mixed with air accumulated in a confined or semiconfined enclosure. The consequences of a gas explosion can be more severe than a cell case explosion.

The vented gases can contain both evaporated solvents and decomposition products, e.g. CO, $CO_2$, $H_2$, $CH_4$ [7,8]. Beside CO and $CO_2$, a large number of different toxic compounds can be released [9,10,11] including fluoride gases. Hydrogen fluoride (HF) has caused most attention and is very toxic [12,13,14]. There are few studies published that report measurements of released HF amounts from commercial Li-ion battery cells during abuse [15,16,17,18,19] and some on HF release during electrolyte fire tests [20]. The fluorine in the cells comes from the Li-salt, e.g. $LiPF_6$, but also from electrode binders, e.g. PVdF, electrode materials and coatings, e.g. fluorophosphates [21,22] and $AlF_3$-coated cathodes [5,23,24], as well as from fluorine containing additives, e.g. flame retardants. Battery safety is complex and a holistic perspective is

essential, for example by introducing $AlF_3$-coatings, the risk for a thermal runaway to occur can decrease while the one for emission of toxic fluoride gases might increase as well as the one of gas explosion.. The overall safety is therefore difficult to evaluate, and depending on battery size and scenarios, it might be improved or worsened.

There are many different types of abuse tests available [25] and a common one is external heating. There are several types of external heating methods for Li-ion battery cells, e.g. heating in an oven [6,25], by IR radiation [18,19,26,27,28], by cartridge or other heaters [29,30,31], in a closed chamber using e.g. accelerated rate calorimeter (ARC) [5,32] or other types [8,33,34]. So far most studies have tested new/fresh cells, i.e. non-aged cells, and few studies are yet available investigating the influence of ageing on safety. Still it is essential to have a high battery safety level over the complete battery life time, since properties of the components may change during ageing. Ageing is typically seen in terms of calendar and cycle ageing. In order to shorten test time, storing and cycling the cells are often performed at increased temperatures, e.g. 35-55 °C, however, at these temperatures the results will differ from those obtained during use at ambient temperature, e.g. 20 °C because of other side and decomposition reactions. The ageing processes of Li-ion cells are non-linear and complex [35,36,37] and not yet fully understood. For example, during ageing the solid electrolyte interphase (SEI) layer is changed and SEI plays an important role and in the pre-stage of the thermal runaway.

Roth and Doughty [38] studied the thermal stability of calendar aged Sony 18650 cells by ARC-tests and found that aged cells, up to 70 °C, showed higher exothermic onset temperatures. Wu et al. [39] studied 0.75 Ah non-commercial graphite/LCO Li-ion cells after 10 and 200 cycles and found that in nail penetration abuse tests thermal safety decreased after 200 cycles. Röder et al. [40] studied 2 Ah graphite/LMO-NMC Li-ion 18650 cells stored at 60 °C up to 36 weeks and found in ARC-tests that exothermic reactions and thermal runaway onset temperatures are lower for cells aged 36 weeks. In contrast, Zhang et al. [41] studied 4.6 Ah graphite/LMO Li-ion cells stored at 55 °C for a duration between 10 and 90 days and found that the onset temperature of self-heating and thermal runaway increased for increased ageing. Fleischhammar et al. [42] studied the influence of cycle ageing on the thermal response in ARC tests for 1.5 Ah graphite/LMO-NMC high-power Li-ion 18650 cells and found significantly lower onset temperatures for first exothermic response as well as for the thermal runaway, with starting temperatures as low as 30.7 °C, and also found lithium plating on the anode for cells undergoing 1C cycling at -10 °C. Friesen et al. [43] studied safety in ARC tests of graphite/NMC 18650 fresh and cycle aged cells using 1C at 0 °C down to 70% state of health (SOH). Cells showed decreased thermal safety, aged cells had as low as 30 °C, onset temperatures as well as earlier thermal runaway. The same authors also studied safety by nail penetration abuse tests and found that aged cells have a delayed but more reactive thermal runaway. In general, formation of lithium metal-plating on the anode at low temperature cycling and/or at too high charging currents poses increased risks for Li-ion batteries [42,43,44,45].

In this work Li-ion cell safety is studied for non-cycled cells stored at 20 °C and 60 °C as well as for cells aged by 100, 200 or 300 deep C/2 cycles, all are of the same cell type, a commercial 6.8 Ah nom graphite/$LiCoO_2$ Li-ion cell. The safety is assessed by abuse testing in form of external

heating (oven) accompanied with FTIR gas measurements. One ARC test is performed for comparison of the safety evaluation methods.

# 2. Experimental

## 2.1 Cells tested

The cells, from the same batch of commercially available lithium-ion cells, had nominal capacity and voltage of 6.8 Ah and 3.75 V, respectively, a lithium cobalt oxide (LCO) cathode, a graphite anode, a polymeric separator and prismatic packaging, see Table 1 for detailed cell specifications. The cells contained fluorine due to the presence of $LiPF_6$ salt in the electrolyte, however, other parts in the cell might also contain fluorine, see examples in the introduction section. Anyhow, the cell was not analyzed for other potential sources of fluorine.

**Table 1** Specification of the commercial Li-ion cell, from cell datasheet, electrolyte from TG-FTIR analysis [46] and separator from DSC-analysis [47].

| Parameter | Value |
|---|---|
| Nominal voltage | 3.75 V |
| Nominal capacity | 6.8 Ah (20 °C, C/5 to 2.5 V cut-off) |
| Packaging | Jellyroll in aluminum hard prismatic can |
| Weight | 140.2 g |
| Cycle life according to datasheet | >70% capacity after 600 cycles with 0.5C, 100% DOD, 20 °C |
| Max continuous discharge current | 14 A |
| Max recommended continuous charge current | 7A |
| Anode | Graphite |
| Cathode | Lithium cobalt oxide, $LiCoO_2$ |
| Electrolyte | Salt: lithium hexafluorophosphate, $LiPF_6$<br>Organic solvents: EC, DMC, EA<br>Additives found: VC, presumable low molecular weight ketone |
| Separator | Shutdown separator, PE-PP |

## 2.2 Electrical characterization

Four-wire electrochemical impedance spectroscopy (EIS) in the frequency range 100 kHz - 5 mHz, with 60 points logarithmically distributed, was performed using a *Metrohm Autolab PGSTAT 302N* and the *Metrohm Nova 1.11 software* in the Galvanostatic mode with an amplitude of 0.1 A. The cell was at ambient temperature, about 20 °C, in a Faraday cage. Sense and current measurement cables were twisted and separated, in opposite circles, to minimize interference.

The capacity of each cell was measured using either a multichannel *Digatron battery tester* or a *Metrohm Autolab* with *Booster 20 A module*. For the capacity measurements used voltage limits of 2.50 V and 4.20 V, a current of 1.4 A (about C/5) and a cut-off charge current of 0.05 A. After the first charge, three complete discharge-charge cycles was applied. Before ageing, the discharge-capacity was measured in the first of the three cycles while after ageing the discharge-capacity of the third cycle was used to determine the cell capacity.

The battery cells were fully charged "First charge" (100% SOC) before the EIS measurement. The cycle numbers presented in this paper do not include the three charge-discharge cycles used to measure the cell capacity.

## 2.3 Ageing procedure

### 2.3.1 Ageing by cycling

The cells were cycled individually using a *Digatron battery tester*, with 100% depth of discharge (DOD) between 4.20 V and 2.50 V. The current of 3.4 A (C/2), was applied for both charge and discharge and a cut-off charge current of 0.34 A (C/20). The cells were cycled at ambient temperature, average temperature of 21 °C, with forced convection cooling. Each cell had a temperature sensor attached on the largest side surface.

### 2.3.2 Ageing by temperature

Fully charged cells were stored for 10 months in a 60 °C oven, which is the maximum allowed storage temperature according to the cell manufacturer's data sheet. The cells were stored at 20 °C before and after storing at 60 °C.

### 2.3.3 Complete cell ageing history

Firstly, the cells were stored un-used in their shipment boxes at room temperature, about 20 °C, during 12 months. Secondly, the cells underwent their first charge and the capacity and impedance was measured for each cell. Thirdly, cells selected for cycle ageing underwent cycling up to about two months (for 300 cycles) . Fourthly, the capacity and the impedance were measured and the cells were stored at room temperature. Fifthly, a few non-cycled cells were selected and stored in a 60 °C oven for 10 months

The external heating abuse tests were performed about 2 years and 4 months after the manufacturing date. Therefore, all cells were of equally long calendar age, but during their life time, some cells had been cycled and some had been stored at 60 °C for part of its lifetime (10 of 28 months).

## 2.4 External heating abuse tests

### 2.4.1 General setup

In total 14 external heating abuse tests were performed. The battery cells were individually heated using a thermostatically controlled oven, *Binder FED 115,* with an inner volume of 115

liter. The battery cell was centrally placed inside the oven and mechanically fastened with steel wire (0.8 mm diameter) on a brick, see Fig. 1. The oven was turned on 1 minute after the start of the test and set to 300 °C, utilizing the maximum heating rate capability of the oven.

The oven was custom-made with four 50 mm diameter access ports, sealed with silicon plugs and was equipped with an internal fan set to maximum speed in order to homogenize the internal temperature. The ventilation outlet, placed on the back of the oven, was set to be fully closed. However, it was not a perfect sealing and during the abuse tests it was partially deformed. The oven door was closed by the handle in the first test but since the door opened during the gas explosions, the door was instead fastened by duct tape in the following tests. Also, one of the silicon plugs on top of the oven was attached relatively loosely, to act as a pressure vent.

Between each test the oven was lightly cleaned/washed to minimize potential interference from e.g. particle contaminations. The glass door window (triple-glass) did not mechanically break but was heavily polluted and etched so it was replaced a few times, to have reasonable video quality.

The cell voltage and temperature were measured at 1 Hz using an *Agilent 34972A* with *Agilent 34902A reed multiplexer module.* The cell voltage was measured via a type K thermocouple cable fixed by twisting the cables in small drilled holes (0.8 mm diameter) in the electrical tab connectors. The Li-ion cell surface temperature was measured using type K thermocouples attached with glass fiber tape (*3M, electrical tape Scotch*, 19 mm wide), measured at up to six locations, T1-T6, see Fig. 1D. Thermocouples of type K were also used to measure the ambient temperature (outside of the oven) and the internal oven temperature, the latter one measured at two locations, as seen in e.g. Fig. 1 A and B. The abuse tests were video recorded by a camera placed outside the oven door window. In some tests, a second video camera was also used, placed at a distance, varying between about 2 and 7 meters, from the oven.

Cell thickness was manually measured using a caliper (gap about 150 mm long) and the cell thickness value noted was the greatest value, which was found at about the mid-mid center position on the largest side of the cell.

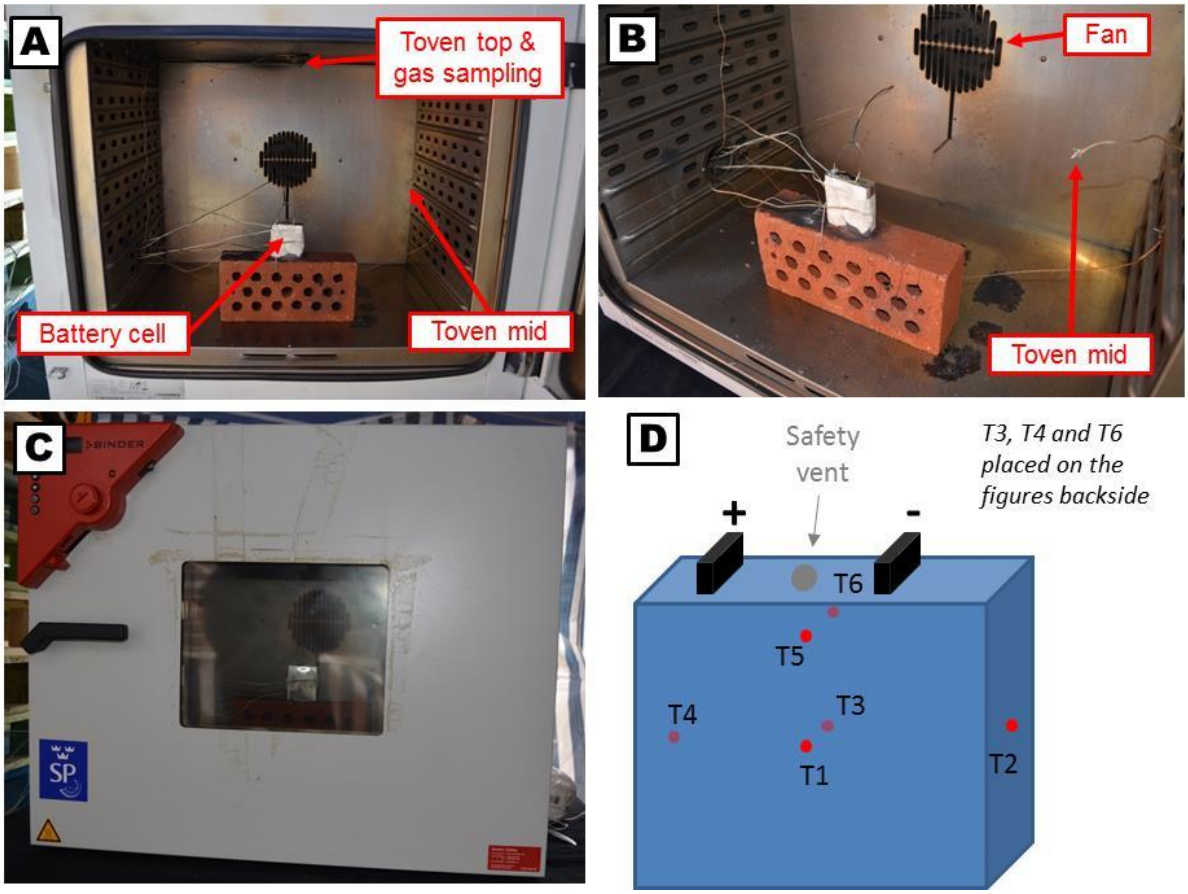


**Fig. 1.** Photos (**A-B**) showing the battery cell placed inside the oven, photo (**C**) showing the oven with closed door, the battery cell can be seen through the glass window of the oven door, the schematic drawing (**D**) shows the placement of the six thermocouples on the cell surface.

### 2.4.2 Specific setup for measurements of gas emissions using FTIR

In four of the tests, FTIR measurements of the gas emissions were performed using a *Bruker Alpha* FTIR spectrophotometer with accuracy of 0.19 $cm^{-1}$. The *transmission* module was used with a gas cell of 7 cm long optical path and $CaF_2$ windows. The non-heated gas cell had a volume of 12.4 mL and was fed via a non-heated 0.73 m long HDPE hose of 1 mm inner diameter and 3 mm outer diameter, having a dead volume of 0.57 mL. The sampling was conducted from a central top position in the oven using an aspirator pump with a controlled flow. The temperature sensor at the top of the oven was located right at the gas outlet. All measurements and elaboration were managed with the accompanying software *OPUS v7.2* inclusive of the package *Reactmon* for sequencing.

In order to have rapid measurements, the following settings were selected: resolution of 4 $cm^{-1}$, average of 8 scans. This resulted in a new averaged spectrum about every 12 seconds and an acceptable signal to noise ratio. Atmospheric compensation for $H_20$ and $CO_2$ was applied. Two

different flows were used in the experiments, 10 liter/hour (test 3 and 10) and 100 liter/hour (test 5 and 8). A new background scan was made before the start of each measurement series. The start times for the FTIR and the other measurements were synchronized. The time delay from gas release in the oven until detection by FTIR was approximately 1 spectrum (12 seconds).

For the FTIR measurements, the baseline of the background spectrum is shifting during the relatively long measurement series probably due to water condensation in the FTIR measurement cell. To compensate for such shifts, a baseline correction of each absorbance trace of a specific wavenumber against time was performed using the OPUS software built-in *Rubberband* correction method.

# 3. Results and discussion

### 3.1 Ageing – capacity fade and impedance

The cell in test 12, was supposed to be cycled to 300 cycles but failed during the cycling process after reaching 229 cycles and it was not possible to charge or discharge it any more. The cells in test 13 and 14 were initially fully charged and stored in 60 °C for 10 months and after this time the voltage had dropped to less than 1 V. The thickness of these cells had increased from 18.5 mm to 21.3 mm (about 15%), however the cell weights were not changed, indicating that the cells had not leaked or vented. The other cells in this investigation had all a thickness of 18.5 mm before and after the cycle ageing.

Capacity data prior to and after ageing are presented in Table 2. The SOH is the relative remaining capacity, calculated by the present C/5-discharge capacity divided by the initial C/5-discharge capacity. After the cycling, the cells had reached the following SOH, about 94% (100 cycles), 91% (200 cycles) and 89% (300 cycles). The cells in test 1 and 4 had lower initial discharge capacity, as shown in Table 2, because they were cycled 3 times prior to the capacity measurements. However, even though the cells in test 1 and 4 were cycled 3 times (for details, see note in Table 2), they are here referred to as 0 cycle cells. Fig. S1 shows the C/2 discharge capacity degradation during cycling for the cycled cells.

Fig. 2 shows the impedance measurements for cells with different cycling ageing. The impedance plot, Fig. 2A, has the typical appearance for lithium-ion batteries, including high frequency inductance, depressed overlapping semicircles at intermediate frequencies and a low frequency spike, each corresponding to cell and connector impedance, SEI and charge transfer effects, and mass transport, respectively [48]. The average series resistance determined from the intersection with the real axis in the complex impedance plot in Fig. 2A for this cell type was originally 13.2 mΩ and increased after 300 cycles to 14.4 mΩ (a 9% increase). In Fig. 2B the results are plotted as phase angle versus the logarithm of frequency. Two peaks are found in this plot, one at frequencies just above 0.1 Hz and one at about 2 Hz. While the low frequency peak increases in size with increasing cycle aging the second peak more or less disappears already after a few cycles. Anyhow, already after 3 cycles distinct differences are detected and the plot of phase angle thus offers another perspective to illustrate the influence of ageing.

Similar plots have been published earlier for lithium-ion cell but without a more detailed discussion [49,50]. For aged batteries with same electrode chemistry (graphite/LCO) the low frequency semicircle in the impedance plot has been assigned to electrolyte oxidation at the cathode [45] and it might therefore be suggested that the growth of the peak in phase angle above 0.1 Hz in this this case is also due to oxidation at the cathode. This may be likely since the cells were charged to a relatively high upper cut-off voltage of 4.20 V, yet within the cell manufacturer's specifications.

**Table 2** Cell data for cycled and none-cycled cells, capacities measured as discharge capacities with 1.4 A (a C-rate of about C/5).

| Test No. | Cycle ageing and cell status | Initial discharge capacity (Ah) | Capacity after ageing (Ah)** | Calculated capacity loss (Ah) | Calculated SOH (%) |
|---|---|---|---|---|---|
| **1** | 0 | 6.50 *** | N/A | N/A | N/A |
| **2** | 0 | 6.63 ** | N/A | N/A | N/A |
| **3** | 0 | 6.56 ** | N/A | N/A | N/A |
| **4** | 0 | 6.47 *** | N/A | N/A | N/A |
| **5** | 100 | 6.72 * | 6.26 | 0.46 | 93.2 |
| **6** | 100 | 6.64 * | 6.23 | 0.41 | 93.8 |
| **7** | 100 | 6.62 * | 6.25 | 0.37 | 94.4 |
| **8** | 200 | 6.60 * | 6.04 | 0.56 | 91.5 |
| **9** | 200 | 6.73 * | 6.05 | 0.68 | 89.9 |
| **10** | 300 | 6.53 * | 5.84 | 0.69 | 89.4 |
| **11** | 300 | 6.68 * | 5.95 | 0.73 | 89.1 |
| **12** | Dead cell, sudden death after 229 cycles | 6.63 * | N/A | N/A | N/A |
| **13** | Dead cell, 0 cycles, stored in 60°C during 10 months | 6.71** | N/A | N/A | N/A |
| **14** | Dead cell, 0 cycles, stored in 60°C during 10 months | 6.69** | N/A | N/A | N/A |

** Using Digatron battery tester*

*** Using Metrohm Autolab PGSTAT 302N*

**** Using Metrohm Autolab PGSTAT 302N, lower value because the cell was prior charge-discharged three times using 3.4 A (C/2) with 0.34 A cutoff charge current. The impact of these three additional cycles in terms of cycling ageing is regarded as negligible.*

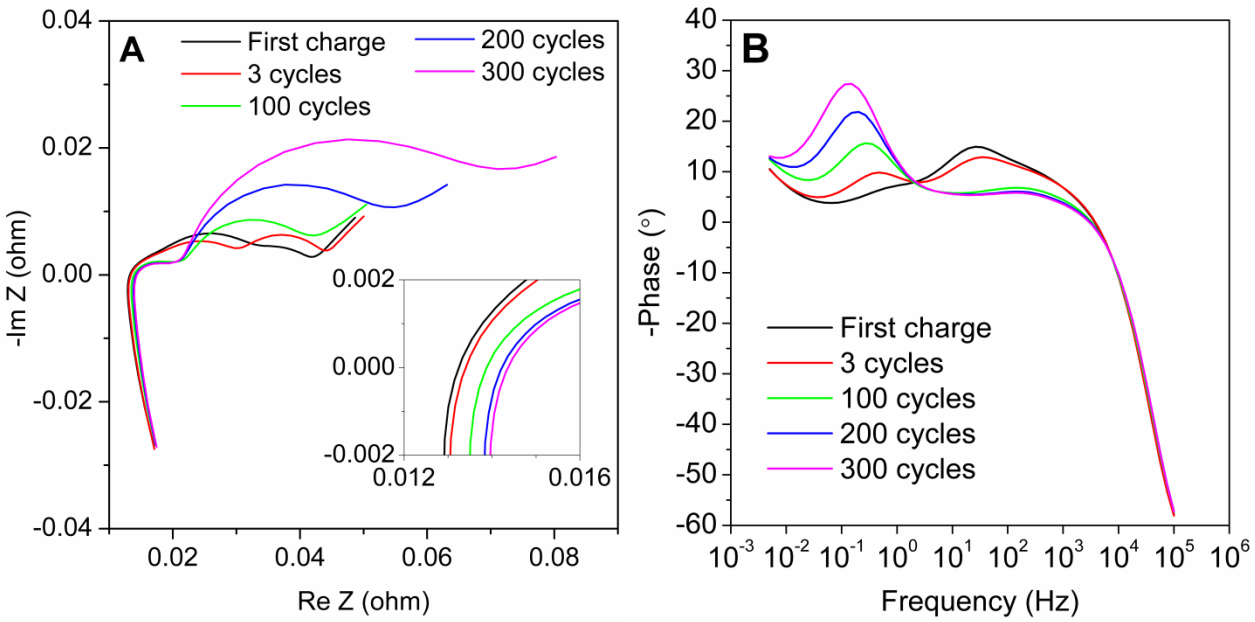


**Fig. 2.** (**A**) Complex Impedance, between 100 kHz and 5 mHz for different number of battery cycles at 100% SOC, real vs imagine parts with insets around the origin, and (**B**) phase vs frequency. Average values, calculated for each cycle number from all available cells, except for "3 cycles" where only one cell was measured.

### 3.2 External heating abuse

In tests 1-11, the cells were fully charged (100 % SOC), but had different cycling ageing, ranging from 0 to 300 cycles. The cells in test 12-14 were dead (non-functional) cells, thus the SOC was not possible to determine. The cell in test 12 suffered "sudden death" during cycling after 229 cycles. The cells used in test 13-14 had been stored for 10 months at 60 °C and had self-discharged or failed during that time and therefore had an OCV less than 1 V, that is below 0% SOC-level.

#### 3.2.1 Overview results

Results from the external abuse tests of the fourteen cells of various ageing and status, working cells as well as dead cells are presented in Table 3. In all tests, the temperature rate increased rapidly when the temperature reached the thermal runaway temperature, and all cells underwent a thermal runaway. For test 1-11, there were short (less than a second) and typical smaller flares, sparks and jet flames coming out of the cell after the thermal runaway, see examples in Fig. 3. In some cases the cell was on fire for longer time and with larger flames, referring to the term "fire" in Table 3. The fire was typically followed by a smaller flame fire, see Table 3, which indicate the presence of one or several flames over an extended period of time. Furthermore, the terms "non-fire" or "without fire" are used when there was no ignition of the battery or its gases, this does not take into account the initial short flares/sparks/jet flames. The term "gas explosion" refers to a delayed ignition of the accumulated flammable gases released

from the battery mixed with air inside the oven, which in the present case resulted in a pressure wave forcing the oven door to open. Gas explosions are common phenomena in fire science [51] however not often discussed with regard to Li-ion battery fires. In this study, as seen in Table 3, the tests for all working cells was either resulting in non-fire or in a gas explosion followed by fire. Furthermore, for about half of the working cells and for all levels of cycle ageing a gas explosion occurred followed by a fire during about 30 seconds and a subsequent small flame fire for about 20-50 seconds thereafter. For the dead cells, test 12-14, the results were significantly different, the video analysis did not show any flares/sparks/jet flames, nor fire or gas explosion occurred.

**Table 3** Overview results from external heating abuse tests.

| Test No. | Cycle ageing and cell status | FTIR gas measurement | Total test time (min) | Thermal runaway and major venting* (min:sec) | Thermal runaway outcome Time as min:sec | Weight loss (%) | Thickness after test (mm) |
|---|---|---|---|---|---|---|---|
| **1** | 0 | - | 105 | 68:39 | • Flares/sparks/jet flames<br>• No fire or explosion | 22.3 | 25.5 |
| **2** | 0 | - | 127 | 64:24 | • Flares/sparks/jet flames<br>• No fire or explosion | 22.9 | 26.0 |
| **3** | 0 | YES | 84 | 68:16 | • Flares/sparks/jet flames<br>• **Gas explosion** @ 68:30<br>(oven door fully opened, camera still attached and observes the accompanied fire)<br>• 32 sec Fire<br>• 14 sec small flame fire (above cell vent) | 22.4 | 27.1 |
| **4** | 0 | - | 84 | 62:55 | • Flares/sparks/jet flames<br>• **Gas explosion** @ 63:08<br>(oven door opened about 10 cm, camera still attached and observes the accompanied fire)<br>• 32 sec Fire<br>• 38 sec small flame fire (above cell vent). | 22.1 | 28.0 |
| **5** | 100 | YES | 84 | 61:54 | • Flares/sparks/jet flames<br>• No fire or explosion | 23.1 | 27.0 |
| **6** | 100 | - | 75 | 59:22 | • Flares/sparks/jet flames<br>• **Gas explosion** @ 59:33<br>(oven door fully opened, camera still attached and observes the accompanied fire)<br>• 32 sec fire | 24.0 | 27.2 |

| | | | | | | | |
|---|---|---|---|---|---|---|---|
| | | | | | • 40 sec small flame fire (above cell vent) | | |
| **7** | 100 | - | 84 | 61:43 | • Flares/sparks/jet flames<br>• No fire or explosion | 22.7 | 25.9 |
| **8** | 200 | YES | 94 | 60:39 | • Flares/sparks/jet flames<br>• Lighter **Gas explosion** @ 61:05 ( door not opened, minor pressure wave on oven backside, camera still attached and observes the accompanied fire)<br>• 81 sec Fire | 22.2 | 27.8 |
| **9** | 200 | - | 86 | 62:26 | • Flares/sparks/jet flames<br>• No fire or explosion | 22.8 | 27.2 |
| **10** | 300 | YES | 94 | 63:30 | • Flares/sparks/jet flames<br>• **Gas explosion @** 63:46 (oven door opened a few cm (door reclosed after about 1 min), camera blown off)<br>• No camera to observe any fire | 21.9 | 28.0 |
| **11** | 300 | - | 87** | 61:21*** | Power blackout* @ 61:17 (unfortunately just before TR)<br>• No camera to observe any possible fire<br>• No explosion heard, oven door not opened. | 22.7 | 29.0 |
| **12** | Dead cell, sudden death after 229 cycles | - | 84 | 68:36 | • No flares/sparks/jet flames<br>• No fire or explosion | 14.8 | 23.9 |
| **13** | Dead cell, 0 cycles, stored in 60°C during 10 months | - | 86 | 73:36 | • No flares/sparks/jet flames<br>• No fire or explosion | 17.9 | 23.5 |
| **14** | Dead cell, 0 cycles, stored in 60°C during 10 months | - | 87 | 72:04 | • No flares/sparks/jet flames<br>• No fire or explosion | 18.2 | 23.9 |

** The major venting happened at the very same time as the thermal runaway temperature is reached, rapidly increasing the temperature rate. The "major venting" is also in this paper referred to as the "3rd vent".*

*** Power blackout at the test facility, data logging, oven camera and external heating switched*

*off during about 9 minutes (no data logging during 9 min 39 seconds). Secondary video camera outside still functional (laptop-battery pack-powered) and was uses to observe time for major venting and assumed to be time for TR.*
**** Determined by secondary video camera outside oven.*

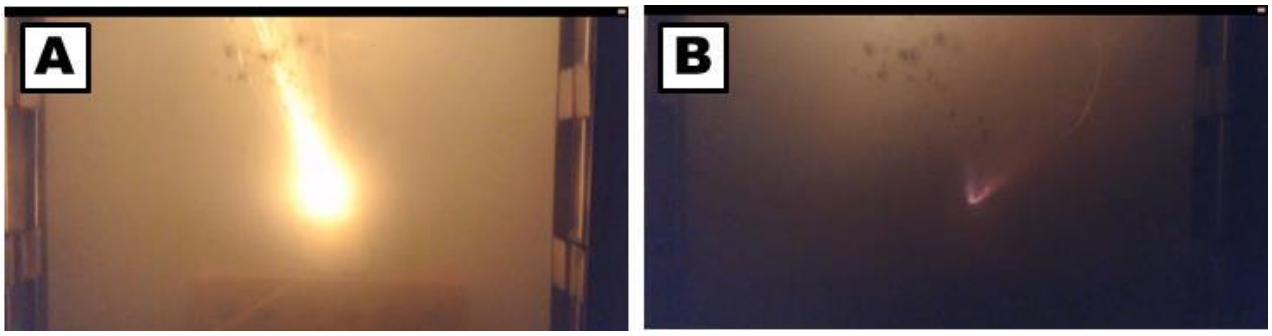


**Fig. 3.** Two video pictures at thermal runway @ time 59:22 in test 6, showing a relative large jet flame **(A)** and smaller flares next after in time **(B)**, neither of them ignited the cell or the gas mixture in the oven.

For all tests, the video analysis showed that the cell safety vent, located on the top of the cell, opened at the same time as the thermal runaway temperature was reached, releasing large amounts of smoke that rapidly filled up the oven volume. The color of the released smoke was typically white or light grey. In case the cell safety vent would not open, e.g. due to malfunction or bad design, a cell case explosion can occur, a dangerous situation including the risk for ejection of ballistic projectiles. There are thus two types of battery explosions, the single cell case explosion (due to internal pressure build-up) and the gas explosion, a delayed ignition of gas emission released from battery cell(s) mixed with air, that can be more severe.

The working cells lost more weight and were more swollen (thicker) than the dead cells. The weight losses were in average 22.6 % for the working cells and 17.0 % for the dead cells. The working cells increased their thickness from 18.5 mm to an average to 27.2 mm (an increase of 47 %) while the dead cells in average were 23.8 mm thick after the external abuse.

The total test times varied somewhat as seen in Table 3, resulting in different heating exposure times. There was occasionally an accidental variation in the test times due to gas explosion, e.g. when the gas explosion slammed the oven door open, the test was considered finished. The variation of the total test time was also due to varying ambient conditions and few intendent longer to study its influence. The weight loss and cell thickness increase was not significantly affected by the varied test run time, suggesting that all major effects regarding cell material loss and cell case occurred within the time frame of the shortest test time (75 min in test 6).

### 3.2.2 Temperature results

The temperature results from the external heating abuse tests are presented in Table 4. The thermal runaway temperature values in Table 4 are determined as the temperature when the rapid increase in temperature occurs. For active cells the thermal runaway temperature was

easily determined while for the dead cells, and in particular for test 12, it was less distinct. The dead cells have a significantly higher thermal runaway temperature, lower temperature rise rate and lower peak temperatures. The results for the dead cells with 0 cycles and stored for a part of its lifetime at 60 °C for 10 months, tests 13-14, show high reproducibility.

**Table 4** Temperature results from the external heating abuse tests.

| Test No. | Cycle ageing and cell status | Thermal runaway temperature (°C) | Max single sensor (°C) | Max Tavg 2 (°C) | ΔT (°C) | Δt (sec) | Max dTavg2 (°C $sec^{-1}$) | Tavg2 sensors used |
|---|---|---|---|---|---|---|---|---|
| **1** | 0 | 195 | 636 | 600 | 405 | 65 | 30 | T1, T4 |
| **2** | 0 | 195 | 646 | 582 | 387 | 94 | 22 | T1, T3, T5, T6 |
| **3** | 0 | 192 | 530 | 450 | 258 | 16 | 72 | T1, T2, T3, T4, T5, T6 |
| **4** | 0 | 192 | 663 | 562 | 369 | 40 | 31 | T2, T3, T5, T6 |
| **5** | 100 | 190 | 579 | 523 | 333 | 73 | 25 | T1, T3, T4, T5 |
| **6** | 100 | 191 | 647 | 580 | 389 | 74 | 37 | T3, T5 |
| **7** | 100 | 187 | 567 | 524 | 337 | 84 | 23 | T1, T2, T3, T4, T5, T6 |
| **8** | 200 | 189 | 605 | 570 | 382 | 49 | 25 | T1, T2, T3, T4, T5, T6 |
| **9** | 200 | 188 | 529 | 490 | 302 | 87 | 17 | T1, T4, T5, T6 |
| **10** | 300 | 191 | 604 | 534 | 343 | 29 | 39 | T1, T4, T5, T6 |
| **11** | 300 | >188* | N/A | N/A | N/A | N/A | N/A | N/A, Power blackout |
| **12** | Dead cell. sudden death after 229 cycles | 205 | 361 | 339 | 134 | 129 | 4 | T1, T2, T3, T4, T5 |
| **13** | Dead cell. 0 cycles. stored in 60°C during 10 months | 201** | 540 | 460 | 260 | 76 | 10 | T3, T4, T5, T6 |
| **14** | Dead cell. 0 cycles. stored in 60°C during 10 months | 203 | 547 | 463 | 260 | 75 | 9 | T1, T2, T4, T5 |

** The average cell surface temperature was 188 °C when power blackout occurred. The thermal runaway happened about 5 seconds later.*

*** T1 thermocouple failed at the beginning of the test, so instead of calculated the average as T1 and T3, the average value was calculated using the five temperature sensors T2-T6.*

The cell surface temperature sensors, T1-T6, are in general reliable at temperatures up to the thermal runaway. The thermal runaway temperature values were calculated as an average of sensors T1 and T3 for all tests expect for test 13 (see note in Table 4). Above the thermal runaway temperature, the sensors record quite different temperatures and occasionally detach from the cell due to the high temperature, cell expansion and eventual gas explosions. Therefore another average value, Tavg2, was used to find the maximum average cell surface temperature, the corresponding rate of temperature increase and the time duration (step time) for that increase. Tavg2 was calculated using all usable sensors of T1-T6, specified in Table 4. Usable sensors were defined as sensors that had not lost cell surface contact. Since the number and positions of the usable cell temperature sensors varied the results presented in Table 4 naturally varies. The thermal runaway temperature values are thus rather well-defined while the maximum temperature values spread more.

The cell surface temperature sensors show relatively similar temperature values before thermal runaway, in contrast to the large temperature variations between the sensors after the thermal runaway. Fig. 4 shows cell voltage, average temperature rate and temperature measurements for test 7, which was one of few tests having all six temperature sensors usable during the complete test. The cell surface temperatures in Fig. 4 vary up to approximately 100 °C. In other tests, local cell surface temperature variations were up to about 300 °C at the most. For this type of measurements, it is important to use multiple cell surface temperature sensors combined with proper validation methods to obtain reliable temperature measurements.

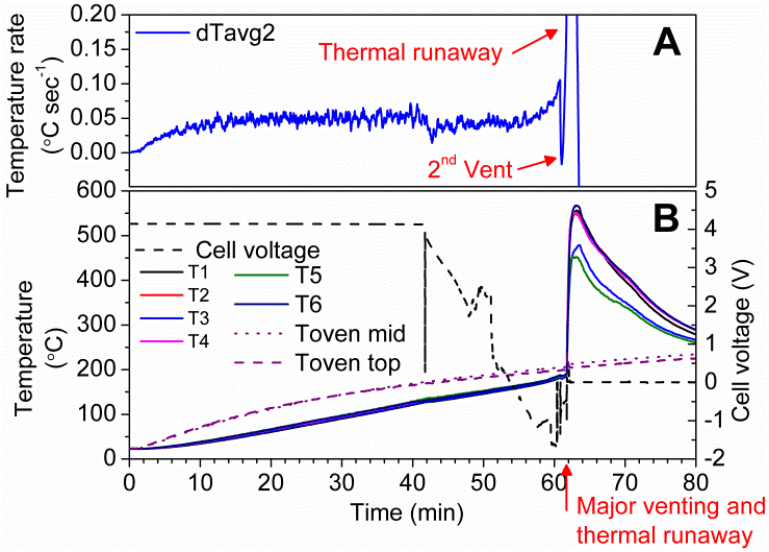


**Fig. 4.** Results from test 7, **(A)** showing the derivate of the average cell surface temperature, dTavg2, and **(B)** showing the cell voltage, the temperature values from the battery surface temperature sensors, T1-T6, and from the two temperature sensors in the oven, Toven mid and Toven top.

Fig. 5A shows the average cell surface temperature prior to and during the early stage of the thermal runaway and all tests are time synchronized to the thermal runaway temperature, which is also marked in the figure. The temperature drops some minutes before the thermal runaway, seen for some of the curves, in particular clearly seen for the blue lines (100 cycles) and identified as due to gas release, in this paper referred to as the 2nd vent. Fig. 5B shows the thermal runaway temperature values vs the number of ageing cycles, the latter showing a shallow minimum between 100 and 200 cycles. In one of the tests, test 11, a total power blackout occurred at the test site seconds before the thermal runaway. The time for major venting in test 11 could anyway be determined using a battery operated outside camera. The time between the last logged data point at 188 °C and the observed gas release and its corresponding thermal runaway was about 5 seconds, although a short time the temperature rate increase is relative rapid. The temperature heating curve for test 10 and 11 followed each other very well up to the blackout.

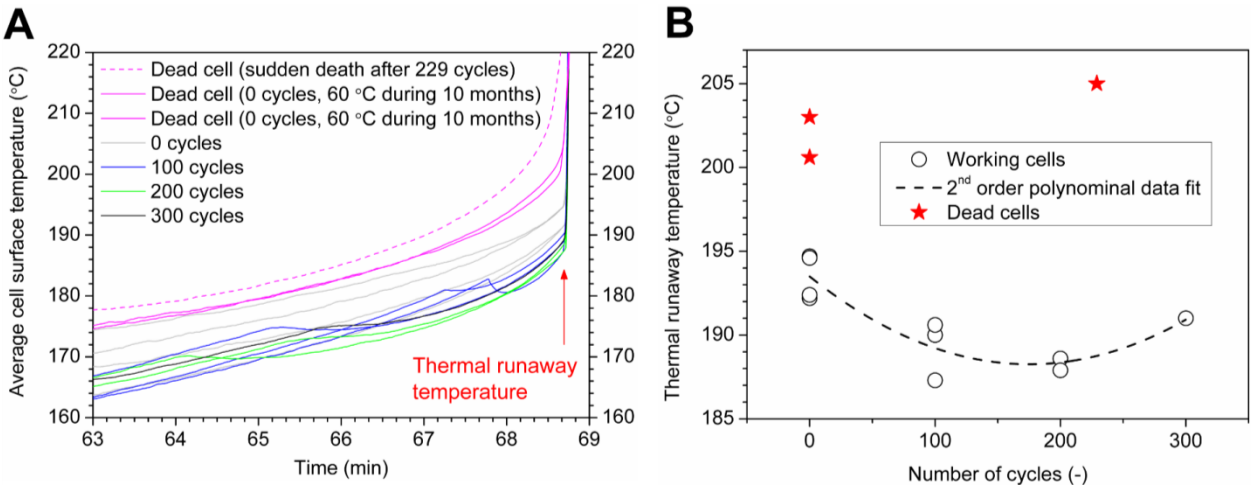


**Fig. 5.** The average cell surface temperature calculated as average of the sensors T1 and T3, **(A)** showing temperature vs time, the time-scales have been synchronized to the thermal runaway temperature, (**B**) showing the thermal runaway temperature vs cycle ageing (number of cycles). The test results shown in the figure A are time-temperature synchronized to the rapid temperature rise at the thermal runaway temperature, using the time in test 1 as reference time.

The thermal runaway temperature values for the same type of cell depend on the test method and on its definition, as well as the location, number and measurement quality of the temperature sensor(s) used. It is crucial to be aware of this when comparing thermal runaway temperatures and onset temperature values from different studies. The value of thermal runaway temperature presented in this paper is the very last temperature point before the start of the rapid temperature increase, seen in Fig. 5A. The thermal runaway temperature values

presented here are about 190 °C for the working cells, and range between 201 and 205 °C for the dead cells. Similar temperature values have been reported [8,25,43,52].

If the external heating had stopped at some time before the thermal runaway temperature, the cells could still go to thermal runaway depending on the cell temperature, cell's own heat-generation rate and ambient conditions such as cell cooling rate. However, the experimental method used in this work did not use a heating step increase method with pauses. Another common method used in the Li-ion battery safety field is the ARC test, according to a Heat-Wait-Search (HWS) procedure, where the battery cell is heated up with high sensitivity and the heating is halted if exothermic heat is detected from the battery cell, monitoring the exothermic cell reactions under adiabatic conditions. For ARC-measurements the onset temperature of thermal runaway can be defined as the temperature when the self-heating rate (SHR) is > 0.2 °C $min^{-1}$ and the thermal runaway temperature when SHR > 10 °C $min^{-1}$ [5,43]. The temperature where the exothermic reactions and the self-heating starts is test equipment specific and typically occurs when SHR > 0.02 °C $min^{-1}$ [43].

The heating time in ARC is typically long, which allows time for boiling/venting and potential side-reactions at high temperatures to occur, e.g. electrolyte degradation and breakdown of SEI and electrode materials, which may affect the test results compared to if the cell is heated up more rapidly. In a hypothetical case, if the electrolyte would have enough time to boil/vent at lower temperatures, no thermal runaway can occur at higher temperatures since no electrolyte-electrode reactions can occur creating the thermal runaway. The heating test time of about 60 minutes used in the present paper, also gives time for side reactions and electrolyte boiling/venting, however less time compared to the ARC test method. As a comparison, a cell from the same batch at 100% SOC was externally abused in an accelerated rate calorimetry (ARC) test chamber by the National University of Singapore. If a thermal runaway temperature is determined from the ARC measurement in a similar principle way as used in the oven experiment, the result is approximately 140 °C, the temperature vs time curve can be seen in Fig. S2. The results for the two measurements thus differ by about 50 °C.

### 3.2.3 Results combined with gas measurements

Fig. 6 shows the measurements of temperature, cell voltage and gas emissions for test 5, a cell which was aged by 100 deep cycles. Three vents were detected. The first vent, releasing dimethyl carbonate (DMC) and ethyl acetate (EA) vapours, occurred at the same time as the cell voltage went down to about 0 V. The cell voltage drop started when the surface temperature was about 130 °C. This temperature is very close to the first melting temperature of the cell's shutdown separator, as can be seen in Fig. S3. Differential scanning calorimetry (DSC) measurements on two commercial separators, one PP monolayer and one trilayer shutdown separator PP/PE/PP, as well as the separator extracted from a non-abused battery cell, are shown in Figure S3. Due to the melting of the separator the temperature is expected to show some decrease since the process is endothermic, instead the cell surface temperature measurement clearly shows a temperature increase during 12 seconds. A possible explanation for the observed temperature increase could be that the cell undergoes an internal cell short

circuit generating heat, however it should only be possible in case the shutdown separator would have a failure/melting of both separator material layers. The second vent also releases ethylene carbonate (EC), 3.5 min before the thermal runaway, and the cell temperature clearly decreased during this venting due to the cooling effect of the outflowing gas. The first and the second vents were not seen or heard on the video, and were determined only from the FTIR gas measurement. The boiling temperature for DMC and EA is significantly lower than for EC, as seen in Table 5. The third vent, also referred to as the major venting in Table 3, occurred when the cell safety vent opened completely, the cell went into thermal runaway and the gas emissions also contained HF besides DMC, EA and EC. HF and $POF_3$ (not shown in Fig. 6) were simultaneously detected for the first time in the third vent/major vent that is clearly visible and audible on the video. Fig. 7 shows the gas emission, temperature and cell voltage results for test 10, a cell aged with 300 cycles which is similar to test 5, however undergoes a gas explosion. The video of the thermal runaway and gas explosion from test 10 can be seen in the supplementary materials, Video S1.

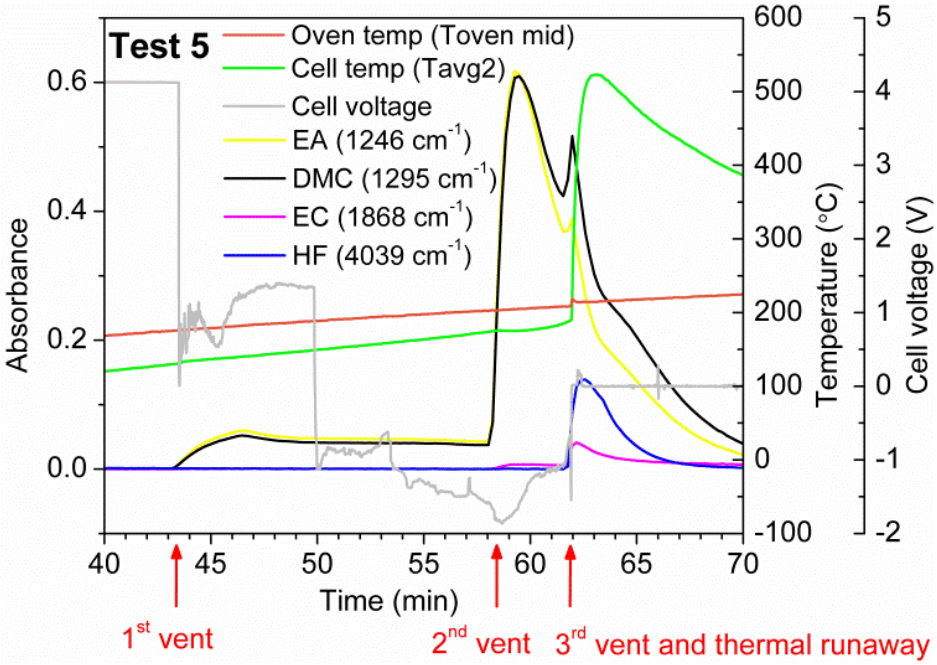


**Fig. 6.** Measurements of temperature, cell voltage and gas emissions for test 5 with 100 cycles. The three separate vents and thermal runaway are marked with arrows.

**Table 5** Flammability data for the electrolyte solvents in the cell.

| Electrolyte solvent | Molecule weight (g $mol^{-1}$) | Boiling temperature (°C) [53] | Autoignition temperature (°C) [53] | Flash point (°C) [53] | Flammable limits lower / upper (%) [54] |
|---|---|---|---|---|---|
| Ethyl acetate (EA) | 88 | 77 | 427 | -3 | 2.2 / 9 |
| Dimethyl carbonate (DMC) | 90 | 91 | 458 | 16 | 4.22 / 12.87 |
| Ethylene carbonate (EC) | 88 | 248 | 465 | 143 | 3.6 / 16.1 |

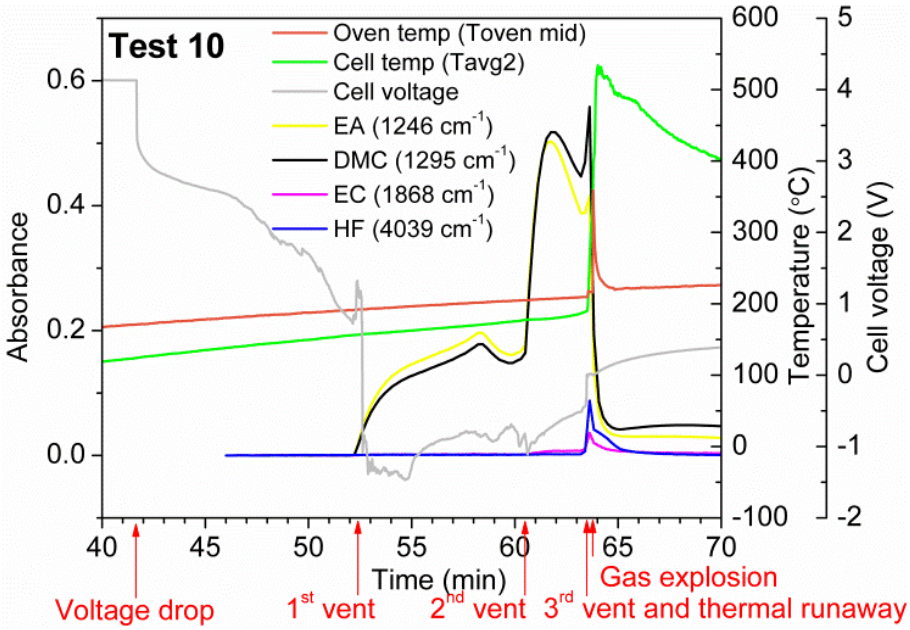


**Fig. 7.** Measurements of temperature, cell voltage and gas emissions for test 10 with 300 cycles. The video camera went off due to explosion so there was no camera to observe the occurrence of fire. Due to the explosion the oven door was opened and the gas emission amounts rapidly decreased.

### 3.2.4 Gas explosions

For the working cells, gas explosions were relatively common, i.e. an explosion happened in 5 out of 11 cases, and happened for all levels of cycle ageing in the investigated range (0-300 cycles). In test 3, 4, 6 and 10 the oven door flung open, the camera was blown off/moved and a bang was heard when the gases in the oven ignited. For the gas explosion in test 8, the gases ignited, but the development was different, less powerful. The time between thermal runaway/major venting until ignition was 26 seconds in test 8 while in the other four cases the gas explosion occurred 11-16 seconds (with an average of 13.5 seconds) after the thermal

runaway. If the oven had been perfectly sealed and without the pressure release counteractions, the gas explosions had probably been more severe. The tests involving gas explosions, i.e. test 3, 4, 6, 8 and 10, all showed a higher rate of temperature increase, dTavg2, see Table 4, with maximum values ranging between 25 to 72 °C $sec^{-1}$. Test 1 had a maximum value of 30 °C $sec^{-1}$, hence the cell might have been close to a gas explosion, however, it did not happen and neither the gases nor the cell did catch fire.

From the video analysis it was seen that all working cells, test 1-11, generated visible flames and sparks, however even though the oven was filled with released smoke and emitted gas no ignition occurred until at a later stage. For an explosion to occur, the mixture of gases and air must be within certain limits and an ignition source must be present. In the first about 10 seconds of battery gas emissions from the 3rd vent, these criteria might not have been fulfilled. The smoke and gas in 3rd vent filled the oven in about 2-3 seconds and thereafter it was not possible to clearly determine the presence of flames or sparks from the video due to the low visibility in the smoke. Before the third vent/thermal runaway, the oven was filled with gas emissions originating from the 1st vent as well as the significantly larger release of the 2nd vent detected by FTIR, so the jet flames and sparks observed just after the safety vent opened in the third vent did not ignite these gases, in none of the tests.

For all cells with 0, 100 and 200 cycles the cell thickness expansion was larger if the cells had gone through a gas explosion, for the 300 cycle cells, it was the opposite. The fact that cells involved in a gas explosion were thicker might indicate that those cells did build up a higher pressure inside the cell before the safety vent completely opened, even though the cell was already partially opened (proven by the 1st and 2nd vents).

It is not possible to exactly determine the ignition source when the gas mixture finally ignited. The ignition could have started inside or outside the cell. The ignition source of the gas explosion could be due to sparks or flames originating from the thermal runaway or an internal cell short circuit due to separator melting, or simply from autoignition of the hot gas mixture. The cell surface temperature was at least for some time higher than 465 °C for all working cells, thus above the auto ignition temperature for EA, DMC and EC, see Table 5. Furthermore, the cell internal temperature was probably higher than the measured surface temperature. The cell might possibly contain flame retardants in the electrolyte, which could be the reason for the unidentified bands found at 1466 $cm^{-1}$ and 1319 $cm^{-1}$ by Bertilsson et al. [46]. This might explain why none of the cells had an instant ignition and not all tests had a delayed gas ignition/gas explosion.

Table 5 shows flammability data for DMC, EA and EC. The autoignition temperature is the lowest temperature at which a flammable mixture of the solvent can spontaneously ignite. The flashpoint is the lowest temperature at which the liquid can be ignited with an ignition source. The flammability range within which limits a gas mixture can be ignited and cause what is called a gas explosion. When a flammable mixture is ignited it will typically expand 5-8 times due to the temperature increase, i.e. it will cause an overpressure of 5-8 bars if confined. Note that many building structures such as doors and windows can withstand a pressure difference of less than 100 mbar. A rather small amount of electrolyte is needed in order to create a flammable

mixture. In one cubic meter about 30 liters (3 % of 1 $m^3$) of solvent in the gas phase is needed. Using the ideal gas law one obtains that 30 litres corresponds to about 100 g of solvent. This means that evaporating 1 kg of electrolyte solvent can result in a flammable mixture of 10 $m^3$. However, as the 5-8 bar over pressure that is created upon ignition of a flammable mixture in a confined space is far above what most structures can withstand.

For the oven volume of 115 liter 100 g $m^{-3}$ means that about 12 g (corresponding to 8 % of the cell weight) of released electrolyte will result in reaching the lower flammability limit (LFL) in the oven. The working cells lost between 31-34 g in weight, while the dead cells lost 21-26 g, and consist of several cell parts, e.g. electrolyte, separator, etc, and indicating that LFL would probably be reached relative easily in all the tests, yet not all did ignite/explode. It is important to consider that due to the non-ideal behavior gases and gas mixtures the LFL might vary from the one stated for each gas and also the gas concentration will have some variations within the oven volume.

### 3.2.5 Toxic gas emissions

Gas emissions of HF and $POF_3$ were measured in all four tests where the FTIR gas measurement was employed, regardless if there was a fire or not. HF is very toxic while $POF_3$ can be seen as a precursor of HF by hydrolysis and therefore may be considered toxic. The sources of fluorine can be several as discussed in the introduction, however a major fluorine source is typically the Li-salt $LiPF_6$ producing HF and $POF_3$ according to Yang et al. [55],

$LiPF_6 \rightarrow LiF + PF_5$ (1)

$PF_5 + H_2O \rightarrow POF_3 + 2HF$ (2)

$POF_3 + 3H_2O \rightarrow H_3PO_4 + 3HF$ (3)

As seen from eqs. 2-3, water/humidity is needed in order to produce HF. The cell interior, e.g. the electrolyte, might contain very small traces of water but they generally disappear in the first cycles of the battery by contributing to the formation of the SEI layer. In normal conditions and at moderate temperature increase, the cell is still fully sealed. When the cell sealing breaks, at the 1st vent, gas emissions are let out in oven air which contains humidity. There is thus a potential for humid air to react with cell materials in the 1st and 2nd vents, however HF and $POF_3$ are not yet detected. The large cell opening of the cell safety vent occurs in the third vent, and this is the only vent phase where HF as well as $POF_3$ are detected.

It is an interesting question why HF and $POF_3$ are detected only in the 3rd vent and not during the 1st and 2nd vents where the cell is open. Possibly, in the first and second vents the electrolyte solvents are boiling off and emitted as single compounds without the Li salt. In the third vent, the gas release is so strong, as is clearly observed from video, that it can release not only the most volatile part of the electrolyte but the remaining electrolyte including part of the $LiPF_6$. Thereafter the $LiPF_6$ containing electrolytes can react with the humidity in the oven and produce HF and $POF_3$.

The temperature also influence the HF formation, however the temperature differences in the three vents are relative low. For the four tests having gas measurement, the temperature of the gas sampled at the gas outlet, was 174-185 °C in the first vent and 193-197 °C in the second vent. In the third vent, where HF and $POF_3$ were detected, the temperature ranged between 203 and 240 °C and the air temperature rose to more than 300 °C in the cases when a gas explosion occured. The gas temperature was however recorded in the oven and not in the measured FTIR gas cell. However, during the external heating, warm oven air is continuously sucked into the gas sampling tubes and gas cell thus warming them. For the higher flow rate used in test 5 and 8, the gas volume of the sampling system (hose and gas cell) was about 13 mL while the flow rate was about 28 mL $sec^{-1}$, so ambient cooling effect was probably relative low. For the lower flow rate used in test 3 and 10, about 2.8 mL $sec^{-1}$, the refilling time was anyway less than 5 seconds. It should also be noted that the gas sampling flow rates correspond to about one or less volume change of the oven volume, which is 115 L, per hour. The oven is not perfectly air tight so a relatively small yet essential air inflow that facilitate more time-accurate FTIR measures. Conversely, when the oven door opened due to gas explosions, the FTIR gas emission data did not show accurate data.

Fig. 8A shows a FTIR vibrorotational spectrum of HF vapor originating in the oven, and Fig. 8B shows detection of $POF_3$ at an earlier time in test 5. $POF_3$ is detected by its characteristic band at 1416 $cm^{-1}$, which is assigned to the prohibited Q-branch of the ΔJ=0 P=O stretching mode [55]. The bands at 1456 $cm^{-1}$ and 1375 $cm^{-1}$ correspond to residual evaporation of DMC [56] and EA [57], respectively. Simultaneously the P-F asymmetric stretching mode of $POF_3$ is also detected at 989 $cm^{-1}$ [55]. The time sample at 79.6 min of the test 5 in Fig. 8A shows that HF is still present at 79.6 min, that is 17.7 min after the thermal runaway temperature. The FTIR measurement shows that HF is present during a longer time than $POF_3$ which can be explained by that $POF_3$ is a less chemically stable and intermediate compound, decomposing according to eq. (3).

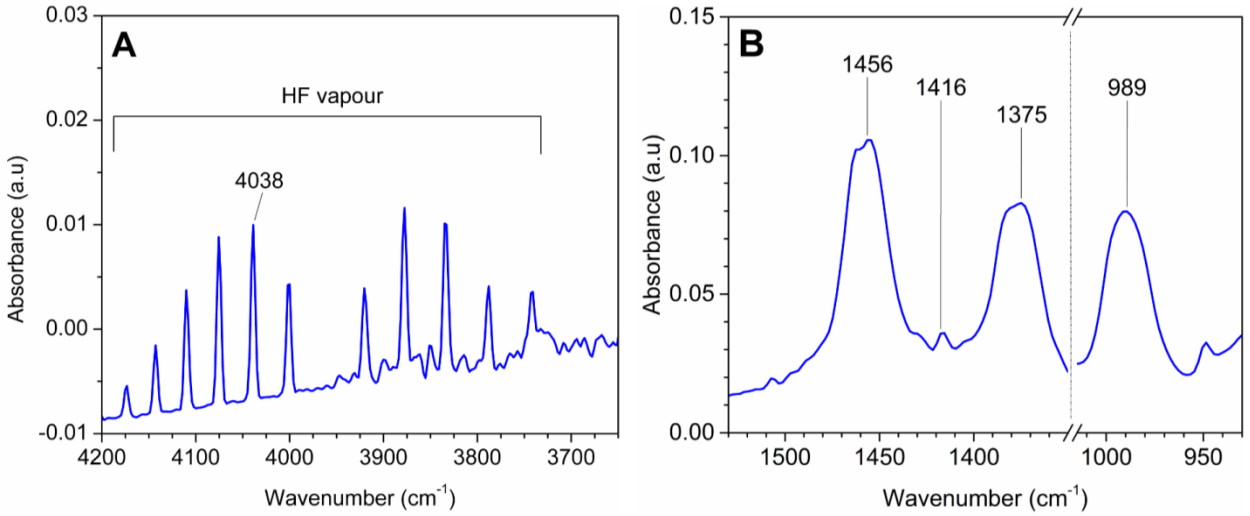


**Fig. 8.** FTIR measurement in test 5, (**A**) showing HF emission at time 79.6 min and (**B**) showing $POF_3$ emission at time 61.8 min.

### 3.2.6 Gas detection

The gas emissions released from a Li-ion battery are both toxic and flammable. If the gas is not immediately ignited there is a risk for a delayed ignition when the flammable gas-air mixture reaches the flammability range in case there is an ignition source, e.g. the hot battery cell itself. If the gases are confined by e.g. the battery system box itself or in the outer installation box/room, this will result in a potentially severe gas explosion.

In particular for large Li-ion battery systems, it can be an essential strategy to have the ability to collect gas emissions and ventilate them out in a safe way. If gas sensors are used, they could possibly detect the level of hydrocarbons and the gas explosion risks. Gas sensors could also be used to detect toxic gases, e.g. HF sensing. There might therefore be a need of having multiple and dynamic gas sensors to detect early cell venting. The first and second vents detected in the present tests are not visually observed or audible and thus not easily detected without gas sensors. However, the cell equipped with six cell surface temperature sensors, shows a temperature drop when the gases are released in the second step. The first vent is not clearly seen in the temperature data, but it indicated by the voltage drop to 0 V. A voltage drop to 0 V can indicate other types of events with and without gas release.

The second vents are quite clearly seen in Fig. 5A, when the average cell surface temperature suddenly drops, just a few minutes before the thermal runaway. The change in temperature rate in the second vent is also clearly seen in Fig. 4, where the dTavg2 rapidly drops before its very rapid increase at thermal runaway temperature. Adequate cell surface temperature sensor(s) in a battery pack could therefore potentially predict and detect a large release of gas. Battery packs of today typically do not have one temperature sensor per cell, instead e.g. 1-2 temperature sensors per battery module (e.g. 20 cells) are used. Anyhow, there is no universal standard and this type of sensing can vary a lot, making presumed gas detection warnings from battery cell surface temperature measurements not functional, except in case of a gas release in cell(s) in direct contact with the installed temperature sensor. The major venting during cell safety vent opening that releases large amounts of smoke and gas, is rather easily seen visually. Battery systems typically have a high tightness class, e.g. IP67, which hinder gas release and potentially increase risks of gas explosion if gases are finally released.

# 4. Conclusions

Hard prismatic $LiCoO_2$-graphite cells with a nominal capacity of 6.8 Ah were abused by external heating in an oven. The study included cycle aged cells, non-cycled cells stored at 60 °C as well as non-cycled cells stored in room temperature. Both working and non-working cells were investigated. Upon the external heating, all cells underwent thermal runaway releasing smoke and gas. For about half of the working cells, the gases accumulated in the oven ignited causing a gas explosion about 15 seconds after the thermal runaway and the major smoke and gas

release. Whether the cells had or had not been the subject of cycling did not influence the occurrence of the gas explosions, they occurred at all cycle ageing levels from 0 to 300 full deep cycles. The gases were analyzed using FTIR. Gas emission of toxic hydrogen fluoride was detected both with and without fire. Another emitted potentially toxic gas and a HF precursor, $POF_3$, was also detected simultaneously with HF. The thermal runaway temperature was about 190 °C and was shown to have a weak correlation with the number of cycles in the ageing process, having a minimum value between 100 and 200 cycles, within the tested cycle range of 0-300 cycles.

Three dead cells were tested, one that experienced sudden death during cycling after 229 cycles and two cells that had not been cycled but instead stored at 60 °C for 10 months. The dead cells also went into thermal runaway; however, they were significantly less reactive with increased thermal runaway temperatures and a lower rate of temperature increase. These cells did not emit any sparks or flames and there was no resulting fire or gas explosion. The work presented here shows the importance of a full assessment of the gases released, their toxicity, flammability and conditions for explosion, in order to be able to design appropriate safety measures in the application and also to be able to select what cells to use in different applications. The monitoring of the temperature and of gas release is shown as a method of an early detection of gas threat and an imminent thermal runaway.

# Acknowledgements

The Swedish Energy Agency and Carl Tryggers Stiftelse för Vetenskaplig Forskning are acknowledged for their financial support. Several persons at RISE Research Institutes of Sweden and Chalmers University of Technology have been involved in this work and are gratefully acknowledged. Sven Byheden for cycling ageing. Ingvar Karlson for support during abuse testing. Antti Rytinki for capacity and impedance measurements. Prof. Lu Li, National University of Singapore, is acknowledge for conducting the ARC measurement.

# Supplementary materials

Supplementary data related to this article.

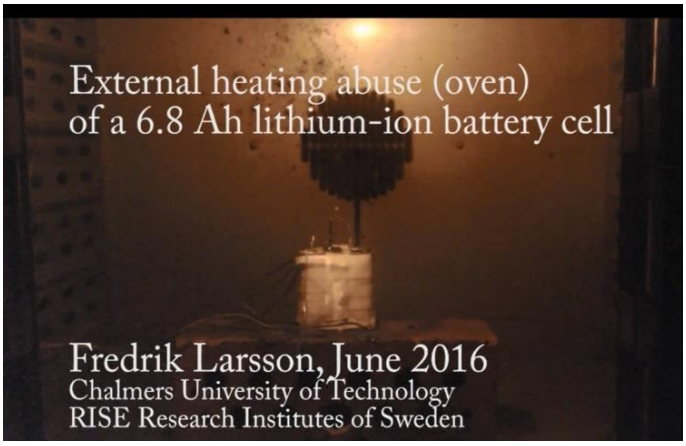


**Video S1.** For test 10 showing the third vent and thermal runaway and the gas explosion from the delayed ignition.

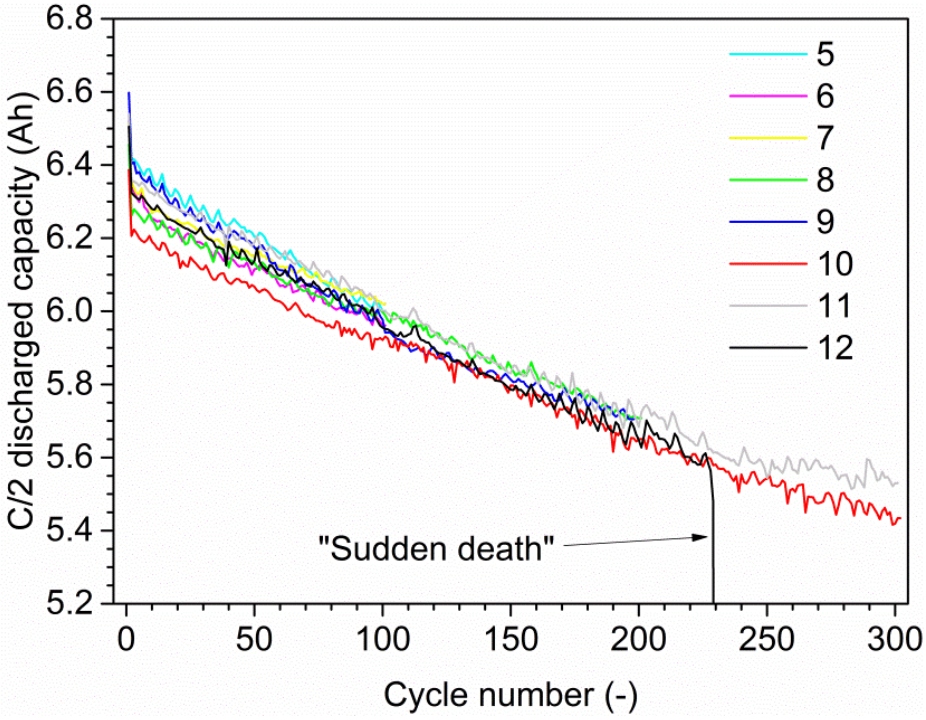


**Fig. S1.** The C/2 discharged capacity degradation during C/2-rate cycling for the cycled cells later external abused in test 5-12.

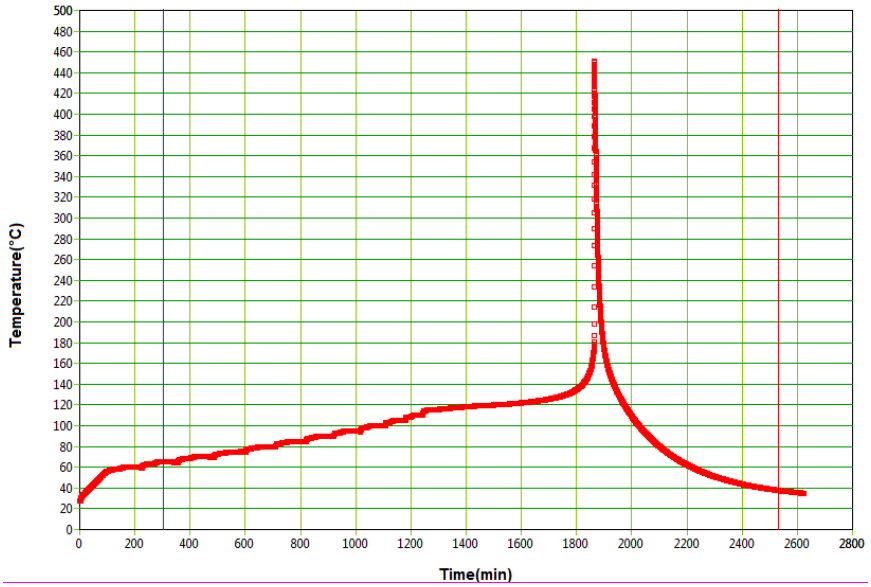


**Fig. S2.** The temperature development vs time for the cell at 100% SOC undergoing external heating abuse by ES-Accelerating Rate Calorimeter (ES-ARC) test chamber from Thermal Hazard Technology (THT, UK), using heat-wait-seek procedure with the following ARC settings: self-heating rate sensitivity of 0.02 °C $min^{-1}$, start temperature of 60 °C with heating steps of 5 °C increments and wait time of 15 minutes after each heating step, end temperature of 305 °C.

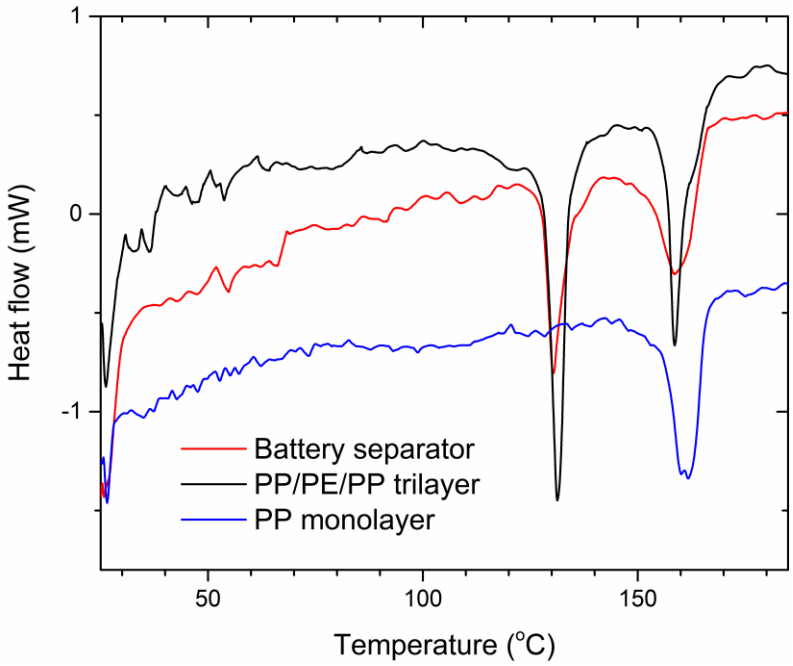


**Fig. S3.** Differential scanning calorimetry (DSC) measurement of the extracted separator from the battery cell and for two other reference separators. The samples were purged with $N_2$ and heated between 25 °C and 185 °C using a heating rate of 5 °C $min^{-1}$ in a liquid $N_2$ cooled Mettler DSC-30.

# References


1 F. Larsson, J. Andersson, P. Andersson, B.-E. Mellander, J. of The Electrochem. Soc. 163 (2016) A2854–A2865.
2 C. F. Lopez, J. A. Jeevarajan, P. P. Mukherjee, J. Electrochem. Soc. 162 (9) (2015) A1905-A1915.
3 J. Lamb, C. J. Orendorff, L. A. M. Steele, S. W. Spangler, J. of Power Sources 283 (2015) 517-523.
4 E. P. Roth, C. J. Orendorff, The Electrochem. Soc. Interface summer 2012 (2012) 45-49.
5 D. Doughty, E. P. Roth, The Electrochem. Soc. Interface summer 2012 (2012) 37-44.
6 F. Larsson, P. Andersson, B.-E. Mellander, Batteries 2 (2016) 9.
7 J. Lamb, C. J. Orendorff, E. P. Roth, J. Langendorf, J. of The Electrochem. Soc. 162 (10) (2015) A2131-A2135.
8 A. W. Golubkov, D. Fuchs, J. Wagner, H. Wiltsche, C. Stangl, G. Fauler, G. Voitic, A. Thaler, V. Hacker, RSC Adv. 4 (2014) 3633-3642.
9 J. Sun, J. Li, T. Zhou, K. Yang, S. Wei, N. Tang, N. Dang, H. Li, X. Qiu, L. Chen, Nano Energy 27 (2016) 313–319.
10 N. P. Lebedeva, L. Boon-Brettz, J. of The Electrochem, Soc. 163 (6) (2016) A821-A830.
11 A. Nedjalkov, J. Meyer, M. Köhring, A. Doering, M. Angelmahr, S. Dahle, A. Sander, A. Fischer, W. Schade, Batteries 2 (2016) 5.
12 Documentation for immediately dangerous to life or health concentrations (IDLHs) for hydrogen fluoride (as F), The National Institute for Occupational Safety and Health (NOISH) (1994).
13 Acute exposure guideline levels for selected airborne chemicals: volume 4, subcommittee on acute exposure guideline levels, ISBN: 0-309-53013-X, Committee on Toxicology, National Research Council (2004).
14 A. Middelman, Hygiensiska gränsvärden AFS 2015:7, Hygieniska gränsvärden. Arbetsmiljöverkets föreskrifter om hygieniska gränsvärden och allmänna råd om tillämpningen av föreskrifterna, ISBN 978-91-7930-628-1, ISSN 1650-3163, Swedish Work Environment Authority (2015).
15 F. Larsson, P. Andersson, P. Blomqvist, B.-E. Mellander, “Toxic fluoride gas emissions from lithium-ion battery fires”, manuscript submitted to Scientific Reports.
16 F. Larsson, P. Andersson, P. Blomqvist, A. Lorén, B.-E. Mellander, J. Power Sources 271 (2014) 414–420.
17 F. Larsson, P. Andersson, P. Blomqvist, B.-E. Mellander, Gas emissions from Lithium-ion battery cells undergoing abuse from external fire, Conference proceedings of Fires in vehicles (FIVE) 2016, Baltimore, 5-6 October 2016, edited by P. Andersson, B. Sundström, SP Technical Research Institute of Sweden, Borås, Sweden, (2016) p. 253-256
18 A. Lecocq, G. G. Eshetu, S. Grugeon, N. Martin, S. Laruelle, G. Marlair, J. Power Sources 316 (2016) 197-206.
19 P. Ribière, S. Grugeon, M. Morcrette, S. Boyanov, S. Laruelle, G. Marlair, Energy Environ. Sci. 5 (2012) 5271-5280.
20 P. Andersson, P. Blomqvist, A. Loren, F. Larsson, Fire and Materials 40 (2016) 999–1015.

21 Y.-U. Park, D.-H. Seo, B. Kim, K.-P. Hong, H. Kim, S. Lee, R. A. Shakoor, K. Miyasaka, J.-M. Tarascon, K. Kang, Tailoring a fluorophosphate as a novel 4 V cathode for lithium-ion batteries, Scientific Reports 2 (2012) article number 704.
22 G. F. Ortiz, M. C. López, Y. Li, M. J. McDonald, M. Cabello, J. L. Tirado, Y. Yang, Enhancing the energy density of safer Li-ion batteries by combining high-voltage lithium cobalt fluorophosphate cathodes and nanostructured titania anodes, Scientific Reports 6 (2016) article number 20656.
23 A. Aboulaich, K. Ouzaouit, H. Faqir, A. Kaddami, I. Benzakour, I.Akalay, Materials Research Bulletin 73 (2016) 362–368.
24 Y.-K. Sun, M.-J. Lee, C. S. Yoon, J. Hassoun, K. Amine, B. Scrosati, Adv. Mater. 24 (2012) 1192–1196.
25 F. Larsson, B.-E. Mellander, J. of The Electrochem. Soc. 161(10) (2014) A1611-A1617.
26 P. Ping, Q. Wang, P. Huang, K. Li, J. Sun, D. Kong, C. Chen, J. of Power Sources 285 (2015) 80-89.
27 P. Huang, Q. Wang, K. Li, P. Ping, J. Sun, Scientific Reports 5 (2015) article number 7788.
28 Y. Fu, S. Lu, K. Li, C. Liu, X. Cheng, H. Zhang, J. of Power Sources 273 (2015) 216-222.
29 B. D. Gould, A. F. Durkin, H. V. Pham, F. W. Williams, Characterization of the heat release rate of lithium-ion battery failures from thermal abuse, 44th Power Sources Conference 2010, ISBN: 978-1-61782-064-9, Las Vegas, Nevada, USA, 14-17 June 2010, (2010) 5-7.
30 T. Maloney, Extinguishment of lithium-ion and lithium-metal battery fires, U.S. Department of Transportation, DOT/FAA/TC-13/53, January 2014 (2014).
31 X. Liu, Z. Wu, S. I. Stoliarov, Analysis of Energy Release during Thermally-induced Failure of Lithium Ion Batteries: Implications for Vehicle Fire Safety, Conference proceedings of Fires in vehicles (FIVE) 2016, Baltimore, 5-6 October 2016, edited by P. Andersson, B. Sundström, SP Technical Research Institute of Sweden, Borås, Sweden (2016) p. 83-94.
32 E.P. Roth, Abuse response of 18650 Li-ion cells with different cathodes using EC:EMC/LiPF6 and EC:PC:DMC/LIPF6 electrolytes, ECS Transactions 11 (19) 19-41 2008, 10.1149/1.2897969
33 C.-Y. Jhu, Y.-W. Wang, C.-M. Shu, J.-C. Chang and H.-C. Wu, Thermal explosion hazards on 18650 lithium ion batteries with a VSP2 adiabatic calorimeter, J. of Hazardous Materials, 192, 99 (2011).
34 Chia-Yuan Wen, Can-Yong Jhu, Yih-Wen Wang, Chung-Cheng Chiang, Chi-Min Shu, Thermal runaway features of 18650 lithium-ion batteries for $LiFePO_4$ cathode material by DSC and VSP2, J. Therm Anal. Calorim. 109 (2012) 1297-1302
35 J. Vetter, P. Novák, M.R. Wagner, C. Veit, K.-C. Möller, J.O. Besenhard, M. Winter, M. Wohlfahrt-Mehrens, C. Vogler, A. Hammouched, J. of Power Sources 147 (2005) 269–281.
36 M. Klett, R. Eriksson, J. Groot, P. Svens, K. Ciosek Högström, R. Wreland Lindström, H. Berg, T. Gustafson, G. Lindbergh, K. Edström, J. of Power Sources 257 (2014) 126-137.
37 J. Groot, M. Swierczynski, A. Irina Stan, S. Knudsen Kær, J. of Power Sources 286 (2015) 475-487.
38 E.P. Roth, D.H. Doughty, J Power Sources 128 (2004) 308-318.
39 M.-S. Wu, P.-C. J. Chiang, J.-C. Lin, Y.-S. Jan, Electrochimica Acta 49 (2004) 1803–1812.
40 P. Röder, B. Stiaszny, J. C. Ziegler, N. Baba, P. Lagaly, H.-D. Wiemhöfer, J. of Power Sources 268 (2014) 315-325.

41 Jianbo Zhang, Laisuo Su, Zhe Li, Ying Sun, Ningning Wu, Batteries 2 (2016) 12.
42 M. Fleischhammer, T. Waldmann, G. Bisle, B.-I. Hogg, M. Wohlfahrt-Mehrens, J. of Power Sources 274 (2015) 432-439.
43 A. Friesen, F. Horsthemke, X. Mönnighoff, G. Brunklaus, R. Krafft, M. Börner, T. Risthaus, M. Winter, F. M. Schappacher, J. of Power Sources 334 (2016) 1-11.
44 J. Jeevarajan, Safety of commercial lithium-ion cells and batteries In: Gianfranco Pistoia (ed) Lithium-Ion Batteries Advances and Applications, Elsevier, Amsterdam, The Netherlands, (2014), p. 387-407.
45 R. Fathi, J. C. Burns, D. A. Stevens, H. Ye, C. Hu, G. Jain, E. Scott, C. Schmidt, J. R. Dahn, J. Electrochem. Soc. 161 (2014) A1572-A1579.
46 S. Bertilsson, F. Larsson, M. Furlani, I. Albinsson, B.-E. Mellander, "Lithium-ion battery electrolyte emissions analyzed by coupled thermogravimetric/Fourier-transform infrared spectroscopy", manuscript submitted to Journal of Power Sources.
47 S. Bertilsson, Thermal and infrared analysis of a lithium-ion battery electrolyte and its vapours for safety assessments, Master's Thesis, Chalmers University of Technology, (2017).
48 T. Osaka, D. Mukoyama, H. Nara, J. Electrochem. Soc., 162 (2015) A2529-A2537 and references therein.
49 P. Singh, R. Vinjamuri, X. Wang, D. Reisner, Electrochim. Acta 51, (2006) 1673-1679.
50 U. Westerhoff, K. Kurbach, F. Lienesch, M. Kurrat, Energy Technol. 4 (2016) 1620 – 1630.
51 R. J. Harris, The investigation and control of gas explosions in buildings and heating plants, British gas corporation, Midlands, England (1983).
52 F. Larsson, B.-E. Mellander, Energy storage system safety in electrified vehicles, Conference proceedings of Fires in vehicles (FIVE) 2012, Chicago, 27-28 September 2012, edited by P. Andersson, B. Sundström, SP Technical Research Institute of Sweden, Borås, Sweden (2012), p. 303-306.
53 G. Eshetu, S. Grugeon, S. Laruelle, S. Boyanov, A. Lecocq, J.-P. Bertrand, G. Marlair, Phys. Chem. Chem. Phys. 15 (2013) 9145-9155.
54 MSDS for EA, DMC and EC, https://www.sciencelab.com (accessed 13 July 2017)
55 H. Yang, G. V. Zhang, P. N. Ross Jr, J. of Power Sources 161 (2006) 573-579.
56 H. Bohets, B. J. van der Veken, Phys. Chem. Chem. Phys. 1 (1999), 1817–1826.
57 T.-K. Ha, C. Pal, P. N. Ghosh, Spectrochimica Acta 48A (8) (1992), 1083–1090.

# Paper IV

Journal of Power Sources 271 (2014) 414–420

Contents lists available at ScienceDirect

Journal of Power Sources

journal homepage: www.elsevier.com/locate/jpowsour

# Characteristics of lithium-ion batteries during fire tests

Fredrik Larsson [a, b, *], Petra Andersson [a], Per Blomqvist [a], Anders Lorén [a], Bengt-Erik Mellander [b]

[a] SP Technical Research Institute of Sweden, Brinellgatan 4, SE-501 15 Borås, Sweden
[b] Department of Applied Physics, Chalmers University of Technology, SE-412 96 Göteborg, Sweden

## HIGHLIGHTS

- Fire tests on commercial lithium–iron phosphate cells and laptop battery packs.
- Heat release rate (HRR) measured, higher state of charge (SOC) gives higher HRR peaks.
- Toxic emissions of HF and $POF_3$ (not detected) quantitatively measured.
- Higher total HF emission for lower SOC values.

## ARTICLE INFO

*Article history:*
Received 24 June 2014
Received in revised form
5 August 2014
Accepted 8 August 2014
Available online 15 August 2014

*Keywords:*
Lithium ion
Battery
Hydrogen fluoride
Phosphorous oxyfluoride
Heat release rate
Fire

## ABSTRACT

Commercial lithium-ion battery cells are exposed to a controlled propane fire in order to evaluate heat release rate (HRR), emission of toxic gases as well as cell temperature and voltage under this type of abuse. The study includes six abuse tests on cells having lithium–iron phosphate (LFP) cathodes and, as a comparison, one test on conventional laptop battery packs with cobalt based cathode. The influence of different state of charge (SOC) is investigated and a limited study of the effect of water mist application is also performed. The total heat release (THR) per battery energy capacity are determined to be 28–75 kJ $Wh^{-1}$ and the maximum HRR values to 110–490 W $Wh^{-1}$. Hydrogen fluoride (HF) is found in the released gases for all tests but no traceable amounts of phosphorous oxyfluoride ($POF_3$) or phosphorus pentafluoride ($PF_5$) are detected. An extrapolation of expected HF emissions for a typical automotive 10 kWh battery pack exposed to fire gives a release of 400–1200 g HF. If released in a confined environment such emissions of HF may results in unacceptable exposure levels.



## 1. Introduction

Lithium-ion batteries are widely used since they offer great benefits compared to many other battery technologies. Advantages such as high energy and power density, long life time and the possibility of fast charging make them attractive for consumer products and electrified vehicles. Nevertheless Li-ion batteries contain reactive and flammable materials, therefore safety issues are a concern and a number of incidents involving Li-ion batteries have been reported over the last couple of years [1–4]. Overheating of the batteries may result in exothermal reactions and lead to a thermal runaway with excessive amounts of heat, gas emissions, fire and potentially explosion/rapid dissembling [1,5–6]. Even in case there is no thermal runaway, a heated battery can still vent flammable and toxic gases. Examples of toxic gases that may originate from such events are hydrogen fluoride, HF, and phosphorous oxyfluoride, $POF_3$. The toxicity of HF is quite well known [7] since it is formed during several chemical decomposition processes and fires but the toxicity of the $POF_3$ is currently unknown. Actually, the toxicity of $POF_3$ might act with other poisoning mechanisms than just by formation of three equivalents of HF. Therefore, critical limits of exposure might be lower for $POF_3$ than for HF as in the chlorine analog $POCl_3$/HCl [8]. The origin of the fluorine compounds is primarily the battery electrolyte but emissions can also come from the binder (e.g. PVdF) of the active electrode materials. The electrolyte usually contains flammable organic solvents some of which are volatile at modest temperatures (below 100 °C) and the commonly used Li-salt, lithium hexafluorophosphate, $LiPF_6$, has a limited thermal stability upon

* Corresponding author. Department of Applied Physics, Chalmers University of Technology, SE-412 96 Göteborg, Sweden. Tel.: +46 10 5165928; fax: +46 33 125038.
*E-mail addresses:* fredrik.larsson@sp.se, vegan@chalmers.se (F. Larsson).

http://dx.doi.org/10.1016/j.jpowsour.2014.08.027
0378-7753/

heating. The decomposition of $LiPF_6$ can be described, according to Yang et al. [9] and Kawamura et al. [10], by:

$$LiPF_6 \rightarrow LiF + PF_5 \quad (1)$$

$$PF_5 + H_2O \rightarrow POF_3 + 2HF \quad (2)$$

$$LiPF_6 + H_2O \rightarrow LiF + POF_3 + 2HF \quad (3)$$

$$POF_3 + H_2O \rightarrow POF_2(OH) + HF \quad (4)$$

When $LiPF_6$ is heated in a dry and inert atmosphere it decomposes to lithium fluoride, LiF, which is a solid compound at temperatures below 845 °C and phosphorus pentafluoride, $PF_5$, which is a gas and a strong Lewis acid, see Eq. (1). In the presence of water/moisture $PF_5$ produces $POF_3$, and HF (Eq. (2)). $LiPF_6$ can also react directly with water/moisture to form LiF, $POF_3$ and HF according to Eq. (3). In fact, $LiPF_6$ is highly susceptible to hydrolysis by even trace amounts of moisture [11]. Furthermore, Kawamura et al. [10] suggested that $POF_3$ could react with water and form $POF_2(OH)$ and HF according to Eq. (4).

The decomposition of electrolytes containing $LiPF_6$ forming HF is complex and has mainly been studied at ambient temperature and during heating (but not in situations where there is a fire) [12–19]. Besides emissions containing fluorine and vaporized solvents, a Li-ion cell can also emit other gases, e.g. $H_2$, CO, $CO_2$, $CH_4$, $C_2H_6$ and $C_2H_4$ [20–22]. Gases can actually be emitted from batteries under several types of abuse conditions such as overheating, overcharge [23], short circuit, fires etc. A few studies are published on heat release rate (HRR) and emissions of toxic gases from Li-ion batteries in fire conditions. Ribière et al. [24] used a Tewarson fire calorimeter to study the HRR and toxic gases from commercial 2.9 Wh pouch cells with $LiMn_2O_4$ (LMO) cathode and graphite anode and found e.g. that the total HF release was higher for lower state of charge (SOC) values. Eshetu et al. [25] studied fire properties and toxicity for commonly used Li-ion battery electrolytes but without Li-salt and thus without the possibility to produce HF.

This paper presents results from fire tests of commercially available Li-ion battery cells. Parameters such as heat release rate, cell voltage and surface temperature are measured as well as HF and $POF_3$ emissions. The influence of application of water is examined to a limited extent by introducing water mist into the flames.

## 2. Experimental

The tests were conducted using the measurement and gas collection system of a Single Burning Item (SBI) apparatus, that is normally used for classification of building materials according to the European Classification scheme EN13823 [26]. The experimental setup is shown in Fig 1. The cells/batteries were placed on a wire grating (large gratings about 4 cm × 10 cm) as seen in Fig 2. A propane burner was placed underneath the cells/batteries and was ignited two minutes after the start of the test. The HRR of the burner alone was approximately 15 kW. Abuse tests were performed on 7 Ah EiG LFP pouch cells, 3.2 Ah K2 LFP cylindrical cells, and on 16.8 Ah Lenovo laptop battery packs, see Table 1.

Test 1–5 used commercially available pouch cells with lithium–iron phosphate (LFP), $LiFePO_4$, cathode and carbon based anode. Each test consisted of five cells that were mechanically fastened together with steel wire (0.8 mm diameter). The terminal tabs of the cells were cut for all cells but the mid one (the third cell), for which the cell voltage was measured. On both sides of the third cell type K thermocouples were centrally attached measuring the cell surface temperature. Temperature values presented in this

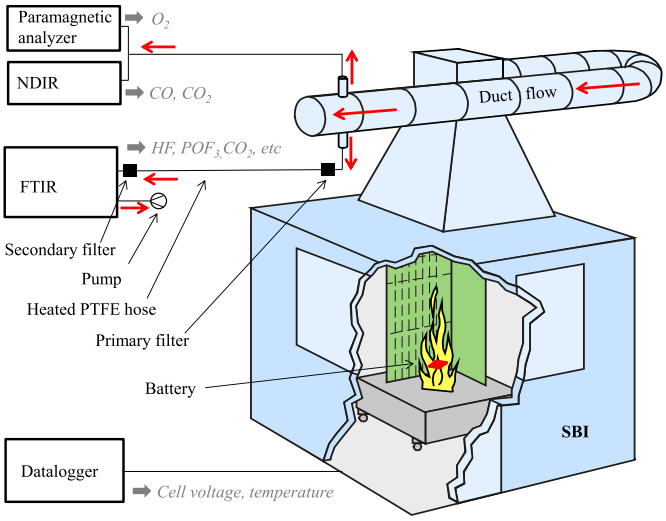


**Fig. 1.** Schematic illustration over experimental setup.

paper are the average of these thermocouple readings. The temperature and cell voltage was measured with a sample rate of 1 Hz using a data logger, *Pico Technology ADC-24*. In test 3, water mist was manually applied as a spray into the flames above the battery to study any influence from additional water on the composition of the gas emissions. In test 6, nine K2 26650-cells, i.e. cylindrical cells 26 mm in diameter and 65 mm long, were placed standing up next to each other inside a box. The box had side walls made of non-combustible silica board and steel net at the bottom and top. It was used as a safety precaution to avoid possible projectiles. In test 7, two identical laptop battery packs were used and placed inside a steel net and fastened on the wire grating.

The cells in test 1–6 were set to the selected SOC-level, according to Table 1, by a charge/discharge procedure using an ordinary laboratory power aggregate and a *Digatron* battery test equipment. The two laptop battery packs in test 7 were fully charged using a laptop computer. All batteries were unused but had different calendar aging. The EiG cells were approximate 2–3 years old, the K2 cells were approximate 1–2 years old and the laptop battery pack was less than 6 months old.

The laptop battery packs in test 7 differ from the other test objects. First, they consist of not only the cells but also electrical connectors, plastic housing and electronic circuits. Secondly, they

**Fig. 2.** The 5-cells pack of EiG cells placed on a wire grating.

**Table 1**
Test objects.

| Test no. | Battery type | No. of cells | Nominal capacity (Ah) | Weight (g) | Test condition |
|---|---|---|---|---|---|
| 1 | EiG ePLB-F007A | 5 | 35 | 1227.9 | 100% SOC |
| 2 | EiG ePLB-F007A | 5 | 35 | 1229.7 | 100% SOC |
| 3 | EiG ePLB-F007A | 5 | 35 | 1229.3 | 100% SOC + water mist |
| 4 | EiG ePLB-F007A | 5 | 35 | 1228.6 | 0% SOC |
| 5 | EiG ePLB-F007A | 5 | 35 | 1227.6 | 50% SOC |
| 6 | K2 LFP26650EV | 9 | 28.8 | 734.8 | 100% SOC |
| 7 | Lenovo laptop battery packs | 12[a] | 33.6 | 639.0 | 100% SOC |

[a] Two laptop battery packs were used at the same time, each with 6 cells.

have cobalt based cell chemistry with a higher cell voltage, 3.7 V vs 3.2 V for the LFP-cells. Thirdly, in each battery pack, 3 cells are electrically connected in series increasing the voltage to 11.1 V.

All tests were video recorded. The tests were performed during two days and in the beginning of each day a blank test was conducted in order to be able to subtract the burner influence on the HRR values and to make a blank for the gas analysis. The burner was active for a varying duration in the different tests, between 17 and 32 min, i.e. as long as a heat release contribution from the battery was still present. The fire emissions from the test object were collected in a ventilation duct. In test 1–2 a duct flow of 0.6 $m^3\ s^{-1}$ was used but in order to increase emission concentrations in the ventilation the duct flow was decreased to 0.4 $m^3\ s^{-1}$ in test 3–7.

A *Servomex 4100 Gas purity analyser* was used to measure the oxygen content of the flow by a paramagnetic analyzer and CO and $CO_2$ were determined by a non-dispersive infrared (NDIR) sensor. The HRR was calculated using the method of oxygen consumption and was corrected for $CO_2$ [26]. A part of the flow in the ventilation duct was extracted for on-line FTIR analysis. This sub-flow was extracted through an 8.5 m sampling PTFE hose, heated to 180 °C, using a pump (3.5 L $min^{-1}$) located after the FTIR measurement cell. The sampled gas is passed through a primary filter (*M&C* ceramic filter, heated to 180 °C) before the heated hose and thought a second filter (*M&C* sintered steel filter, heated to 180 °C) before the FTIR. After each test the primary filter was chemically analyzed for fluoride content since it is known that HF may be partly adsorbed by this type of filter [27]. The fluoride adsorbed by the filter was determined by method B.1 (b) of the SS-ISO 19702:2006 Annex B standard, where the filter is leached in water in an ultrasonic bath for at least 10 min. Thereafter the fluoride content in the water is measured by ion chromatography with a conductive detector. The amount of HF is calculated by assuming that all fluoride ions present in the filter derives from HF. The concentration of the emitted gas was measured by Fourier transform infrared spectroscopy (FTIR) using a *Thermo Scientific Antaris IGS analyzer* (*Nicolet*) with a gas cell. The spectral resolution of the FTIR was 0.5 $cm^{-1}$. The gas cell was of 0.2 L, had a path length of 2.0 m, a cell pressure of 86.7 kPa was maintained and the cell was heated to 180 °C. Each spectrum used 10 scans which gave a new spectrum every 12 s. There is a natural time delay between the gas measurement of the SBI and the FTIR in the measurement setup. The HRR and FTIR results presented in this paper were therefore time synchronized by overlaying of $CO_2$ measurements from the FTIR and the NDIR.

FTIR is a suitable technique to measure the concentrations of HF and $POF_3$ in the emitted fire gases. The FTIR was calibrated for a number of compounds, e.g. HF, when delivered from the supplier. However, it was found that the HF calibration was not accurate enough so it was recalibrated, see Andersson et al. [28] for a detailed description of the calibration procedure. The FTIR was also calibrated for $POF_3$. $PF_5$ could only be qualitatively determined by its spectral signature [28] but no traces of $PF_5$ could be found in the fire tests probably due to that the $PF_5$ is highly reactive. The detection limits were 2 ppm for HF and 6 ppm for $POF_3$. The spectral bands used for Classical Least Square (CLS) type quantification of HF and $POF_3$ are stated in Table 2.

**Table 2**
The spectral bands used for HF and $POF_3$.

| Spectral bands ($cm^{-1}$) | Type of band |
|---|---|
| *HF* | |
| 4203–4202 | HF R-branch stretching mode [29] |
| 4175–4172 | HF R-branch stretching mode [29] |
| *$POF_3$* | |
| 1418–1413 | P–O stretching mode [9] |
| 874–868 | P–F symmetric stretching mode [9] |

## 3. Results and discussion

The HRR results for the EiG battery cells with 0%, 50% and 100% SOC are shown in Fig. 3. High SOC values give high HRR peaks and the temperature and voltage measurements in Fig. 4 confirm that cells with high SOC value give a more reactive response, with rapid temperature increase and earlier voltage breakdown. Studies using other techniques confirm our results that battery cells with higher SOC are more thermally reactive, using e.g.; fire calorimeter [24], accelerating-rate calorimetry (ARC) [5] and VSP2 adiabatic calorimeter [30]. The HRR from the nine K2 cells in test 6 and the two complete laptop battery packs in test 7 can be seen in Fig. 5. The laptop pack includes the plastic box and have Li-ion cells with the more reactive cobalt based cathode, while the K2 cells (as well as the EiG cells) have LFP cathodes which are known to be significantly more stable [5,31–34]. The higher HRR values for the laptop cells are thus expected.

Outbursts from fully charged cells (100% SOC) of EiG, K2 and laptop packs were visually observed, see Fig. 6 for a typical example. The outbursts originate from ignition of the rapid gas release from a cell upon opening due to excessive cell pressure and correspond to the sharp spikes in the HRR curves, see Figs. 3 and 5. In most cases, one HRR-spike could be detected for each individual cell. For EiG cells with 50% and 0% SOC no spikes were observed in the HRR curves, instead two broad maxima were found. The orientation of the cells on the wire grating varied due the different packaging types (pouch, cylindrical, complete battery pack) which might have influenced the results. However, tests 1–5 used the same cell type and setup. The results of tests 6–7 can be seen as examples of possible events for these types of cells.

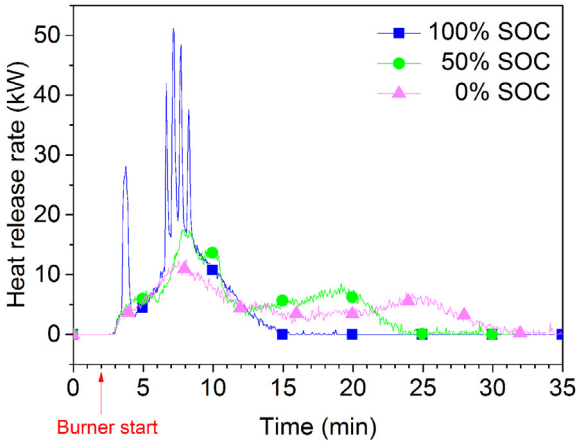


**Fig. 3.** Heat release rate for EiG cells with 0%, 50% and 100% SOC.

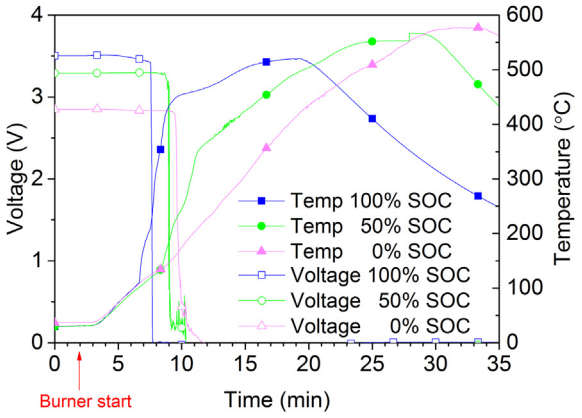


**Fig. 4.** Mid cell temperature and voltage for EiG with 0%, 50% and 100% SOC.

The fire test on EiG cells with 100% SOC was repeated two times (tests 1–2) without water mist application and one time (test 3) with water mist applied approximately 6.5 min after burner start. Fig. 7 shows HRR, HF emission rate, voltage and temperature for the mid cell, in test 2. Rapidly propagating flames released from the battery cells were visually observed five times during the test and denoted outbursts, marked in Fig. 7, and coincided with the five spikes in the HRR curve. The hydrogen fluoride concentration showed a rapid increase at the end of the HRR peak and the HF maximum plateau was reached just after the HRR spikes. The delay between HF production and HRR is not due to gas transport time since it is compensated by $CO_2$ synchronization, the reason is due to delay times in the sampling system. As expected, the temperature of the mid cell showed a steep increase connected to the HRR peaks, the outbursts and the voltage breakdown. The maximum temperature reached in this measurement was 521 °C. Test 1 and test 2 show similar values and behavior, the variation between the tests is due to the nature of the fire characteristics.

Fig. 8 shows test 3 where 100% SOC EiG cells were tested with water mist application. Most of the results of the tests with and without water mist are similar, but the maximum HF concentration recorded at the time of applying the water mist into the flames is approximately twice as high as that in tests 1–2. However, the total amount of measured HF from FTIR and absorbed by the primary filter is of the same order for all tests 1–3. The water mist was certainly not the only source of water in this experiment, in addition to water existing in the atmosphere water is produced by the

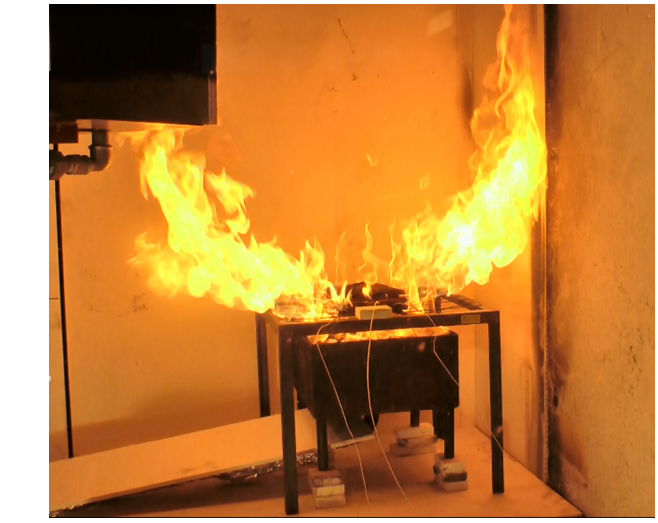

**Fig. 6.** Outbursts from EiG 100% SOC (test 1).

combustion process. In the general case of combustion of hydrocarbons water is produced:

$$C_nH_m + (m/4 + n)O_2 \rightarrow nCO_2 + (m/2)H_2O \quad (5)$$

and in the oxidation of ethylene carbonate (EC), $C_3H_4O_3$, a commonly used Li-ion solvent, water is thus produced according to:

$$2C_3H_4O_3 + 5O_2 \rightarrow 6CO_2 + 4H_2O \quad (6)$$

When propane, $C_3H_8$, is combusted, 1 mol of propane produces 4 mol of water according to Eq. (5). In test 1–3 the 15 kW propane burner was active during 17 min and given the heat of combustion of propane, 2044 kJ $mol^{-1}$, the amount of water produced from the burner can be calculated to be approximately 550 g.

The water concentration in the exhaust duct was measured by the FTIR, see Fig. 9 for the results of test 1–3. The water concentration shown for test 3 is scaled (factor 0.4/0.6) due to the lower duct flow in order to allow a comparison with the measured values of test 1–2. The outbursts result in an increased water concentration and the effects on the measured water concentration from the applied water mist is also clearly seen. Calculated from the measured data, the mass of the added water mist was around 400 g

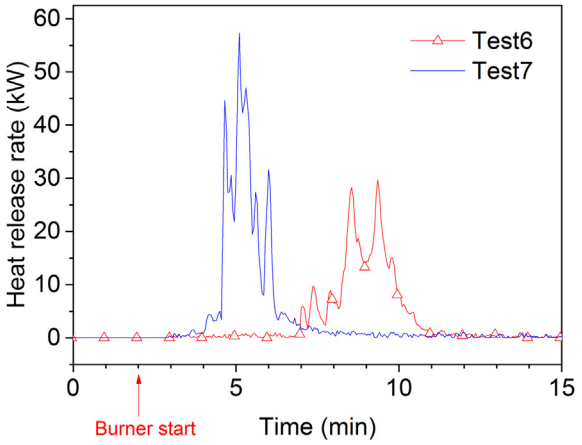


**Fig. 5.** Heat release rate for K2 cells (test 6) and laptop battery packs (test 7).

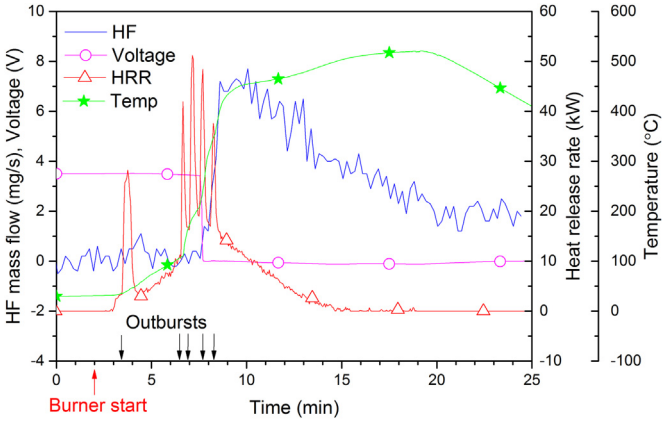


**Fig. 7.** Resultsf EiG 100% SOC (test 2).

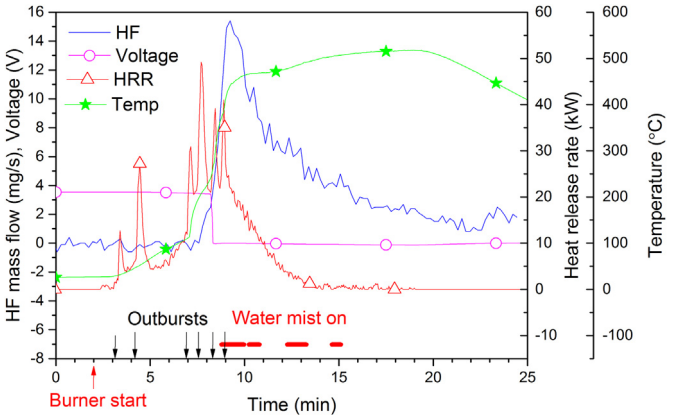


**Fig. 8.** Results for EiG 100% SOC with water mist (test 3).

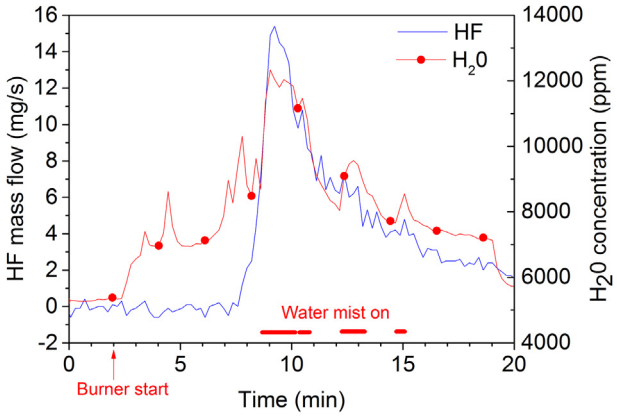


**Fig. 10.** HF mass flow and water concentration for test 3.

while around 350 g water was released due to the combustion of battery materials. The water in the duct flow from ambient air was around 1500 g for test 3 and 2300 g in test 1–2 (due to higher duct flow rate). The time of the water mist application was relatively short and the water mist was applied in the reaction zone, thus the impact from this source of water was potentially high which is also seen in Fig. 9. The amounts of water from ambient air were large but the impact should have been low since only part of the air flow passed the reaction zone above the battery and no effect on the HF concentration was observed due to the higher ambient water content in the duct flow in test 1–2 compared to test 3. Fig. 10 shows the correlation between HF production and water concentration for test 3. No HF production directly associated with the outbursts can be seen but the application of water mist seems to influence the HF production. However, the added water mist only temporarily increased the emission of HF but did not change the total amount of HF produced. Anyhow, only one test with water mist application was performed and the correlation between the water mist application and the increased HF peak production could possibly depend on other factors than the additional water introduced by the water mist.

Fig. 11 shows the measured production rate of HF for all EiG tests. For 0–50% SOC the peaks are broadened compared to the peaks for the 100% SOC cells and the total amount of measured HF is about double that of the 100% SOC cells. Detailed results from all the tests can be found in Table 3. Total yields in mg $g^{-1}$ are calculated as total amount of HF divided per weight loss of the batteries. In test 7 the weight loss also included the burning of pack materials, e.g. plastic housing. Total yields in mg $Wh^{-1}$ are calculated as total amount HF in mg divided by total energy capacity, Wh, of the batteries for each test. Whichever of these yield values that are used, the EiG cells with 0% or 50% SOC showed the highest HF values. The measured data indicate a relationship between SOC and the total released HF emissions, with increased total amounts of HF emission for lower SOC. Ribière et al. [24] found somewhat similar results by studying single cells with 100%, 50% and 0% SOC, showing an increasing total amount of HF emissions for decreasing SOC value. The reason for this is unknown and an investigation of the relationship would require further studies. The HF concentrations measured were in all cases well above the detection limit but no significant amounts of $POF_3$ could be detected in any of the tests. FTIR measurements on samples of similar electrolytes with $LiPF_6$ in a cone calorimeter have shown the production of $POF_3$ to be in the order of 1/20 of the HF production [28]. The detection limit of $POF_3$ in the FTIR measurements is 3 times higher than for HF, thus there could have been $POF_3$ present during the measurements which has not been detectable.

The HRR values presented in this paper are calculated using the oxygen consumption method. This technique is well accepted and used in fire calorimetry measurements. For the case of battery fires, the technique might however have some limitations since it will not account for energy liberated by Joule heating through electrical

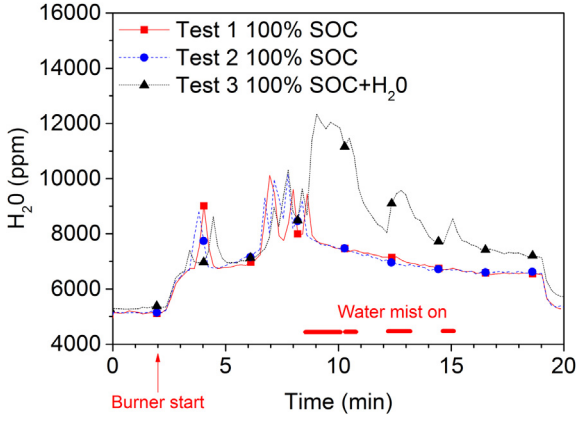


**Fig. 9.** Water concentrations measured in test 1–3. The increased water level in test 3 due to water mist application is clearly seen.

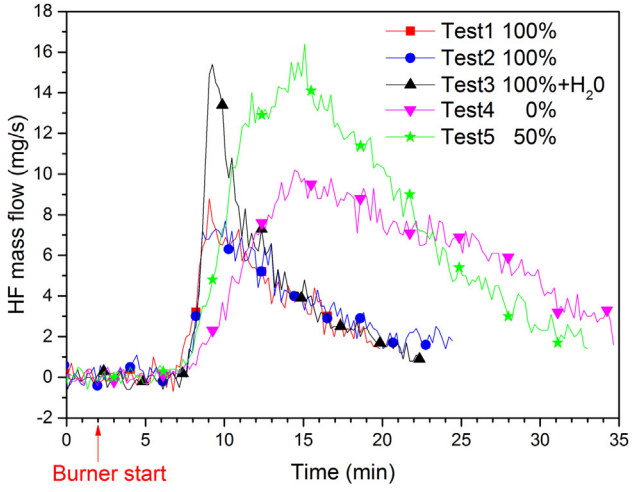


**Fig. 11.** HF mass flow for EiG cells with different SOC (indicated by % in figure legend) in tests 1–5.

**Table 3**
Detailed results of heat release rate, energy release, hydrogen fluoride emissions for test 1–7.

| Test no. | Weight loss (g) | Max heat release (kW) | Total heat release (kJ) | Hydrogen fluoride | | | | | |
|---|---|---|---|---|---|---|---|---|---|
| | | | | Max production rate (g $s^{-1}$) | Total amounts from FTIR (g) | Total amounts from filter (g) | Total amounts (g) | Total yields (mg $g^{-1}$) | Total yields (mg $Wh^{-1}$) |
| 1 | 346 | 55 | 7731 | 0.0088 | 3.2 | 1.7 | 4.9 | 14 | 44 |
| 2 | 342 | 51 | 7526 | 0.0077 | 3.9 | 2.4 | 6.3 | 18 | 56 |
| 3 | 341 | 49 | 8095 | 0.0154 | 4.2 | 1.5 | 5.7 | 17 | 51 |
| 4 | 353 | 13 | 8314 | 0.0102 | 9.7 | 1.6 | 11.3 | 32 | 100 |
| 5 | 354 | 17 | 8452 | 0.0164 | 12.0 | 1.9 | 13.9 | 39 | 120 |
| 6 | 145 | 29 | 2766 | 0.0029 | 1.2 | 1.0 | 2.2 | 15 | 24 |
| 7 | 258 | 57 | 3470 | 0.0011 | Not detected | 1.9 | 1.9 | 7.3 | 15 |

discharge, e.g. internal short circuits in a cell due to melted separator. Ribière et al. [24] estimates the error to be max 10% and thereby claim the oxygen consumption method to the usable. Besides the issue with Joule heating, the Li-ion battery can release its own oxygen [5]. The oxygen release varies with different Li-ion cell chemistries, and is typically lowest for LFP. In this test method a large amount of air is passed in the duct flow and the effect of released oxygen is regarded as negligible.

In order to simplify an estimation of the heat and gas emission hazards for this type of lithium-ion batteries the values have been normalized to the energy capacity of the batteries. Table 4 shows such values from our study as well as calculated values using data from Ribière et al. [24]. Again, note that the values for the laptop battery pack also accounts for the plastic housing. The EiG cells have about the double total heat release, 67–75 kJ $Wh^{-1}$, compared to the other batteries in Table 4. Also, the influence of SOC levels is small compared to the differences between the battery types. The maximum HRR per Wh calculated from our experimental data, 110–490 W $Wh^{-1}$, is, however, lower than the values reported by Ribière et al. [24], 300–1900 W $Wh^{-1}$, who used a different test procedure. Normalized values for the total HF release vary in our study between 15 and 124 mg $Wh^{-1}$, a wider range than that found by Ribière et al. [24].

In general, the measured values of the amount of HF produced in fire tests are comparatively high and could pose a serious hazard if released in an enclosed environment. For example, the 7 Ah EiG battery cell can typically be used in a plug-in electric vehicle (PHEV) and a 10 kWh battery pack of a PHEV could consist of 448 such cells (a battery system of 112 cells in series and 4 cells in parallel; cell voltage 3.2 V nominal, pack voltage 358.4 V nominal). If we extrapolate our results for the 5-cell packs by multiplying by a factor of 448/5 = 89.6, it may represent a scenario of a complete fire of a PHEV battery pack. The extrapolation gives 400–1200 g HF depending on the state of charge for the EiG cells where high SOC gives lower HF. Even though the extrapolation is extensive and therefore can be questionable the result is in the same order of magnitude as that reported by Lecocq et al. [35] who conducted complete vehicle fire tests including HF measurements of two electric vehicles (EV) with fully charged batteries (100% SOC) and on two similar gasoline powered combustion engine passenger cars (none-EV). Lecocq et al. [35] measured significant HF emissions from all four vehicles, both EV and similar none-EV, and suspected that the HF emissions from all vehicles could in part originate from air conditioner system. Using the values in Lecocq et al. [35], and calculating the difference in total HF release between the EV and the similar none-EV an estimate of the contribution to the HF release from the Li-ion battery can be found to be 919 g for a 16.5 kWh Li-ion battery and 657 g for a 23.5 kWh Li-ion battery. Scaling these values for a 10 kWh battery results in 280–557 g of released HF.

If we assume that all the emitted HF is released within a closed passenger compartment of 5 $m^3$ of an electrified vehicle we obtain HF concentrations between 80 and 240 g $m^{-3}$. NOISH (The National Institute for Occupational Safety and Health) in USA stated the IDLH (Immediately Dangerous To Life or Health) value for HF to 30 ppm corresponding to a concentration of HF in air of 0.025 g $m^{-3}$ [7]. Our values which are similar to those of Lecocq et al. [35] exceed the IDLH by about four orders of magnitude. The reported HF values from Ribière et al. [24] also by far exceed the IDLH value. However, the experimental data reported here comes from a limited study and the calculation assumes a somewhat extreme theoretical situation which differs from real fire situations, i.e. all HF is emitted and trapped in the compartment and that the passenger stays in the compartment. Anyhow, even if the emission occurs in a much larger volume, e.g. in a garage, the HF levels can still be very high. The reported HF values thus indicate that a critical situation might occur in the case of a thermal event in a Li-ion battery pack. Although we could not directly detect the presence of $POF_3$, it may also be present in considerable amounts since indications are that HF and $POF_3$ is produced with a ratio of about 1:20 [28].

**Table 4**
Total heat release, maximum HRR value and total HF release, normalized values for energy capacity.

| Battery | Nominal energy capacity (Wh) | Normalized total heat release (kJ $Wh^{-1}$) | Normalized maximum HRR (W $Wh^{-1}$) | Normalized total HF release (mg $Wh^{-1}$) |
|---|---|---|---|---|
| Five EiG cells | 112 | 67–75 | 110–490 | 44–124 |
| Nine K2 cells | 92 | 30 | 310 | 24 |
| Two laptop battery packs | 124 | 28 | 460 | 15 |
| Single cell, calculated from Ribière et al. [24] | 11 | 28–35 | 300–1900 | 37–69 |

## 4. Conclusions

The tests show that lithium-ion battery cells exposed to fire are significantly more reactive at 100% SOC than at lower SOC values and energetic outbursts were observed. The HRR peak values thus varied in a rather wide range, between 13 and 57 kW for batteries with approximately 100 Wh energy capacity. The normalized total heat release per energy capacity was 28–75 kJ $Wh^{-1}$ and the normalized maximum HRR values were 110–490 W $Wh^{-1}$.

The amount of HF released varied between 15 and 124 mg $Wh^{-1}$. Lower SOC values gave higher amounts of HF. Extrapolation of data shows that the potential HF release from a 10 kWh PHEV battery is in the range 400–1200 g HF. If this amount of HF would be released inside a passenger compartment of 5 $m^3$ the HF concentration would be 80–240 g $m^{-3}$, that is magnitudes higher than acceptable short time exposure levels. Besides HF, there may also be significant emissions of $POF_3$, a compound which might be more toxic than HF.

Although these estimates are based on an extrapolation and can be regarded as a hypothetical case it highlights the risks associated with toxic emissions at battery fires and the need to find replacements for the fluorine content in the Li-salt and binder used in Li-ion battery cells. The influence of additional water in form of water mist seemed to increase the HF emissions momentarily, however the total HF release was the same. Further studies of the relationship between water and HF emissions in fires are needed in order to thoroughly evaluate potential risks related to the use of water as firefighting medium in electric vehicle fires.

## Acknowledgments

The authors gratefully acknowledge the Swedish Energy Agency and the FFI-program as well as the Swedish Fire Research Board for financial support. Several persons at SP Fire Technology are acknowledged for their contribution to this work, including Lars Pettersson and Magnus Samuelsson.

## References

[1] Z.J. Zhang, P. Ramadass, W. Fang, in: G. Pistoia (Ed.), Lithium-ion Batteries Advances and Applications, Elsevier, Amsterdam, 2014, pp. 409–435.
[2] Q. Wang, P. Ping, X. Zhao, G. Chu, J. Sun, C. Chen, J. Power Sources 208 (2012) 210–214.
[3] D. Lisbona, T. Snee, Process Saf. Environ. Prot. 89 (2011) 434–442.
[4] http://edition.cnn.com/2014/01/14/travel/787-dreamliner/, 2014-05-13.
[5] D. Doughty, E.P. Roth, Electrochem. Soc. Interface (Summer 2012) 37–44.
[6] F. Larsson, P. Andersson, B.-E. Mellander, in: B. Sandén, P. Wallgren (Eds.), Systems Perspectives on Electromobility, Chalmers University of Technology, Göteborg, 2014, ISBN 978-91-980973-9-9, pp. 33–44.
[7] Documentation for Immediately Dangerous to Life or Health Concentrations (IDLHs) for Hydrogen Fluoride (as F), The National Institute for Occupational Safety and Health (NOISH), USA, May 1994. http://www.cdc.gov/niosh/idlh/7664393.html.
[8] Middelman, Hygiensiska gränsvärden AFS 2011:18, Hygieniska gränsvärden Arbetsmiljöverkets föreskrifter och allmänna råd om hygieniska gränsvärden, Swedish Work Environment Authority, Sweden, 2011, ISBN 978-91-7930-559-8. ISSN:1650-3163.
[9] H. Yang, G.V. Zhuang, P.N. Ross Jr., J. Power Sources 161 (2006) 573–579.
[10] T. Kawamura, S. Okada, J.-i. Yamaki, J. Power Sources 156 (2006) 547–554.
[11] Q.-S. Wang, J.-H. Sun, G.-Q. Chu, X.-L. Yao, C.H. Chen, J. Therm. Anal. Calorim. 89 (1) (2007) 245–250.
[12] C.G. Barlow, Electrochem. Solid-State Lett. 2 (8) (1999) 362–364.
[13] S.E. Sloop, J.B. Kerr, K. Kinoshita, J. Power Sources 119–121 (2003) 330–337.
[14] C.L. Campion, W. Li, W.B. Euler, B.L. Lucht, B. Ravdel, J.F. DiCarlo, R. Gitzendanner, K.M. Abraham, Electrochem. Solid-State Lett. 7 (7) (2004) A194–A197.
[15] C.L. Campion, W. Li, B.L. Lucht, J. Electrochem. Soc. 152 (12) (2005) A2327–A2334.
[16] S.F. Lux, I.T. Lucas, E. Pollak, S. Passerini, M. Winter, R. Kostecki, Electrochem. Commun. 14 (2012) 47–50.
[17] H. Yang, X.-D. Shen, J. Power Sources 167 (2007) 515–519.
[18] M.D.S. Lekgoathi, B.M. Vilakazi, J.B. Wagener, J.P. Le Roux, D. Moolman, J. Fluor. Chem. 149 (2013) 53–56.
[19] Hammami, N. Raymond, M. Armand, Nature 424 (2003) 635–636.
[20] T. Ohsaki, T. Kishi, T. Kuboki, N. Takami, N. Shimura, Y. Sato, M. Sekino, A. Satoh, J. Power Sources 146 (2005) 97–100.
[21] E.P. Roth, C.J. Orendorff, Electrochem. Soc. Interface (Summer 2012) 45–49.
[22] D.P. Abraham, E.P. Roth, R. Kostecki, K. McCarthy, S. MacLaren, D.H. Dought, J. Power Sources 161 (2006) 648–657.
[23] M.D. Chatelain, T.E. Adams, Proc. Power Sources Conf. 42 (2006) 87–89.
[24] P. Ribière, S. Grugeon, M. Morcrette, S. Boyanov, S. Laruelle, G. Marlair, Energy Environ. Sci. 5 (2012) 5271–5280.
[25] G.G. Eshetu, S. Grugeon, S. Laruelle, S. Boyanov, A. Lecocq, J.-P. Bertrand, G. Marlair, Phys. Chem. Chem. Phys. 15 (2013) 9145–9155.
[26] EN 13823:2010, Reaction to Fire Tests for Building Products – Building Products Excluding Floorings Exposed to the Thermal Attack by a Single Burning Item, European Committee for Standardization, Brussels, 2010.
[27] ISO 19702:2006, Toxicity Testing of Fire Effluents – Guidance for Analysis of Gases and Vapours in Fire Effluents Using FTIR Gas Analysis, International Organization for Standardization, Geneva, 2006.
[28] P. Andersson, P. Blomqvist, A. Lorén, F. Larsson, Investigation of Fire Emissions from Li-ion Batteries, SP Report 2013:5, SP Technical Research Institute of Sweden, Båras, Sweden, 2013, ISBN 978-91-87461-00-2.
[29] J.M. Hollas, Modern Spectroscopy, thirdrd ed., John Wiley & Sons, Chichester, 1996.
[30] C.-Y. Jhu, Y.-W. Wang, C.-M. Shu, J.-C. Chang, H.-C. Wu, J. Hazard. Mater. 192 (2011) 99–107.
[31] H. Joachin, T.D. Kaun, K. Zaghib, J. Prakash, J. Electrochem. Soc. 156 (6) (2009) A401–A406.
[32] G. Chen, T.J. Richardson, J. Electrochem. Soc. 156 (9) (2009) A756–A762.
[33] G. Chen, T.J. Richardson, J. Power Sources 195 (2010) 1221–1224.
[34] K. Zaghib, J. Dubé, A. Dallaire, K. Galoustov, A. Guerfi, M. Ramanathan, A. Benmayza, J. Prakash, A. Mauger, C.M. Julien, J. Power Sources 219 (2012) 36–44.
[35] Lecocq, M. Bertana, B. Truchot, G. Marlair, in: P. Andersson, B. Sundström (Eds.), Conference Proceedings of Fires in Vehicles (FIVE) 2012, SP Technical Research Institute of Sweden, Borås, Sweden, 2012, pp. 183–193.

# Paper V

# Toxic fluoride gas emissions from lithium-ion battery fires

Fredrik Larsson[1,2,*], Petra Andersson[2], Per Blomqvist[2], Bengt-Erik Mellander[1]

[1] Department of Physics, Chalmers University of Technology, Kemivagen 9, SE-41296 Gothenburg, Sweden
[2] Safety and Transport, RISE Research Institutes of Sweden, Brinellgatan 4, SE-50115 Boras, Sweden
* correspondence: vegan@chalmers.se, fredrik.larsson@ri.se

## Abstract

Lithium-ion battery fires generate intense heat and considerable amounts of gas and smoke. Although the emission of toxic gases can be a larger threat than the heat, the knowledge of such emissions is limited. This paper presents quantitative measurements of heat release and fluoride gas emissions during battery fires for seven different types of commercial lithium-ion batteries. The results have been validated using two independent measurement techniques and show that large amounts of hydrogen fluoride (HF) may be generated, ranging between 20 and 200 mg/Wh of nominal battery energy capacity. In addition, 15-22 mg/Wh of another potentially toxic gas, phosphoryl fluoride ($POF_3$), was measured in some of the fire tests. Gas emissions when using water mist as extinguishing agent were also investigated. Fluoride gas emission can pose a serious toxic threat and the results are crucial findings for risk assessment and management, especially for large Li-ion battery packs.

Lithium-ion batteries are a technical and a commercial success enabling a number of applications from cellular phones to electric vehicles and large scale electrical energy storage plants. The occasional occurrences of battery fires have, however, caused some concern especially regarding the risk for spontaneous fires and the intense heat generated by such fires[1,2,3,4,5]. While the fire itself and the heat it generates may be a serious threat in many situations, the risks associated with gas and smoke emissions from malfunctioning lithium-ion batteries may in some circumstances be a larger threat, especially in confined environments where people are present, such as in an aircraft, a submarine, a mine shaft, a spacecraft or in a home equipped with a battery energy storage system. The gas emissions has however only been studied to a very limited extent.

An irreversible thermal event in a lithium-ion battery can be initiated in several ways, by spontaneous internal or external short-circuit, overcharging, external heating or fire, mechanical abuse etc. This may result in a thermal runaway caused by the exothermal reactions in the battery[6,7,8,9,10], eventually resulting in a fire and/or explosion . The consequences of such an event in a large Li-ion battery pack can be severe due to the risk for failure propagation[11,12,13]. The electrolyte in a lithium-ion battery is flammable and generally contains lithium

hexafluorophosphate ($LiPF_6$) or other Li-salts containing fluorine. In the event of overheating the electrolyte will evaporate and eventually be vented out from the battery cells. The gases may or may not be ignited immediately. In case the emitted gas is not immediately ignited the risk for a gas explosion at a later stage may be imminent. Li-ion batteries release a various number of toxic substances[14,15,16] as well as e.g. CO (an asphyxiant gas) and $CO_2$ (induces anoxia) during heating and fire. At elevated temperature the fluorine content of the electrolyte and, to some extent, other parts of the battery such as the polyvinylidene fluoride (PVdF) binder in the electrodes, may form gases such as hydrogen fluoride (HF), phosphorus pentafluoride ($PF_5$) and phosphoryl fluoride ($POF_3$). Compounds containing fluorine can also be present as e.g. flame retardants in electrolyte and/or separator[17], in additives and in the electrode materials, e.g. fluorophosphates[18,19], adding additional sources of fluorine.

The decomposition of $LiPF_6$ is promoted by the presence of water/humidity according to the following reactions[20,21];

$$LiPF_6 \rightarrow LiF + PF_5 \quad (1)$$

$$PF_5 + H_2O \rightarrow POF_3 + 2HF \quad (2)$$

$$LiPF_6 + H_2O \rightarrow LiF + POF_3 + 2HF \quad (3)$$

Of these $PF_5$ is rather short lived. The toxicity of HF and the derivate hydrofluoric acid is well known[22,23,24] while there is no toxicity data available for $POF_3$, which is a reactive intermediate[25] that will either react with other organic materials or with water finally generating HF. Judging from its chlorine analogy $POCl_3/HCl$[24], $POF_3$ may even be more toxic than HF. The decomposition of fluorine containing compounds is complex and many other toxic fluoride gases might also be emitted in these situations, however, this study focuses on analysis of HF and $POF_3$.

Although a number of qualitative and semi-quantitative attempts have been made in order to measure HF from Li-ion batteries under abuse conditions, most studies do not report time dependent rates or total amounts of HF and other fluorine containing gases for different battery types, battery chemistries and state-of-charge (SOC). In some measurements reported, HF has been found, within limited SOC-variations, during the abuse of Li-ion battery cells[15,16,26], as well as detected during the abuse of battery packs[27]. However, time-resolved quantitative HF gas emission measurements from complete Li-ion battery cells undergoing an abusive situation have until now only been studied to a limited extend; for a few SOC-values, including larger commercial cells[28,29], a smaller-size commercial cell[30] and a research cell (i.e. non-commercial cell)[31]. Time-resolved quantitative HF measurements on the gas release from complete electric vehicles including their Li-ion battery packs during an external fire have also been performed[32]. Other types of gas emissions from Li-ion cells during abuse have been the subject of a somewhat larger number of investigations[33,34,35,36,37,38,39,40,41]. Since the electrolyte typically is

the primary source of fluorine, measurements of fluorine emissions from battery type electrolytes have been studied. For example, fire or external heating abuse tests have been performed on electrolytes[42,43,44,45,46] and the quantitative amounts of HF and $POF_3$ have been measured in some cases[45,46]. Other studies of electrolytes exposed to moderate temperatures, 50-85 °C, show the generation of various fluorine compounds[20,21,47,48,49] and some studies include both electrolyte and electrode material[50,51].

Our quantitative study of the emission gases from Li-ion battery fires covers a wide range of battery types. We found that commercial lithium-ion batteries can emit considerable amounts of HF during a fire and that the emission rates vary for different types of batteries and SOC levels. $POF_3$, on the other hand, was found only in one of the cell types and only at 0% SOC. The use of water mist as an extinguishing agent may promote the formation of unwanted gases as in eqs. (2)–(3) and our limited measurements show an increase of HF production rate during the application of water mist, however, no significant difference in the total amount of HF formed with or without the use of water mist.

**Lithium-ion battery fire tests**

The experiments were performed using an external propane burner for the purpose of heating and igniting the battery cells as described in the Methods section. Seven different types of batteries, type A-G, were investigated, from seven manufacturers and with different capacity, packaging type, design and cell chemistry, as specified in Table 1. Type A had a lithium cobalt oxide (LCO) cathode and carbon anode, types B to E had lithium-iron phosphate (LFP) cathode and carbon anode, type F had nickel cobalt aluminum oxide (NCA) and lithium aluminum titanium phosphate (LATP) electrodes while type G was a laptop battery pack with unspecified battery chemistry. All electrolytes contained $LiPF_6$. Most of the cells were tested for different SOC levels, from fully charged, 100% SOC, to fully discharged, 0% SOC. The study included large-sized automotive-classed cells, i.e. series production cells of high industry quality, with long life time etc.

The heat release rate (HRR) and the emitted HF for B-type cells with different SOC values are shown in Figure 1. Only the 100 % SOC cells show several distinct peaks, corresponding to intense flares, when the cells vented and the emitted gas burn, for all other cells the heat release as a function of time is more smooth. These behaviors are reproducible also for the other tested cell types, e.g., only the 100% SOC cells show the more violent heat release peaks with intense flares.

Table 1 Details of the tested Li-ion battery cells.

| Battery | Numbers of batteries per test | Type | Nominal capacity per battery (Ah) | Nominal voltage per battery (V) | Cell packaging |
|---|---|---|---|---|---|
| A | 5-10 | LCO ($LiCoO_2$) | 6.8 | 3.75 | Prismatic hard Al-can |
| B | 2 | LFP ($LiFePO_4$) | 20 | 3.2 | Pouch |
| C | 5 | LFP ($LiFePO_4$) | 7 | 3.2 | Pouch |
| D | 9 | LFP ($LiFePO_4$) | 3.2 | 3.2 | Cylindrical |
| E | 5 | LFP ($LiFePO_4$) | 8 | 3.3 | Cylindrical |
| F | 2 | NCA-LATP ($LiNiCoAlO_2$-$LiAlTiPO_4$) | 30 | 2.3 | Pouch |
| G | 2 | Laptop pack* | 5.6 | 11.1 | Cylindrical |

* Each laptop battery pack has 6 cells of type 18650; arranged 2 in parallel and 3 in series.

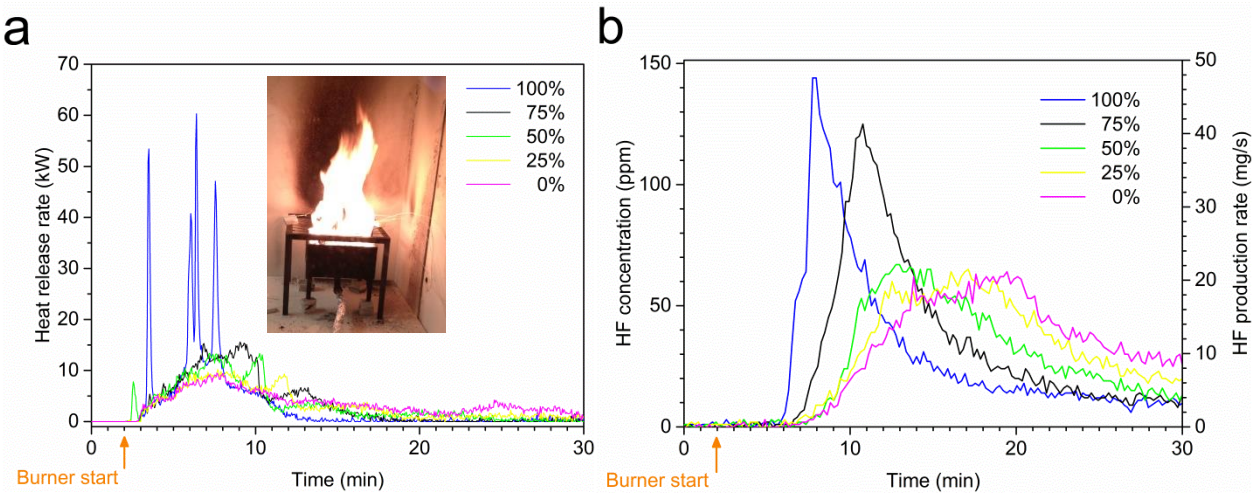


Figure 1 Results for type B cells, for 0-100% SOC with intermediate SOC-steps of 25 %, exposed to an external propane fire; (a) showing the heat release rate (burner HRR contribution is subtracted), the inset photo shows burning battery cells during the test; (b) showing the HF release both as the measured concentrations as well as the calculated HF production rates. The HF production rates are calculated from the measured HF concentration by the Ideal gas law taking into account the ventilation flow, see Methods. The starting time of the heating process is marked on the time axis.

The measurements of the gas emissions during the fire tests show that the production of HF is correlated to the increase in HRR although somewhat delayed. From Figure 1b it is evident that the higher SOC value, the higher values for the peak HF release rate. The total amount of HF

varies considerably for the different battery types, see Figure 2a. The amount of HF produced, expressed in mg/Wh, where Wh is the nominal battery energy capacity, is approximately 10 times higher for the cell with the highest values compared to the cells with the lowest values. The different relative amount of electrolyte and filler materials in the cells could be the simple explanation of this variation but information on those amounts are difficult to access for commercial batteries. The highest HF values are found for the pouch cells, a possible explanation would be that hard prismatic and cylindrical cells can build a higher pressure before bursting, rapidly releasing a high amount of gases/vapors from the electrolyte. Due to the high velocity of the release and thus the short reaction time, combustion reactions might be incomplete and less reaction products might be produced. In the test involving type G the cylindrical cells were layered horizontally, thus having a different venting direction and possibly increased wall losses, which combined with a very energetic response, might suggest why HF was detected only from the filter analysis and not detected by FTIR-analysis. The tested pouch cells of type B and C burned for longer time and with less intensity. The pouch cell of type F, however, burned faster, possibly due to its different electrode materials. The SOC influence on the HF release was less significant and the trend in Figure 2a shows higher HF values for 0% than for 100% SOC, however with clear peaks at 50% SOC. Although these results are reproducible, they are difficult to explain. In other studies[30,31], significantly narrower in test scope, involving smaller-sized cells and using a somewhat different abuse method, it was found that the total amount of HF measured by real-time FTIR was higher for decreasing SOC (tests conducted at 100%, 50% and 0% SOC).

The HRR curve is used to calculate the total heat release (THR) which corresponds to the energy released from the burning battery. THR is obtained by integrating the measured HRR (with the burner contribution subtracted) over the complete test time. Figure 2b shows the energy ratio, that is how much energy is produced by the burning battery, compared to the amount of nominal electrical energy capacity a fully charged battery can deliver to an external circuit. The energy ratio is therefore a comparison between the chemical and the electrical energy of the Li-ion battery cell. The energy ratio varies considerably for the different cell types but is approximately constant for each cell, independent of SOC level. There are some similarities in Figures 2a and 2b for the pouch cells, type B and C, which give the highest values in both cases, although in reverse order. This might indicate a higher amount of combustibles, e.g. electrolyte, in these cells compared to the other cells. It is also interesting to see that the energy ratio varies significantly between the tested cells, ranging from 5 to 21. This is important knowledge for fire protection and fire fighting. The energy ratio thus refers to a nominal fully charged battery while in normal use only a part of the SOC-window is used, for example half (50%) of the SOC-window (corresponding to cycling the battery between e.g. 30% and 80% SOC). If instead, the total heat release divided by the used electric battery capacity in the specific application is considered, higher energy ratio values are obtained. A summary of the results is shown in Table 2.

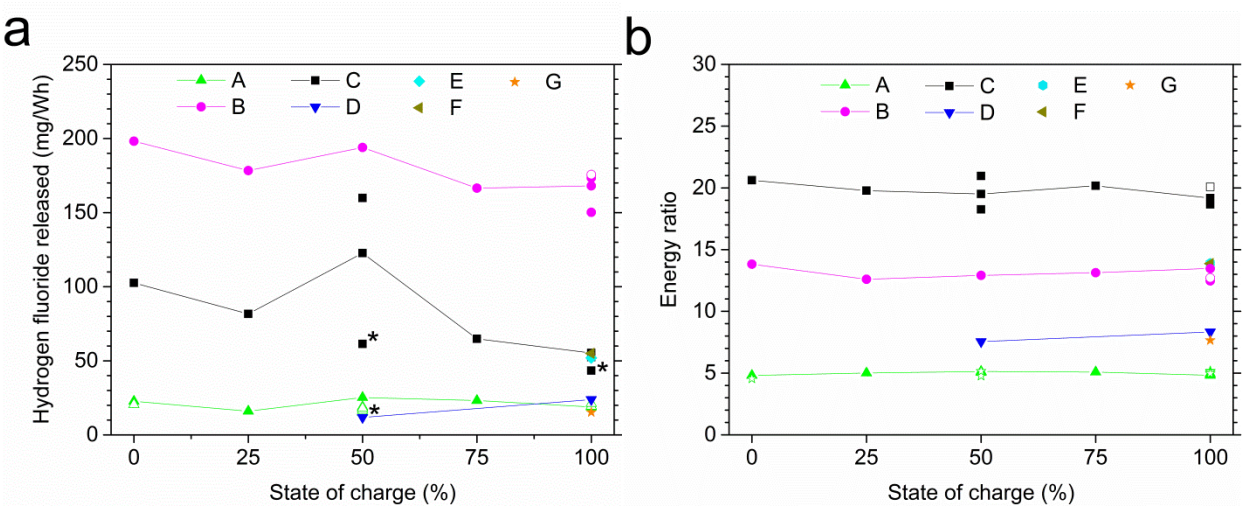


Figure 2 Total amount of HF measured by FTIR, normalized to nominal electrical energy capacity (a) and the energy ratio (b), for seven types of Li-ion battery cells and with various state of charge levels. Non-filled symbols indicate a repetition variant, e.g. applying water mist. The lines are intended as a guide for the eye. The energy ratio is a dimensionless value calculated by taking the total heat release from the battery fire divided by the nominal electrical energy capacity. Note that for 100% SOC the values are overlapping for type C, E and F as well as for type A, D and G in (a) and type B, E and F in (b).

** Low value for type C at 50% and 100% SOC and type D at 50% SOC due to that a pre HF-saturation was not applied, therefore a part of the HF release was likely to be saturated in the gas sampling system, see Methods.*

Table 2 Main test results normalized to nominal energy capacity, when applicable including various SOC-levels.

| Battery | Nominal energy capacity (Wh) | Normalized total HF detected with FTIR (mg/Wh) | Normalized maximum HRR (W/Wh) | Normalized THR (kJ/Wh) |
|---|---|---|---|---|
| A | 128 | 15-25 | 243 - 729 | 17 - 19 |
| B | 128 | 150 – 198 | 78 - 633 | 45 - 50 |
| C | 112 | 43 – 160 | 116 - 491 | 66 - 75 |
| D | 92 | 12 – 24 | 207 - 315 | 27 - 30 |
| E | 132 | 52 | 235 | 50 |
| F | 138 | 55 | 384 | 50 |
| G | 124 | 15 | 460 | 28 |

The measured heat release from an overheated battery may include several aspects, e.g. the battery temperature increase and the combustion of released gases. Variations due to the type of battery cell, the initiation method, e.g. if the test is done as an external fire test, an external heating or an overcharge test, and the test method, e.g. access to ambient oxygen (inert, under-ventilated or well-ventilated fire), and the presence of an external igniter, can greatly affect the amount of measured heat release. Energy release from a internal cell event in a confined environment can, for example, be lower than the energy release from the same cell in case of external fire. Thus energy ratios published using other methods and other types of Li-ion cells can be significantly different[7,52, 53].

For all tested battert types and selected SOC-levels, $POF_3$ could only be measured quantitatively for type A battery cells at 0% SOC. Repeated measurements confirmed the presence of $POF_3$ only for type A and only for 0% SOC. No $POF_3$ could thus be detected in any of the other tests. $POF_3$ is an intermediate compound and the local combustion conditions in every test, will influence the amounts of $POF_3$ generated. This shows the importance of investigating many different set-ups when evaluating emitted gases.

In Figure 3 the HRR, the average surface temperature of the five cells as well as the HF and $POF_3$ production rates are shown for type A cells at 0% SOC. The $POF_3$ curve is less noisy than the HF curve due to different signal-to-noise ratios of the FTIR instrumentation at the different wavenumbers. There is a secondary peak in HRR approximately 5 minutes after the main heat event, this peak does not correspond to any peaks in the mass flow of HF or $POF_3$. The explanation for this could be that the second peak in the heat release rate involves burning of mainly non-fluorine containing compounds. The temperature curve shows a rapid increase above the melting temperature of the alumina cell case at about 660 °C. At these temperatures the alumina is molten and has formed a puddle on the burner bed beneath the battery cells. The thermal conditions in and around the thermocouples and the remains of the batteries have therefore changed considerably causing the apparent temperature increase.

In addition to the time resolved measurements with the FTIR, gas-washing bottles were used to determine the total fluorine content in the gas emissions during the tests. A comparison between the different measurement methods used can be seen in Figure 4 for type A cells. Note that the FTIR measurements are performed only to detect HF and $POF_3$, other fluoride compounds are not included. It is interesting to note that for 0% SOC the total amount of fluoride measured by the gas-washing bottle technique matches rather well with the FTIR and primary filter analysis. For other SOC values the fluoride content is higher from the gas-washing bottle measurements. Still, the general trend observed in the FTIR measurements for different SOC values is more or less confirmed by the gas-washing bottle measurements.

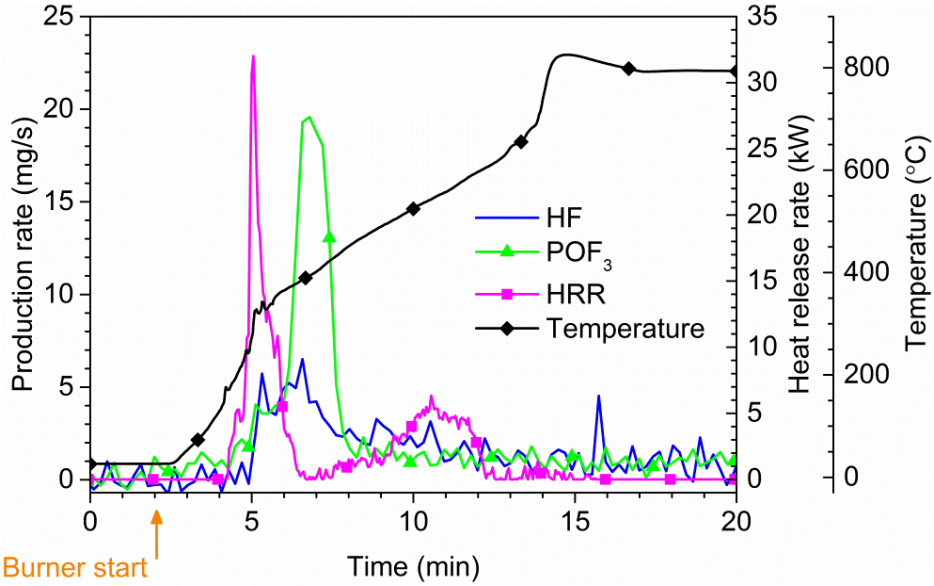


Figure 3 Results for a test with 5 type A cells at 0% SOC showing HF and $POF_3$, HRR and average surface temperature of the battery cells.

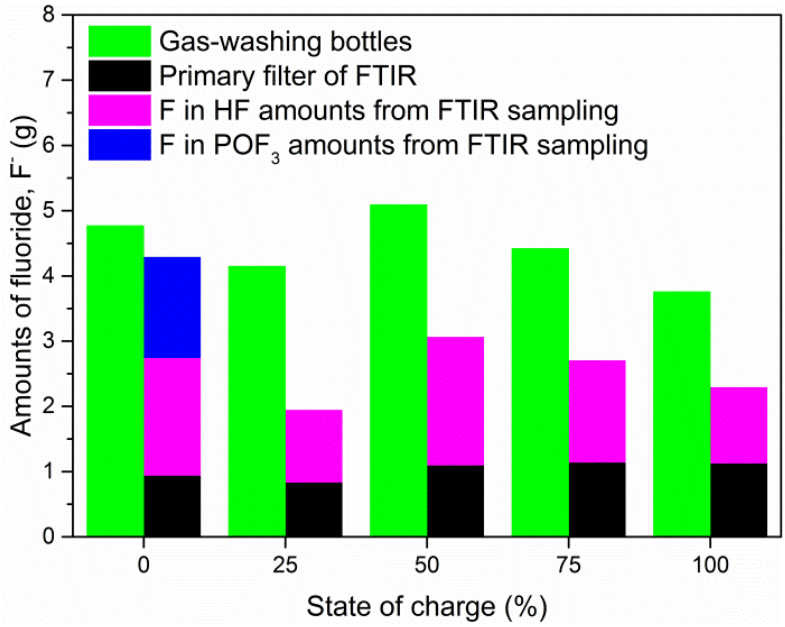


Figure 4 Total amount of measured fluoride, $F^-$, for type A, for 0-100 % SOC with intermediate steps of 25 %. The amount of $F^-$ from the FTIR is calculated from the measurement results for $POF_3$ and HF, while the amount of fluoride from gas-washing bottles and primary filter analyses is measured as water soluble fluoride.

Gas-washing bottles were also used for some of the tests involving battery types B and C. These batteries showed higher amounts of released HF compared to type A. The ratio between the total values of released flouride from FTIR plus filter analysis and from the gas-washing bottles for type B and C was between 0.89 and 1.02, indicating a better correlation between FTIR and gas-washing bottles measurement when HF gas emissions are higher.

The total amount of $POF_3$ measured by FTIR for type A at 0% SOC was 2.8 g (for 5-cells) and 3.9 g (for 10 cells). Hence, the normalized total $POF_3$ production was 15-22 mg/Wh of nominal battery energy capacity. Abuse studies measuring $POF_3$ are few, Andersson et al.[46] found both HF and $POF_3$ when burning mixtures of propane and Li-ion battery electrolytes with a HF:$POF_3$ production ratio between 8:1 and 53:1. Besides HF and $POF_3$ measurements, several distinct non-assigned peaks were found in the FTIR measurements, e.g. at 1027 $cm^{-1}$ and 1034 $cm^{-1}$, which have also been seen in other studies[46]. They are compatible with the typical C-O stretching energies of low molecular weight alcohols in gas phase but also with in-plane stretching of aromatic compounds. This indicates the complexity and the limited knowledge in this area.

**Water mist measurements**

In order to study the effects of water on gas emissions, fire tests have also been performed where a water mist was applied during the fire. The reason for this experiment is that water is the preferred extinguishing agent for a lithium-ion battery fire. The intention in this study was however not to extinguish the fire completely. One potential problem regarding the use of water mist is that the addition of water may, in principle, increase the rate of formation of HF, see eqs. (2) and (3).

Figure 5 shows the results for type B cells with and without exposure to water mist, note that both the HRR and HF production are delayed when water mist is used. In this limited study, the peak of the HF production rate increased by 35% when using water, however no significant change in the total amounts of the HF release could be seen. A similar result has been reported in a previous study[28]. The water mist was applied during two different periods of time, as marked in Figure 5, adding a total of 851 g of water in the reaction zone, however, several other large sources of water were also present in the experiment, i.e. water production from the propane combustion and from humidity in the air. The water mist is cooling the fire and the top surface of the pouch cell was for some time partly covered with liquid water; this is the reason that the battery fire is delayed as seen in Figure 5. The water mist might actually also clean the air by collecting fume particles and HF can be bound to water droplets, thus possibly lowering

the amount of HF in the smoke duct and increasing the non-measured amount of very toxic hydrofluoric acid on the test area surfaces (e.g. walls, floor, smoke duct walls).

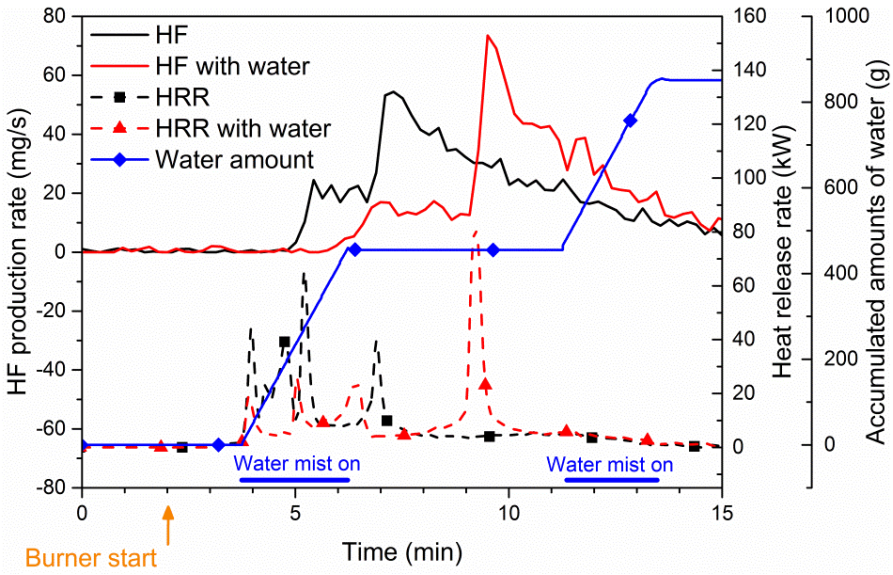


Figure 5 Results for type B cells at 100% SOC with and without the use of water mist.

**Repeatability**

Repeated tests were performed for battery types A-C for selected SOC-levels. Some of the repetitions included a variant, e.g. including water mist; see Methods. In Figure 2 all available test data are presented. Since the test repetitions are not clearly observable in Figure 2 the results are also presented in Table 3 showing the mean values and standard deviations and the number of performed tests. While the ranges in Table 2 include data for all tested SOC-values, Table 3 shows test data for repeated measurements including repetition variants.

Table 3 Detailed results for all available repetitions. Values presented as mean values followed by the standard deviation, in case the data parameter was not measured in all tests the value in bracket declares the number of available tests used for the specific data parameter value.

| Battery | SOC (%) | Number of tests | Normalized total HF detected (mg/Wh) | | Normalized maximum HRR (W/Wh) | Normalized THR (kJ/Wh) |
|---|---|---|---|---|---|---|
| | | | From FTIR | From gas-washing bottles | | |
| A | 100 | 6 | 19.8 ± 1.2 [3] | 29.1 ± 3.1 [5] | 612 ± 102 | 18.1 ± 0.46 |
| | 50 | 7 | 18.5 ± 3.9 [6] | 36.7 ± 3.3 [6] | 416 ± 39 [6] | 18.0 ± 0.61 [6] |
| | 0 | 2 | 21.6 ± 1.5 | 38.3 ± 1.6 | 214 ± 53 | 16.8 ± 0.66 |
| B | 100 | 4 | 166.8 ± 11.5 | 191.3 ± 11.3 [2] | 538 ± 77 | 46.9 ± 1.9 |
| C | 100 | 3 | 53.9 ± 2.0 [2]* | N/A | 461 ± 27 | 69.5 ± 2.6 |
| | 50 | 3 | 141.3 ± 26.3 [2]* | N/A | 149 ± 5 | 70.5 ± 4.9 |

***** For FTIR data for battery type C, one data point of 50% and one data point at 100% SOC are excluded as outliers since they were low due to that a pre HF-saturation was not applied in the test, see Methods.

Figure 6 shows the repeatability results for four tests of battery type B for 100% SOC. The time evolution of HRR varies in the fire tests as seen in Figure 6a. In fire tests there are always natural variations, however comparing the tests with 100% SOC, in Figure 6a, with those with lower SOC-values presented in Figure 1a, the repeatability of the 100% SOC tests is significant. The third repetition (black line) in Figure 6a is delayed due to that it included an application of water mist, as discussed above. Although the appearance of the HRR plots of the four tests differs in Figure 6a the THR (the integrated HRR) values are rather similar. Figure 6b shows the HF release for the same four tests of type B at 100% SOC. Repetition 2 and 3 were performed in the third test period, without secondary FTIR filter, and therefore Repetition 2 occurs earlier while Repetition 3 is delayed due to the applied water mist, as discussed above. For the four tests of type B at 100% SOC the mean value of the total FTIR detected HF release is 166.8 mg/Wh with a standard deviation of 11.5 mg/Wh, as seen in Table 3. Comparing Figure 1b and Figure 6b, shows that for 100% SOC the HF release is faster and reaches a higher value. Repetition 1 in Figure 6b shows lower HF release peak values, however, the total HF release value from the FTIR measurement of 168 mg/Wh is close to the average value (166.8 mg/Wh, as seen in Table 3).

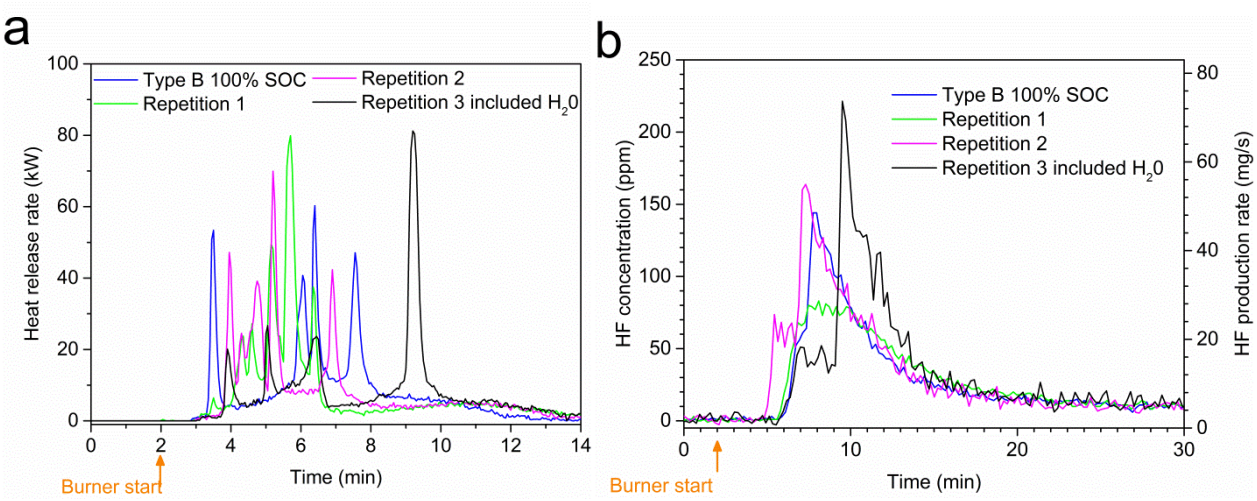


Figure 6 Repeatability for four tests of type B cells at 100% SOC, (a) shows the heat release rate (burner HRR contribution is subtracted) and (b) shows the HF release, both as the measured concentrations as well as the calculated HF production rates.

**Conclusions**

This study covered a broad range of commercial Li-ion battery cells with different chemistry, cell design and size and included large-sized automotive-classed cells, undergoing fire tests. The method was successful in evaluating fluoride gas emissions for a large variety of battery types and for various test setups.

Significant amounts of HF, ranging between 20 and 200 mg/Wh of nominal battery energy capacity, were detected from the burning Li-ion batteries. The measured HF levels, verified using two independent measurement methods, indicate that HF can pose a serious toxic threat, especially for large Li-ion batteries and in confined environments. The amounts of HF released from burning Li-ion batteries are presented as mg/Wh. If extrapolated for large battery packs the amounts would be 2-20 kg for a 100 kWh battery system, e.g. an electric vehicle and 20-200 kg for a 1000 kWh battery system, e.g. a small stationary energy storage. The immediate dangerous to life or health (IDLH) level for HF is 0.025 g/m$^3$ [22] (30 ppm) and the lethal 10 minutes HF toxicity value (AEGL-3) is 0.139 g/m$^3$ [23] (170 ppm). The release of hydrogen fluoride from a Li-ion battery fire can therefore be a severe risk and an even greater risk in confined or semi-confined spaces.

This is the first paper to report measurements of $POF_3$, 15-22 mg/Wh, from commercial Li-ion battery cells undergoing abuse. However, we could only detect $POF_3$ for one of the battery

types and only at 0% SOC, showing the complexity of the parameters influencing the gas emission. No $POF_3$ could be detected in any of the other tests.

Using water mist resulted in a temporarily increased production rate of HF but the application of water mist had no significant effect on the total amount of released HF.

The research area of Li-ion battery toxic gas emissions needs considerable more attention. Results as those presented here are crucial to be able to conduct a risk assessment that takes toxic HF gas into account. The results also enable strategies to be investigated for counteractions and safety handling, in order to achieve a high safety level for Li-ion battery applications. Today we have a rapid technology and market introduction of large Li-ion batteries but the risks associated with gas emissions have this far not been possible to take into consideration due to the lack of data.

**Acknowledgments**

The Swedish Energy Agency and its FFI-program, and Carl Tryggers Stiftelse för Vetenskaplig Forskning are acknowledged for their financial support. Several persons at RISE Research Institutes of Sweden and Chalmers University of Technology have been involved in this work and are gratefully acknowledged.

**Author contributions**

F. Larsson planned the experiments, partially together with P. Andersson and B.-E. Mellander. P. Andersson made the initial data process of the SBI heat release data. P. Blomqvist planned and performed the FTIR and gas-washing bottles measurements and made the initial data processing. F. Larsson prepared the batteries and performed the measurement and data analyses of temperature, cell voltage and water mist, and did the post-measurements and final data processing. Water mist setup was planned and constructed by B.-E. Mellander and F. Larsson. All four authors were involved in the analyses of the data and wrote the paper.

**Additional Information**

**Competing financial interests:** The authors declare no competing financial interests.

## Methods

Seven types of Li-ion batteries were exposed to an external propane fire. Fire characteristics, gas emissions, battery temperatures and cell voltages were measured. In total 39 fire tests were conducted of which 20 were within the base test matrix, 19 were repeated measurements of selected battery types and SOC-levels of which 10 included a variant, e.g. water mist for fire-fighting. The amounts of emitted fluoride gases were measured with two parallel and independent techniques, FTIR (time resolved concentration measurements and total values achieved by integration of the time resolved curve) and gas-washing bottles (total values). The experimental setup is schematically shown in Figure 7.

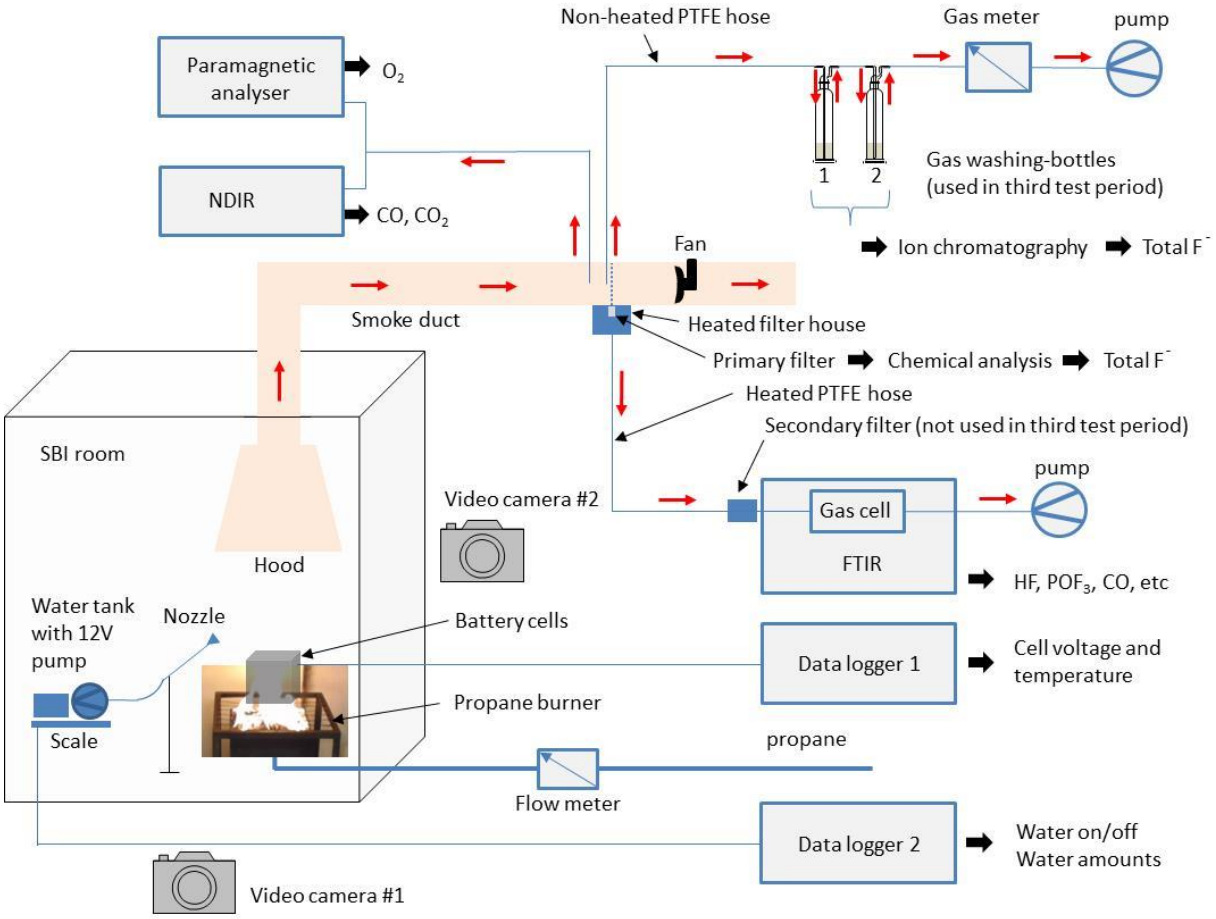


Figure 7 Schematic illustration of the experimental setup.

The gas collecting system and measurement system of the *Single Burning Item (SBI) method* (EN 13823[54]), which is normally used for reaction-to-fire classification of construction products according to EN 13501-1[55] was used in the tests. The tests were performed in three different

test periods; the second test period was conducted about 1 year after the first and the third test period was conducted about 2.5 years after the first. Each test period involved several days of testing. The measurement equipment, as specified in the text below, was somewhat varying between the three test periods.

## Batteries

Six different types of Li-ion battery cells, type A-F, and one Li-ion battery pack, type G, were tested as seen in Table 1. The number of cells used in each test was varied in order to achieve similar electrical energy capacity per test. The batteries were placed on wire gratings just above a 16 kW propane burner. The wire grating was made of steel wire about 2 mm thick over a surface of about 300 x 300 mm. The quadrants of the grating were 40 x 100 mm. The cells were not electrically connected to each other (except the laptop packs of type G, see note in Table 1). Type A-F was pure battery cells while type G was a complete laptop battery pack which included plastics box, electronics and cables. The chemical content of the polymer materials in the auxiliary components of the battery pack of battery type G is not known. It is possible, however not likely, that fluorine was included in some of the components, which in that case could have resulted in the production of HF. For battery type A, 5 cells/test was used except in two variant tests in which 10 cells/test were used.

The influence of different state of charge was investigated, for some battery types the complete SOC-window ranging from 0% to 100%, with intermediate steps of 25%, was investigated. The SOC levels included for each battery type and the numbers of repetitions per test type, i.e. the fire test matrix, is seen in Table 4. All parameters were not measured in all of the tests. Measurement of HRR and corresponding THR was conducted in 38 tests, FTIR in 35 tests and gas-washing bottles were used in 19 tests.

The selected SOC level in each test was set using a charge/discharge procedure using ordinary laboratory equipment as well as dedicated battery test equipment, i.e. a *Digatron battery tester* and *Metrohm Autolab PGSTAT302N* with 20 A booster module. The cells were first fully charged by constant current followed by constant voltage (CC-CV) according to the manufacturer's instructions. For cells intended for tests with less than 100% SOC, the cell was discharged to the selected SOC level, using constant discharge current (CC). A relative low current rate, about C/5, was used and voltage and current rates were within the manufacturer limits. In most cases each battery type was tested during the same test period. However, the tests for type C and D were split in several test periods, for type C repetitions on 50% SOC were conducted in all three test periods, and for type B repetitions at 100% SOC were made in two test periods, the latter one included a water mist test.

All batteries were unused and the calendar life time of the cells before the tests were approximately 6-12 months for type A, F and G and between approximately 2-3 years for type B-E. The pouch cells; type B, C and F was mechanically tied together with steel wires (0.8 mm diameter). The type A hard prismatic cells were tight together in packs of five cells, "5-cell-pack", using steel straps (1 x 13 mm). The hard prismatic and cylindrical cells were placed in boxes to protect test personnel from potential projectile hazards in case of cell explosions due to excessive pressure. The 5-cell-pack of type A was placed standing up, with the cell safety vents releasing straight upright in direction to the hood and smoke duct, inside a custom-made steel-net-box, see Figure 8. Additionally, the 5-cell-pack of type A was fastened to the bottom of the steel-net-box with steel wire (0.8 mm diameter) in the corners to avoid it moving around due to e.g. explosion/rupture/venting. Type D and E cells were placed standing up in custom-made boxes made of non-combustible silica board and steel net at the top and bottom. Type G was placed in a steel net. The protective boxes and steel net were fastened in the wire gratings with steel wire and steel straps to avoid movement due to response to the fire. Care was taken to avoid external short circuiting when placing the battery on the wire gratings as well as avoiding accidental external electrical inter-cell-connections, e.g. for pouch cells the electrical tab terminals were cut. Still the battery test setup allowed that the separators and electrical insulation in the cells could melt due to the heat exposure which could cause various internal and external electrical contacts.

The battery surface temperature was measured with several type K thermocouples; the number of sensors varied for the different battery types. Battery cell surface temperature values presented in this paper are average values over the cell. Cell voltages were measured for type A, B, C and F battery tests. Cell voltage and thermocouple readings was sampled with 1 Hz using two types of data loggers, *Agilent 34972A using an Agilent 34902A reed multiplexer module* (for the third test period) and *Pico Technology ADC-24* (for the first and second test period).

Table 4 Detailed test matrix of the fire tests.

| Battery | Number of tests per SOC-level | | | | | Number of tests |
|---|---|---|---|---|---|---|
| | 0 % | 25 % | 50 % | 75 % | 100 % | |
| A | 1 + 1* | 1 | 3 + 4* | 1 | 3 + 3* | 17 |
| B | 1 | 1 | 1 | 1 | 3 + 1* | 8 |
| C | 1 | 1 | 3 | 1 | 2 + 1* | 9 |
| D | | | 1 | | 1 | 2 |
| E | | | | | 1 | 1 |
| F | | | | | 1 | 1 |
| G | | | | | 1 | 1 |
| Total number of tests | | | | | | 39 |

* repetition includes a variant, e.g. water mist or 2x5-cell-pack (for battery type A).

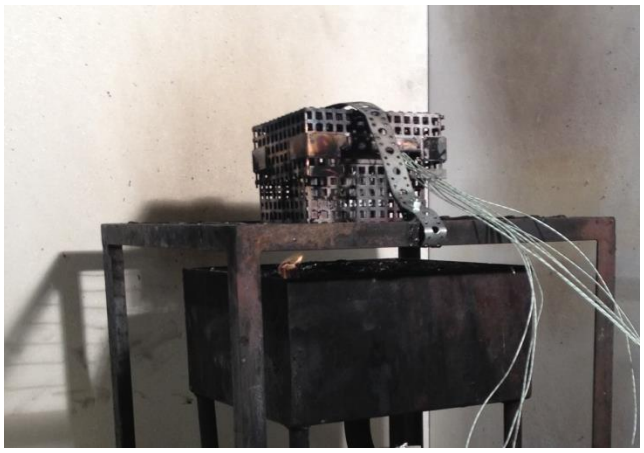

Figure 8 Photo of test type A, showing the 5-cell-pack inside a steel-net-box placed on the wire gratings. The sand bed for the propane burner is underneath the wire grating, a pilot flame (seen in front left corner of the burner) is used to ignite the propane gas.

## Test procedure

The propane burner was started 2 minutes into each test, as indicated with arrows in the result figures in the paper. The burner was active as long as there was a heat contribution from the burning batteries; therefore, the burner was active for different durations of time for different batteries and SOC-levels. When the heat release from the batteries was no longer detectable, the power of the propane burner was doubled, i.e. to 32 kW, in order to be sure to fully burn out any residues of the batteries, for increased personnel safety. The fire emissions were collected in the hood and transferred in the smoke duct having a ventilation flow of 0.4 $m^3/s$, with the exception that 0.6 $m^3/s$ was used in two tests with 100 % SOC for type C. For these cases the values were scaled down to the lower flow values making the results from the two flow rates comparable. The SBI-room, see Figure 7, had a ventilation inlet from an adjacent indoor laboratory hall (which had fresh air inlet from the ventilation system in the building), supplying ambient air with temperature about 20 °C entering beneath the propane burner. We consider the amount of ambient air to be sufficient to provide an oxygen-rich environment and thereby consider the battery fire as well-ventilated. However for some tests, during the rapid and energetic gas outbursts, a full combustion might not have occurred in these short time periods.

All tests were video recorded and for the majority of the tests an additional camera was used set at 90 degree angle from the other video camera, allowing simultaneous recording from two sides of the battery fire.

A part of the smoke duct flow was sampled to a *Servomex 4100 Gas purity analyser* where the oxygen content was measured by a *paramagnetic analyser* and CO and $CO_2$ were measured by a *non-dispersive infrared sensor (NDIR)*. By combing these two measurements, the heat release rate (HRR) is calculated using the oxygen consumption method corrected by $CO_2$[54]. Each test day started with a blank test, i.e. using only the propane burner, to measure the HRR of the burner alone and measure blanks for FTIR and gas-washing bottles. In the presented HRR values of the battery tests the burner contribution to the HRR (about 16 kW, with slight daily variations, established by the blank tests) has been subtracted. The combined expanded uncertainty is +/-5 kW for the HRR-values. By integrating the HRR values over the entire test, subtracting the HRR from the burner, the total heat release (THR) from the battery cells could be established. The oxygen consumption method is common in fire calorimetry, however when using it with batteries, the joule heating from electrical discharge within the cells is not accounted for, therefore the values of HRR and THR do not include the Joule heating. During the external fire tests, it is difficult to measure how much a battery cell is electrically discharged when the separator is melting. The energy ratios presented in Figure 2b do not include any Joule heating as clearly stated by its definition. For 0% SOC the influence from Joule heating is in principle zero, however small amounts of joule heating might possibly be liberated when going to zero voltage even though other processes might occur. Li-ion cells can also release oxygen during thermal runaway and this could affect the measured $O_2$ levels. The amount of oxygen release varies for different electrode materials, e.g. LFP typically releases less oxygen than LCO. However, the ventilation flow is large and the $O_2$ released from the battery cells is regarded as negligible.

## Gas measurements

Besides the gas measurements in the SBI apparatus, measurements of gases were also conducted by online Fourier transform infrared spectroscopy (FTIR). The FTIR offers broad and diverse spectra of gases, the focus was however on fluoride gas emissions. The FTIR used was a *Thermo Scientific Antaris IGS analyzer (Nicolet)* with a gas cell. The gas cell was heated to 180 °C and had a volume of 0.2 L, 2.0 m path length and a cell pressure of 86.7 kPa which was maintained during the tests. The spectral resolution of the FTIR was 0.5 $cm^{-1}$ (accuracy 0.01 $cm^{-1}$) and 10 scans where used to collect a spectrum every 12 s, giving both accurate intensity, as well as relatively rapid measurements with its five spectrum per minute rate. A part of the duct flow, taken along the full duct pipe width (in the mid height of the pipe) from around 15 sampling holes (about 2 mm diameter, directed opposite to flow, pipe end was closed), was taken to online FTIR measurement. This sub-flow was extracted through a primary filter inside a heated filter house (180 °C) and then extracted through an 8.5 m sampling PTFE hose, heated to 180 °C, and then through a secondary filter and finally through the gas cell of the FTIR. The sub-flow was selected to be 3.5 L/min using a pump located after the FTIR gas cell. Between each

test the FTIR sampling system was flushed with $N_2$ gas and a new background spectrum was measured. There is a natural delay time between the FTIR and the heat release measurement. In order to time synchronize them, the $CO_2$ measurements from both the FTIR and the NDIR (part of the heat release rate measurement) were overlayed.

One primary filter (M&C ceramic filter, type "F-2K") was used per test and was chemically analysed for fluoride content after the test. It is known that HF may be partly adsorbed by this type of filter[56]. The fluoride amount absorbed by the filter was determined by leaching the filter in an ultrasonic water bath for at least 10 min and thereafter the fluoride content in the water was measured by ion chromatography with a conductive detector, according to the method B.1 (b) of the SS-ISO 19702:2006 Annex B standard. The amount of HF is calculated by assuming that all fluoride ions present in the filter derives from HF. The secondary filter (M&C sintered steel filter), heated to 180 °C, was the same in all tests in the first and second test period. In the third test period the secondary filter was removed in order to decrease delay time and losses. The third test period started with burning 10 cells of type A in order to saturate the FTIR sampling system with HF and it was conducted because in the first and the second test period the first tests had indicated low HF values, HF was potentially lost during saturation of the gas collecting system.

The FTIR was calibrated[29,57] for HF and $POF_3$. The minimum detection limit (MDL) for HF was 1.7 ppm and the limit of quantification (LOQ) was established to 5.7 ppm. The detection limit for $POF_3$ was 6 ppm[29]. $PF_5$ was also qualitatively detectable by the FTIR[29] but not quantitatively calibrated. A classical least square (CLS) method was used for the quantification of HF and $POF_3$ using the spectral bands specified in Table 5. The relative error of the HF prediction is lower than 10 rel-%.

For all measurements, except type G, the measured ppm levels of HF were above the detection level. For $POF_3$, the maximum concentration was 11 ppm (5-cells) and 19 ppm (10-cells).

When the FTIR measurement stopped, HF levels were, in some of the tests, still somewhat above the detection limit, even though no HRR contribution was measured from the batteries. It is also possible that the HF was temporarily clogged in the sampling system. Some HF might not have been collected in the measurements and the effect of this error is largest for the batteries that give the lowest values. Thus the reported values might underestimate the released gas emissions.

Table 5 FTIR spectral band used for measurements of $POF_3$ and HF.

| Spectral bands ($cm^{-1}$) | Type of band |
|---|---|
| $POF_3$ | |
| 868 - 874 | P-F symmetric stretching mode[20] |
| 1413 - 1418 | P-O stretching mode[20] |
| HF | |
| 4172 - 4175 | HF R-branch stretching mode[58] |
| 4202 - 4203 | HF R-branch stretching mode[58] |

In order to further improve the accuracy of the FTIR measurements, a data offset determination and a subsequent adjustment of the HF values was performed. The improvement was greatest for tests with lower concentrations, closer to the MDL value, e.g. type A with 5 cells with low values during relatively short periods of time. With 10 cells per test, the type A batteries gave higher signal-to-noise levels. The FTIR measurements started around 8 minutes before the burner was started. The calculated average HF ppm noise level was treated as an offset that had both negative and positive values, ranging from extreme values of about -2 to 3.5 ppm. This offset was compensated for by assuming a constant offset value and adding positive or negative offset values to the total HF release value. Note that the reported concentration values in ppm are only valid for the measurements in the smoke duct of our specific test equipment and method. The HF and $POF_3$ concentration values (in ppm) were used for calculating the corresponding production rates (in mg/s) using the ideal gas law and taking into account the measured ventilation flow rate in the smoke duct.

In the third test period the total amounts of water soluble fluorides were determined using gas-washing bottle technique. This was made in order to validate the results from the FTIR measurements with a separate measurement technique. The water soluble fluorides were collected in the bottles and the amount of HF was calculated by assuming that all fluoride ions present derives from HF. The sample gas was extracted from the center of the smoke duct using a non-heated 6 mm (o.d.) diameter PTFE sampling tube with a length of about 1.5 m. The sampling was made using two gas-washing bottles connected in series each containing 40 mL of an alkaline buffer solution (20 mM $Na_2CO_3$/20 mM $NaHCO_3$). The second bottle was used to capture any losses from the first bottle. The sampling flow was 1.0 normal-L/min and the total sampled volume during a test was measured by a calibrated gas volume meter. The sampling flow rate was checked before the start of each test using a *Gilian Gilibrator-2 NIOSH Primary Standard Air Flow Calibrator* gas flow meter. The procedure during a test was to continuously sample during the full test time. When the test was completed, the sampling tube was disconnected from the exhaust duct to allow rinsing of the tube with buffer solution, about 30 mL in the first gas-washing bottle, to collect any fluoride deposited on the inner walls of the

tubing, in order to minimize losses in the tube. Since the tube was rinsed, heating of the tube was not necessary (any condensation in tube was collected anyhow). Analysis of fluorine content of the absorption solutions was made using High Performance Ion Chromatography (HPIC). The contents of the two gas-washing bottles were analyzed separately. The bottles were rinsed with distilled water between each test in order to minimize any interference between tests.

## Water mist test

In the water mist tests, a custom-made equipment was constructed, including a 12 V automotive pump and water container which was placed on a scale measuring the weight of the water. The scale readings and the on/off manual switching (of the 12V) was recorded with 1 Hz using *Pico Technology ADC-24* with a custom-made *LabVIEW* program. The water mist was sprayed on or above the batteries using a metal nozzle. In order for precise time synchronization, the on/off 12V signal was recorded by both data loggers (data logger 1 and data logger 2). A blank test, i.e. using only the propane burner and without batteries, was performed in order to calibrate the setup. The water flow was around 190 g water per min and consisted of deionized water.

## References


1 Samsung Note 7: Press Conference Details, Samsung US, Our safety promise, http://www.samsung.com/us/explore/committed-to-quality/?CID=van-brd-brd-0119-10000141, Date of access: 06/04/2017.

2 Prigg, M. Nasa reveals shocking video of secretive military 'RoboSimian' EXPLODING as its batteries catch fire (2016), http://www.dailymail.co.uk/sciencetech/article-3883158/Nasa-reveals-shocking-video-secretive-military-RoboSimian-EXPLODING-batteries-catch-fire.html, Date of access: 06/04/2017

3 Aircraft Serious Incident Investigation Report, JA804A. Japan Transport Safety Board (2014), Available online: http://www.mlit.go.jp/jtsb/eng-air_report/JA804A.pdf, Date of access: 13/02/2017.

4 Auxiliary Power Unit Battery Fire, Japan Airlines Boeing 787-8, JA829J, Boston, Massachusetts; NTSB/AIR-14/01. National Transportation Safety Board (2014), Available online: http://www.ntsb.gov/investigations/AccidentReports/Reports/AIR1401.pdf, Date of access: 13/02/2017.

5 Chevrolet Volt battery incident overview report, *National Highway Traffic Safety Administration (NHTSA)*, DOT HS 811 573 (2012).

6 Doughty, D. & Roth, E. P. A general discussion of Li ion battery safety. *The Electrochem. Soc. Interface*, **summer 2012**, 37-44 (2012).

7 Larsson, F. & Mellander, B.-E. Abuse by external heating, overcharge and short circuiting of commercial lithium-ion battery cells. *J. of The Electrochem. Soc.* **161(10)**, A1611-A1617 (2014).

8 Larsson, F., Andersson, P. & Mellander, B.-E. Are electric vehicles safer than combustion engine vehicles? in *Systems perspectives on Electromobility* (eds. Sandén, B. & Wallgren, P.) 33-44 (Chalmers University of Technology, 2014).

9 Finegan, D. P. et al. In-operando high-speed tomography of lithium-ion batteries during thermal runaway. *Nat. Commun*. **6**, 6924 (2015).

10 Larsson, F., Andersson, P. & Mellander, B.-E. Lithium-ion battery aspects on fires in electrified vehicles on the basis of experimental abuse tests. *Batteries* **2**, 9 (2016).

11 Lopez, F. L., Jeevarajan, J. A. & Mukherjee, P. P. Experimental analysis of thermal runaway and propagation in lithium-ion battery modules. *J. of The Electrochem. Soc* **162 (9)**, A1905-A1915 (2015).
12 Lamb, J., Orendorff, C. J, Steele, L. A. M. & Spangler, S. W. Failure propagation in multi-cell lithium-ion batteries. *J. of Power Sources* **283**, 517-523 (2015).
13 Larsson, F., Anderson, J., Andersson, P. & Mellander, B.-E. Thermal modelling of cell-to-cell fire propagation and cascading thermal runaway failure effects for lithium-ion battery cells and modules using fire walls. *J. of The Electrochem. Soc.* **163 (14)**, A2854-A2865 (2016).
14 Lebedeva, N. P. & Boon-Brettz, L. Considerations on the chemical toxicity of contemporary Li-ion battery electrolytes and their components. *J. of The Electrochem. Soc.* **163 (6)**, A821-A830 (2016).
15 Sun, J. et al. Toxicity, a serious concern of thermal runaway from commercial Li-ion battery. *Nano Energy* **27,** 313–319 (2016).
16 Nedjalkov, A. et al. Toxic gas emissions from damaged lithium ion batteries - analysis and safety enhancement solution. *Batteries* **2**, 5 (2016).
17 Liu, K. et al. Electrospun core-shell microfiber separator with thermal-triggered flame-retardant properties for lithium-ion batteries. *Sci. Adv.* **3**, e1601978 (2017).
18 Park, Y.-U. et al. Tailoring a fluorophosphate as a novel 4 V cathode for lithium-ion batteries. *Scientific Reports* **2**, 704 (2012).
19 Ortiz, G. F. et al. Enhancing the energy density of safer Li-ion batteries by combining high-voltage lithium cobalt fluorophosphate cathodes and nanostructured titania anodes. *Scientific Reports* **6**, 20656 (2016).
20 Yang, H., Zhuang, G. V. & N. Ross Jr, P. Thermal stability of $LiPF_6$ salt and Li-ion battery electrolytes containing $LiPF_6$. *J. of Power Sources* **161,** 573-579 (2006).
21 Kawamura, T., Okada, S. & Yamaki, J.-i. Decomposition reaction of $LiPF_6$-based electrolytes for lithium ion cells. *J. of Power Sources* **156**, 547-554 (2006).
22 Documentation for immediately dangerous to life or health concentrations (IDLHs) for hydrogen fluoride (as F). *The National Institute for Occupational Safety and Health (NOISH)* (1994).
23 Acute exposure guideline levels for selected airborne chemicals: volume 4, subcommittee on acute exposure guideline levels. ISBN: 0-309-53013-X. *Committee on Toxicology, National Research Council* (2004).
24 Middelman, A. Hygiensiska gränsvärden AFS 2015:7, Hygieniska gränsvärden. Arbetsmiljöverkets föreskrifter om hygieniska gränsvärden och allmänna råd om tillämpningen av föreskrifterna. ISBN 978-91-7930-628-1. ISSN 1650-3163. *Swedish Work Environment Authority* (2015).
25 Guéguen, A. et al. Decomposition of $LiPF_6$ in high energy lithium-ion batteries studied with online electrochemical mass spectrometry. *J. of The Electrochem. Soc.* **163 (6)**, A1095-A1100 (2016).
26 Chatelain, M. D. & Adams, T. E. Lithium ion gas sampling of vented cells. *Proceedings of the Power Sources Conference* **42**, 87-89 (2006).
27 Blum, A. F. & Long Jr, R. T. Hazard assessment of lithium ion battery energy storage systems. *Fire Protection Research Foundation* (2016).
28 Larsson, F., Andersson, P., Blomqvist, P., Lorén, A. & Mellander, B.-E. Characteristics of lithium-ion batteries during fire tests. *J. of Power Sources* **271**, 414-420 (2014).
29 Larsson, F., Andersson, P., Blomqvist, P. & Mellander, B.-E. Gas emissions from Lithium-ion battery cells undergoing abuse from external fire in *Conference proceedings of Fires in vehicles (FIVE) 2016* (eds. Andersson, P. & Sundstrom, B.) 253-256 (SP Technical Research Institute of Sweden, 2016).
30 Ribière, P. et al. Investigation on the fire-induced hazards of Li-ion battery cells by fire calorimetry. *Energy Environ. Sci.* **5**, 5271-5280 (2012).
31 Lecocq, A. Scenario-based prediction of Li-ion batteries fire-induced toxicity. *J. of Power Sources* **316**, 197-206 (2016).
32 Lecocq, A., Bertana, M., Truchot, B. & Marlair, G. Comparison of the fire consequences of an electric vehicle and an internal combustion engine vehicle in *Conference proceedings of Fires in vehicles (FIVE) 2012* (eds. Andersson, P. & Sundstrom, B.) 183-193 (SP Technical Research Institute of Sweden, 2012).
33 Ohsaki, T. et al. Overcharge reaction of lithium-ion batteries. *J. of Power Source* **146**, 97-100 (2005).
34 Abraham, D. P. et al. Diagnostic examination of thermally abused high-power lithium-ion cells. *J. of Power Sources* **161**, 648-657 (2006).
35 Roth, E. P. Abuse response of 18650 Li-ion cells with different cathodes using EC:EMC/$LiPF_6$ and EC:PC:DMC/$LiPF_6$ electrolytes. *ECS Transactions* **11 (19),** 19-41 (2008).
36 Golubkov, A. W. et al. Thermal-runaway experiments on consumer Li-ion batteries with metal-oxide and olivin-type cathodes. *RSC Adv.* **4**, 3633-3642 (2014).

37 Golubkov, A. W. et al. Thermal runaway of commercial 18650 Li-ion batteries with LFP and NCA cathodes – impact of state of charge and overcharge. *RSC Adv.* **5**, 57171-57186 (2015).
38 Spinner, N. S. et al. Physical and chemical analysis of lithium-ion battery cell-to-cell failure events inside custom fire chamber. *J. of Power Sources* **279**, 713-721 (2015).
39 Fu, Y. et al. An experimental study on burning behaviors of 18650 lithium ion batteries using a cone calorimeter. *J. of Power Sources* **273**, 216-222 (2015).
40 Huang, P., Wang. Q., Li, K., Ping, P. & Sun, J. The combustion behavior of large scale lithium titanate battery. *Scientific Reports* **5**, 7788 (2015).
41 Ping, P. et al. Study of the fire behavior of high-energy lithium-ion batteries with full-scale burning test. *J. of Power Sources* **285**, 80-89 (2015).
42 Roth, E. P. & Orendorff, C. J. How electrolytes influence battery safety. *The Electrochem. Soc. Interface*, **summer 2012**, 45-49 (2012).
43 Eshetu, G. G. et al. In-depth safety-focused analysis of solvents used in electrolytes for large scale lithium ion batteries. *Phys. Chem. Chem. Phys.* **15**, 9145-9155 (2013).
44 Lamb, J., Orendorff, C. J., Roth, E. P. & Langendorf, J. Studies on the thermal breakdown of common Li-ion battery electrolyte components. *J. of The Electrochem. Soc.* **162 (10)**, A2131-A2135 (2015).
45 Eshetu, G. G. et al. Fire behavior of carbonates-based electrolytes used in Li-ion rechargeable batteries with a focus on the role of the $LiPF_6$ and LiFSI salts. *J. of Power Sources* **269**, 804-811 (2014).
46 Andersson, P., Blomqvist, P., Lorén, A. & Larsson, F. Using Fourier transform infrared spectroscopy to determine toxic gases in fires with lithium-ion batteries. *Fire and Materials* **40 (8)**, 999-1015 (2016).
47 Lux, S. F. The mechanism of HF formation in $LiPF_6$ based organic carbonate electrolytes. *Electrochem. Comm.* **14**, 47–50 (2012).
48 Lux, S. F., Chevalier, J., Lucas, I. T. & Kostecki, R. HF formation in $LiPF_6$-based organic carbonate electrolytes. *ECS Electrochem. Lett.* **2 (12)**, A121-A123 (2013).
49 Wilken, S., Treskow, M., Scheers, S., Johansson, P. & Jacobsson, P. Initial stages of thermal decomposition of $LiPF_6$-based lithium ion battery electrolytes by detailed Raman and NMR spectroscopy. *RSC Adv.* **3**, 16359-16364 (2013).
50 Hammami, A., Raymond, N. & Armand, M. Runaway risk of forming toxic compounds. *Nat.* **424**, 635-636 (2013).
51 Campion, C. L. et al. Suppression of toxic compounds produced in the decomposition of lithium-ion battery electrolytes. *Electrochem. and Solid-State Lett.* **7 (7)**, A194-A197 (2004).
52 Liu, X. et al. Heat release during thermally-induced failure of a lithium ion battery: impact of cathode composition. Fire Safety Journal **85**, 10-22 (2016).
53 Lyon, R. E. & Walters, R. N. Energetics of lithium ion battery failure. J. of hazardous materials **318**, 164-172 (2016).
54 EN 13823:2010. Reaction to fire tests for building products – building products excluding floorings exposed to the thermal attack by a single burning item. *European Committee for Standardization* (2010).
55 EN 13501-1:2007+A1:2009. Fire classification of construction products and building elements - part 1: classification using data from reaction to fire tests. *European Committee for Standardization* (2009).
56 ISO 19702:2006. Toxicity testing of fire effluents -- guidance for analysis of gases and vapours in fire effluents using FTIR gas analysis. *International Organization for Standardization (2006).*
57 Andersson, P., Blomqvist, P., Lorén, A. & Larsson, F. Investigation of fire emissions from Li-ion batteries. *SP Technical Research Institute of Sweden*. SP Report 2013:5 (2013).
58 Hollas, J. M. Modern Spectroscopy, 3ed. (John Wiley & Sons, 1996).

# Paper VI

# Gas Emissions from Lithium-Ion Battery Cells Undergoing Abuse from External Fire

Fredrik Larsson[1,3,*], Petra Andersson[2], Per Blomqvist[2] and Bengt-Erik Mellander[3]
[1]Electronics, SP Technical Research Institute of Sweden, Borås, Sweden
[2]SP Safety, SP Technical Research Institute of Sweden, Borås, Sweden
[3]Department of Physics, Chalmers University of Technology, Göteborg, Sweden

## ABSTRACT

Heat release rate, total heat released and toxic gas emissions were measured during exposure of commercial lithium-ion (Li-ion) battery cells to an external propane burner fire. Hydrogen fluoride (HF) was found in all tests and the released HF emissions measured via online FTIR range between 12-81 mg/Wh. Gas-washing bottles were used as a secondary measurement technique in one of the tests. The gas washing bottle and the FTIR measurements were in the same order of magnitude proving the usefulness of the FTIR technique even if there is an accumulation of HF in the filters used in the beginning of the test. The HF release for a large battery pack exposed to fire could thus in a worst case scenario result in a very large volume of toxic gases.

**KEYWORDS:** lithium-ion battery, gas emission, toxic gases, safety, fire, HRR

## INTRODUCTION

Currently Li-ion has taken the position as the dominant choice for batteries used in portable battery powered consumer products. Li-ion batteries have also been introduced in electrified vehicles, in the electrical power grid and in ships. The Li-ion battery has attractive properties in form of power and energy densities, long life time, fast chargeability and no memory-effect, but has some potential drawbacks when it comes to safety.

The high energy densities of Li-ion batteries give potential for a rapid de-energizing. Additionally, the electrolyte used in Li-ion batteries is flammable. Compared to many other battery technologies, the Li-ion battery requires substantial efforts in order to manage its intrinsic safety shortcomings. The voltage and temperature ranges must be monitored and controlled. The Li-ion cell must be protected against physical damage (e.g. penetration and deformation) and from short circuit. In case of a severe failure, the Li-ion cell can undergo a thermal runaway which is a rapid exothermic reaction resulting in a fast temperature increase, gassing, fire and potentially an explosion. Furthermore, the gases released from the cell are toxic; of special interest is the production of hydrogen fluoride (HF) [1-3]. This work presents fire tests that have been performed on commercial Li-ion cells where HF is measured.

## EXPERIMENTAL SET-UP

The Single Burning Item apparatus (SBI) was used to measure typical fire characteristics, e.g. Heat Release Rate (HRR), CO and $CO_2$ production in addition was HF measured. Multiple commercial Li-ion cells were exposed to external fire by a 16 kW propane burner. Table 1 shows the details of the cylindrical and pouch cells, including state-of-charge (SOC), used in the four tests, A-D, performed. The cells were not electrically connected to each other and not under electrical load during the tests. The cylindrical cells were placed in boxes to protect from flying projectiles and the LTO cells were both fastened to each other and fastened to the wire grating with steel wire, as seen in Figure 1. For test D the center temperature between the two cells and both cell voltages (CV) were measured every second. Gases were measured online by FTIR, particular interest was given to the emission of hydrogen fluoride (HF). The FTIR gave one spectrum every 12 seconds based on 10 scans. Detailed descriptions on the experimental set-up can be found in Larsson et. al. [1].

*Table 1 Test overview.*

| Test | Cell type | No. of cells | Nom voltage (V) | Total nom capacity (Ah) | Electrode chemistry Anode – cathode | Cell packaging | SOC (%) |
|---|---|---|---|---|---|---|---|
| **A** | K2 LFP26650EV | 9 | 3.2 | 28.8 | Carbon – LFP | Cylindrical | 100 |
| **B** | K2 LFP26650EV | 9 | 3.2 | 28.8 | Carbon – LFP | Cylindrical | 50 |
| **C** | Lifetech X-1P | 5 | 3.3 | 40 | Carbon – LFP | Cylindrical | 100 |
| **D** | Leclanché LTO | 2 | 2.3 | 60 | LTO – NCO | Pouch | 100 |

*Figure 1 Experimental setup before burner start for test B (left), test C (mid) and test D (right).*

In addition to the FTIR measurements, gas-washing bottles were used in test D in order have a second measurement technique to sample the total amount of released fluorides. The assumption here was that the absolute majority of water soluble fluorides would be HF. Two gas-washing bottles, each containing 40 mL of a carbonate/bicarbonate buffer solution, were connected in series. The flow through the bottles was 1.0 nL/min and a calibrated gas volume meter was used to measure the total sampled volume. High Performance Ion Chromatography (HPIC) was used for the analysis of the absorption solutions. The sample gas was continuously extracted from the centre of the exhaust duct during the full test time. After the test the sampling tube was rinsed to collect any HF deposited inside the tube in order to minimize any losses of HF for the analysis.

## RESULTS AND DISCUSSION

Figure 2 shows HRR and HF mass flow for the K2 cells (test A and B). The fully charged cell shows higher HRR peaks, similar to the results in Larsson et. al. [1], also the case with 50% SOC shows some peaks in contradiction to how the 50% SOC pouch cells behaved in Larsson et. al. [1]. This is probably due to that cylindrical cells can withstand more pressure before the safety valve releases the gas. The HF gas emission peaks are higher for 100% than for 50% SOC. However, the K2 50% test was the first run in the test series and it has later proved that the measurement systems, e.g. the FTIR sampling system (tubes and secondary filter etc) is catching HF before it gets saturated on HF. It is thus difficult to make a direct comparison between the 50 % and 100% SOC tests in this case, as a part of the released HF was saturated in the FTIR sampling, and lower HF values are therefore measured for K2 50%. It could also be noted that the test with K2 50% SOC was run about one year later than the one with 100% SOC. About nine “sound bangs” were heard for the test B with 50% SOC, corresponding to cell opening (e.g. safety vent) in each K2 cell while eight “sound bangs” were heard for the test A with 100% SOC, suggesting that one K2 cell did open in some other way, e.g. a softer/earlier safety vent opening, or that two cells opened at the same time.

Figure 3 shows HRR and HF gas emissions for test C. In the test, one of the five cylindrical Lifetech cells exploded and the cell interior was expelled [3]. The reason for this was that the safety vent did not open, and this happening elucidate that the safety mechanics (in this case, the safety vent) can malfunction. Figure 4 shows the results for test D. The center temperature between the two cells reaches about 600 °C. The production of HF is about 2 minutes delayed after the HRR, similar to test A-C. The cell voltage breakdown in the bottom cell occurs at the same time as HF gas emissions and cell temperature increases rapidly, suggesting the occurrence of thermal runaway starting in the bottom cell. The cell voltage of the top cell breaks down about 1 minute later. The battery cells burnt

relatively fast (i.e. giving high HRR).

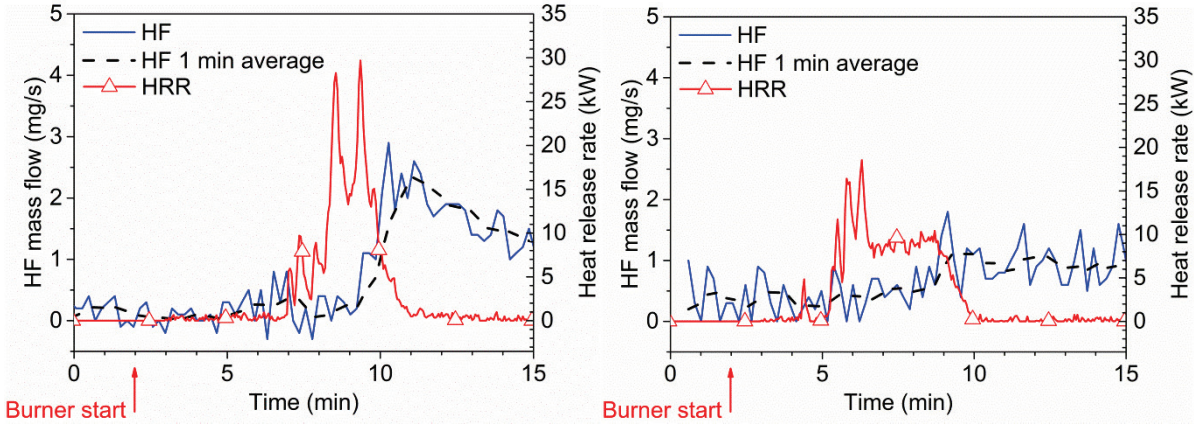


*Figure 2* *Results for K2, test A 100% SOC (left) and test B 50% SOC (right). The* "1 min average" is calculated by 5 points moving average of each 12 seconds spectrum.

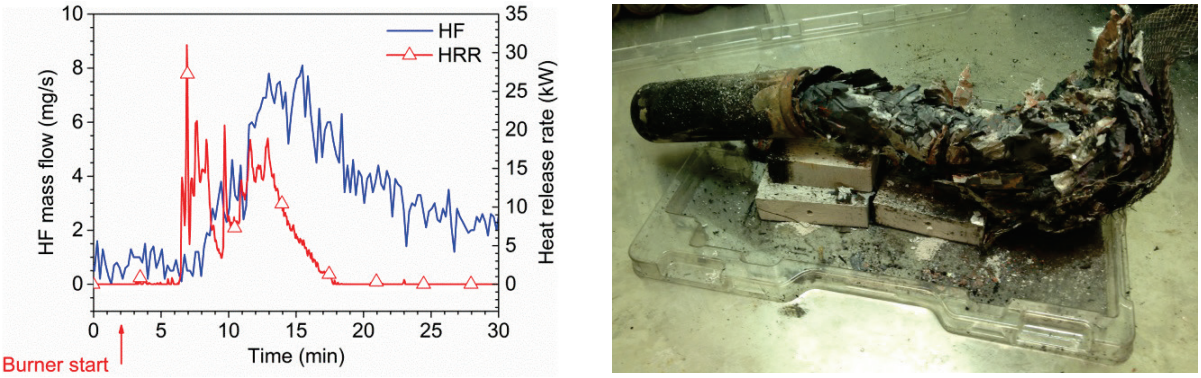


*Figure 3* *Results for test C, Lifetech 100% SOC. The photo is taken during tear-down analysis and showing the cell interior expelled out. The cell was caught by the steel net in the protective test box.*

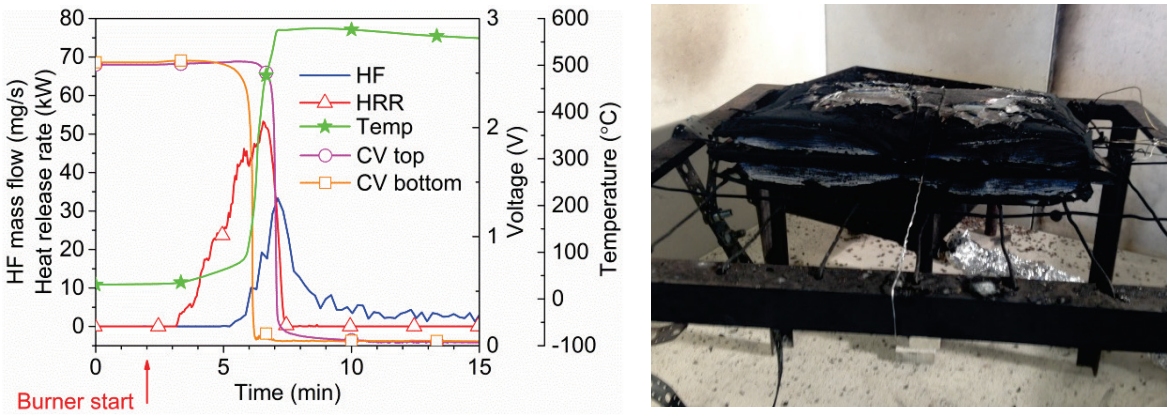


*Figure 4* *Results for test D. The photo is taken from the long side, after the test is complete.*

The detection limit for HF for the equipment used in this investigation is 2 ppm [1]. The peak ppm levels for the tests in Figures 2-4 are 9 ppm (test A), 5 ppm (test B), 16 ppm (test C) and 100 ppm (test D), all well above the detection limit. Detailed results for the tests are shown in Table 2. The weight loss of the battery cells was between 19 and 25 %. The total amounts of HF gas emissions were between 12 and 81 mg/Wh and 7 and 27 mg/g (where g corresponds to the weight loss). The secondary measurement with gas-washing bottle technique in test D, gave about twice the amount of HF, however still in the same order or magnitude as the FTIR measurement.

An electrified vehicle today could have a battery pack ranging between 10-90 kWh. Battery packs in heavy-duty electrified vehicles (buses, trucks, etc), in ships and in stationary electrical grid could have significantly larger battery systems. Extrapolating for a worst case scenario of a 100 kWh battery pack (e.g. 400 VDC, 250 Ah), the amount of released HF could be 1200-8000 g. The IDLH (Immediately Dangerous to Life or Health) value for HF is 0.025 g/m$^3$ [4]. If the HF gas emissions would be homogenously distributed this amount of HF has to be diluted in more than 50 000 - 300 000 m$^3$ of air not to exceed the IDLH value. This volume corresponds e.g. to a total fire in an electric vehicle with 100 kWh battery pack parked in a 15000 – 100000 m$^2$ garage of 3 m in height. Another example of a larger 1 MWh battery pack in e.g. a stationary storage in an apartment-complex would result in a volume corresponding to about 1500 – 10000 apartments of 300 m$^3$ each (e.g. 100 m$^2$ with 3 m in height). These examples assume that the gases are not vented away but stay in the building. However, it is important to note that all fires produce smoke and one should also for that reason not stay within the room/building if there is a fire going on.

*Table 2. Detailed results of HRR, total heat release (THR, integrated HRR) and HF gas emission release. The energy capacity in Wh is calculated by nominal voltage times nominal capacity.*

| Test | Weight loss (g, %) | Max HRR (kW) | THR (kJ) | Hydrogen fluoride | | | | | |
|---|---|---|---|---|---|---|---|---|---|
| | | | | Amounts from FTIR (g) | Amounts from filter (g) | Total amounts (g) | Amounts from gas washing bottles (g) | Total yields (mg/g) | Total yields (mg/Wh) |
| **A** | 145 g 19.7 % | 29 | 2766 | 1.2 | 1.0 | 2.2 | N/A | 15 | 24 |
| **B** | 155 g 21.0 % | 19 | 2502 | 0.7 | 0.4 | 1.1 | N/A | 7 | 12 |
| **C** | 406 g 24.6% | 31 | 6605 | 6.3 | 1.3 | 7.6 | N/A | 19 | 58 |
| **D** | 419 g 19.1% | 53 | 6893 | 4.8 | 1.6 | 6.4 | 11.2 | 15-27 | 46-81 |

## CONCLUSIONS

The total amounts of HF gas emissions measured in these tests on commercial Li-ion cells were 12-81 mg/Wh for the different batteries tested. The HF release for a large battery pack exposed to fire could thus in a worst case scenario result in a very large volume of toxic gases.

## ACKNOWLEDGEMENTS

The Swedish Energy Agency, the Swedish Fire Research Board and Carl Tryggers Stiftelse för Vetenskaplig Forskning are greatly acknowledged for their support. Several technical staff colleagues at SP Safety have contributed to this work.

## REFERENCES

1. Larsson, F., Andersson, P., Blomqvist, P., Lorén, A., and Mellander, B.-E., “Characteristics of lithium-ion batteries during fire tests”, *Journal of Power Sources*, 271, 414-420, 2014.
2. Andersson, P., Blomqvist, P., Lorén, A., and Larsson, F., “Using Fourier transform infrared spectroscopy to determine toxic gases in fires with lithium-ion batteries”, *Fire and Materials*, DOI: 10.1002/fam.2359, in press.
3. Larsson, F., Andersson, P., and Mellander, B.-E., “Lithium-Ion Battery Aspects on Fires in Electrified Vehicles on the Basis of Experimental Abuse Tests”, *Batteries*, 2, 9, 2016.
4. Documentation for Immediately Dangerous to Life or Health Concentrations (IDLHs) for Hydrogen Fluoride (As F); The National Institute for Occupational Safety and Health (NOISH): Washington, DC, USA, 1994.

# Paper VII

*Journal of The Electrochemical Society*, **163** (14) A2854-A2865 (2016)
0013-4651/2016/163(14)/A2854/12/$33.00 © The Electrochemical Society

# Thermal Modelling of Cell-to-Cell Fire Propagation and Cascading Thermal Runaway Failure Effects for Lithium-Ion Battery Cells and Modules Using Fire Walls

**Fredrik Larsson,[a,b,z] Johan Anderson,[b] Petra Andersson,[b] and Bengt-Erik Mellander[a]**

[a]*Department of Physics, Chalmers University of Technology, SE-412 96 Goteborg, Sweden*
[b]*SP Technical Research Institute of Sweden, SE-501 15 Boras, Sweden*

A model is presented for predicting the cell-to-cell propagation of a thermal runaway/fire in a lithium-ion battery cell to neighboring cells by simulating the temperature development in neighboring cells. The modelling work comprises of two major steps; setting up a model of the cells including the thermal properties of the cells, and then validating the model through experiments where the boundary conditions in the validation test must be determined carefully. The model is developed to allow a fast evaluation of several different preventive means of thermal insulation, it is not modelling the pack and cells to a great detail. Still the experimental validation indicates that the model is good enough to fulfil its purpose of the model. A feasibility study using the model is conducted assessing two different types of fire walls between battery modules of 10 cells. The results show that there is a substantial risk for a cascading of thermal events in a battery pack, although cooling systems and fire walls may mitigate these risks.


Manuscript submitted July 1, 2016; revised manuscript received September 23, 2016. Published October 22, 2016.

Lithium-ion (Li-ion) batteries offer great performance in terms of energy and power densities. Today millions of Li-ion batteries are used in various consumer products (e.g. mobile phones and laptop computers) and growing numbers of Li-ion batteries are also used in electrified vehicles and other applications (e.g. stationary grid power). However, compared to many other battery technologies Li-ion is less thermally stable. If the cell temperature is increased beyond a certain threshold, a thermal runaway can occur, resulting in a rapid temperature increase and possibly other related adverse effects such as release of gas and smoke, fire, and rupture/explosion. There are numerous types of abuse situations that can result in an overtemperature inducing a thermal runaway, such as mechanical, electrical and thermal abuse. On cell level, the thermal runaway response during abuse conditions depends e.g. on cell chemistry, cell design, size of battery and abuse type.[1–10] In order to avoid large consequences it is important that a thermal runaway in a single Li-ion cell does not propagate to involve several modules or a complete battery pack.

In order to prevent the Li-ion battery cell from going into thermal runaway, different safety measures are necessary. The design of the battery pack and its application integration plays an important role in preventing cell failure propagation. For example, an adequate design of the battery pack and the electrified vehicle for protection against battery deformation in case of a crash[11] is of key importance as a mechanically damaged battery could result in both external and internal short circuits of the battery cells, which could lead to thermal runaway. In order to protect from electrical abuse, passive and active safety actions should be taken. Monitoring of individual cells by a Battery Management System (BMS) is necessary to protect each cell from e.g. overvoltage, undervoltage, overtemperature and overcurrent. The BMS should be designed to give high safety also in case of failure of e.g. a sensor. However, for some abuse scenarios the BMS cannot protect the battery. A first example is in case a spontaneous internal short circuit develops in a cell, external systems like the BMS are in this case unable to prevent the development. A second example is for thermal abuse situations in case of an external heating by e.g. fire or extreme sunlight. For electrified vehicles, the fire source could be the vehicle itself, an adjacent building or another vehicle involved in a fire or crash etc. The consequences of such a situation may, however, be controlled on the system level by an appropriate system design.

In case of a thermal runaway in a single Li-ion cell it is important to stop or at least delay its spreading to adjacent cells, since the effects from a cascading thermal runaway scenario of a complete battery pack could be devastating. Battery packs in electrified vehicles can consist of thousands of battery cells. In general, the design of a battery pack plays an important role for fire propagation; e.g. thermal management system, mechanical support structure cell-to-cell respective module-to-module, potential use of fire walls, and division of a battery pack into different sub-packs are important design aspects. Understanding fire propagation between Li-ion cells in a battery pack consisting of multiple cells is therefore important in order to minimize large-scale effects.

There are relatively many simulation studies available about general heat generation and cooling of Li-ion batteries during normal cycling (battery charge/discharge) within the battery specifications.[12–20] Furthermore, Li-ion cells and battery packs with multiple cells have been simulated during abusive conditions; by external heating in oven,[21–24] external heating by cell heating element,[25] short circuiting,[23,26–28] overcharging[23] and mechanical deformation/crash/nail penetration.[23,29–32] Spotnitz et al.[33] performed a numerical study on the influence of various heat transfer modes for the thermal runaway propagation cell-to-cell for a battery pack with 8 cylindrical cells of type 18650. Maloney[34] studied fire propagation and extinguishment experimentally on 5 cylindrical cells in which the fire was initiated in one cell using an external heater. Lamb et al.[35] studied thermal runaway propagation initiated by a single cell thermal runaway using nail penetration. Their work covered series and parallel connected modules with 10 cylindrical 18650 cells and with 5 pouch cells and it was found that the thermal contact between the cells was a dominating factor for the propagation characteristics.

Lopez et al.[36] experimentally initiated a thermal runaway in one cell with external heating and studied the cell-to-cell propagation for 18650 cells as well as for small prismatic cells. By investigating different cell inter-spacing and electrical tab connections they concluded that for the prismatic cells, which had two vents on the cell side, fire protection materials between the cells were required in order to hinder fire propagation. Further experimental studies of thermal runaway propagation have been performed for 18650 cells by Spinner et al.[37] and for a prismatic cell module by Feng et al.[38,39] and Huang et al.[40]

A review covering safety focused modelling has also been published recently by Abada et al.[41] However, simulations of lithium-ion battery fire abuse situations have rarely been studied. Anderson et al.[42] used CFD simulations with subsequent thermal modelling to study the fire resistance of a battery pack in a gasoline pool fire test according to United Nations Regulation No. 100[43] and a heat propagation simulation of cell-to-cell fire propagation for five Li-ion pouch cells has recently been performed by Anderson et al.[44,45],and Andersson et al.[46]

An electrified vehicle could have an energy capacity ranging between e.g. 10 and 100 kWh containing hundreds of cells in order to achieve a high enough energy capacity and battery pack voltage. Even larger battery packs can be found in e.g. stationary grid applications and onboard ships. Cell-to-cell fire propagation in a large battery pack

[z]E-mail: vegan@chalmers.se; fredrik.larsson@sp.se

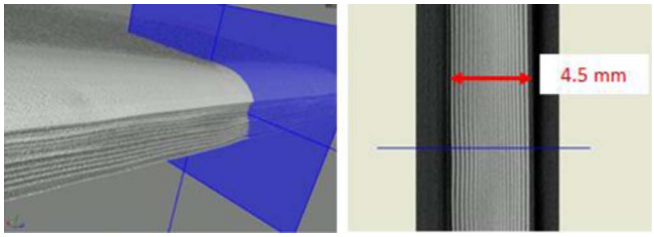


**Figure 1.** X-ray photos of the battery cell, a 3D photo (left) and a 2D cross-section (right) where the blue line indicate the cross-section area.

could result in severe consequences. Therefore a model to predict cell-to-cell propagation is important in order to design and validate safe Li-ion battery systems.

This paper presents a thermal model for cell fire propagation, intended for studying the cell-to-cell propagation on a battery system level. It is desired to have a conservative model that will result in somewhat higher temperatures than in the experimental study, in order to be on the safe side when evaluating cell-to-cell propagation effects. The paper first describes the battery cell and the numerical model and tool. Secondly, a validation of the model is conducted using experimental data. Finally, the model is applied to a fictive part of a battery pack, where cell and module fire propagation is studied with and without firewalls.

## Thermal Model

***Battery cell model.—***The starting point for the modelling work is a commercial Li-ion battery cell, EiG ePLB-F007A, a pouch prismatic cell with a nominal capacity of 7 Ah and a nominal energy capacity of 22.4 Wh. The cell's physical size is about 220 × 145 × 4.5 mm. The Li-ion cell has a lithium-iron phosphate (LFP), $LiFePO_4$, cathode and a carbon anode. The physical structure of the cell is a multilayered repeatable structure; negative current collector of copper, anode, separator, cathode, positive current collector of aluminum. Figure 1 shows X-ray photos of the pouch cell where the multilayered structure is clearly seen. The total number of layers is of the order of 150 layers.

The cell was modelled in 3D as a square block with the same dimensions as the pouch cell. Modelling the detailed structure of the cells would result in far too long simulation times and the cell was thus modelled as a homogenous material but with anisotropic thermal conductivity in the plane (in the two planar directions parallel to the multilayered cell, x- and y-directions) and across the cells (perpendicular to the multilayerad cell stack structure, z-direction) due to the layered structure.[44] The thermal property values used for the battery cell are shown in Table I. The density was simply established by measuring the physical cell volume and the cell weight. Specific heat and thermal conductivity values used in the simulation were estimated from literature values by Wu et al.[47] Ideally, careful measurements of these quantities at elevated temperatures would be needed but are generally difficult to obtain. The effects of varying thermal properties were studied previously[44–46] and thus this study was conducted using one particular set of values only.

When modelling more than one cell in this work, the cells were assumed to be in perfect contact with each other at all times with a thin, thermally resistive layer in between cells to represent the pouch packaging material. Cell swelling was thus not included in the model. The packaging material was modelled as a lumped heat capacity material i.e. the temperature change in the material depends only on the thickness and thermal conductivity, i.e. thermal inertia is ignored. The thermally resistive layer was assumed to have a thickness of 160 μm per cell (320 μm between two cells) and a thermal conductivity k = 0.22 W/(mK) for the overall pouch packaging materials, these data are calculated based on data from Svens et al.[48] with three layers consisting of 88 μm polypropylene, 45 μm aluminum and 27 μm polyamide.

**Table I. Values of the thermal properties of the Li-ion battery cell used for the simulations.**

| Type | Density ρ [kg/m$^3$] | Specific heat $c_p$ [J/(kg K)] | Thermal conductivity k [W/(m K)] |
|---|---|---|---|
| Cell interior | 1965 | 1243 | $k_x = k_y = 21$ and $k_z = 0.48$ |
| Cell packaging layer | N/A | N/A | 0.22 |

**Table II. The numerical characteristics for three sizes of grid resolutions for 5 battery cells tightly packed.**

| Grid resolution | Numbers of elements | Degrees of freedom | Solution time [Minutes] | Accuracy [Max relative errror] |
|---|---|---|---|---|
| Coarse | 8000 | 17000 | 1.1 | <3.5% |
| Normal | 18000 | 27000 | 2.5 | <1.8% |
| Fine | 38000 | 50000 | 9.0 | N/A |

***Heat transfer model and boundary conditions.—***The thermal model solves the heat conduction equation determining the local temperature in the cell. The heat diffusion is governed by,

$$\rho c_p \frac{\partial T}{\partial t} = \nabla \cdot (k \nabla \mathrm{T}) + \dot{Q} \quad [1]$$

where $\dot{Q}$ is the total power generated within the battery cell, representing in the present case the energy generated in a thermal runaway. Note that to be able to compute the temperature, T, with good accuracy according to Eq. 1 the temperature dependent density, ρ, specific heat capacity, $c_p$, and thermal conductivity, $k$, are needed. In addition, the thermal conductivity can be anisotropic for inhomogeneous materials, e.g. layered materials inside battery cells.

Furthermore, boundary conditions are needed to solve the equation, i.e. the radiative heat flux expressed as,

$$\dot{Q}_r = \varepsilon\sigma \left(T_{gas}^4 - T^4\right) \quad [2]$$

and the convective heat flux,

$$\dot{Q}_c = h_c \left(T_{gas} - T\right) \quad [3]$$

where ε is the emissivity, σ the Stefan-Boltzmann constant (5.67 × $10^{-8}$ W/(m$^2$K$^4$)), $h_c$ the convective heat transfer coefficient and $T_{gas}$ the gas temperature. T in Eqs. 2 and 3 is the temperature on the boundary of the cell. Note that the radiation and gas temperature are assumed to be the same, denoted $T_{gas}$.

***Simulation tool.—***The battery cell(s) were modeled in 3D with the Finite-Element Method (FEM) utilizing the heat transfer module in COMSOL Multiphysics program version 5.1. The heat transfer module in Comsol solves Eq. 1 with the boundary conditions in Eqs. 2–3 by standard Finite-Element (FE) analysis.

The accuracy of the FE solution in Comsol was first evaluated using a grid sensitivity study. To be able to perform many repeated simulations, the total simulation time has to be acceptable and with only a limited loss of accuracy. The numerical characteristics using three different grid resolutions; course, normal and fine, for 5 battery cells tightly packed (a "5-cell-pack") are shown in Table II. The "degrees of freedom" for the model are the lengths of the temperature state vector that are the unknowns in the finite element analysis. The "solution time" is the runtime for the model of the 5-cell-pack to finish. The "accuracy" means the maximum error relative to the solution obtained by the fine grid. As seen in Table II the solution converges at the level of fine where the solution does not change with increasing resolution, however small deviations as well as good computational performance are found already for the normal resolution. The grid resolution normal was chosen for the rest of the studies here resulting

**Figure 2.** Photo of 5-cell-pack placed on wire-gratings.

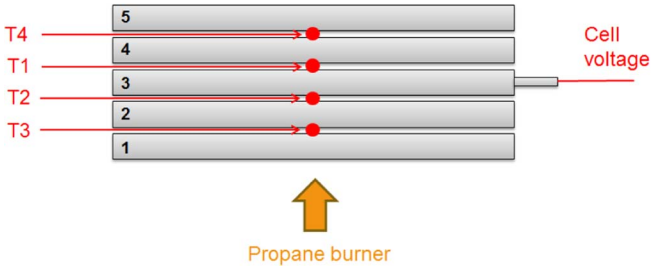


**Figure 3.** Schematic illustration of the test setup showing the placement of the four thermocouples between the five cells; T1, T2, T3 and T4, and cell voltage measured of the third (mid) cell.

**Table III. Test overview of 5-cell-packs.**

| Test No. | SOC (%) | Thermocouples used | Burner HRR (kW) |
|---|---|---|---|
| A | 100 | T1, T2 | 16.4 |
| B | 75 | T1, T2, T3, T4 | 16.9 |
| C | 0 | T1, T2 | 16.4 |

in a maximum error from the numerical solution due to the limit in grid size of 1.8%, as seen in Table II.

### Model Validation - Experimental

As an experimental validation of the model a scenario using five commercial Li-ion cells tied together using steel wires (0.8 mm diameter) was chosen. These cells were exposed to the heat from a 16 kW propane burner with physical dimensions of about 300 × 300 mm. The 5-cell-pack was placed on wire gratings with propane burner beneath as seen in Figure 2. The gas and measurement collection system of the *Single Burning Item (SBI) method* (EN13823[49]) was used for these tests. Battery cells with different state of charge (SOC) were used in the tests, varying from 100% to 0% SOC, denoted Test A, B and C, see Table III. The tests were conducted both to measure the heat release rate (HRR) of a cell undergoing a thermal runaway and also to measure the temperatures between the cells to provide validation data for the thermal model and the cells. The propane burner was started at time 0 in each test. The concentrations of $O_2$, CO and $CO_2$ in the duct flow were measured utilizing a *Servomex 4100 Gas purity analyzer,* more specifically by using a paramagnetic analyzer for $O_2$ and a non-dispersive infrared (NDIR) sensor for CO and $CO_2$. The HRR was calculated using the method of oxygen consumption and corrected for $CO_2$ according to EN13823.[49] The oxygen consumption method is well-established in fire calorimetry. However, there might be some limitations for its use for Li-ion batteries, e.g. since it does not include heat generated from Joule heating in case of separator meltdown and the following internal cell short circuit, electrically discharging the cell. However, this deviation is likely to be relatively small.[50,51]

The temperatures between the cells were measured using type K thermocouples. Figure 3 schematically shows the placement of the four thermocouples, T1-T4. In some tests only T1 and T2 were measured as shown in Table III. Temperatures and the cell voltage of the middle (third) cell were measured at 1 Hz using a data logger, Pico Technology ADC-24. The cell voltage of the mid (third) cell was measured. The terminal tabs of the other cells were cutoff in order to avoid short circuiting of the cells during the tests. Figure 4 shows some photos from test A. The HRR from the propane burner alone was measured each test day prior the battery pack tests, as a blank test, in order to accurately measure the HRR from the burner. The HRR from the burner for the different tests is presented in Table III. The HRR contribution from the burner has been subtracted in all figures presenting HRR from battery cells in this paper. Figure 5 shows the HRR for various SOC for the 5-cell-packs. For the experiment with 100% SOC, distinct outbursts of released energy were detected, while for the other SOC levels no such peaks were detected. The heat release rate of fires is naturally varying even when all controllable parameters are the same. It is thus impossible to exactly reproduce the results of an experiment but as shown in Figure 6, where test A is repeated, a very similar behavior is observed in repeated experiments. Figure 7 shows the measured temperatures and HRR for test A and test B. All measured temperatures show a two step process, with a lower heat increase rate up to a certain temperature, around a cell surface temperature of 100–150°C and then the second step is initiated with a significantly more rapid temperature increase rate, up to a temperature platau at around 400–500°C. For test B, the measured temperatures T4 start to rise before temperature T1 and in fact follow temperature T2 rather close, as seen in Figure 7. This seems to be due to that the top cell starts to burn before the cell underneath which is indicated by the videos taken during the test. The two stage temperature development could be due to that when a cell starts to burn underneath another cell, the temperature recording point between the cells will heat more rapidly. Also the thermal properties of the cell will change as the electrolyte and separator material disappears from the cell and thus the thermal conductivity will likely increase, since separator and electrolyte have lower heat conductivity values then the metal parts.

(a) (b) (c)

**Figure 4.** Test A, (a) photo during fire test, photos after the test are taken from above (b) and from the longer side of the cell (c).

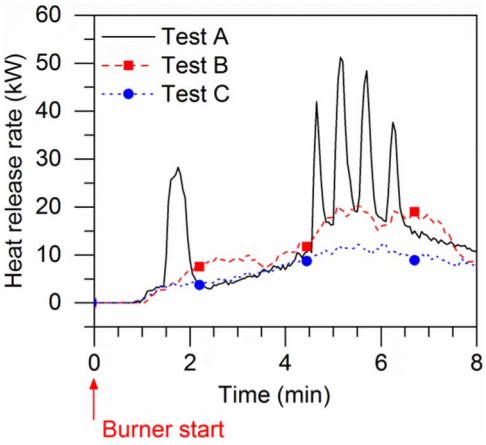


**Figure 5.** Experimentally measured HRR for Test A (100% SOC), Test B (75% SOC) and Test C (0% SOC).

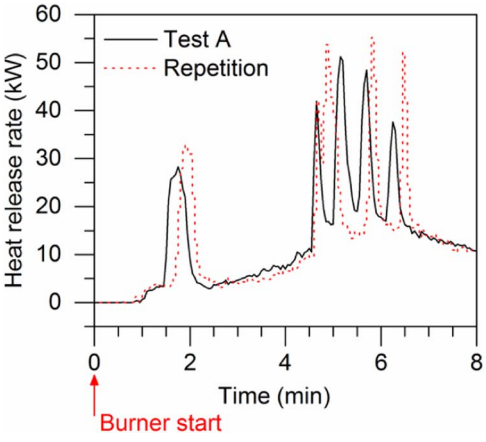


**Figure 6.** Experimentally measured HRR for 100% SOC, Test A and a repetition, to show repeatability.

However, possible loss of physical contacts between the parts of the cell may also lead to a decreased thermal heat conductivity.

The generated heat release in the five battery cells, $\dot{Q}$ in Eq. 1, can be determined by the measured HRR while subtracting the burner contribution to the HRR. For the numerical simulation, finding the total heat release for a single cell is necessary. The bottom cell, closest to the propane burner, will be the first of the five battery cells to catch fire/go into thermal runaway. It is therefore important to distinguish the heat release of the initiating bottom cell from that of the other four cells in the tests. For the 100% SOC case, the HRR from the bottom cell can be relatively well determined by observing the HRR data, including the first outburst peak but not the second outburst peak in the HRR graph, seen in Figure 5. For lower SOC, which does not show these outbursts, it is more difficult to establish the HRR release of the bottom cell. It was therefore assumed for all SOC-levels that the HRR curve for the initiating cell (the cell in the bottom of the set-up) is the HRR-curve until 1/5 of the total heat release (THR, integrated HRR) is reached as indicated in Table IV.

**Table IV. Total heat release from the 5-cell-packs.**

| Test No. | SOC (%) | Total heat release, THR (kJ) | 1/5 of THR (kJ) | Test time when 1/5 of THR is reached (min) |
|---|---|---|---|---|
| A | 100 | 7526 | 1505 | 4.2 |
| B | 75 | 8132 | 1626 | 4.5 |
| C | 0 | 8314 | 1663 | 5.3 |

The 5-cell-pack used for the experimental validation did not have any inter-cell material. In should be noted that using pouch cells in a real battery pack would typically require use of an inter-cell support structure, e.g. aluminum plates, for mechanical support and thermal management of the pouch cell. Such a rigid structure could also decrease/hinder cell swelling in case of overtemperatures. Inter-cell materials also play an important role for cell-to-cell thermal propagation. The experiment was set up to provide validation data for the simulation model, for that purpose no inter-cell materials were used neither desired.

## Boundary Conditions for Model Validation

In order to predict the time evolution of the temperatures in an object subject to fire, a well-defined fire source is needed, see e.g. Anderson et al.[42] For modelling purposes, a test with a mock-up was performed under otherwise similar conditions as the 5-cell-pack fire tests, in order to characterize the burner accurately. The mock-up had the dimensions 222 × 147 × 40 mm, see Figure 8, and was constructed of Promatect clad with custom made plate thermometers.[52] The dimensions of the mock-up were determined by estimations of relative swelling, by post video analysis, of the Li-ion pouch cells during real test conditions and the thickness of the mock-up was thus larger than that of the initial five cells, but lower than the final height of the swelled 5-cell-pack. Although the moisture level is very low in Promatect it was dried for around 48 h in order to further reduce moisture content.

The objective of the mock-up test is to estimate the impact of the fire source on each side of the mock-up by measuring the adiabatic surface temperature (AST) on each side using plate thermometers and by that comparing the numerical model with the experimental set-up. The mock-up was instrumented with type K Inconel plate thermometers that were approximately 40 mm x 100 mm in size to fit

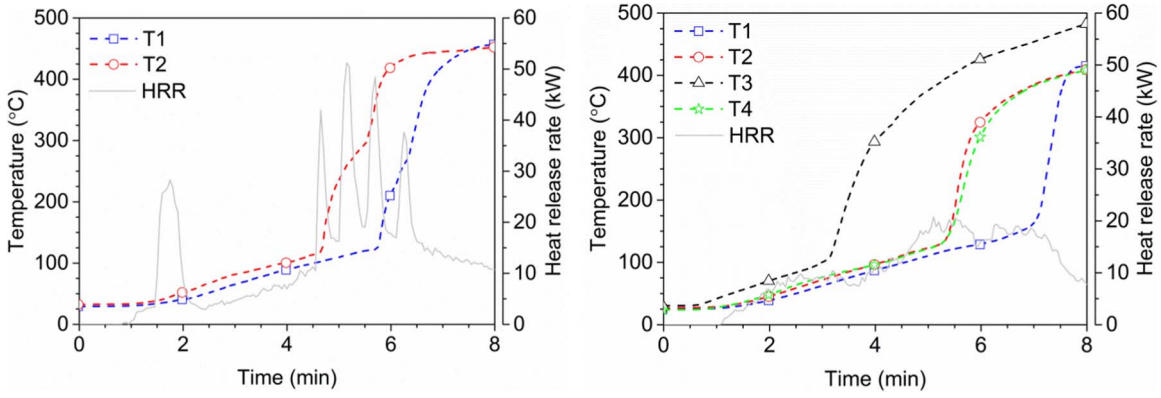


**Figure 7.** Experimentally measured temperatures and HRR, for Test A 100% SOC (left) and for Test B 75% SOC (right).

**Figure 8.** The mock-up with applied instrumentation before the test.

on four sides of the mock-up. The AST is defined as the temperature on the surface of an object that cannot absorb any heat. AST is an artificial temperature that describe the local conditions around the test object and replaces the radiation and convection temperature, in Eqs. 2 and 3. Since it is adiabatic conditions $\dot{Q}_{Tot} = 0$ which gives,

$$0 = \dot{Q}_{Tot} = \dot{Q}_r + \dot{Q}_c = \varepsilon\sigma\left(T_{gas}^4 - {T_{AST}}^4\right) + h_c\left(T_{gas} - T_{AST}\right) \quad [4]$$

where $T_{AST}$ is the adiabatic surface temperature.

Typically AST is described as,

$$\dot{Q}_{AST} = h\left(T_{AST} - T\right) \quad [5]$$

The heat flow, $\dot{Q}_{AST}$, is determined per unit of time and area where $h$ is the heat transfer coefficient. However, due to the limitations of the physical extension of the object's height, the size of the plate thermometers were smaller than the normal 100 mm x 100 mm, indicating that the smaller sized thermometers may experience a somewhat different convection radiation equilibrium than normal sized plate thermometers.

The impact of the propane fire source was modelled using the Fire Dynamics Simulator (FDS) program version 6.1.1[53] to determine the gas temperatures, $T_{gas}$ in Eqs. 2 and 3, around the cells and the heat transfer coefficient, $h_c$ in Eq. 3. The impact is limited to be represented as a set of heat transfer coefficient and temperature on the upper, lower and side boundaries, respectively. FDS uses a computational fluid dynamics (CFD) model solving the Navier-Stokes equations in the limit of low-speed, thermally-driven flow with an emphasis on smoke and heat transport from fires. The propane fire source was modelled in a $1 \times 1 \times 1$ cm$^3$ grid in FDS using default values for propane with 30 $\times$ 30 grid cells over the burner surface. A grid sensitivity study was performed according to the FDS user's guide[53] for $5 \times 5 \times 5$ cm$^3$ and $1 \times 1 \times 1$ cm$^3$ grids and the finer grid was deemed to have enough resolution for the present purposes. Note that for a pre-simulation estimation of grid resolution by calculating the characteristic fire size,

$$D^* = \left(\frac{\dot{Q}}{\rho_\infty c_p T_\infty \sqrt{g}}\right)^{2/5} \quad [6]$$

results in 3.68 for the coarse mesh and 18.4 for the fine mesh for $D^*/\delta x$, of which the latter is appropriate for this kind of analysis according to McGrattan el al.[53] The characteristic fire size divided by the grid cell size ($D^*/\delta x$) is a relevant quantity to determine mesh resolution and should be in the range 10 – 20, where $D^*$ is determined by the Eq. 6. Here, $\rho_\infty$ is the ambient density of air, $T_\infty$ is the ambient temperature of air, $c_p$ is the specific heat of air and g is the gravitational acceleration. Time slices of the simulation are shown in Figure 9 where the representation of the flames can be seen in the left figure and the temperature field surrounding the mock-up can be seen on the right. The fire source was modelled using the HRRPUA option in FDS, i.e. the HRR per unit area over the burner surface was defined using the measured HRR from the mock-up test to determine this value. The HRR of the propane burner was measured to 16.5 kW in a blank test prior the mock-up test. In the FDS software, the gas temperatures on each side of the mock-up were monitored together with the heat transfer coefficient. The results are presented in Table V, the gas temperatures and heat transfer coefficients are mean values calculated for the period 5 to 15 minutes after the burner start.

**Table V. The gas temperature and heat transfer coefficient for the mock-up from FDS simulations, mean values for the time period 5 to 15 minutes.**

| Parameter | Lower | Upper | Side |
|---|---|---|---|
| Gas temperature, $T_{gas}$ [°C] | 555 | 119 | 649 |
| Heat transfer coefficient, $h_c$ [W/(m$^2$K)] | 9.96 | 4.65 | 9.48 |

The gas temperatures and heat transfer coefficients found in the modelling using the FDS were then used in a COMSOL Multiphysics model of the mock-up in order to make sure that the boundary conditions found in the FDS simulation resulted in appropriate levels of temperature increase for the mock-up. By comparing the simulation results from COMSOL with experimental data a validation of the complete numerical method could be achieved. The heat transfer to the mock-up was modelled in COMSOL assuming radiation from the surrounding gas on all sides, i.e. for promatec and inconcel plate thermometers, with emissivity $\varepsilon = 0.8$. The thermal conductivity $k = 0.099$ W/(mK), density $\rho = 280$ kg/m$^3$ and specific heat capacity $c_p = 2200$ J/(kgK) of Promatect were taken from Häggkvist's[54] measured data at 100°C. The model includes thin Inconel plates on the side to simulate the conditions of the experiment, however to have reliable results at the plates an increased number of grid cells are needed at these locations. In total the model consists of approximately 70000 grid cells. Temperatures from the simulation and the experimental

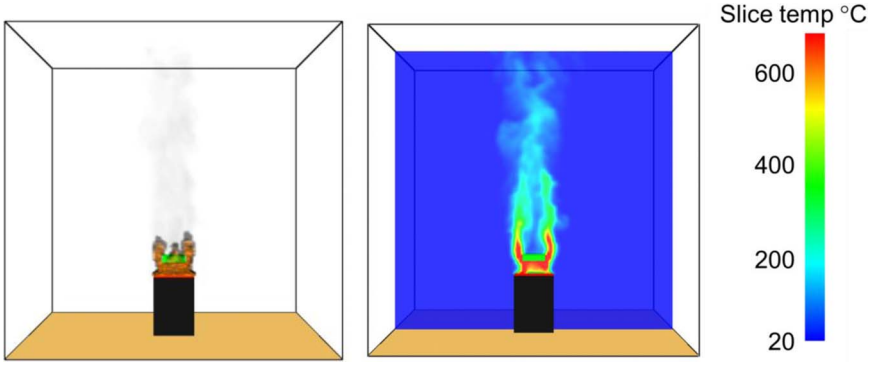


**Figure 9.** Time slices of the FDS simulation of the mock-up, showing the flames (left) and the temperature in the vicinity of the mock-up (right).

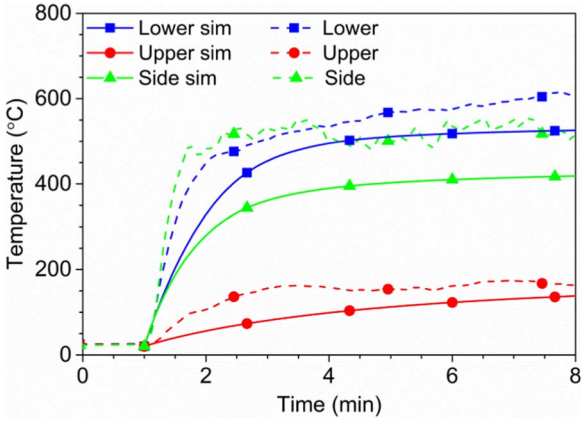


**Figure 10.** Comparison of simulated (solid lines) and measured values (dashed lines) of the surface temperature for three sides of the mock-up.

data of the mock-up are shown in Figure 10. As seen from the figure the agreement is reasonably good for the top and bottom surfaces although a bit on the non-conservative side, while the temperature on the sides is underestimated in the simulation. This is probably due to that in the experimental test there was a small distance between the steel plates and the Promatect on the sides which allowed much higher heat transfer to the steel plates on the sides where the plate was exposed to gas on both sides. Using an emissivity $\varepsilon = 1.0$ would result in somewhat higher simulated temperatures, however it is expected[54] that the emissivity of the object is closer to $\varepsilon = 0.8$ and it was therefore chosen.

The thermal properties of Promatec and of the battery cell are very different. Therefore, analogous FDS simulations were performed for a Li-ion 5-cell-pack in order to obtain gas temperatures and heat transfer coefficients also for this case, the results of which are shown in Table VI. In the FDS model, the 5-cell-pack was modelled as a rectangular box with the dimensions before test and thermal properties adopted from Table I. As in the previous case of the mock-up, reported values are mean values over the period 5 to 15 minutes after burner start. The impact from the natural variations of the propane burner is studied by comparing 16.4 and 16.9 kW HRR in Table VI and Table VII. As seen from the tables, the variation in the values of $T_{gas}$ and $h_c$ is maximum 4% but typically lower.

**Table VI. The gas temperature and heat transfer coefficient for the 5-cell-pack from FDS simulations for Test A with 16.4 kW HRR from the propane burner.**

| Parameter | Lower | Upper | Side |
|---|---|---|---|
| Gas temperature, $T_{gas}$ [°C] | 537 | 111 | 610 |
| Heat transfer coefficient, $h_c$ [W/(m$^2$K)] | 11.00 | 3.42 | 10.60 |

**Table VII. The gas temperature and heat transfer coefficient for the 5-cell-pack from FDS simulations for Test B with 16.9 kW HRR from the propane burner.**

| Parameter | Lower | Upper | Side |
|---|---|---|---|
| Gas temperature, $T_{gas}$ [°C] | 538 | 116 | 615 |
| Heat transfer coefficient, $h_c$ [W/(m$^2$K)] | 11.10 | 3.48 | 10.50 |

## Model Validation Results

In order to validate the model results for the 5-cell-pack from the FEM simulation are compared with experimental measurements for 75% and 100% SOC. For each SOC level, the heat transfer boundary conditions from the FDS simulation as presented in Table VI and Table VII were used as input to the FEM simulations, with the emissivity of $\varepsilon = 0.8$ on all sides. The measured HRR presented in Figure 5 was used as input for each SOC-level of the 5-cell-pack and was deposited homogenously into the bottom cell. The HRR curve from Figure 5, was deposited only into the bottom cell during the complete simulation, even though the measured HRR curve also comes from additional cells. The reason for this is that detailed information of the HRR and the precise time for the start reactions from individual cells are difficult to obtain. For 100% SOC level, five peaks are visible in the HRR graph, however it is unclear which peak correspond to which cell. For 75% SOC and lower there are no visible peaks and the HRR is smoother making it difficult to validate without ending up in curve fitting. Most of the HRR development has occurred during the first 8 minutes of the test, as seen in Figure 7, and the simulation time is thus chosen to be 8 minutes for the validation. There is of course an error due to that all HRR is distributed only into the bottom cell. After a certain time, the first (bottom) cell is considered to be fully burned, and the time for this is presented in Table IV, showing that after around 4.5 minutes the fire for the first cell is completed, suggesting that simulation times beyond 4.5 minutes have increased errors. This modelling choice is done in order to reduce the number of degrees of freedom keeping in mind that the model is intended for cell-to-cell propagation and not for a detailed cell level analysis.

Figure 11 shows both the measured and simulated results for the four temperatures in the 75% SOC case. In Figure 11a the simulated temperatures are derived with a model including both the HRR from the burner and the HRR from the battery cells. In Figure 11b only the HRR from the burner is used in order to investigate the impact for the burner alone. The simulated temperatures are therefore naturally

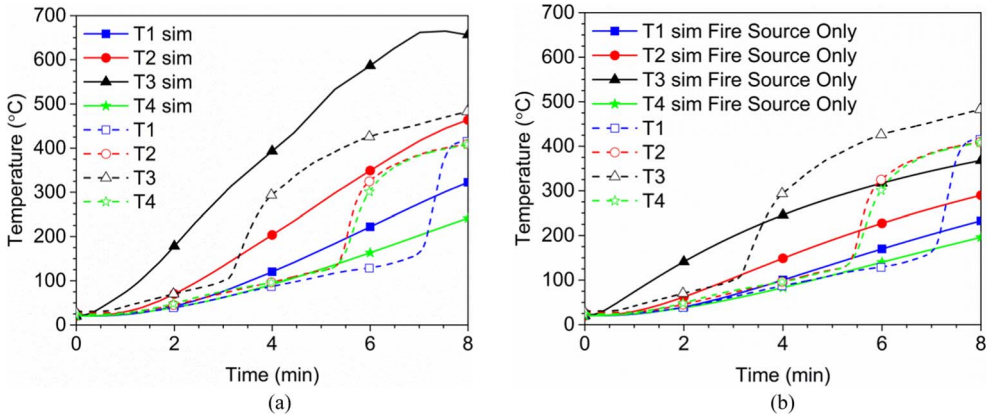


**Figure 11.** The temperature increase for simulated (solid lines) and measured (dashed lines) values as a function of time at positions T1 – T4, for test B 75% SOC. In the simulation both HRR from battery cells and from the fire source is applied (left) but only the HRR from the fire source (right).

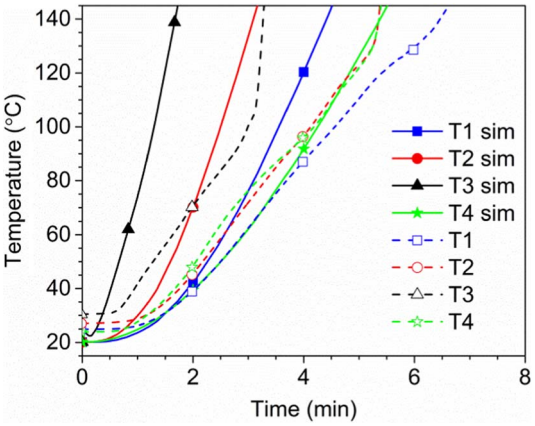


**Figure 12.** A magnification of Figure 11a for temperatures scale 15–145°C.

higher in Figure 11a than in Figure 11b, simply because more heat is present in Figure 11a. The contributions to the temperature increase from the burner and the burning battery cells, in Figure 11a and Figure 11b, are of the same magnitude. The temperatures predicted by the simulation are higher than the measured temperatures up to around 6 minutes after burner start. In Figure 11b, the simulation of the temperature closest to the burner (T3) shows the largest discrepancy between predicted and measured temperature which is natural since the heat contributed by the bottom cell is not included. The heat release in the bottom cell started already after one minute as seen in Figure 5. In the simulation there is a large deviation between the temperature T2 and T4, whereas the measured temperatures T2 and T4 are unexpectedly similar. The reason for this is believed to be due to the construction of the thermal model where the heat originates from the bottom cell in contrast to the experimental measurements where all cells are contributing to the heating. Figure 12 shows a magnification of Figure 11a up to 145°C. The simulated values differs from the experimental values and Figure 12 shows the limitations of the model. As discussed below, the model was deemed as good enough to continue with a feasibility study. In Figure 13, the temperature (T1-T2) as a function of time is shown for the test with 100% SOC. In this test, no temperature measurements were performed for positions T3-T4. The two step process is clearly seen in the experimental measurements. First the cell surface temperature increases relatively slowly up to a breaking point at around a cell surface temperature of 120°C, and then it increases rapidly until reaching a plateau at around 450°C. In the initial phase the simulations overpredict the temperature increase. The simulations do not capture the second phase where the temperature increases more rapidly. The simulated heat release in only the bottom

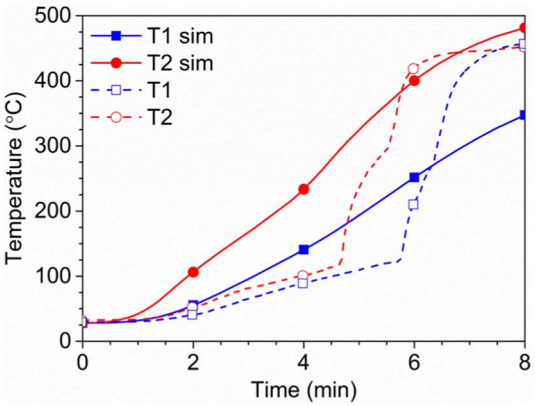


**Figure 13.** The simulated (solid lines) and measured (dashed lines) temperatures as a function of time at position T1 and T2, for test A 100% SOC.

cell and the heat transfer coefficient change when the electrolyte and separator have disappeared, which is expected to occur in the experiment but not included in the model, is believed to explain the major difference. However, the heat conductivity in the bottom cell is believed to increase first of the five cells, due to decrease of electrolyte and separator, resulting in higher heat conduction to the second cell, thereby somewhat decreasing the discrepancy between the simulation and the measurements. The model does not cover the battery chemical reactions and the unpredictable nature of fire and flame propagation also prohibits an exact prediction of the temperatures. Also, the assumptions and the parameters for the materials involved where kept as general as possible to provide a rather straight-forward model for a general purpose use. Curve fitting in order to obtain a better agreement between experimental and simulated data was not performed. For a more detailed discussion, the overprediction of the temperature in the first phase could be due to that the evaporation of the electrolyte is not considered, also the cells are assumed to be in perfect thermal contact with each other. The simulated temperatures, shown in Figure 11 and Figure 13, are higher than the experimental values for time up to around 6 minutes. This is in contrast to the results for the mock-up where the simulated temperatures, shown in Figure 10, were lower than the experimentally found values. No further investigation of this discrepany was conducted, however the reason for the difference in the mock-up case was probably due to the plate thermometers not being in good contact with the promatec cladding allowing exposure to the hot gases on both sides.

A sensitivity analysis was performed where the following parameters were varied; HRR (Table VI and Table VII), distance from the propane burner (within ± 1.5 cm) and material properties of the battery pack, yielding new sets of boundary conditions. Two different material properties were evaluated, one with the battery data (Table I) and the other to be Promatect material (insulated material). However, it was found that taking all these variations into account the variation in the final temperatures between the cells were less than ±7.5°C at 150°C and ±26°C at 500°C.

The fire/thermal runaway process is complex including both evaporation/melting (phase transition) and combustion of e.g. electrolyte and polymer materials, and at the same time internal short circuits and electrolyte-electrode reactions may take place. It is difficult to accurately capture the full depth of these processes and at the same time have a simple enough model to be able to simulate a large number of battery cells on a battery system level. For the purpose of this work, the model results were considered good enough and also on the safe side (an overestimation of the temperatures), especially up to 6 minutes, to allow a study of cell-to-cell propagation on a battery system level. A conservative result is desirable since the methodology is to be used in simulating propagation events in systems and modules consisting of many cells. The validation tests, involving the external propane burner, were used to validate the model. The thermal model can be used without external heating. Thereby, simulation of thermal propagation without external heat and with only heat originating from the internal battery cell. The heat from the cell is considered fully combusted and established by THR measurements from external fire abuse. However, in case of another abuse situation, e.g. a spontaneous internal cell short circuit, the released heat could differ since the cell might not be fully combusted. In principle, for the same battery cell type and status (same ageing etc.), any abuse type which results in thermal runaway and total combustion of the cell materials, the THR should be equal to the measured THR in Table IV. Total combustion is typically difficult to obtain and in case this is not fulfilled, the measured THR in Table IV offer a conservative input as the most severe case.

The thermal properties used as presented in Table I, were carefully selected from available literature values with anisotropic thermal conductivity due the layer structure. However, the temperature dependence of these parameters has not been taken into account as no such information could be found in the literature. In addition the overall properties will change also due to consumption of material. In the extreme case of a completely burnt out battery cell, there will

be no electrolyte or separator left while current collectors (aluminum sheets and copper sheets) and parts of the original electrode layers (e.g. carbon and LFP) may remain relatively intact, with properties that differ significantly from the original cell. During the thermal event the cell density is changed due to loss of material by combustion and cell venting, however, also cell volume is changed due to swelling. The weight of the 5-cell-pack after the complete test has decreased by approximately 28% (350 g for 5 cells) of the original weight for all tests and SOC levels. Our model uses a constant density and effects of changing density are thus neglected. Also the thermal conductivity is kept constant. Especially during a thermal runaway the cell pouch is prone to swelling, as observed during the tests although the steel wires binding the cells together partly inhibit the swelling. The swelling changes the area of direct contact to the neighboring pouch cell while in the model the cells are assumed to be in direct contact with each-other during the entire test. It should also be noted that due to the swelling of the cells, the heat transfer to the thermocouples will change, therefore the measured temperatures might not entirely represent only the cell surface temperature. The error originating from the assumed surrounding gas temperatures as well as the heat transfer coefficients to the battery cells are however small as seen in the performed sensitivity study.

A simple but useful condition determining a thermal runaway is to set a critical onset temperature. Typically thermal runaway onset temperatures found in the literature are of the order of 120–150°C,[5] since at about 120°C the solid electrolyte interphase (SEI) layer typically starts to breakdown. The SEI layer protects the carbon anode from direct contact with the electrolyte. Without the SEI layer exothermal reactions between the anode and electrolyte can start, initiating a potential thermal runaway phase and cathode-electrolyte reactions. The cathode-electrolyte reactions have a relatively strong dependence on the cathode material used. Electrolyte composition and additives can also play a large role in thermal runaway characteristics. However also the boiling temperature of the electrolyte is important. Dimethyl carbonate (DMC) is a common organic solvent used in Li-ion electrolyte mixtures. DMC has a boiling temperature of 90°C and thus the cell will release content before the actual thermal runaway starts. The physical processes determining the thermal runaway onset temperature are rather complex and can vary greatly for different Li-ion battery cells. The time from an abuse situation until a thermal runaway occurs can also be extended, e.g. three weeks, as in the case of a Chevrolet Volt post crash test fire event.[55] One should also be aware of the difference between the temperature where self-heating processes start which later may lead to a thermal runaway, and the very distinct "point of no return" onset temperature that is instantly followed by a thermal runaway. Larsson and Mellander[7] studied the onset thermal runaway temperatures for some different commercial Li-ion chemistries by external heating and found the latter type of onset temperature to be about 200°C ± 20°C. The "point of no return" is typically associated with the breakdown of the cathode, resulting in high-rate exothermic reactions between the electrolyte and the cathode. The melting temperature of a typcial Li-ion polymer separator made of polyethylene (PE) or polypropylene (PP) is typically about 130°C and 160°C,[9] respectively, and if the separator is melted an internal cell short-circuit can start between the anode and the cathode, increasing the cell temperature further, which can lead to a thermal runaway. Note that there are also ceramically reinforced separators on the market with increased melting temperature, typically above 200°C.

### Model Application to a Battery Module with Fire Walls

In order to assess events on a battery system level the model described above was extended to model a part of a battery pack. For this purpose a 3D model was constructed in Comsol Multiphysics comprising 20 battery cells, 2 fire walls and 11 aluminum cooling plates seen in Figure 14. In this design, a battery module consists of 10 cells. In Figure 14, one complete battery module (with 10 cells, cell number 6–15) and two half-battery modules (with 5 cells, cell number 1–5 and respectivily cell number 16–20) are presented. Each battery

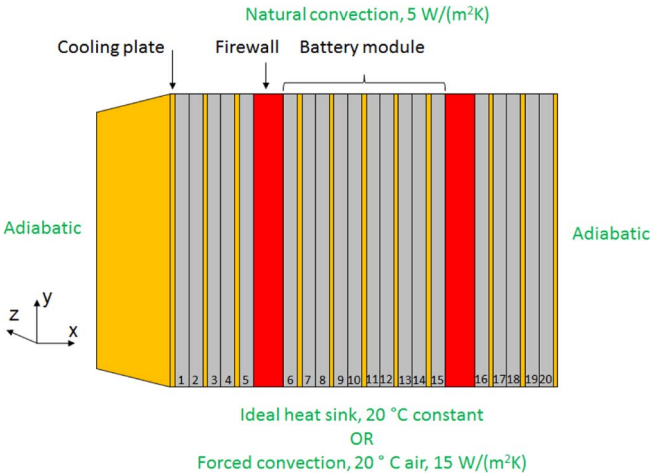


**Figure 14.** Schematic 3D drawing of the simulated part of a battery system, consisting of 20 cells (gray) with 1 mm aluminum cooling plates between every second cell (orange) and module separation from the neighbor module by fire walls (red) on each module side. The cells are counted as 1 to 20 with start in the leftmost battery cell, as seen in the drawing. The dimensions and the thermal property data of the battery cells are the same as in the previous model, the latter can be found in Table I. The boundary conditions of each side are shown (green text).

cell has a 1 mm thick aluminum cooling plate on one side of the cell. On each side of the middle module there are fire walls, as illustrated in Figure 14. The inter-cell aluminum cooling plates play an important role for thermal management; supporting cooling, and heating in case of cold weather, of the cells during normal use (discharge/charge) and are thus critical in order to achieve a long battery life time. The plate also provides mechanical support. During usage and aging a Li-ion pouch cell is prone to swelling, of the order of a few percent, and therefore an additional inter-cell material, e.g. a thin and soft foam, could be used between the cells to absorb this swelling, however, in this model this type of material is not included. The boundaries of the model are treated as adiabatic on four sides simulating a worst case scenario where additional battery modules are present. The top side has a natural convection with a heat transfer coefficient of 5 W/(m$^2$K). This condition was selected in order to simulate a situation with cell electrical interconnections, electronics and circuit-boards (part of Battery Management System) on top surrounded by more or less "trapped" air. The bottom side has either an ideal heat sink kept at a constant temperature of 20°C, to simulate liquid cooling, or a forced convective condition to ambient air of 20°C having a heat transfer coefficient of 15 W/(m$^2$K), representative of air cooling. The numerical model of this system is represented by approximately 700000 grid cells compared to around 18000 grid cells for the 5-cell-pack (see Table II) and takes approximately two hours to run on a workstation. The model do not cover heat transport through electrical battery cell interconnections. The heat transfer from battery vent products and smoke is distributed through the HRR in the thermal runaway cell only and not distributed over several cells. The exact path the vent products will take is difficult to predict. Distributing the heat produced in the cell it originates from, will provide a conservative estimate.

Aluminum is a potential fire wall material in battery systems, due to its relatively light weight and excellent properties for thermal management. The relatively low melting temperature of aluminum, 660°C, may however be a disadvantage since it can be less than typical Li-ion battery fire temperatures. A second material as a fire wall was evaluated, glass fiber (duct liner), was chosen since it has significantly different thermal properties. The evaluation of glass fiber as a fire wall material should rather be understood as a fire protection material to compare with aluminum, rather than claiming that glass fiber would be an appropriate material selection for a fire wall in a future real battery

**Table VIII. Thermal properties of the fire wall materials.**

| Fire wall material | Density ρ [kg/m$^3$] | Specific heat $c_p$ [J/(kg K)] | Thermal conductivity k [W/(m K)] |
|---|---|---|---|
| Aluminum | 2700 | 903 | 238 |
| Glass fiber (duct liner)[56] | 32 | 840 | 0.038 |

system. Glass fiber (duct liner) cannot support mechanical stability, furthermore, the influence of environmental stress (temperature, humidity, vibration in case of electric vehicle) using glass fiber is neither known nor studied. To our knowledge, the use of aluminum is rather common in battery systems, potentially even as "fire walls", however, no information has been found of battery packs using glass fiber. Aluminum and glass fiber firewalls were investigated in this study using different wall thickness in order to investigate their mitigating effect, see Table VIII for thermal properties of the materials.

A number of different simulations have been performed, where placement of the thermal event was changed. The temperatures in adjacent cells and cells directly on the opposite side of the fire wall were assessed. Furthermore, the influence of fire wall thickness for a scenario with a complete module fire was also investigated.

A delay of the heat propagation can significantly mitigate the adverse effects of a thermal runaway event and is thus of high interest. Here, a few different scenarios where the thermal runaway event occurs in different locations such as in the middle of the module or in the cell closest to the fire wall are considered. Two SOC levels are assessed, 75% and 100% SOC, and their corresponding HRRs. However, for most simulations, 100% SOC is used since it was the most rapid energy release. A cell thermal runaway is run up to approximately 1/5$^{th}$ of the THR, according to Table IV, and then the simulation continues to study the temperature development in the cooling phase.

The temperature inside a cell adjacent to a thermal runaway event determines when and if a cascade process of thermal runaways may happen in a battery pack. There is naturally a great interest to be able to predict and mitigate effects of single cells experiencing a thermal runaway. For evaluation of cell-to-cell propagation, a temperature in the cell in excess of about 120–150°C is needed for a thermal event to start. In order to have a high safety margin, an even lower temperature value could be chosen, e.g. 80–100°C. In this study we have chosen 100°C as the critical temperature when a cell goes into thermal runaway. In Figure 15, the 100°C critical temperature is marked with an orange dashed line and labeled "Limit". In case not stated otherwise, the presented temperature for a specific cell number is the cell surface temperature located on the side that is closest to the heat source.

In Figure 15 the different boundary conditions and different SOC levels are investigated for the case of a thermal event in cell 10. The HRR is deposited in the cell at time 0 and during 210 s (3.5 min) in both SOC cases and the cell is then allowed to cool down. The time 210 s is derived from the time when 1/5$^{th}$ of THR is reached, according to Table IV, but the time value is decreased since the HRR from the battery cells will start to generate heat after approximately 1 min, as seen in Figure 5. In Figure 15 the temperatures as a function of time are shown where the temperatures (in mid y-axis) are shown for the adjacent cells, cell 9 and cell 11. From the results it can be seen that an ideal heat sink kept at 20°C would efficiently delay or even stop further propagation of an event, however this condition is rarely fulfilled. Furthermore it is likely that a thermal event would first propagate in cell 9 not protected by the 1 mm Al cooling plate. Further away from the thermal event the temperatures are well on the safe side.

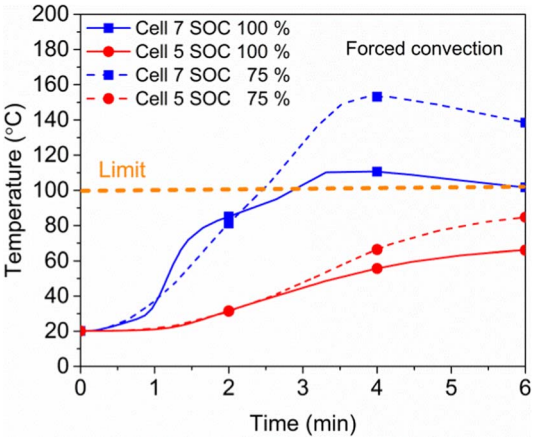


**Figure 16.** The thermal runaway starts in cell 6, closest to the firewall, and the temperature development is shown for the two neighboring cells, for both 100% and 75% SOC, with forced convection on the bottom side. Fire wall of aluminum with a thickness of 5 mm.

Figure 16 displays the temperature as a function of time where the thermal event is placed in cell 6, immediately on the right hand side of the fire wall in Figure 14. In this simulation, forced convection is exclusively assumed on the lower side. It is found that the fire wall can delay the thermal event by significantly reducing the temperatures however the event would propagate to the cell 7 on the right. Also in this case, further away from the event the temperatures are well below 100°C. Similar to the results in Figure 15 the temperature development for the 75% SOC case starts somewhat lower than for 100% SOC but after 2–3 minutes the 75% SOC case results in higher temperatures.

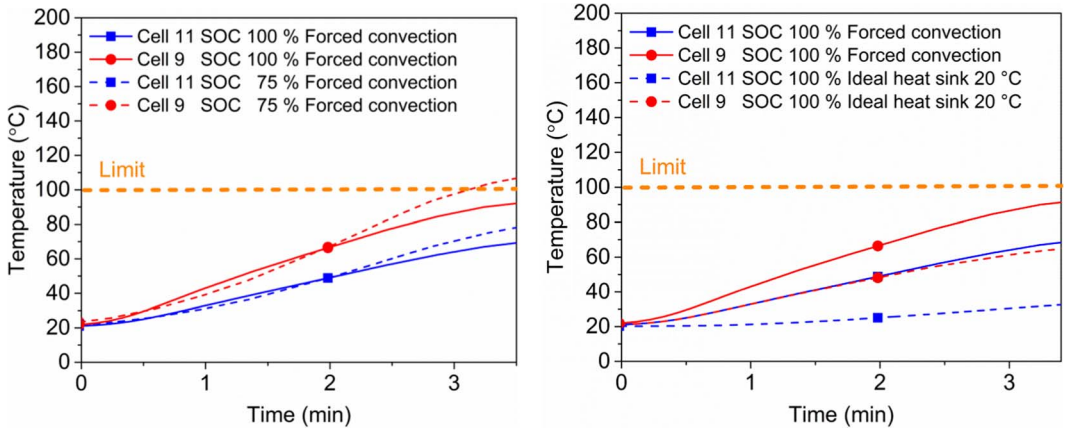


**Figure 15.** The thermal runaway starts in cell 10 and the temperature development is shown for the two neighboring cells; comparing 100% and 75% SOC with forced convection on the bottom side (left), and comparing forced convection with 20°C heat sink at the bottom for 100% SOC (right). Fire wall of aluminum with a thickness of 5 mm.

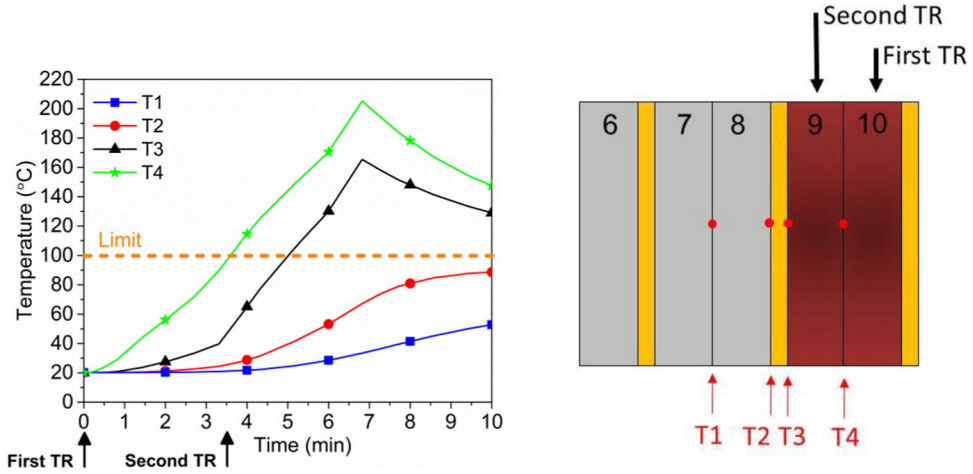


**Figure 17.** The thermal runaway (TR) starts in cell 10, then the heat propagates and after 3.5 minutes a second thermal runaway is initiated in cell 9, for 100% SOC, with forced convection on the bottom side and with a fire wall of aluminum with a thickness of 5 mm. (a) shows the temperature development for 4 locations (T1-T4) in the adjacents cells, (b) schematically shows the placement of T1-T4.

Considering the two cases above it seems quite plausible that a thermal event would propagate to the adjacent cell and thus a model to further simulate this case was implemented. Here it is assumed that a thermal event occurs as in Figure 15, in cell 10, however after 3.5 min a second thermal event is started in cell 9 increasing the temperatures further. A forced convection boundary is assumed for the lower face in the model. In Figure 17 the temperatures as a function of time are shown for 4 locations. Here it is less likely that the event would propagate to cell 8 and 11; however if it would go from cell to cell fire walls could significantly delay the event. This indicates that a thermal event may propagate from cell to cell and thus efficient fire walls need to be implemented to delay or partly stop a catastrophic event.

In order to evaluate the fire walls in terms of being able to stop or delay a module-to-module propagation, all 10 cells (cell 6–15) within a module with 100% SOC had thermal runaway initiated at the same time. Figure 18 shows the cell temperature on the other side of the firewall for the two types of firewall materials and with different thicknesses; 0, 5, 10 and 20 mm. A thickness of 0 mm corresponds to that there is no fire wall present. The temperature reduction is higher for aluminum than for glass fiber. Figure 19 shows the temperature in the middle of the fire wall, for the thicknesses 5, 10 and 20 mm. Aluminum has more than 6000 times higher thermal conductivity than glass fiber, as seen in Table VIII, resulting in removal of significantly more heat from the fire wall to adjacent cells and cooling system. Spreading the heat to a neighboring cell may actually be beneficial in case the temperature increase of the adjacent cell can be kept low, thus the heat may be distributed to a large volume, i.e. many battery cells.

The model does not consider heat transfer through the electrical connections between the battery cells. External heating studies on smaller sized Li-ion cells[25] have shown that the heat transfer through the cell tabs by electrical connectors can have an important impact on the cell-to-cell propagation. The same study found that cell spacing could have a significant influence on cell propagation. In another study[35] on smaller sized cells during nail penetration abuse different propagation characteristics were found for series and parallel connected cells. Even within the parallel connected cells, different electrical cell routing showed significant effect on the cell-to-cell propagation.[25] In the present model all battery cell components are combusted, however in an overheated Li-ion cell vent gas and smoke as well as electrolyte leakage can occur which can influence the heat generation. In addition, considering the smoke and fire complexity, the results could vary considerably for different cell responses to the heating. Also the design of the battery module and pack effects e.g. the contributions of vent gases and electrolyte leakage. Cell propagation is thus a complex issue with many parameters and much is still unknown. In this study relatively large cells were used, no cell spacing (in x-direction, see Figure 14) is used and the cells are not electrically connected to each other. Furthermore, the thermal runaway data is derived from external abuse tests by fire.

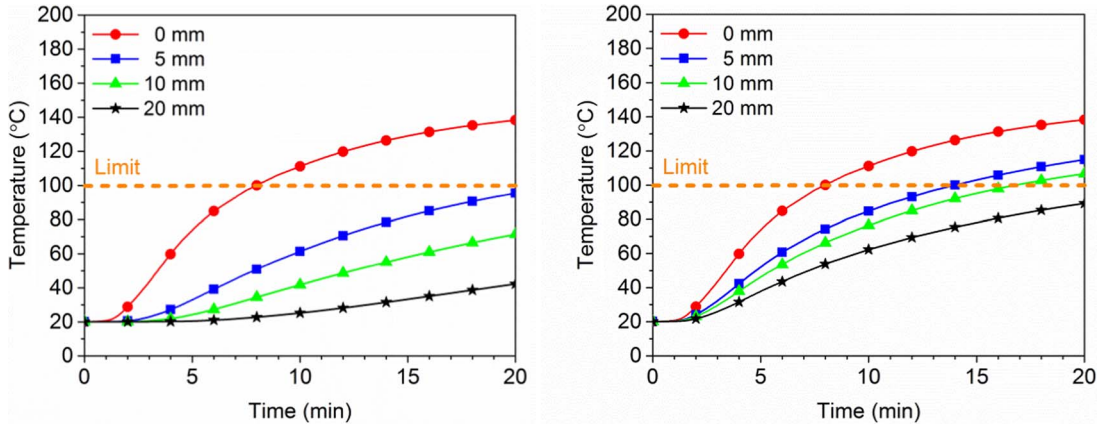


**Figure 18.** Temperatures in the cell adjacent (cell 5 and cell 16, due to symmetry) to the fire wall, where a thermal event occurs at the same time in all ten cells (cell 6–15) in a module; for aluminum (left) and for glass fiber (right) fire wall.

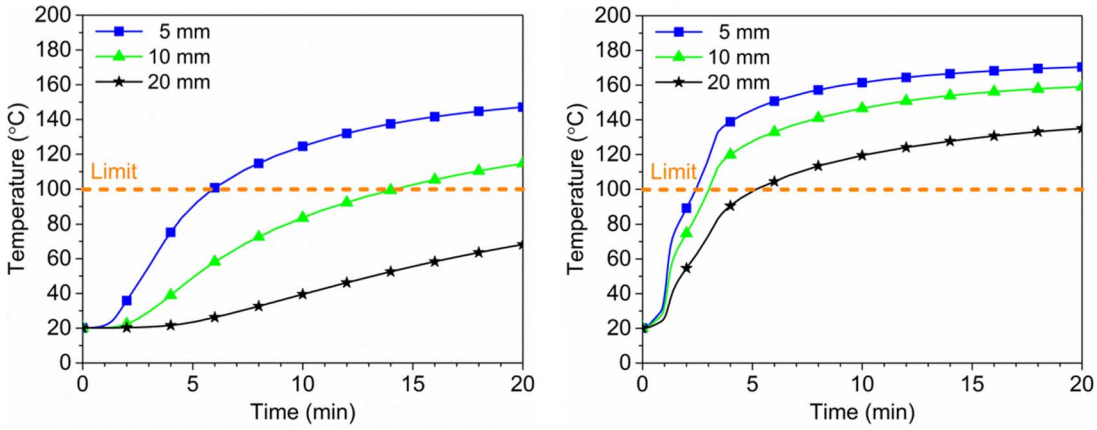


**Figure 19.** Temperatures in the center of the fire wall, where a thermal event occurs at the same time in all ten cells (cell 6–15) in a module; for aluminum (left) and for glass fiber (right) fire wall.

## Conclusions

This paper presents an attempt to predict the propagation of a thermal runaway/fire in a cell to neighboring cells by simulating the temperature development in the cells. The modelling work comprises of two major steps. In the first step, the model is setup of the cells including their thermal properties and then validating the model through experiments were the boundary conditions in the validation test need to be determined carefully. The validation step include an external heat source, however, the model can be used without any external heat source. In the second step, the model is applied to assessing fire walls of different material and thicknesses between modules in a battery pack.

The model is developed to require moderate computer running time in order to be used for a fast evaluation of several different means of preventive insulation, it is thus not modelling the pack and cells in great detail and it overpredicts the temperature increase in the adjacent cell compared to the validation experiment at the early stages of the test. The thermal inertia of the cell packaging material is neglected and the cells are assumed to be in perfect thermal contact with each other unless there is a fire wall or other materials in between the cells. The thermal properties are taken from literature data, the temperature dependence of the properties is not taken into consideration, however anisotropic heat conduction is taken into account by different conductivities in the plane of the cell compared to across the cell which is due to the layered structure of the cells. The thermal inertia induced by its thermal properties can be of importance close to the temperature where the electrolyte starts to evaporate. Joule heating by electrical short circuit as well as electrode-electrolyte reactions are neglected. In the validation experiment the cells are exposed to a fire from below which gives the temperature rise in the cells and then the subsequent fire of each cell. As the cells are consumed the thermal properties will change radically. This results in a different slope of the temperature rise in each cell as the different cells are consumed. In the model validation all heat is assumed to be developed in the bottom cell and since the thermal properties are constant the temperature rise has about the same slope throughout the simulation. However, as the purpose of the model is to screen different means to prevent propagation of a thermal runaway to neighboring cells, and the overprediction is a conservative result, the model is considered good enough.

A feasibility study using the model is conducted assessing two different types of fire walls between modules consisting of 10 cells. Different thicknesses of the fire walls are used and the initiation point of the thermal runaway is varied. In addition, other means to cool the cells are investigated, like using a cooling liquid. The results show that there is a substantial risk for the spreading of thermal events in a battery pack, although cooling systems and fire walls may limit these risks.

The tested 5-cell-pack has an energy capacity of 0.112 kWh while a battery pack for an electrified vehicle typically could have between 10 and 100 kWh, equal to 450 to 4500 cells of the tested cell type. Even if larger capacity cells are used, hundreds of cells are needed in order to achieve a high enough battery pack voltage. There can be even larger battery packs in e.g. stationary grid applications and on ships. Cell-to-cell fire propagation in a large battery pack could result in considerable damage. Therefore, using experiments and simulations of cell-to-cell propagation is important in order to design and validate safe Li-ion battery systems.

## Acknowledgments

The Swedish Energy Agency and the Swedish Fire Research Board are gratefully acknowledged for their financial support. Several technical staff colleagues at SP Fire Research have contributed to this work.

## References

1. E. P. Roth and D. H. Doughty, *J. of Power Sources*, **128**, 308 (2004).
2. E. P. Roth, *ECS Transactions*, **11**(19), 19 (2008).
3. J. Jeevarajan, "Safety of commercial lithium-ion cells and batteries", *Chapter 17 in Lithium-Ion Batteries: Advances and Applications*, edited by G. Pistoia, Elsevier, Amsterdam, The Netherlands, p. 387 (2014).
4. Z. J. Zhang, P. Ramadass, and W. Fang, "Safety of lithium-ion batteries", *Chapter 18 in Lithium-Ion Batteries: Advances and Applications*, edited by G. Pistoia, Elsevier, Amsterdam, The Netherlands, p. 409 (2014).
5. D. Doughty and E. P. Roth, *The Electrochem. Soc. Interface, summer*, **2012**, 37 (2012).
6. W. Golubkov, D. Fuchs, J. Wagner, H. Wiltsche, C. Stangl, G. Fauler, G. Voitic, and A. Thaler, *RSC Adv.*, **4**, 3633 (2014).
7. F. Larsson and B.-E. Mellander, *J. of The Electrochem. Soc.*, **161**(10), A1611 (2014).
8. F. Larsson and B.-E. Mellander, *Conference proceedings of Fires in vehicles (FIVE) 2012*, edited by P. Andersson and B. Sundstrom, SP Technical Research Institute of Sweden, Sweden, p. 303 (2012).
9. F. Larsson, P. Andersson, and B.-E. Mellander, *Batteries*, **2**, 9 (2016).
10. P. Andersson, P. Blomqvist, A. Lorén, and F. Larsson, *Fire and Materials*, in press.
11. F. Larsson, P. Andersson, and B.-E. Mellander "Are electric vehicles safer than combustion engine vehicles?", Chapter 4 in Systems perspectives on Electromobility, edited by B. Sandén and P. Wallgren, *Chalmers University of Technology*, Goteborg, Sweden, ISBN 978-91-980973-9-9, p.33 (2014).
12. D. H. Jeon and S. M. Baek, *Energy Conversion and Management*, **52**, 2973 (2011).
13. W. Wu, X. Xiao, and X. Huang, *Electrochimica Acta*, **83**, 227 (2012).
14. S. Chacko and Y. M. Chung, *J. of Power Sources*, **213**, 296 (2012).
15. L. Fan, J. M. Khodadadi, and A. A. Pesaran, *J. of Power Sources*, **238**, 301 (2013).
16. J. Yi, U. S. Kim, C. B. Shin, T. Han, and S. Park, *J. of The Electrochem Soc.*, **160**(3), A437 (2013).
17. M. Guo and R. E. White, *J. of Power Sources*, **221**, 334 (2013).
18. P. Taheri, M. Yazdanpour, and M. Bahrami, *J. of Power Sources*, **243**, 280 (2013).
19. G. Zhang, L. Cao, S. Ge, C.-Y. Wang, C. E. Shaffer, and C. D. Rahn, *J. of The Electrochem. Soc.*, **161**(10), A1499 (2014).
20. N. Javani, I. Dincer, G. F. Naterer, and G. L. Rohrauer, *Applied Thermal Engineering*, **73**, 307 (2014).

21. T. D. Hatchard, D. D. MacNeil, A. Basu, and J. R. Dahn, *J. of The Electrochem. Soc.*, **148**(7), A755 (2001).
22. G.-H. Kim, A. Pesaran, and R. Spotnitz, *J. of Power Sources*, **170**, 476 (2007).
23. R. Spotnitz and J. Franklin, *J. of Power Sources*, **113**, 81 (2003).
24. P. Peng and F. Jiang, *International J. of Heat and Mass Transfer*, **88**, 411 (2015).
25. C. F. Lopez, J. A. Jeevarajan, and P. P. Mukherjeea, *J. of The Electrochem. Soc.*, **162**(10), A2163 (2015).
26. B. Barnett, D. Ofer, S. Sriramulu, and R. Stringfellow, "Lithium-ion batteries, safety", Chapter 9 in Encyclopedia of Sustainability Science and Technology: *Batteries for Sustainability*, edited by R. J. Brodd, Springer, ISBN 978-0-387-89469-0, p. 285 (2012).
27. K. Smith, G.-H. Kim, E. Darcy, and A. Pesaran, *Int. J. of Energy Res.*, **34**, 204 (2010).
28. S. Santhanagopalan, P. Ramadass, and J. (Z.) Zhang, *J. of Power Sources*, **194**, 550 (2009).
29. E. Sahraei, J. Campbell, and T. Wierzbicki, *J. of Power Sources*, **220**, 360 (2012).
30. E. Sahraei, J. Meier, and T. Wierzbicki, *J. of Power Sources*, **247**, 503 (2014).
31. W. Zhao, G. Luo, and C.-Y. Wanga, *J. of The Electrochem. Soc.*, **162**(1), A207 (2015).
32. J. Xu, C. Lan, Y. Qiao, and Y. Ma, *Applied Thermal Engineering*, **110**, 883 (2017).
33. R. M. Spotnitz, J. Weaver, G. Yeduvaka, D. H. Doughty, and E. P. Roth, *J. of Power Sources*, **163**, 1080 (2007).
34. T. Maloney, "Extinguishment of lithium-ion and lithium-metal battery fires", *U.S. Department of Transportation*, DOT/FAA/TC-13/53, January 2014.
35. J. Lamb, C. J. Orendorff, L. A. M. Steele, and S. W. Spangler, *J. of Power Sources*, **283**, 517 (2015).
36. C. F. Lopez, J. A. Jeevarajan, and P. P. Mukherjee, *J. of Electrochem. Soc.*, **162**(9), A1905 (2015).
37. N. S. Spinner, C. R. Field, M. H. Hammond, B. A. Williams, K. M. Myers, A. L. Lubrano, S. L. Rose-Pehrsson, and S. G. Tuttle, *J. of Power Sources*, **279**, 713 (2015).
38. X. Feng, X. He, M. Ouyang, L. Lu, P. Wu, C. Kulp, and S. Prasser, *Applied Energy*, **154**, 74 (2015).
39. X. Feng, L. Lu, M. Ouyang, J. Li, and X. He, *Energy*,**115**, 194 (2016).
40. P. Huang, P. Ping, K. Li, H. Chen, Q. Wang, J. Wen, and J. Sun, *Applied Energy*, **182**, 659 (2016).
41. S. Abada, G. Marlair, A. Lecocq, M. Petit, V. Sauvant-Moynot, and F. Huet, *J. of Power Sources*, **306**, 178 (2016).
42. J. Anderson, J. Sjostrom, P. Andersson, F. Amon, and J. Albrektsson, *J. of Thermal Science and Engineering Applications*, **6**, 041015 (2014).
43. Addendum 99: Regulation No. 100, Revision 2, *United Nations*, 2013.
44. J. Anderson, F. Larsson, P. Andersson, and B.-E. Mellander, *Conference proceedings of Fires in vehicles (FIVE) 2014*, edited by P. Andersson and B. Sundstrom, SP Technical Research Institute of Sweden, Boras, Sweden, p. 268 (2014).
45. J. Anderson, F. Larsson, P. Andersson, and B.-E. Mellander, *Enhanced Safety of Vehicles (ESV) 2015*, Gothenburg, 2015.
46. P. Andersson, J. Anderson, F. Larsson, and B.-E. Mellander, *2nd European Symposium on Fire Safety Science (ESFSS)*, Nicosia, 2015.
47. B. Wu, Z. Li, and J. Zhang, *J. of The Electrochem. Soc.*, **162**(1), A181 (2015).
48. P. Svens, M. H. Kjell, C. Tengstedt, G. Flodberg, and G. Lindbergh, *Energies*, **6**, 400 (2013).
49. EN 13823:2010, "Reaction to Fire Tests for Building Products – Building Products Excluding Floorings Exposed to the Thermal Attack by a Single Burning Item", *European Committee for Standardization*, Brussels, 2010.
50. P. Ribière, S. Grugeon, M. Morcrette, S. Boyanov, S. Laruelle, and G. Marlair, *Energy Environ. Sci.*, **5**, 5271 (2012).
51. F. Larsson, P. Andersson, P. Blomqvist, A. Lorén, and B.-E. Mellander, *J. of Power Sources*, **271**, 414 (2014).
52. U. Wickstrom, *Fire Technology*, **30**(2), 195 (1994).
53. K. McGrattan, S. Hostikka, R. McDermott, J. Floyd, C. Weinschenk, and K. Overholt, Fire Dynamics Simulator (Version 6) - User's Guide, NIST Special Publication, 1019 (2013).
54. A. Haggkvist, "The plate thermometer as a mean of calculation incident heat radiation", Master thesis, 2009:183 CIV, *Lulea University* (2009).
55. Chevrolet Volt battery incident overview report, *National Highway Traffic Safety Administration (NHTSA)*, DOT HS 811 573, January 2012.
56. J. P. Holman, "Heat Transfer", McGraw-Hill Book Company, New York, USA, 1997.

# Paper VIII

batteries

MDPI

Article

# Overcurrent Abuse of Primary Prismatic Zinc–Air Battery Cells Studying Air Supply Effects on Performance and Safety Shut-Down

**Fredrik Larsson [1,2,*], Antti Rytinki [1], Istaq Ahmed [3], Ingvar Albinsson [4] and Bengt-Erik Mellander [1]**

1 Department of Physics, Chalmers University of Technology, Kemivagen 9, SE-41296 Gothenburg, Sweden; antti.rytinki@outlook.com (A.R.); f5xrk@chalmers.se (B.-E.M.)
2 Electronics, SP Technical Research Institute of Sweden, Brinellgatan 4, SE-50115 Borås, Sweden
3 Volvo Group Trucks Technology, Sven Hultins gata 9, SE-41288 Gothenburg, Sweden; istaq.ahmed@volvo.com
4 Department of Physics, University of Gothenburg, Fysikgarden 1, SE-41296 Gothenburg, Sweden; ingvar.albinsson@physics.gu.se
* Correspondence: vegan@chalmers.se or fredrik.larsson@sp.se; Tel.: +46-10-516-5000

Academic Editor: Andreas Jossen
Received: 27 September 2016; Accepted: 20 December 2016; Published: 3 January 2017

**Abstract:** Overcurrent abuse has been performed on commercial 48 Ah primary prismatic zinc (Zn)–Air battery cells with full air supply as well as with shut-off air supply. Compared to other battery technologies, e.g., lithium-ion batteries, metal–air batteries offer the possibility to physically stop the battery operation by stopping its air supply, thus offering an additional protection against severe battery damage in the case of, e.g., an accidental short circuit. This method may also reduce the electrical hazard in a larger battery system since, by stopping the air supply, the voltage can be brought to zero while maintaining the energy capacity of the battery. Measurements of overdischarge currents and current cut-off by suffocation have been performed to assess the safety of this type of Zn–air battery. The time to get to zero battery voltage is shown to mainly be determined by the volume of air trapped in the cell.

**Keywords:** abuse; air supply; metal–air; overcurrent; overdischarge; primary battery; safety; suffocation; zinc (Zn)–air

## 1. Introduction

New battery technologies offer power and energy densities that make it possible to construct applications with impressive performance. Lithium-ion batteries have, for example, made it possible to produce electric vehicles with reasonable range and there are expectations that the next-generation batteries such as zinc (Zn)–air, lithium–air and fuel flow batteries could provide further strides towards even more competitive products, promoting, among other things, extended electromobility in the future [1,2]. As for all new technologies, it is important to know and understand the potential risks associated with their applications. Lithium-ion batteries have, in general, a good safety record; however, the cells contain reactive materials as well as a volatile and flammable electrolyte. A so-called thermal runaway can occur in Li-ion cells, resulting in excessive heat, emission of toxic gas and eventually fire and/or explosion [3,4]. Safety aspects for lithium-ion batteries have been studied using various types of abuse tests such as overcharge, overdischarge, short circuiting, external heating and fire [5,6]. Such tests are very important in order to evaluate and minimize risks, not only for the different products using these batteries but also for the storage and transportation of the cells as well as for recycling. The risks associated with transporting lithium-ion cells by air have, for example, been a focus recently [7].

Among new developing technologies, the lithium–air battery has attracted considerable attention due to its prospected very high specific energy. The Li–air battery is still far from being commercialized and certain safety concerns are challenging [8]. In contrast to lithium-ion batteries, metal–air batteries in general may offer the possibility to limit battery reactions by stopping the air supply to the cell. One such battery type, the Zn–air battery, is promising in that the energy density is good, typically of the order of 200 Wh/kg or more, the materials used are abundant and the costs of production are expected to be comparatively low [9,10]. The battery has a hydroxide electrolyte, a Zn anode and atmospheric oxygen is reduced at the cathode. The cell is in many respects similar to a fuel cell, and electricity is produced as long as fuel, in this case Zn, and oxygen are available. The cell reactions are:

$$\text{Anode: } Zn + 4OH^- \rightarrow Zn(OH)_4{}^{2-} + 2e^- \quad (1)$$

$$\text{Electrolyte: } Zn(OH)_4{}^{2-} \rightarrow ZnO + H_2O + 2OH^- \quad (2)$$

$$\text{Cathode: } 1/2O_2 + H_2O + 2e^- \rightarrow 2OH^- \quad (3)$$

$$\text{Overall: } Zn + 1/2O_2 \rightarrow ZnO \quad (4)$$

Zn–air batteries are regarded to be very safe, and risks are commonly only associated with possible leakage of the hydroxide electrolyte and the formation of hydrogen by Zn corrosion. Early types of Zn–air batteries contained a mercury amalgam but the present generation of these batteries is mercury-free. Short circuit currents are generally expected to be low, and this should minimize risks associated with external short circuits, but traditional abuse tests on these types of cells are rare. In this study, primary Zn–air batteries were investigated regarding overcurrent and controlled air supply flow in order to evaluate risks and possibilities related to battery safety. Besides performing an overcurrent abuse test study on Zn–air batteries, the study particularly addresses suffocation as a means to stop battery reactions and thus to cause battery shutdown. For metal–air batteries this is a principal additional safety function that is not available in other battery technologies such as lead-acid, nickel–metal hydride (NiMH) and lithium-ion batteries.

## 2. Experimental

### *2.1. The Zn–Air Cell*

Tests were conducted using primary (non-rechargeable) Zn–air cells as shown in Figure 1 and specified in Table 1. The cell contained 33% potassium hydroxide (KOH) electrolyte and had a Zn anode and an air cathode with nano-sized manganese (Mn) and graphite (C). The outer prismatic cell packaging material was polyethylene. The cell had 40 air holes on one side, with a diameter of about 6 mm, the total air supply area was 1130 $mm^2$. The cells were pre-commercial/commercial cells from QuantumSphere of type MetAir® SC Series 4.8 (QuantumSphere Inc., Santa Ana, CA, USA). Grey duct tape, shown in Figure 1, was placed between the battery pole tabs in order to avoid accidental short circuits. In Table 1, the values for the dimensions are given for the complete cell including outer plastic sealing parts; the battery pole tabs are not included. There is an air-space of about 3–4 mm beneath the cell. The volume is simply calculated by multiplying the dimensions.

This study included a total of eight cells from the same manufacturer. Four of the eight cells were of an early design version. Before this study the new design cells were stored for around 1.5 years, unfortunately with the outer transport seal opened, exposing them to ambient air. The early cell design was stored for around one additional year. However, the cells seem to still have adequate performance. The cells with early design version were used to develop and verify the test method.

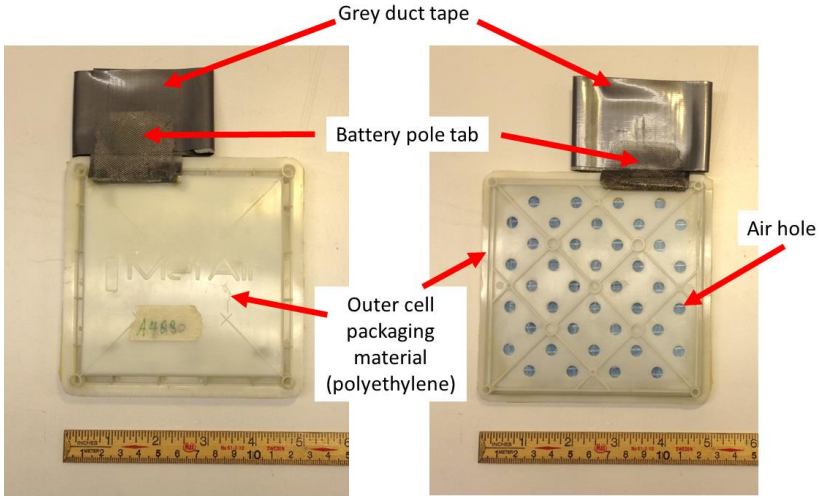


**Figure 1.** (**a**) Front and (**b**) back photos of the Zn–Air cell.

**Table 1.** Cell properties.

| Parameter | Value | Unit |
|---|---|---|
| Nominal open circuit voltage (*OCV*) | 1.4 | V |
| Nominal voltage | 1.1 | V |
| Rated maximum continuous discharge current | 4 | A |
| Rated capacity at 1 A discharge | 48<br>53 | Ah<br>Wh |
| Dimensions | Prismatic shape, 126 × 126 × 14 | $mm^3$ |
| Volume | 0.22 | L |
| Weight | 270 | g |
| Calculated energy density | 196 | Wh/kg |

### *2.2. Measurement Setup*

Two different experimental setups were used. One where the cell had full air supply from the surrounding air, and one where it was suffocated completely. Impedance measurements were performed in free air.

#### 2.2.1. Open Air Setup

The cell was in this case placed inside a suffocation bag but the cell was not suffocated, see Figure 2. For open air measurements the bag was not needed but was used for consistency and to eliminate the presence of the bag as a variable. The bag itself had a square hole which fits over square air intake area of the cell. The four legs of the cell fit into four holes in the corners of the bags hole. This keeps the cell in place relative to the bag. Cable connections, using copper crocodile clamps, were placed close to the base of the cells tabs. Current wires (for discharge current) and sense wires (for cell voltage measurement) were well separated from each other. The zip lock of the bag was sealed as much as possible. The measurement cables were shielded and kept well separated to make it easy to keep an overview of the system.

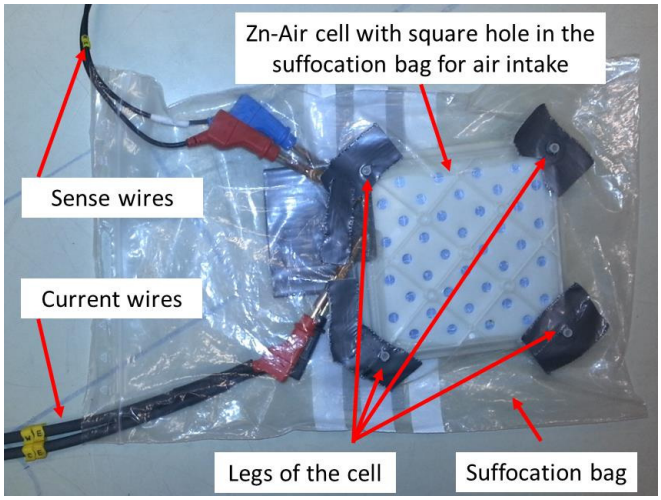


**Figure 2.** Open air setup, the back side of the cell with the air holes, shown in the figure, had free access to air.

### 2.2.2. Suffocation Setup

In addition to the steps for open air measurement, three more items were used for the suffocation setup. Figure 3a shows the suffocation plate (to the right) consisting of a square aluminum plate with a 1 cm layer of hard plastic foam followed by a layer of very soft foam, and covered in a plastic sheet (total 0.18 kg). When pressed against the air intake of the cell, the foam deformed and created a tight seal on the cell. A large aluminum heat sink (1.57 kg) and a 2.05 kg weight were placed on top of the suffocation plate so their weight made the seal tighter. When lifting the suffocation in a "first sealed, then open" experiment, all three items were lifted at once for accurate timing.

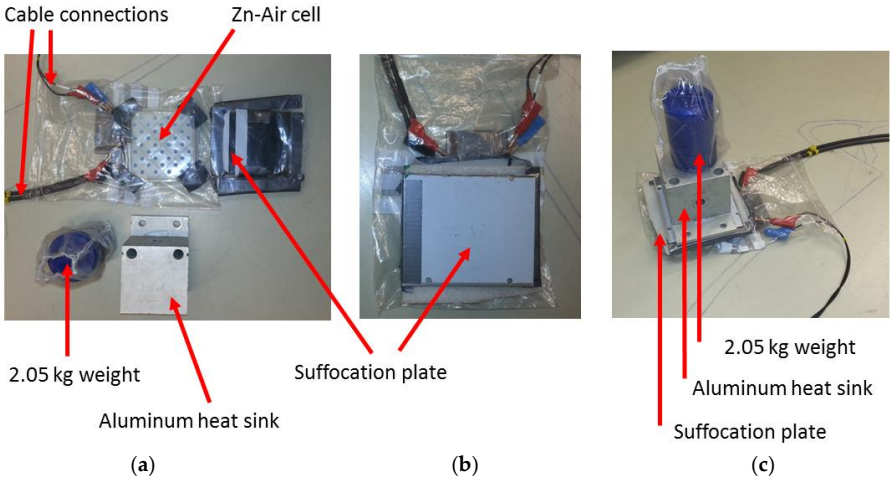


**Figure 3.** Suffocation setup. (**a**) All parts are separated from each other; (**b**) suffocation plate is placed over the cell; and (**c**) the aluminum heat sink and 2.05 kg weight is placed on top of the cell and suffocation plate.

### *2.3. Impedance Measurement*

The impedance was measured using a Metrohm Autolab PGSTAT 302N (Metrohm Autolab B.V., Utrecht, The Netherlands) with Booster 20 A module (Metrohm Autolab B.V.) and Metrohm Nova 1.11 Software (Metrohm Autolab B.V.). Four-wire measurements were used, in ambient room temperature, about 20 °C, in free air, with galvanostatic mode and an amplitude of 10 mA, frequency range 10 mHz–100 kHz, with 50 points logarithmically distributed.

### *2.4. Discharging Measurement*

The discharging measurements were also performed using the Metrohm Autolab PGSTAT 302N with a Booster 20 A module. Current and voltage were recorded at a rate of one measurement per second. The cell was orientated airside up, in order to easily control the air supply to the cell surface. The cell was placed in ambient room temperature (around 20 °C). The cell tabs were further separated by a large piece of duct tape (seen in Figures 1 and 2) attached to the cell to avoid any risk of short circuit. The bottom of the cell was sealed by the cell design; however, an additional seal composed of a plastic bag and tape was used for all the experiment performed in this study. The suffocation was applied according to the setup described in Section 2.2.2. A rest period of at least 2 h was used between two sequential discharging experiments until the open circuit voltage (*OCV*) was stabilized.

## 3. Results and Discussion

In all tests, a 60-s rest phase prior the start of the discharging was used for monitoring, and a longer rest phase of 900 s was used after discharging to record the recovery of the cell potential. Note that the given times in the paper are referring to the time from the start of discharge, i.e., add 60 s to the value, to correspond to the time scales in the figures.

The maximum allowed continuous discharge current of the cells is 4 A according to the manufacturer. Two types of measurements were performed. For the first type, each cell was discharged at 4 A both in open air and suffocated for 150 s or until the cell potential reached 0 V. A total of four tests were conducted for each cell, two in open air and two suffocated. In Figure 4, the results for one of the cells (cell 1) are shown. The time to reach 0 V during suffocation was 120 s. In the second type of measurement, the sealing of the cell was lifted at a pre-determined time. Also, in this type of experiment, an initial 60 s rest period was used followed by a 240 s, 4 A discharge phase where the suffocation was lifted 75 s after discharge initiation (135 s from the test start), as shown in Figure 4. These results were reproducible; repeated tests on two samples are shown in Figure 5. The experiments show that the cell recovered rapidly to the original *OCV* after suffocation, provided air access was granted. When the cell is open to air, the voltage recovers rapidly; when the cell is sealed during the whole experiment (green curve/symbols in Figure 4), the recovery is slow. The small differences shown in Figure 5 are due to minor differences regarding the voltage when the sealing was removed.

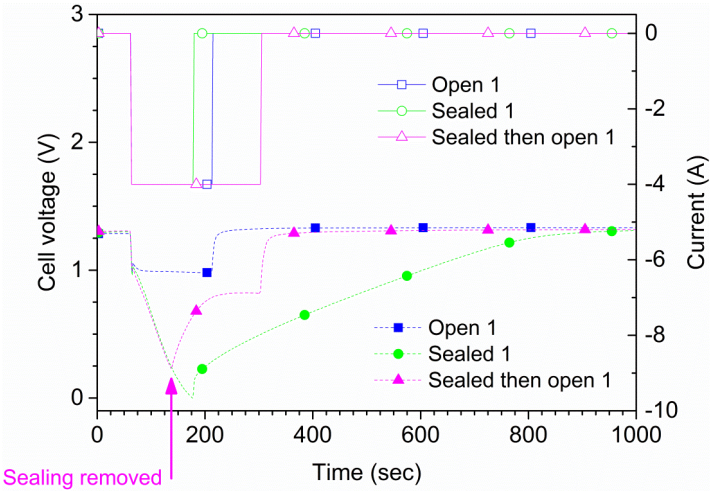


**Figure 4.** Voltage (filled symbols) and current (open symbols) measurements for cell 1 for three different tests using a discharge current of 4 A; in open air; sealed (suffocated) for 150 s or until the cell potential reached 0 V; and first sealed (suffocated) then open in air.

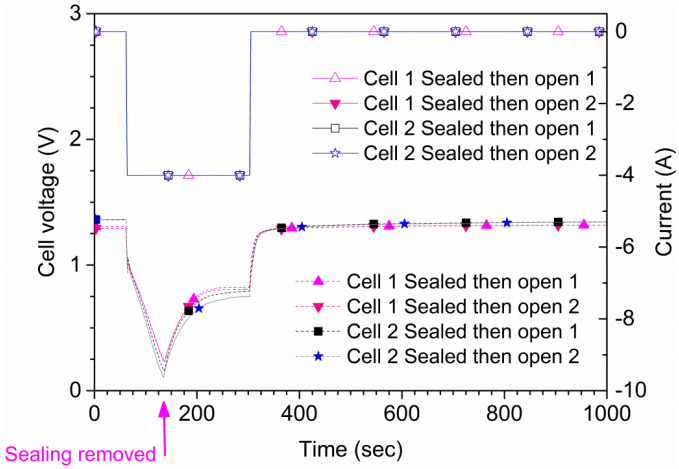


**Figure 5.** Voltage (filled symbols) and current (open symbols) measurements for sealed then open, for two repetitions per cell and for two different cells, cells 1 and 2.

The tests were also performed in order to find the maximum current that a cell can sustain for 2 min, as shown in Figure 6. This current was later used for maximum discharge tests. During the tests, the cell was discharged by a current of 4, 5, 6, 7, 8, 9 and 10 A for 2 min each, in this order. A cutoff triggered at 0.0 V cell potential was used, which stopped the running step and jumped to the next in case 0.0 V was reached. One of the cells showed a voltage of 76 mV at the end of the 8 A step; when changing to 10 A, the voltage rapidly reached 0 V and the test stopped. The other cell shown in Figure 6 showed a larger initial voltage drop and had a lower potential profile during the complete tests. That cell also passed the 8 A step, but not the 10 A step. Therefore, the maximum continuous current is estimated to be 8 A. This current level was used for the additional tests. Since the cells are rated for 4 A, using currents above this value is, by definition, an overcurrent. The short circuit current, $I_{sc}$, i.e., the current through an external conductor with negligible resistance connecting the battery pole tabs, depends on, e.g., the current path size through the battery tabs and the rate of the electrochemical reactions creating the short circuit current. $I_{sc}$ is, in general, time-dependent (as well as dependent on various additional parameters, e.g., cell type and design, temperature, aging, state of charge (*SOC*)) and was not investigated in this study since we needed a continuous current for our measurements; the current used was therefore lower than $I_{sc}$.

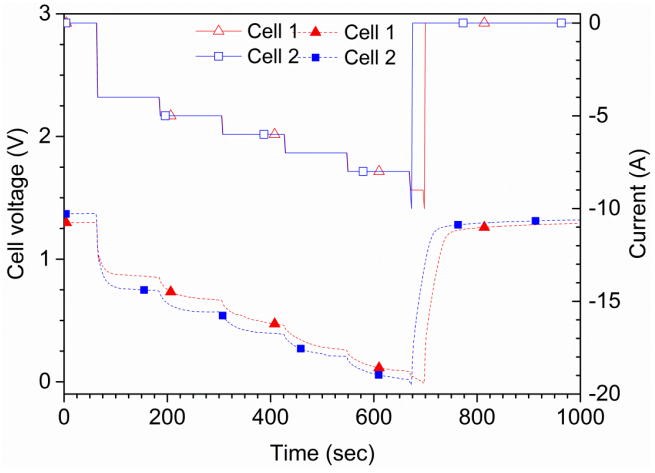


**Figure 6.** Voltage (filled symbols) and current (open symbols) measurements for current increment step for two different cells, cells 1 and 2.

Figure 7 shows the results for the same type of measurements as in Figure 4 but with an 8 A discharge current. With suffocation, 0.0 V was reached 36 s after the start of the discharge in the first run, and after 33 s in a second run (not shown). In open air, the cell delivered 8 A in 120 s; however, by the end of the discharge the voltage was only 14 mV. For the second run of 8 A in open air, the cell reached 0.0 V after 107 s, and did thus not reach the 120 s goal. In the sealed and open air run, the seal was removed at around 0.23 V, 27 s after the start of the discharge. The 8 A current was maintained in this case until 0.0 V was reached 135 s after the start of the discharge. A comparison between 4 A and 8 A is shown in Figure 8 for the three air supply cases.

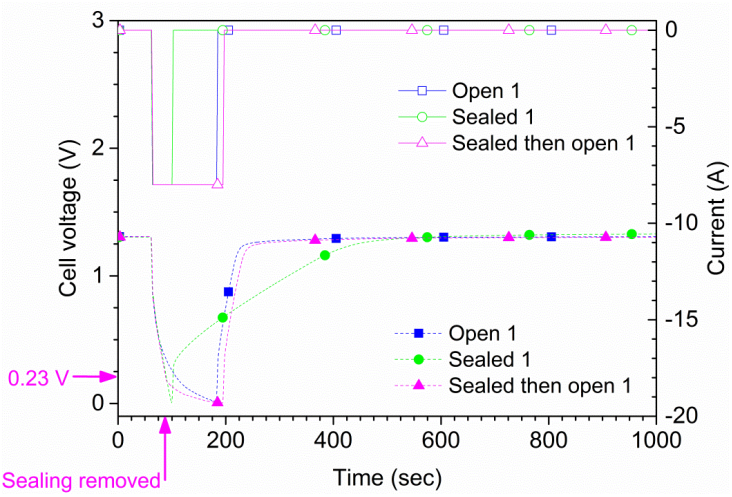


**Figure 7.** Voltage (filled symbols) and current (open symbols) measurements for cell 1 for three different tests using 8 A; open, sealed; and sealed then open.

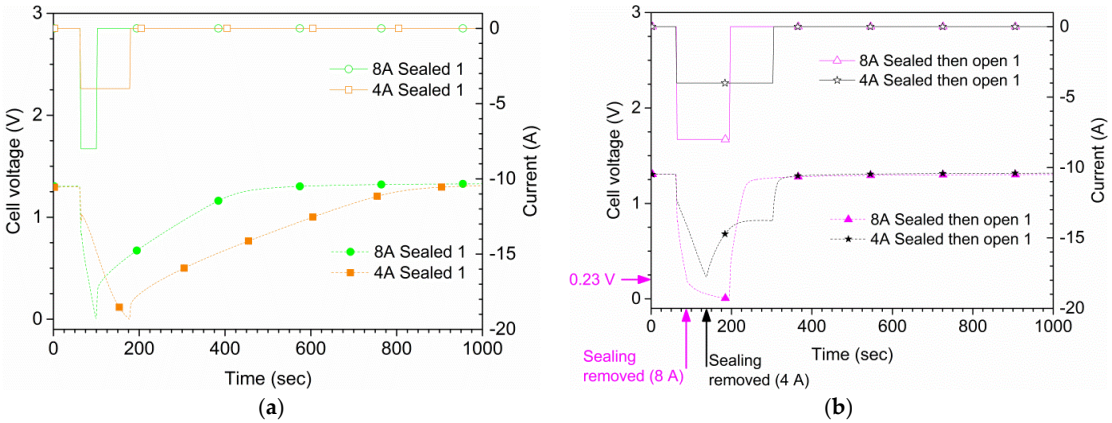


**Figure 8.** Voltage (filled symbols) and current (open symbols) measurements for cell 1 comparing 4 and 8 A with (**a**) sealed, and (**b**) sealed then open cell.

The suffocation experiments show that the potential of the cells rapidly goes to zero when the air supply is stopped. Starting from the cell reactions, Equations (1)–(4), our calculations show that the required air flow to the cell is 0.56 mL/s at a standard temperature and pressure, for a discharge current of 1.0 A. In the present case, for the 4 A discharge, the cell reached 0.0 V after approximately 120 s, corresponding to an air volume of 269 mL trapped inside cell. This volume is very close to the actual volume of the prismatic cell. For the 8 A overcurrent case, the suffocation resulted in a zero potential value already after 36 s, corresponding to an air volume of 161 mL. Of course, in this case the cell potential was decreasing also in open air, so the lower value is not unexpected. It should also be noted that the cell potential recovered quickly when the cells were re-exposed to air.

One of the important safety questions tested is: if the air supply at the cathode is stopped, is it possible to stop the battery operations efficiently in case of an emergency situation? The obtained results show that suffocation of the cell can indeed bring the cell potential to zero within a short period of time and stop further propagation of the internal reactions. The procedure is mainly limited by the volume of the cell packaging. The shutdown time is a function of the available air volume within the battery cell, and in the case of a battery pack also including the free air inside the battery system. For example, for a battery module/pack using a stack of Zn–air cells electrically connected in series and/or parallel, the amount of free air in the battery pack, arising from, e.g., interconnecting cell spacing, should be minimized in order for suffocation to be efficient. However, free air volumes are typically minimized anyway in order to achieve a compact battery pack size. Anyhow, some additional free air volumes might be useful and required for thermal management (cooling/heating) of the battery cells. The shutdown rate using suffocation may also be improved by lowering the available air volume by removing air from the system. In case of an emergency shutdown, the need of reducing the amount of oxygen in the free air volume can be supported by other methods, e.g., by a pump which could rapidly empty the free air volume; however, a too-fast pressure reduction could potentially harm the battery cell. The evaluation and testing of removing air by pumping was, however, not included in this study. In case of a battery pack with considerable free air space available, a shut-off air supply may result in a safe shutdown only after a relatively long time (including possible negative side-effects, e.g., additional pack heating due to ongoing cell discharging, etc.); nevertheless, a shutdown will eventually occur. Suffocation might thus be valuable also in this case as a potential passive safety shutdown method, as a complement to other shutdown techniques. There are faster ways to reach voltage shutdown, e.g., using electrical current fuses, contactors switching off and other circuit breakers. There are also internal cell safety devices for voltage shutdown, e.g., positive temperature coefficient (PTC) devices in case of an overcurrent. Furthermore, the suffocation offers an additional battery safety layer and an alternative means of battery shutdown which is not available in other battery technologies, e.g., Li-ion, NiMH and lead-acid batteries.

An additional essential safety improvement using suffocation for metal–air batteries would be the improved electrical hazard safety. The hazardous voltage in a large battery pack could, in principle, be brought to zero by using suffocation and combining it with a battery management system (BMS) controlled discharge circuit to empty the residual battery voltage. This way the battery would have its energy capacity preserved but with no hazardous voltage present. That could offer significant advantages for personal safety in manufacturing, transport, rescuing, service, maintenance etc. With an engineering design it is probably possible to make the suffocation a passive technique with autonomous safety, e.g., very valuable in a battery electric vehicle crash situation, in large battery packs used in stationary energy storage systems, in vessels, etc. The demonstrated principle of suffocation could thus be a useful safety device in future large battery packs of metal–air cells, e.g., in Li–air battery systems.

In the event of suffocation, a further complication may possibly arise due to hydrogen gas production from the corrosion of Zn:

$$Zn + 2H_2O \rightarrow Zn(OH)_2 + H_2 \quad (5)$$

The safety instruction for Zn–air batteries thus advises to always have good ventilation around the cell. Using suffocation for an emergency stop procedure is, however, not likely to cause safety problems with hydrogen production, since the suffocation will also stop the supply of humid air.

The age and *SOC* of the cell did not seem to influence the results in any substantial way. One cell (cell 1) was, after the previous discharge and overcurrent abuse, tested with 1 A discharge currents in steps of 5 Ah until 0.0 V was reached. The potential dropped significantly only close to the end of life and the internal impedance increased as the capacity was depleted. Figure 9 shows impedance measurements of the same cell during its use, at 0, 3.9 and 25.6 Ah discharge. Impedance plots of zinc–air batteries are complex but can often be described by a low-frequency part mainly related to cathode reactions, possibly also including a Warburg diffusion element, a medium-frequency part

mainly related to the anode; while the high-frequency region shows an inductive response that can be due to electrode porosity, cell geometry and electrical leads [11,12]. The impedance plots in Figure 9 show similar behavior but data are too limited to make an in-depth analysis in this case. Nevertheless, the results show that the series resistance (determined from the intersection with the real axis in the complex impedance plot) increased from about 18.3 mΩ to 28.2 mΩ at end of life (a 54% increase), and that the medium-frequency impedance increased with the increased discharge as expected as the anode is consumed. Also, the low-frequency part is affected, maybe partially as a consequence of the formation of zinc oxide as suggested by Schröder et al. [13]. It can be noted that the 25.6 Ah total discharged capacity is lower than the rated capacity (48 Ah with a 1 A discharge current); however, the cell had underwent abusive tests including higher discharge currents than 1 A, prior to the final discharge procedure with a 1 A discharge current.

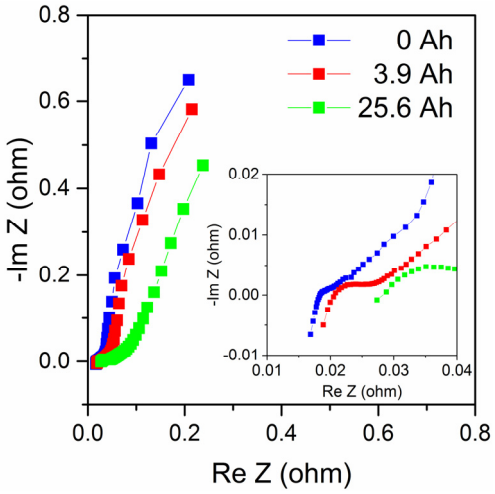


**Figure 9.** Impedance measurements for cell 1 showing real vs. imagined part three times: the beginning of life (0 Ah), intermediate measurement (3.9 Ah), and at the end of the testing (25.6 Ah), with a magnification around the origin in the inset.

## 4. Conclusions

Zn–air batteries are regarded as having a very high safety level since the possibilities for unwanted reactions are low and spontaneous reactions, e.g., as a consequence of an internal error, are unlikely. Furthermore, even if this battery technology is regarded to be very safe, interrupting the flow of air by suffocation could be a useful additional safety device, e.g., in case of internal or external short circuits or in case there is a risk of excessive temperatures, especially for larger battery systems. In this study it has been shown that suffocation may be an efficient method to bring the battery cell potential to zero and thus stop battery reactions within a short time. Using suffocation as a method to halt battery reactions may be a general possibility for batteries with an air cathode to be used in case of, e.g., internal short circuit events or external violence such as nail penetration or deformation in order to shut down a battery system. This method may also reduce the electrical hazard in a larger battery system since, by stopping the air supply, the voltage can be brought to zero while maintaining the energy capacity of the battery. As a consequence, this method may be considered also for emerging battery techniques such as the Li–air battery.

**Acknowledgments:** The authors gratefully acknowledge the Swedish Energy Agency and Carl Tryggers Stiftelse för Vetenskaplig Forskning for financial support.

**Author Contributions:** Fredrik Larsson and Istaq Ahmed conceived the experiments. Fredrik Larsson designed and planned the experiments and Antti Rytinki performed the experiments. All five authors were involved in the analyses of the data and wrote the paper.

**Conflicts of Interest:** The authors declare no conflict of interest.

## References


1. Lee, J.-S.; Kim, S.T.; Cao, R.; Choi, N.-S.; Liu, M.; Lee, K.T.; Cho, J. Metal–air batteries with high energy density: Li–air versus Zn–air. *Adv. Energy Mater.* **2011**, *1*, 34–50. [CrossRef]
2. Li, Y.; Dai, H. Recent advances in zinc–air batteries. *Chem. Soc. Rev.* **2014**, *43*, 5257–5275. [CrossRef] [PubMed]
3. Larsson, F.; Mellander, B.-E. Abuse by external heating, overcharge and short circuiting of commercial lithium-ion battery cells. *J. Electrochem. Soc.* **2014**, *161*, A1611–A1617. [CrossRef]
4. Larsson, F.; Andersson, P.; Mellander, B.-E. Lithium-ion battery aspects on fires in electrified vehicles on the basis of experimental abuse tests. *Batteries* **2016**, *2*, 9. [CrossRef]
5. Larsson, F.; Andersson, P.; Blomqvist, P.; Lorén, A.; Mellander, B.-E. Characteristics of lithium-ion batteries during fire tests. *J. Power Sources* **2014**, *271*, 414–420. [CrossRef]
6. Larsson, F.; Andersson, J.; Andersson, P.; Mellander, B.-E. Thermal modelling of cell-to-cell fire propagation and cascading thermal runaway failure effects for lithium-ion battery cells and modules using fire walls. *J. Electrochem. Soc.* **2016**, *163*, A2854–A2865. [CrossRef]
7. U.S. Department of Transportation. Risks of Fire or Explosion when Transporting Lithium Ion or Lithium Metal Batteries as Cargo on Passenger and Cargo Aircraft. Available online: https://www.faa.gov/other_visit/aviation_industry/airline_operators/airline_safety/safo/all_safos/media/2016/SAFO16001.pdf (accessed on 13 June 2016).
8. Choi, N.-S.; Chen, Z.; Freunberger, S.A.; Ji, X.; Sun, Y.-K.; Amine, K.; Yushin, G.; Nazar, L.F.; Cho, J.; Bruce, P.G. Challenges facing lithium batteries and electrical double-layer capacitors. *Angew. Chem. Int. Ed.* **2012**, *51*, 9994–10024. [CrossRef] [PubMed]
9. Rahman, M.A.; Wang, X.; Wen, C. High energy density metal-air batteries: A review. *J. Electrochem. Soc.* **2013**, *160*, A1759–A1771. [CrossRef]
10. Li, Y.; Gong, M.; Liang, Y.; Feng, J.; Kim, J.-E.; Wang, H.; Hong, G.; Zhang, B.; Dai, H. Advanced zinc-air batteries based on high-performance hybrid electrocatalysts. *Nat. Commun.* **2013**, *4*, 1805. [CrossRef] [PubMed]
11. Ma, H.; Wang, B.; Fan, Y.; Hong, W. Development and characterization of an electrically rechargeable zinc-air battery stack. *Energies* **2014**, *7*, 6549–6557. [CrossRef]
12. Osaka, T.; Mukoyama, D.; Nara, H. Review—Development of diagnostic process for commercially available batteries, especially lithium ion battery, by electrochemical impedance spectroscopy. *J. Electrochem. Soc.* **2015**, *162*, A2529–A2537. [CrossRef]
13. Schröder, D.; Sinai Borker, N.N.; König, M. Performance of zinc air batteries with added $K_2CO_3$ in the alkaline electrolyte. *J. Appl. Electrochem.* **2015**, *45*, 427–437. [CrossRef]